

**AD-A257 299**



②

**NAVAL POSTGRADUATE SCHOOL**  
**Monterey, California**



**DTIC**  
**ELECTE**  
**NOV 17 1992**  
**S A D**

**THESIS**

**EFFECT OF SURFACE COATING ON CYLINDERS  
SUBJECTED TO UNDERWATER SHOCK**

**by**

**John K. Bergersen**

**SEPTEMBER 1992**

**Thesis Advisor:**

**Young W. Kwon**

**Approved for public release; distribution is unlimited.**

**92-29620**



Unclassified  
SECURITY CLASSIFICATION OF THIS PAGE

Form Approved  
OMB No 0704-0188

# REPORT DOCUMENTATION PAGE

1a REPORT SECURITY CLASSIFICATION <b>Unclassified</b>		1b RESTRICTIVE MARKINGS	
2a SECURITY CLASSIFICATION AUTHORITY		3 DISTRIBUTION/AVAILABILITY OF REPORT <b>Approved for public release: Distribution is Unlimited</b>	
2b DECLASSIFICATION/DOWNGRADING SCHEDULE			
4 PERFORMING ORGANIZATION REPORT NUMBER(S)		5 MONITORING ORGANIZATION REPORT NUMBER(S)	
6a NAME OF PERFORMING ORGANIZATION <b>Naval Postgraduate School</b>	6b OFFICE SYMBOL (if applicable) <b>ME</b>	7a NAME OF MONITORING ORGANIZATION <b>Naval Postgraduate School</b>	
6c ADDRESS (City, State, and ZIP Code) <b>Monterey, CA 93943-5000</b>		7b ADDRESS (City, State, and ZIP Code) <b>Monterey, CA 93943-5000</b>	
8a NAME OF FUNDING/SPONSORING ORGANIZATION	8b OFFICE SYMBOL (if applicable)	9 PROCUREMENT INSTRUMENT IDENTIFICATION NUMBER	
8c ADDRESS (City, State, and ZIP Code)		10 SOURCE OF FUNDING NUMBERS	
		PROGRAM ELEMENT NO	PROJECT NO
		TASK NO	WORK UNIT ACCESSION NO
11 TITLE (Include Security Classification) <b>EFFECT OF SURFACE COATING ON CYLINDERS SUBJECTED TO UNDERWATER SHOCK (U)</b>			
12 PERSONAL AUTHOR(S) <b>JOHN K. BERGERSEN</b>			
13a TYPE OF REPORT <b>Master's Thesis</b>	13b TIME COVERED FROM _____ TO _____	14 DATE OF REPORT (Year, Month, Day) <b>SEPTEMBER 1992</b>	15 PAGE COUNT <b>135</b>
16 SUPPLEMENTARY NOTATION <b>The views expressed are those of the author and do not reflect the official policy or position of the Department of Defense or the U.S. Government.</b>			
17 COSATI CODES		18 SUBJECT TERMS (Continue on reverse if necessary and identify by block number)	
FIELD	GROUP	SUB GROUP	
		underwater shock	
19 ABSTRACT (Continue on reverse if necessary and identify by block number) <p>The response of a composite cylinder (metallic cylinder coated with a rubber material) subjected to an underwater explosion was analyzed numerically. Qualitative differences between coated and uncoated cylinders were investigated. The dynamic response of the coated cylinder was found to be adversely affected when impacted by an underwater shock wave under certain conditions of geometry and material properties of the coating. When adversely affected, significant deviations in axial and hoop stress and strain values were observed. The coated cylinder exhibited larger effective plastic strain and higher residual internal energy in the metallic material. Rubber coatings appeared to inhibit energy dissipation from the metallic material to the surrounding water medium. A parametric study of various coatings was performed on both aluminum and steel cylinders. The adverse effects of the coating decreased when the shear modulus of the rubber was increased or when the rubber thickness was increased, indicating the existence of</p>			
20 DISTRIBUTION AVAILABILITY OF ABSTRACT <input checked="" type="checkbox"/> UNCLASSIFIED UNLIMITED <input type="checkbox"/> SAME AS RPT <input type="checkbox"/> DTIC USERS		21 ABSTRACT SECURITY CLASSIFICATION <b>Unclassified</b>	
22a NAME OF RESPONSIBLE INDIVIDUAL <b>Young W. Kwon</b>		22b TELEPHONE (Include Area Code) <b>(408) 646-3385</b>	22c OFFICE SYMBOL <b>ME/kv</b>

DD Form 1473, JUN 86

Previous editions are obsolete

S/N 0102-LF-014-6603

SECURITY CLASSIFICATION OF THIS PAGE

**Unclassified**

Unclassified

SECURITY CLASSIFICATION OF THIS PAGE

Block # 19 continued:

threshold values for these parameters. The results of this study indicate that the stiffness of the coating is a critical factor involving these threshold values.

Approved for public release; distribution is unlimited.

Effect of Surface Coating On Cylinders  
Subjected to Underwater Shock

**DTIC QUALITY INSPECTED 4**

by

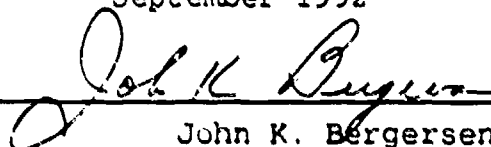
John K. Bergersen  
Lieutenant Commander, United States Navy  
B.S., University of Rochester, 1981

Submitted in partial fulfillment  
of the requirements for the degree of

MASTER OF SCIENCE  
IN MECHANICAL ENGINEERING  
from the  
NAVAL POSTGRADUATE SCHOOL  
September 1992

Accession For	
NTIS	CRA&I <input checked="" type="checkbox"/>
DTIC	TAB <input type="checkbox"/>
Unannounced <input type="checkbox"/>	
Justification	
By	
Distribution /	
Availability Codes	
Dist	Avail and/or Special
A-1	


Author:

  
John K. Bergersen

Approved by:

  
Young W. Kwon, Thesis Advisor

  
Young S. Shin, Second Reader

  
Matthew D. Kelleher, Chairman  
Department of Mechanical Engineering

## ABSTRACT

The response of a composite cylinder (metallic cylinder coated with a rubber material) subjected to an underwater explosion was analyzed numerically. Qualitative differences between coated and uncoated cylinders were investigated. The dynamic response of the coated cylinder was found to be adversely affected when impacted by an underwater shock wave under certain conditions of geometry and material properties of the coating. When adversely affected, significant deviations in axial and hoop stress and strain values were observed. The coated cylinder exhibited larger effective plastic strain and higher residual internal energy in the metallic material. Rubber coatings appeared to inhibit energy dissipation from the metallic material to the surrounding water medium. A parametric study of various coatings was performed on both aluminum and steel cylinders. The adverse effects of the coating decreased when the shear modulus of the rubber was increased or when the rubber thickness was increased, indicating the existence of threshold values for these parameters. The results of this study indicate that the stiffness of the coating is a critical factor involving these threshold values.

## TABLE OF CONTENTS

I. INTRODUCTION . . . . .	1
II. NUMERICAL ANALYSIS . . . . .	4
A. NUMERICAL CODES . . . . .	4
1. Finite Element Code . . . . .	4
2. Boundary Element Code . . . . .	5
3. Structure and Wave Equations . . . . .	5
B. NUMERICAL MODEL . . . . .	8
1. Material Models . . . . .	8
2. Simulated Test Conditions . . . . .	12
3. Finite Element Mesh . . . . .	13
4. Element Compatability . . . . .	15
5. Material Properties . . . . .	16
III. RESULTS AND ANALYSIS . . . . .	18
A. ELEMENT COMPATABILITY . . . . .	18
B. EFFECT OF SURFACE COATINGS ON CYLINDERS . . . . .	25
IV. CONCLUSIONS AND RECOMMENDATIONS . . . . .	110
APPENDIX: COMPOSITE CYLINDER MODEL INGRID INPUT FILE . . . . .	112

LIST OF REFERENCES . . . . .	115
INITIAL DISTRIBUTION LIST. . . . .	117

## LIST OF FIGURES

Figure 1:	Cylinder geometry and test profile. . . . .	12
Figure 2:	Free-field pressure-time history plot. . . . .	13
Figure 3:	Finite element mesh (quarter model). . . . .	14
Figure 4:	Axial strain at position A1 for different shell thickness element configurations. . . . .	19
Figure 5:	Hoop strain at position A1 for different shell thickness element configurations. . . . .	19
Figure 6:	Axial strain at position A2 for different shell thickness element configurations. . . . .	20
Figure 7:	Hoop strain at position A2 for different shell thickness element configurations. . . . .	20
Figure 8:	Axial strain at position A3 for different shell thickness element configurations. . . . .	21
Figure 9:	Hoop strain at position A3 for different shell thickness element configurations. . . . .	21
Figure 10:	Axial strain at position B1 for different shell thickness element configurations. . . . .	22
Figure 11:	Hoop strain at position B1 for different shell thickness element configurations. . . . .	22
Figure 12:	Axial strain at position B2 for different shell thickness element configurations. . . . .	23
Figure 13:	Hoop strain at position B2 for different shell thickness element configurations. . . . .	23
Figure 14:	Axial strain at position B3 for different shell thickness element configurations. . . . .	24
Figure 15:	Hoop strain at position B3 for different shell thickness element configurations. . . . .	24
Figure 16:	Axial strain at position A1 for uncoated and coated aluminum cylinders. . . . .	26
Figure 17:	Hoop strain at position A1 for uncoated and coated aluminum cylinders. . . . .	26
Figure 18:	Axial strain at position A2 for uncoated and coated aluminum cylinders. . . . .	27
Figure 19:	Hoop strain at position A2 for uncoated and coated aluminum cylinders. . . . .	27
Figure 20:	Axial strain at position A3 for uncoated and coated aluminum cylinders. . . . .	28
Figure 21:	Hoop strain at position A3 for uncoated and coated aluminum cylinders. . . . .	28
Figure 22:	Axial strain at position B1 for uncoated and coated aluminum cylinders. . . . .	29



Figure 23:	Hoop strain at position B1 for uncoated and coated aluminum cylinders. . . . .	29
Figure 24:	Axial strain at position B2 for uncoated and coated aluminum cylinders. . . . .	30
Figure 25:	Hoop strain at position B2 for uncoated and coated aluminum cylinders. . . . .	30
Figure 26:	Axial strain at position B3 for uncoated and coated aluminum cylinders. . . . .	31
Figure 27:	Hoop strain at position B3 for uncoated and coated aluminum cylinders. . . . .	31
Figure 28:	Axial strain at position C1 for uncoated and coated aluminum cylinders. . . . .	32
Figure 29:	Hoop strain at position C1 for uncoated and coated aluminum cylinders. . . . .	32
Figure 30:	Axial strain at position C2 for uncoated and coated aluminum cylinders. . . . .	33
Figure 31:	Hoop strain at position C2 for uncoated and coated aluminum cylinders. . . . .	33
Figure 32:	Axial strain at position C3 for uncoated and coated aluminum cylinders. . . . .	34
Figure 33:	Hoop strain at position C3 for uncoated and coated aluminum cylinders. . . . .	34
Figure 34:	Deformation of (a) uncoated aluminum cylinder and (b) composite cylinder #1 at 2.86 msec. . . . .	36
Figure 35:	Deformation of (a) uncoated aluminum cylinder and (b) composite cylinder #2 at 5.86 msec. . . . .	37
Figure 36:	Internal energy of aluminum shell material for uncoated and coated aluminum cylinders. . . . .	38
Figure 37:	Axial strain at position A1 for coated aluminum cylinders with variation of rubber shear modulus. . . . .	40
Figure 38:	Hoop strain at position A1 for coated aluminum cylinders with variation of rubber shear modulus. . . . .	40
Figure 39:	Axial strain at position A2 for coated aluminum cylinders with variation of rubber shear modulus. . . . .	41
Figure 40:	Hoop strain at position A2 for coated aluminum cylinders with variation of rubber shear modulus. . . . .	41
Figure 41:	Axial strain at position A3 for coated aluminum cylinders with variation of rubber shear modulus. . . . .	42
Figure 42:	Hoop strain at position A3 for coated aluminum cylinders with variation of rubber shear modulus. . . . .	42

Figure 43:	Axial strain at position B1 for coated aluminum cylinders with variation of rubber shear modulus. . . . .	43
Figure 44:	Hoop strain at position B1 for coated aluminum cylinders with variation of rubber shear modulus. . . . .	43
Figure 45:	Axial strain at position B2 for coated aluminum cylinders with variation of rubber shear modulus. . . . .	44
Figure 46:	Hoop strain at position B2 for coated aluminum cylinders with variation of rubber shear modulus. . . . .	44
Figure 47:	Axial strain at position B3 for coated aluminum cylinders with variation of rubber shear modulus. . . . .	45
Figure 48:	Hoop strain at position B3 for coated aluminum cylinders with variation of rubber shear modulus. . . . .	45
Figure 49:	Axial strain at position C1 for coated aluminum cylinders with variation of rubber shear modulus. . . . .	46
Figure 50:	Hoop strain at position C1 for coated aluminum cylinders with variation of rubber shear modulus. . . . .	46
Figure 51:	Axial strain at position C2 for coated aluminum cylinders with variation of rubber shear modulus. . . . .	47
Figure 52:	Hoop strain at position C2 for coated aluminum cylinders with variation of rubber shear modulus. . . . .	47
Figure 53:	Axial strain at position C3 for coated aluminum cylinders with variation of rubber shear modulus. . . . .	48
Figure 54:	Hoop strain at position C3 for coated aluminum cylinders with variation of rubber shear modulus. . . . .	48
Figure 55:	Internal energy of aluminum shell material of coated aluminum cylinders with variation of rubber shear modulus. . . . .	49
Figure 56:	Effective plastic strain at position A3 for uncoated and coated aluminum cylinders with large variation of rubber shear modulus. . . . .	50
Figure 57:	Radial velocity at node 49 for uncoated and coated aluminum cylinders with large variation of rubber shear modulus. . . . .	50
Figure 58:	Deformation of uncoated and coated aluminum cylinders with large variation of rubber shear modulus at 2.86 msec. (Scale factor of 5). . . . .	52
Figure 59:	Internal energy of aluminum material for uncoated and coated cylinders with large variation of rubber shear modulus (10 msec. range). . . . .	53

Figure 60:	Internal energy of aluminum material for uncoated and coated cylinders with large variation of rubber shear modulus (2 msec. range) . .	53
Figure 61:	Comparison of internal energy of aluminum shell material of coated cylinder with variation in coefficient of asymmetry. . .	54
Figure 62:	Axial strain at position A1 for coated aluminum cylinders with variation of coefficient of asymmetry. . . . .	55
Figure 63:	Hoop strain at position A1 for coated aluminum cylinders with variation of coefficient of asymmetry. . . . .	55
Figure 64:	Axial strain at position A2 for coated aluminum cylinders with variation of coefficient of asymmetry. . . . .	56
Figure 65:	Hoop strain at position A2 for coated aluminum cylinders with variation of coefficient of asymmetry. . . . .	56
Figure 66:	Axial strain at position A3 for coated aluminum cylinders with variation of coefficient of asymmetry. . . . .	57
Figure 67:	Hoop strain at position A3 for coated aluminum cylinders with variation of coefficient of asymmetry. . . . .	57
Figure 68:	Axial strain at position B1 for coated aluminum cylinders with variation of coefficient of asymmetry. . . . .	58
Figure 69:	Hoop strain at position B1 for coated aluminum cylinders with variation of coefficient of asymmetry. . . . .	58
Figure 70:	Axial strain at position B2 for coated aluminum cylinders with variation of coefficient of asymmetry. . . . .	59
Figure 71:	Hoop strain at position B2 for coated aluminum cylinders with variation of coefficient of asymmetry. . . . .	59
Figure 72:	Axial strain at position B3 for coated aluminum cylinders with variation of coefficient of asymmetry. . . . .	60
Figure 73:	Hoop strain at position B3 for coated aluminum cylinders with variation of coefficient of asymmetry. . . . .	60
Figure 74:	Axial strain at position C1 for coated aluminum cylinders with variation of coefficient of asymmetry. . . . .	61
Figure 75:	Hoop strain at position C1 for coated aluminum cylinders with variation of coefficient of asymmetry. . . . .	61

Figure 76:	Axial strain at position C2 for coated aluminum cylinders with variation of coefficient of asymmetry. . . . .	62
Figure 77:	Hoop strain at position C2 for coated aluminum cylinders with variation of coefficient of asymmetry. . . . .	62
Figure 78:	Axial strain at position C3 for coated aluminum cylinders with variation of coefficient of asymmetry. . . . .	63
Figure 79:	Hoop strain at position C3 for coated aluminum cylinders with variation of coefficient of asymmetry. . . . .	63
Figure 80:	Axial strain at position A1 for coated cylinders with variation of aluminum shell thickness. . . . .	65
Figure 81:	Hoop strain at position A1 for coated cylinders with variation of aluminum shell thickness. . . . .	65
Figure 82:	Axial strain at position A2 for coated cylinders with variation of aluminum shell thickness. . . . .	66
Figure 83:	Hoop strain at position A2 for coated cylinders with variation of aluminum shell thickness. . . . .	66
Figure 84:	Axial strain at position A3 for coated cylinders with variation of aluminum shell thickness. . . . .	67
Figure 85:	Hoop strain at position A3 for coated cylinders with variation of aluminum shell thickness. . . . .	67
Figure 86:	Axial strain at position B1 for coated cylinders with variation of aluminum shell thickness. . . . .	68
Figure 87:	Hoop strain at position B1 for coated cylinders with variation of aluminum shell thickness. . . . .	68
Figure 88:	Axial strain at position B2 for coated cylinders with variation of aluminum shell thickness. . . . .	69
Figure 89:	Hoop strain at position B2 for coated cylinders with variation of aluminum shell thickness. . . . .	69
Figure 90:	Axial strain at position B3 for coated cylinders with variation of aluminum shell thickness. . . . .	70
Figure 91:	Hoop strain at position B3 for coated cylinders with variation of aluminum shell thickness. . . . .	70

Figure 92:	Axial strain at position C1 for coated cylinders with variation of aluminum shell thickness. . . . .	71
Figure 93:	Hoop strain at position C1 for coated cylinders with variation of aluminum shell thickness. . . . .	71
Figure 94:	Axial strain at position C2 for coated cylinders with variation of aluminum shell thickness. . . . .	72
Figure 95:	Hoop strain at position C2 for coated cylinders with variation of aluminum shell thickness. . . . .	72
Figure 96:	Axial strain at position C3 for coated cylinders with variation of aluminum shell thickness. . . . .	73
Figure 97:	Hoop strain at position C3 for coated cylinders with variation of aluminum shell thickness. . . . .	73
Figure 98:	Effective plastic strain at position A1 for coated cylinders with variation of aluminum shell thickness. . . . .	74
Figure 99:	Effective plastic strain at position A2 for coated cylinders with variation of aluminum shell thickness. . . . .	74
Figure 100:	Effective plastic strain at position A3 for coated cylinders with variation of aluminum shell thickness. . . . .	75
Figure 101:	Effective plastic strain at position B1 for coated cylinders with variation of aluminum shell thickness. . . . .	75
Figure 102:	Effective plastic strain at position B2 for coated cylinders with variation of aluminum shell thickness. . . . .	76
Figure 103:	Effective plastic strain at position B3 for coated cylinders with variation of aluminum shell thickness. . . . .	76
Figure 104:	Effective plastic strain at position C1 for coated cylinders with variation of aluminum shell thickness. . . . .	77
Figure 105:	Effective plastic strain at position C2 for coated cylinders with variation of aluminum shell thickness. . . . .	77
Figure 106:	Effective plastic strain at position C3 for coated cylinders with variation of aluminum shell thickness. . . . .	78
Figure 107:	Deformation of coated cylinders with variation of aluminum shell thickness at 2.34 msec. . . . .	79
Figure 108:	Internal energy of aluminum shell material of coated cylinders with variation of aluminum shell thickness. . . . .	80

Figure 109: Axial strain at position A1 for coated aluminum cylinders with variation of rubber thickness. . . . .	92
Figure 110: Hoop strain at position A1 for coated aluminum cylinders with variation of rubber thickness. . . . .	82
Figure 111: Axial strain at position A2 for coated aluminum cylinders with variation of rubber thickness. . . . .	83
Figure 112: Hoop strain at position A2 for coated aluminum cylinders with variation of rubber thickness. . . . .	83
Figure 113: Axial strain at position A3 for coated aluminum cylinders with variation of rubber thickness. . . . .	84
Figure 114: Hoop strain at position A3 for coated aluminum cylinders with variation of rubber thickness. . . . .	84
Figure 115: Axial strain at position B1 for coated aluminum cylinders with variation of rubber thickness. . . . .	85
Figure 116: Hoop strain at position B1 for coated aluminum cylinders with variation of rubber thickness. . . . .	85
Figure 117: Axial strain at position B2 for coated aluminum cylinders with variation of rubber thickness. . . . .	86
Figure 118: Hoop strain at position B2 for coated aluminum cylinders with variation of rubber thickness. . . . .	86
Figure 119: Axial strain at position B3 for coated aluminum cylinders with variation of rubber thickness. . . . .	87
Figure 120: Hoop strain at position B3 for coated aluminum cylinders with variation of rubber thickness. . . . .	87
Figure 121: Axial strain at position C1 for coated aluminum cylinders with variation of rubber thickness. . . . .	88
Figure 122: Hoop strain at position C1 for coated aluminum cylinders with variation of rubber thickness. . . . .	88
Figure 123: Axial strain at position C2 for coated aluminum cylinders with variation of rubber thickness. . . . .	89
Figure 124: Hoop strain at position C2 for coated aluminum cylinders with variation of rubber thickness. . . . .	89
Figure 125: Axial strain at position C3 for coated aluminum cylinders with variation of rubber thickness. . . . .	90

Figure 126: Hoop strain at position C3 for coated aluminum cylinders with variation of rubber thickness. . . . .	90
Figure 127: Effective plastic strain at position A1 for coated aluminum cylinders with variation of rubber thickness. . . . .	91
Figure 128: Effective plastic strain at position A2 for coated aluminum cylinders with variation of rubber thickness. . . . .	91
Figure 129: Effective plastic strain at position A3 for coated aluminum cylinders with variation of rubber thickness. . . . .	92
Figure 130: Effective plastic strain at position B1 for coated aluminum cylinders with variation of rubber thickness. . . . .	92
Figure 131: Effective plastic strain at position B2 for coated aluminum cylinders with variation of rubber thickness. . . . .	93
Figure 132: Effective plastic strain at position B3 for coated aluminum cylinders with variation of rubber thickness. . . . .	93
Figure 133: Effective plastic strain at position C1 for coated aluminum cylinders with variation of rubber thickness. . . . .	94
Figure 134: Effective plastic strain at position C2 for coated aluminum cylinders with variation of rubber thickness. . . . .	94
Figure 135: Effective plastic strain at position C3 for coated aluminum cylinders with variation of rubber thickness. . . . .	95
Figure 136: Deformation of coated aluminum cylinders with variation of rubber thickness at 0.76 msec. (Displacement scale factor of 5). . .	96
Figure 137: Deformation of coated aluminum cylinders with variation of rubber thickness at 2.86 msec. (Displacement scale factor of 5). . .	97
Figure 138: Internal energy of aluminum shell material for coated cylinders with variation of rubber thickness. . . . .	98
Figure 139: Axial strain at position A1 for uncoated and coated steel cylinders. . . . .	100
Figure 140: Hoop strain at position A1 for uncoated and coated steel cylinders. . . . .	100
Figure 141: Axial strain at position A2 for uncoated and coated steel cylinders. . . . .	101
Figure 142: Hoop strain at position A2 for uncoated and coated steel cylinders. . . . .	101

Figure 143: Axial strain at position A3 for uncoated and coated steel cylinders. . . . .	102
Figure 144: Hoop strain at position A3 for uncoated and coated steel cylinders. . . . .	102
Figure 145: Axial strain at position B1 for uncoated and coated steel cylinders. . . . .	103
Figure 146: Hoop strain at position B1 for uncoated and coated steel cylinders. . . . .	103
Figure 147: Axial strain at position B2 for uncoated and coated steel cylinders. . . . .	104
Figure 148: Hoop strain at position B2 for uncoated and coated steel cylinders. . . . .	104
Figure 149: Axial strain at position B3 for uncoated and coated steel cylinders. . . . .	105
Figure 150: Hoop strain at position B3 for uncoated and coated steel cylinders. . . . .	105
Figure 151: Axial strain at position C1 for uncoated and coated steel cylinders. . . . .	106
Figure 152: Hoop strain at position C1 for uncoated and coated steel cylinders. . . . .	106
Figure 153: Axial strain at position C2 for uncoated and coated steel cylinders. . . . .	107
Figure 154: Hoop strain at position C2 for uncoated and coated steel cylinders. . . . .	107
Figure 155: Axial strain at position C3 for uncoated and coated steel cylinders. . . . .	108
Figure 156: Hoop strain at position C3 for uncoated and coated steel cylinders. . . . .	108



## ACKNOWLEDGEMENTS

I would like to express my sincere thanks and appreciation to Dr. Young W. Kwon and Dr. Young S. Shin for their support, guidance, encouragement and infinite patience. I would also like to express my gratitude to the Defense Nuclear Agency, for their continued interest and support of the underwater explosion research at the Naval Postgraduate School.

To LCDR Padraic Fox, LT Jim Chisum and LT William Miller, whose expert tutelage and advice were invaluable in my research, I extend my warmest thanks.

Finally, I dedicate this work to my wife, Carolann, and my four sons, John, Brad, Lance and Brandon. Their love, support and many sacrifices paved the way for completion of this thesis.

## I. INTRODUCTION

Not since World War II has mankind witnessed such dramatic and profound changes as those that have occurred in recent years. Sweeping political and economic reform in the former Soviet Union has not only slowed their military production and affected their deployment of forces, but it has been the impetus that has led the United States to re-evaluate its own strategic planning and policies. Accordingly, the United States Navy has had to re-formulate its "Maritime Strategy".

Although the Soviet threat has diminished, the United States Navy must remain capable of quickly responding to conflicts around the world, as demonstrated in Operation Desert Shield and Operation Desert Storm. To continue to meet all its commitments abroad, amidst a shrinking defense budget, the Navy has placed a premium on development and production of ships and submarines that are technologically superior, cost-effective, easily maintained and perhaps most importantly, survivable. In the 21st century, "shallow water" naval engagements are most likely. In this environment, U.S. warships and submarines will be most vulnerable to mines and depth charges. Although a future adversary may not possess a large arsenal of military firepower, it will likely employ sophisticated weapons, possibly nuclear weapons, capable of inflicting considerable damage without rendering a direct hit.

To counter this threat, the United States Navy has intensified its efforts in research and study of underwater explosions on ship and submarine hulls. No matter how well a ship or submarine might be armored, the effects of a direct hit from a mine, torpedo or depth charge are potentially catastrophic. If however, the explosion were to occur away from the hull, then the ability of the hull to withstand the effects of the shock wave caused by the blast becomes crucial. In an attempt to better understand the effects of blast damage on shock hardening, the Navy has performed underwater explosion tests and analyzed the problem numerically using computer simulations. Knowledge gained through such study should prove invaluable to ship and submarine designers of the future.

The dynamic response of a structure to an underwater explosion is a complex problem due to the interaction between the fluid and structure. Over the past several years, the Naval Postgraduate School has conducted extensive research in the field of underwater shock. This study has involved both physical testing and numerical modeling of uncoated metal cylinders of various configurations such as unstiffened, stiffened, single shell layer and double shell layer models. Ship shock qualifications and even small scale testing can be cost prohibitive and time consuming, therefore much of the work has focused on developing computer models using the numerical analysis technique. Results from earlier studies

[Refs. 1-3] indicate response predictions compare favorably with both analytical solutions and experimental data.

In a recent study conducted by the Navy [Ref. 4], when subjected to an underwater shock wave, damage to a steel test panel increased when it was covered with a low density layer of glass microspheres suspended in water (slurry). This result was unexpected and the reason for this adverse response is still under investigation. It is suspected that compliant coatings may affect the propagation of a shock wave and the dynamic response of a structure.

The objective of this study was to examine the response of a metal cylinder coated with a rubber material, when subjected to an underwater explosion, utilizing the numerical analysis technique. Rubber coated aluminum and steel cylinders were analyzed and a parametric study of various coatings was performed to gain a better understanding of the damage mechanism. Preliminary study seems to indicate that the dissipation of energy from the structure to the surrounding water medium is critical to its dynamic response.

## **II. NUMERICAL ANALYSIS**

### **A. NUMERICAL CODES**

To study the effects of an underwater shock wave on a cylinder, a coupled finite element and boundary element code was utilized. The two codes operate in tandem so that the fluid-structure interaction can be calculated. This code was successfully implemented at the Naval Postgraduate School in 1991 and has since been the primary tool used for studying underwater shock phenomena. Structural calculations were handled by the finite element code while the effects of the propagation of the explosive pressure wave through the water medium were calculated by the boundary element code.

#### **1. Finite Element Code**

The finite element code used in this analysis was VEC/DYNA3D [Ref. 5]. Originally implemented in 1976, it has been widely used in the industrial sector and at many universities. The code is efficient and extremely flexible, offering a wide variety of material models from which to choose.

Input to VEC/DYNA3D was provided by LS-INGRID [Ref. 6], a pre-processor and three dimensional mesh generator. Model configuration, element and material type, boundary

constraints and loading conditions were specified in the pre-processor.

Output from VEC/DYNA3D was provided by LS-TAURUS [Ref. 7], an interactive post-processor that was used to display fringe plots, element, node and material time history plots, and generate data files.

## **2. Boundary Element Code**

The boundary element method code used in this analysis was USA (Underwater Shock Analysis) [Ref. 8]. The USA code computed the transient response of the submerged cylinder to the shock wave. Calculations of the fluid-structure interaction are based on the Doubly Asymptotic Approximation (DAA) theory developed by T.L. Geers [Ref. 9]. The boundary element method precludes the requirement to discretize the water medium since equivalent forces and masses are transferred to the cylinder from the water and are applied at the nodes of a two dimensional mesh which is superimposed on the cylinder surface. As a result, computational efficiency is improved.

## **3. Structure and Wave Equations**

The differential equation for the dynamic response of a structure can be expressed as follows:

$$[M_s] \ddot{x} + [C_s] \dot{x} + [K_s] x = \{f\} \quad (1)$$

where  $[M_s]$ ,  $[C_s]$  and  $[K_s]$  are the structural mass, damping and

stiffness matrices respectively, and  $\{x\}$ ,  $\{\dot{x}\}$  and  $\{x\}$  are the nodal acceleration, velocity and displacement vectors respectively.  $\{f\}$  is the excitation force vector and can be expressed as a function of the incident and scattered pressures of the impinging shock wave and any concentrated loads applied to the structure. Their functional relationship is as follows:

$$\{f\} = - [G] [A_f] \{P_i + P_s\} + \{f_d\} \quad (2)$$

where  $[G]$  is the fluid/structure transformation matrix,  $[A_f]$  is the diagonal area matrix associated with the fluid elements,  $\{P_i + P_s\}$  is the incident and scattered pressure wave vector and  $\{f_d\}$  is the force vector applied to the dry structure. The scattered pressure represents the only unknown quantity, but it can be determined by solving the first order wave equation given below,

$$[M_f] \{\ddot{p}_s\} + \rho c [A_f] \{\dot{p}_s\} = \rho c [M_f] \{\dot{u}_s\} \quad (3)$$

where  $[M_f]$ ,  $\rho$ ,  $c$  and  $\{u_s\}$  are the symmetric fluid mass matrix, fluid density, sound speed and particle velocity vector respectively. Although the general solution is complicated, early and late time solutions to equation (3) can be found by

approximating  $\{P_s\} \gg \{P_s\}$  and  $\{P_s\} \ll \{P_s\}$  respectively and are referred to as the Doubly Asymptotic Approximations. The early time approximation is also referred to as the high frequency approximation or plane wave approximation. The solution is calculated at early times, at locations close to the structure and assumes the shape of the shock wave to be planar. The change in the scattered wave pressure is almost instantaneous, so  $\{P_s\}$  becomes the dominant term. Simplification and integration of equation (3) leads to the following solution:

$$\{P_s\} = \rho c \{u_s\} \quad (4)$$

The late time approximation is also referred to as the low frequency approximation or virtual mass approximation. The solution is calculated when the scattered pressure wave has travelled a significant distance from the structural surface so that the pressure change becomes negligible and the  $\{P_s\}$  term can be ignored. Simplification of equation (3) leads to the following form:

$$[A_r] \{P_s\} = [M_r] \{u_s\} \quad (5)$$

Determination of intermediate time solutions is accomplished by using the DAA relations which bridge the upper and lower limit approximations. A second DAA theory, called DAA2 was



later developed to account for surface curvature effects. DAA2 theory is contained in [Ref. 10].

## **B. NUMERICAL MODEL**

### **1. Material Models**

The behavior of the metal material was based on the Kinematic/Isotropic Elastic-Plastic Model [Refs. 5,6]. In addition to the density, the model required at least two other material properties be specified such as the bulk modulus, Young's modulus, shear modulus or Poisson's ratio. Optional inputs included yield stress, hardening modulus, or hardening parameter. The hardening parameter reflects the type of hardening (Isotropic or Kinematic) the material will experience. When steel was analyzed, strain-rate hardening effects were accounted for and were based on the Cowpers-Symonds Model, shown in equation (6)

$$\sigma_y = \sigma_y [1 + (\frac{d\epsilon/dt}{c})^{1/p}] \quad (6)$$

where  $\sigma_y$  is the yield stress and  $c$  and  $p$  are the strain-rate parameters which were obtained from a previous study [Ref. 3].

The behavior of the rubber material was based on the Compressible Mooney-Rivlin Model [Refs. 5,6]. Mooney pioneered a new approach to analyze the deformation of a soft material such as rubber [Ref. 11]. He stated that classical elastic

theory could not be applied to a highly elastic (hyper-elastic or superelastic) material but that deformation could be accurately represented in terms of its general strain energy density.

Mooney postulated that in addition to being homogeneous and free from hysteresis, a hyper-elastic material possesses the following properties:

- It is isotropic in the undeformed state and remains isotropic in planes that are at right angles to a stretch or squeeze.
- Deformations are isometric, i.e. occur without change in volume.
- In simple shear, shearing stress in any isotropic plane is proportional to the shear force.

Mooney expressed the general strain energy density function of a material,  $W$  as follows:

$$W = C_1 (\lambda_1^2 + \lambda_2^2 + \lambda_3^2 - 3) + C_2 \left( \frac{1}{\lambda_1^2} + \frac{1}{\lambda_2^2} + \frac{1}{\lambda_3^2} - 3 \right) \quad (7)$$

where  $\lambda_1$  is the principal stretch, which is equivalent to  $(1+e_1)$ , where  $e_1$  is strain. Applying conditions for a hyper-elastic material and substituting expressions for  $C_1$  and  $C_2$  as shown below

$$C_1 = \frac{(G+H)}{4} \quad , \quad C_2 = \frac{(G-H)}{4} \quad (8), (9)$$

leads to the following form:

$$W = \frac{G}{4} \sum_{i=1}^3 \left( \lambda_i - \frac{1}{\lambda_i} \right)^2 + \frac{H}{4} \sum_{i=1}^3 \left( \lambda_i^2 - \frac{1}{\lambda_i^2} \right) \quad (10)$$

where  $G$  and  $H$  represent the modulus of rigidity and the modulus characterizing asymmetry of reciprocal deformation respectively. The variable  $H$  is a measure of the ability of a material to store energy when compressed as opposed to when stretched. To express the asymmetry of reciprocal deformation in a more useful form, Mooney defined a new parameter  $\alpha$ , called the coefficient of symmetry, as follows:

$$\alpha = \frac{H}{G} \quad (11)$$

Experimental values for  $G$  and  $\alpha$  were derived for two types of rubber, tread stock and gum stock. Mooney found that the experimental data relating force and elongation, agreed closely with analytical results for soft rubber undergoing up to 400% elongation and 50% compression. Mooney believed that just as the infinitesimal deformation of a hard or moderately elastic material can be characterized by two material properties, shear modulus and Poisson's ratio, deformation of rubber can also be characterized by two properties, shear

modulus and coefficient of asymmetry. Mooney's analysis and development form the basis upon which the numerical model for the rubber material was generated. In the finite element model, the strain energy density function was defined as follows.

$$W = A(I-3) + B(II-3) + C(III^2-1) + D(III-1)^2 \quad (12)$$

where

$$C = 0.5A + B, \quad D = \frac{A(5\nu-2) + B(11\nu-5)}{2(1-2\nu)}, \quad (13), (14)$$

$$2(A+B) = G \quad (15)$$

$\nu$  is Poisson's ratio and  $I, II, III$  are invariants of the right Cauchy-Green tensor. The model required values for the constants  $A$  and  $B$ . By relating the first two terms of the strain energy density equation, equation (12), with equation (7), as expressed by Mooney, equivalent expressions for the two constants were determined and are shown below.

$$A = \frac{G}{4}(1+\alpha), \quad B = \frac{G}{4}(1-\alpha) \quad (16), (17)$$

Since values for  $G$  and  $\alpha$  were given for tread stock and gum stock in Mooney's development, these types of rubber were used in the analysis.

## 2. Simulated Test Conditions

All cases involved identical test conditions. The problem simulated detonation of 60 lbs. of HBX-1 spherically shaped explosive at a horizontal standoff distance of 25 ft. from the cylinder resulting in a side-on attack geometry. The uncoated cylinder models (metal only) were 12 in. in diameter, 42 in. long, 1/4 in. thick (shell thickness) with a 1 in. thick endplate. The composite or coated cylinder models had the same dimensions for the metal material as the uncoated cylinders but in addition were coated with 1/4 in. of rubber material on the outer surface of the cylinder. The shell and coating thicknesses were nominal values and were changed for parametric study. The cylinder geometry/test profile is shown in Figure 1.

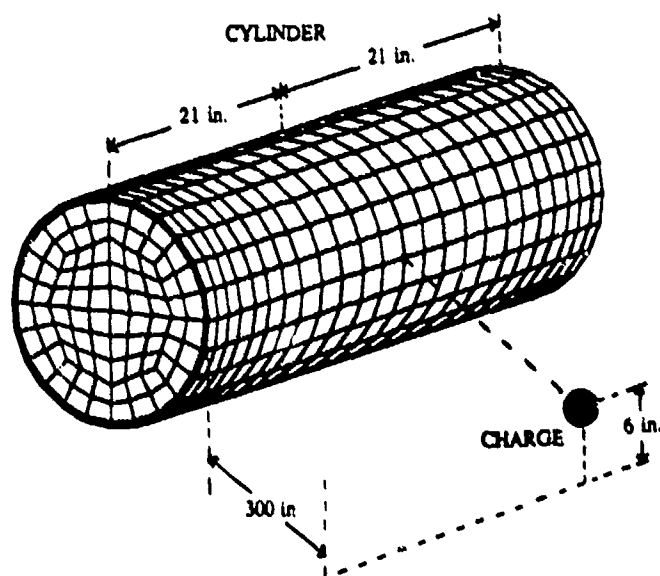


**Figure 1:** Cylinder geometry and test profile.

Actual pressure-time history data from a previous physical test was utilized in the analysis. The pressure-time history plot is shown in Figure 2.

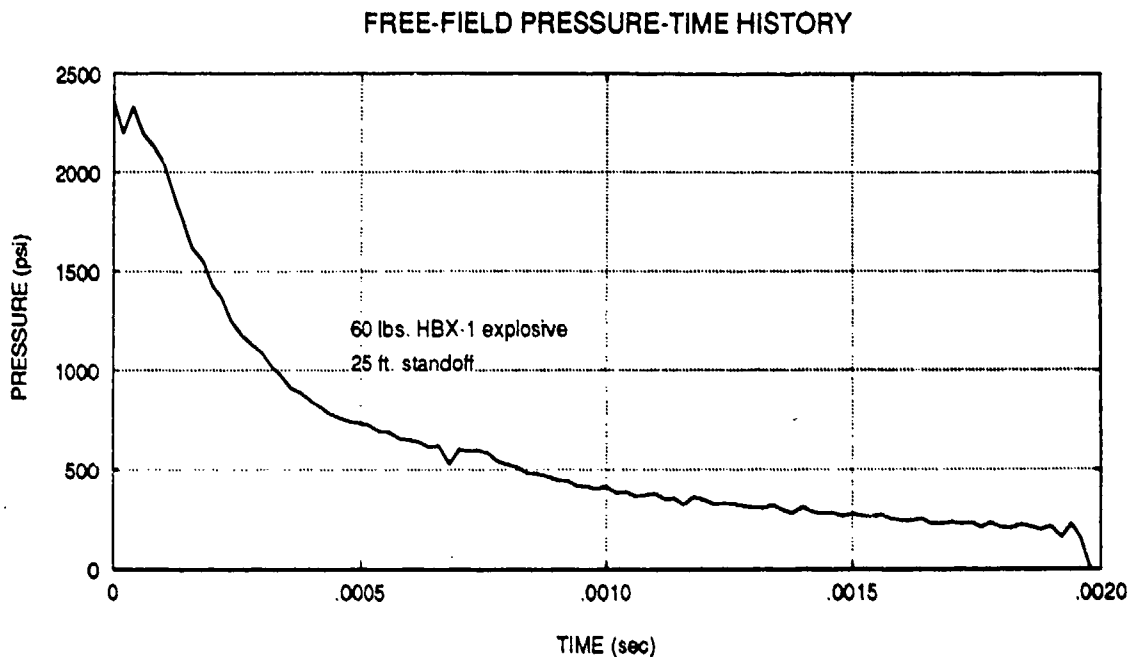
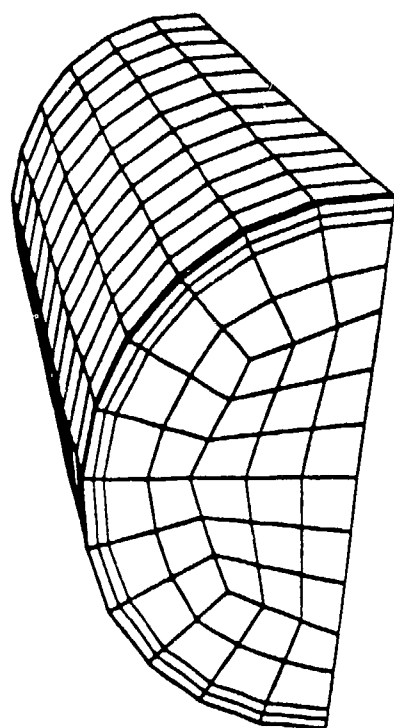


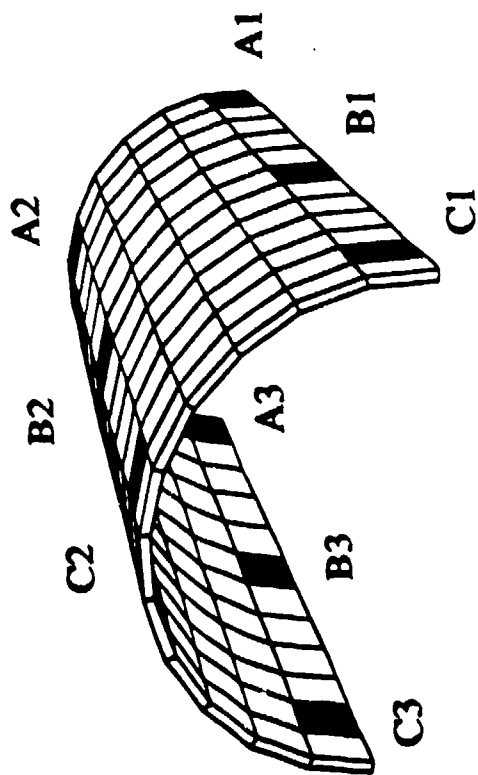
**Figure 2:** Free-Field Pressure-Time History Plot.

### **3. Finite Element Mesh**

The problem geometry involved two planes of symmetry (x-z and y-z planes) which allowed the cylinder to be modeled as a quarter cylinder. This significantly reduced the number of computations in each test. Appropriate boundary constraints were applied along the symmetric planes. The finite element mesh for the quarter model is shown in Figure 3. The metal material consisted of 186 thick shell elements while the rubber material consisted of 198 solid (brick) elements.



RUBBER MATERIAL



METAL SHELL MATERIAL



METAL ENDPLATE

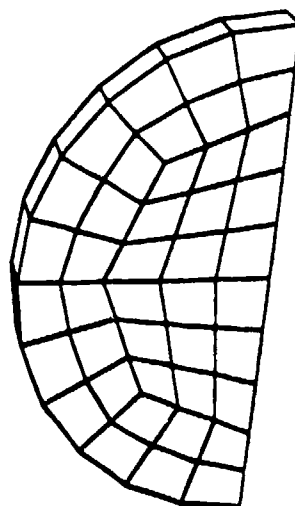


Figure 3: Finite element mesh (quarter model).

Only solid elements could be used for the rubber in this model configuration. A total of 9 locations were analyzed in each case, 3 at the center section of the cylinder, 3 near the endplate and 3 midway between the center section and the endplate. At each section the 3 locations were approximately equally spaced around the surface of the cylinder. A1 represents the element closest to the charge. The metal shell material in Figure 3 shows the element orientation. Unless otherwise specified, all plots reference these element locations. Although the response of the rubber was examined in different cases, the analysis of the metal response was the primary objective, therefore most of the results presented are for the metal material.

#### **4. Element Compatibility**

Since the metal and rubber were modeled using a different type of element, it was necessary to verify the elements were compatible and would give reliable results. This was done by performing a test simulation for three different shell layer configurations, a single thick shell model, a double thick shell (two adjacent single thick shells) model, and a thick shell and brick model, then comparing the responses at various locations. The total shell thickness was the same in all configurations. Results are given in Chapter III.



## 5. Material Properties

Nominal material properties were obtained from a materials handbook. Aluminum, steel and rubber material properties are shown in Tables 1-3 respectively.

**TABLE 1: ALUMINUM (6061-T6) PROPERTIES**

Parameter	Symbol	Value
Density	$\rho$	5.412 slugs/ft <sup>3</sup>
Poisson's ratio	$\nu$	0.33
Young's modulus	$E$	1.08x10 <sup>7</sup> psi
Yield stress	$\sigma_y$	4.0x10 <sup>4</sup> psi
Speed of sound	$a$	16,400 ft/sec

**TABLE 2: STEEL (ASTM A106 grade C) PROPERTIES**

Parameter	Symbol	Value
Density	$\rho$	15.218 slugs/ft <sup>3</sup>
Poisson's ratio	$\nu$	0.30
Young's modulus	$E$	2.9x10 <sup>7</sup> psi
Hardening modulus	$E_{tan}$	1.114x10 <sup>5</sup> psi
Yield stress	$\sigma_y$	4.7x10 <sup>4</sup> psi
Strain-rate parameter	$c$	8.797x10 <sup>4</sup> sec <sup>-1</sup>
Strain-rate parameter	$p$	5.65
Speed of sound	$a$	16,900 ft/sec

**TABLE 3: RUBBER PROPERTIES**

Parameter	Symbol	Value
Density	$\rho$	1.908slugs/ft <sup>3</sup>
Poisson's ratio	$\nu$	0.4991
Speed of sound	$a$	100 ft/sec
Shear modulus (Tread stock)	$G$	95.8 psi
Coef. of asymmetry (Tread stock)	$\alpha$	0.223
Shear modulus (Gum stock)	$G$	48.6 psi
Coef. of asymmetry (Gum stock)	$\alpha$	0.448

### **III. RESULTS AND ANALYSIS**

As discussed in Chapter 2, data was collected at nine different locations on the cylinder, corresponding to the element positions as shown in Figure 3. Results are reported for both axial and hoop directions. The axial direction is parallel to the centerline axis of the cylinder while the hoop direction is tangent to the circumference of the cylindrical shell for a given location. Some data has not been reported since the results are often redundant and can be seen in other plots. For this reason, strain plots are shown in lieu of stress plots since the same features and trends are exhibited in both.

#### **A. ELEMENT COMPATABILITY**

A preliminary study was undertaken to verify element compatability since the metallic material and the coating were modeled using different types of elements. Single thick shell, double thick shell and thick shell/brick element configurations were compared at all "A" and "B" locations and are shown in Figures 4-15. Axial and hoop strain values for the single thick shell and double thick shell cases were essentially identical. The thick shell/brick model deviated slightly from the thick shell models in the magnitude of the response. However, their frequency of oscillation appeared to

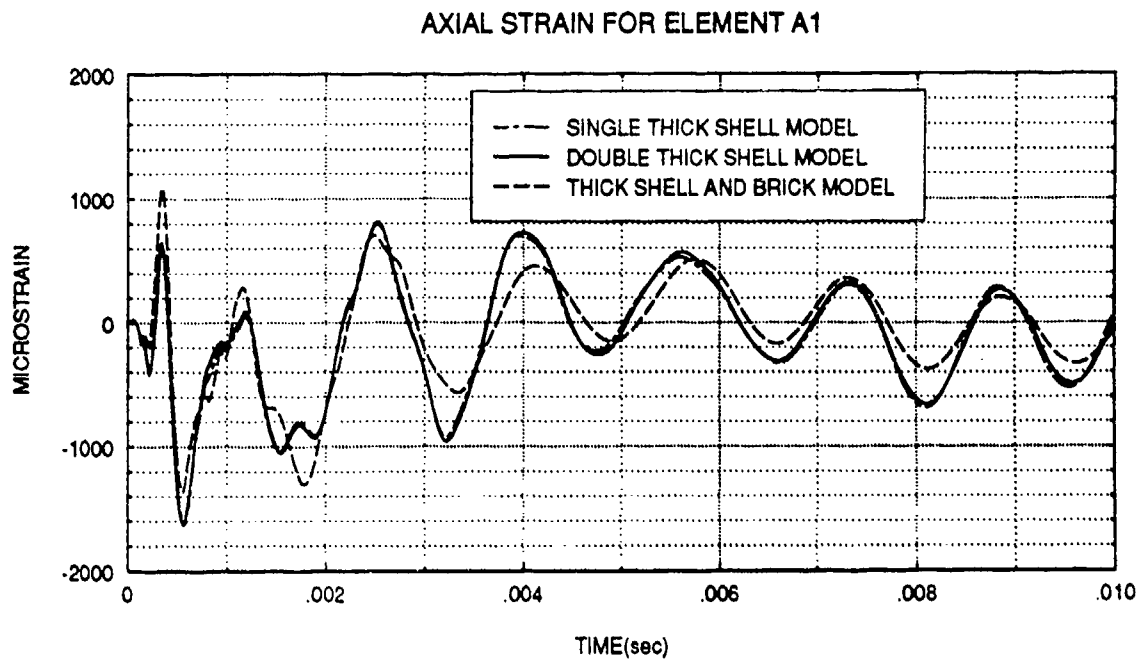


**Figure 4:** Axial strain at position A1 for different shell thickness element configurations.

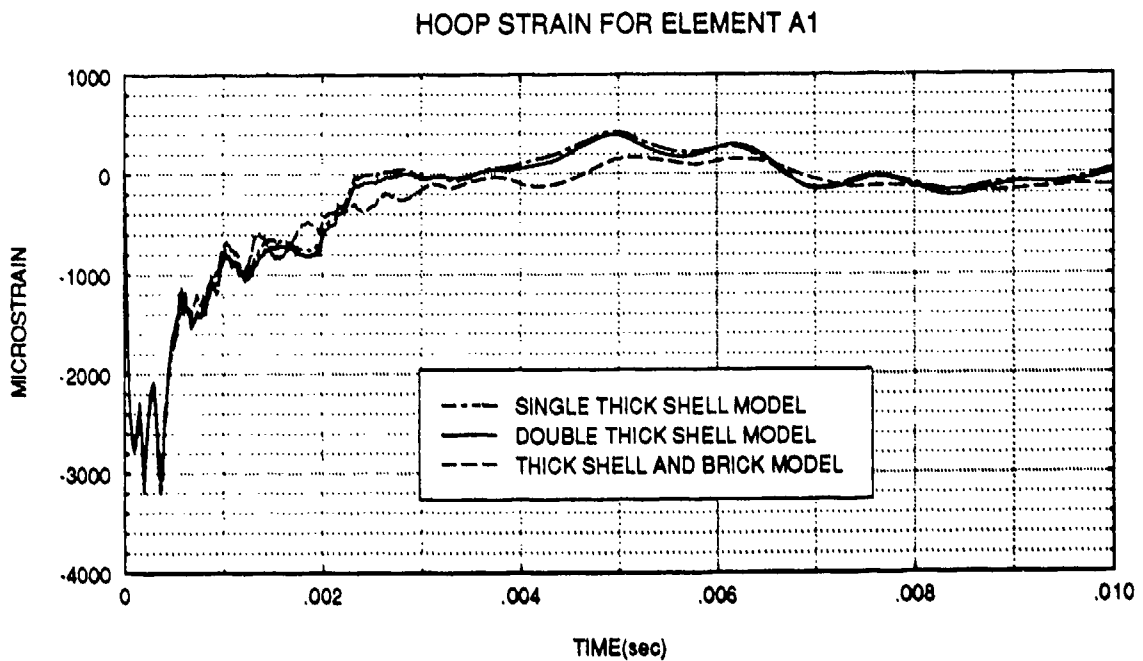


**Figure 5:** Hoop strain at position A1 for different shell thickness element configurations.

### AXIAL STRAIN FOR ELEMENT A2

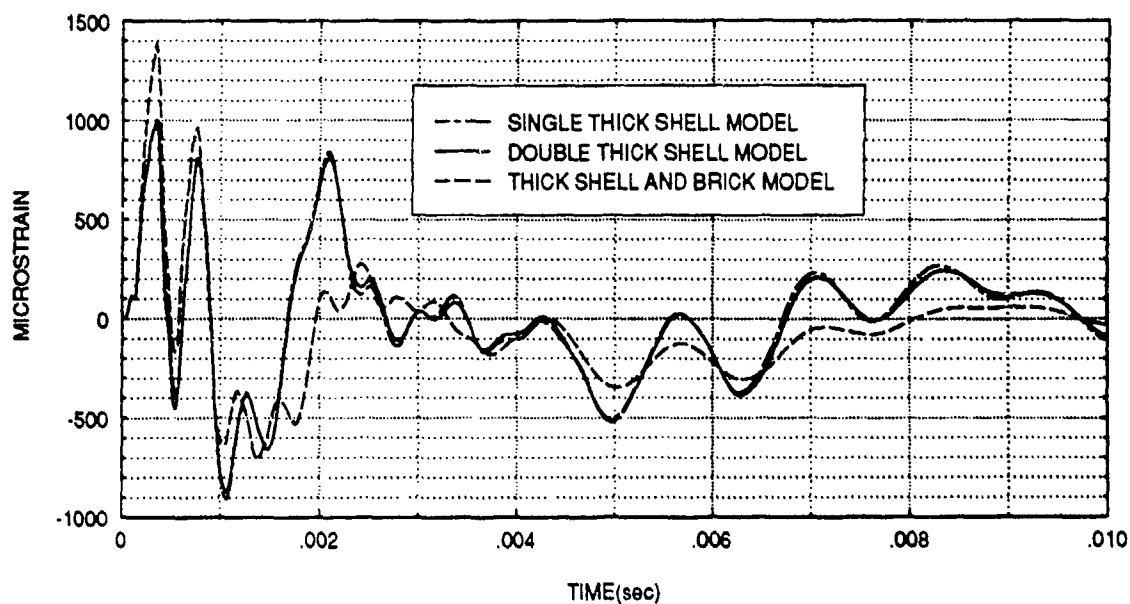


**Figure 6:** Axial strain at position A2 for different shell thickness element configurations.

### HOOP STRAIN FOR ELEMENT A2

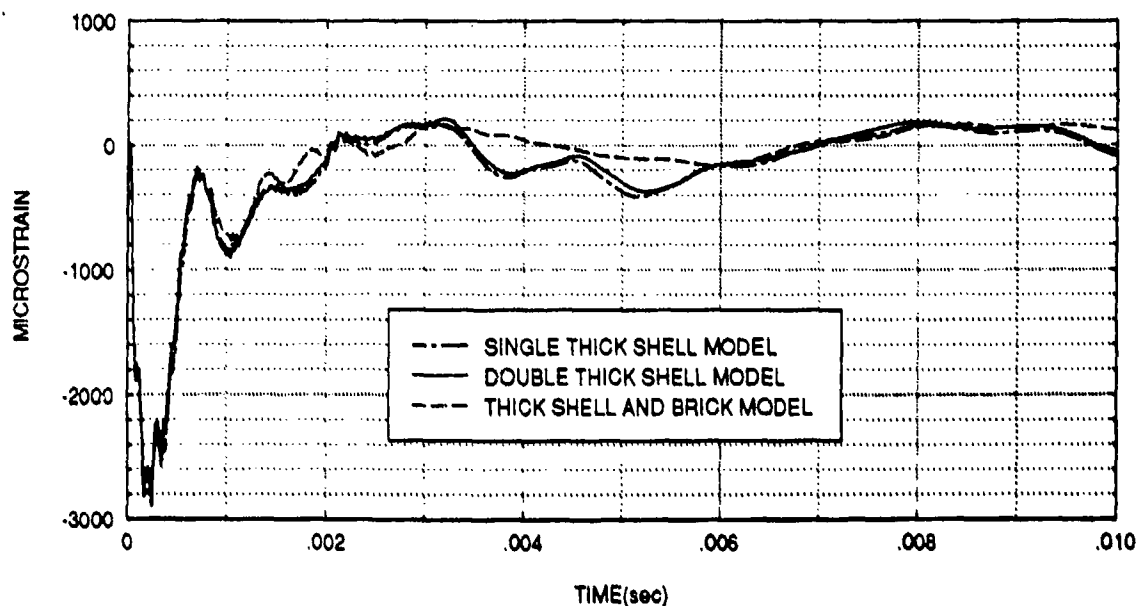


**Figure 7:** Hoop strain at position A2 for different shell thickness element configurations.

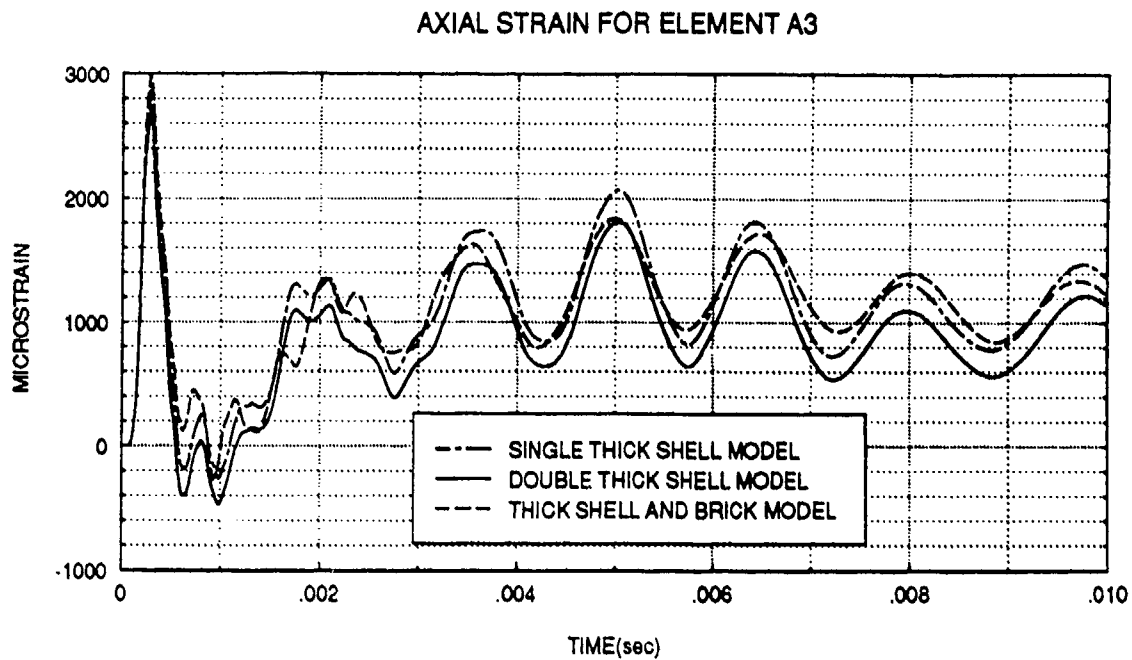


**Figure 8:** Axial strain at position A3 for different shell thickness element configurations.

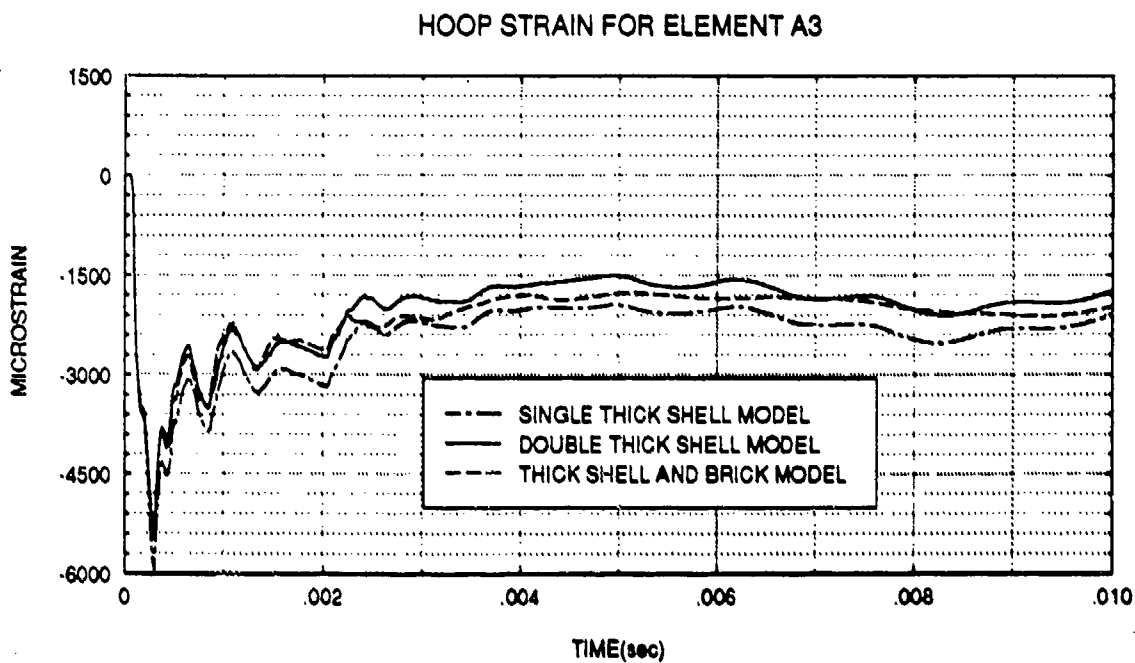


**Figure 9:** Hoop strain at position A3 for different shell thickness element configurations.

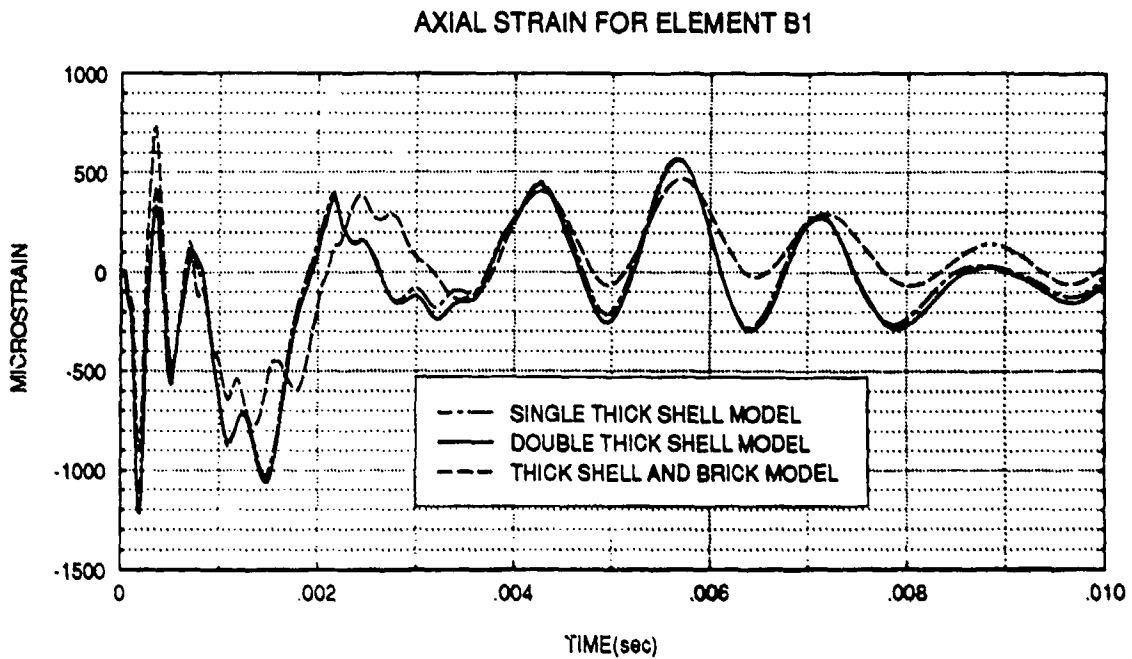


**Figure 10:** Axial strain at position B1 for different shell thickness element configurations.

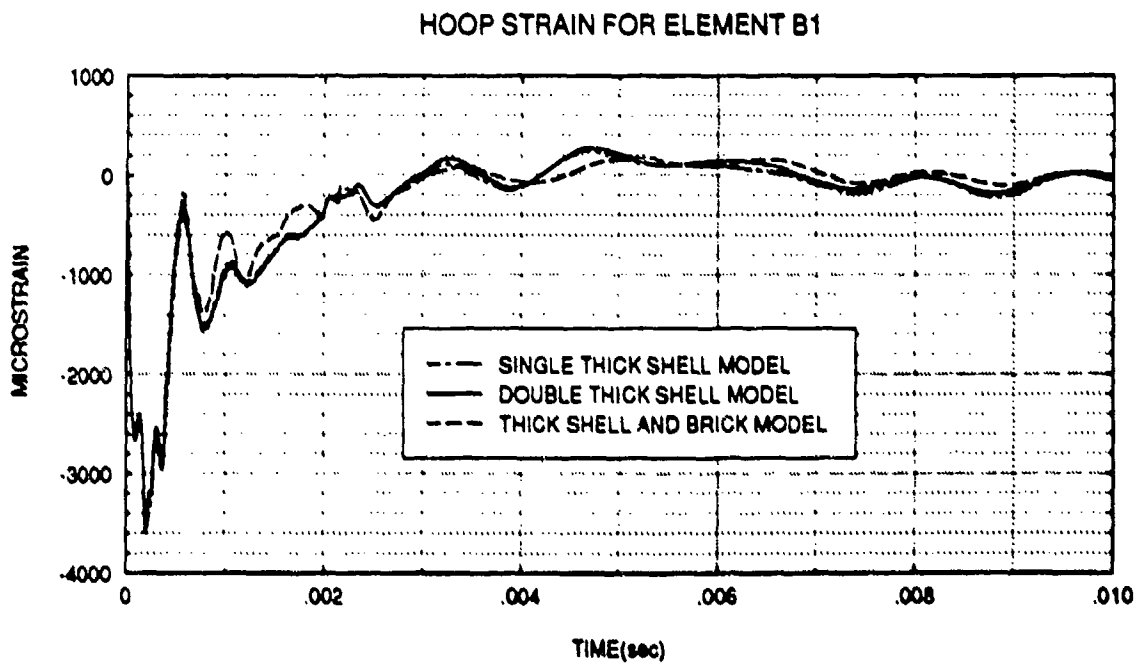


**Figure 11:** Hoop strain at position B1 for different shell thickness element configurations.

### AXIAL STRAIN FOR ELEMENT B2

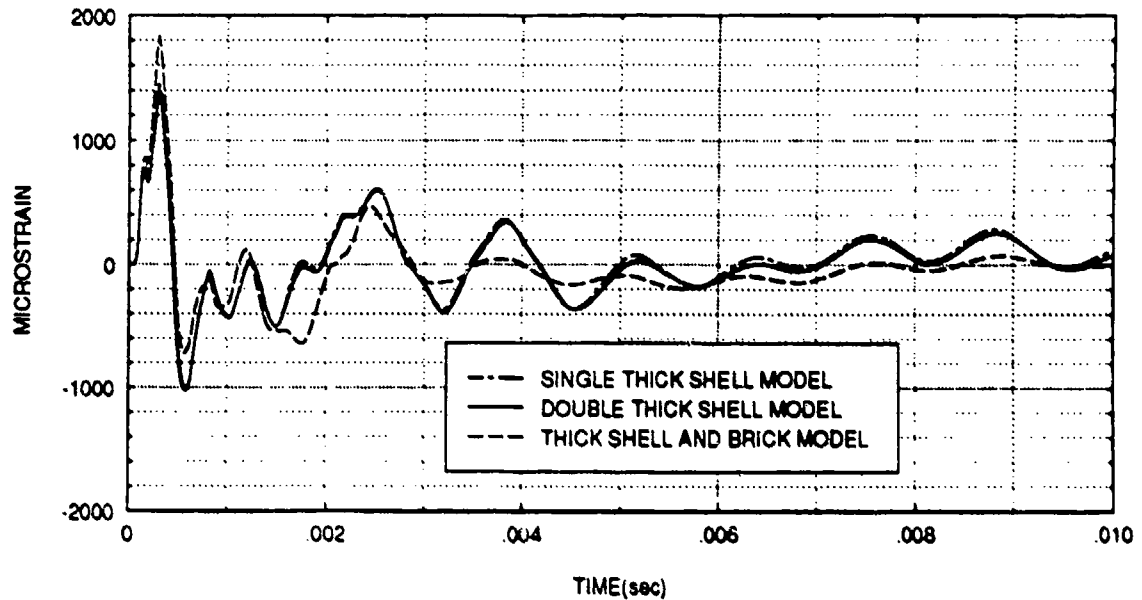


**Figure 12:** Axial strain at position B2 for different shell thickness element configurations.

### HOOP STRAIN FOR ELEMENT B2

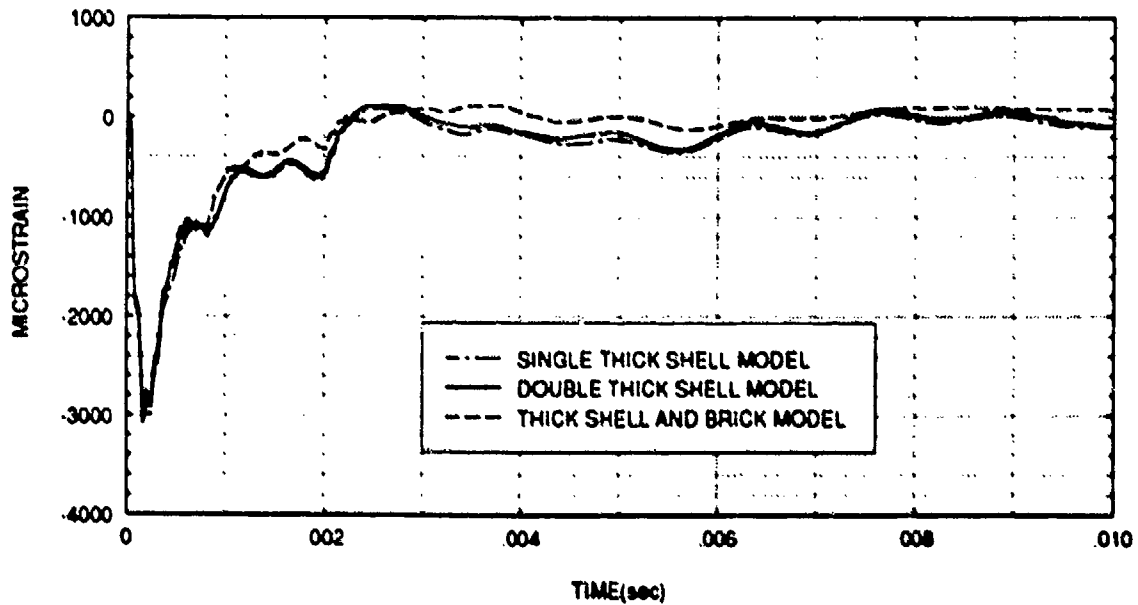


**Figure 13:** Hoop strain at position B2 for different shell thickness element configurations.



# AXIAL STRAIN FOR ELEMENT B3

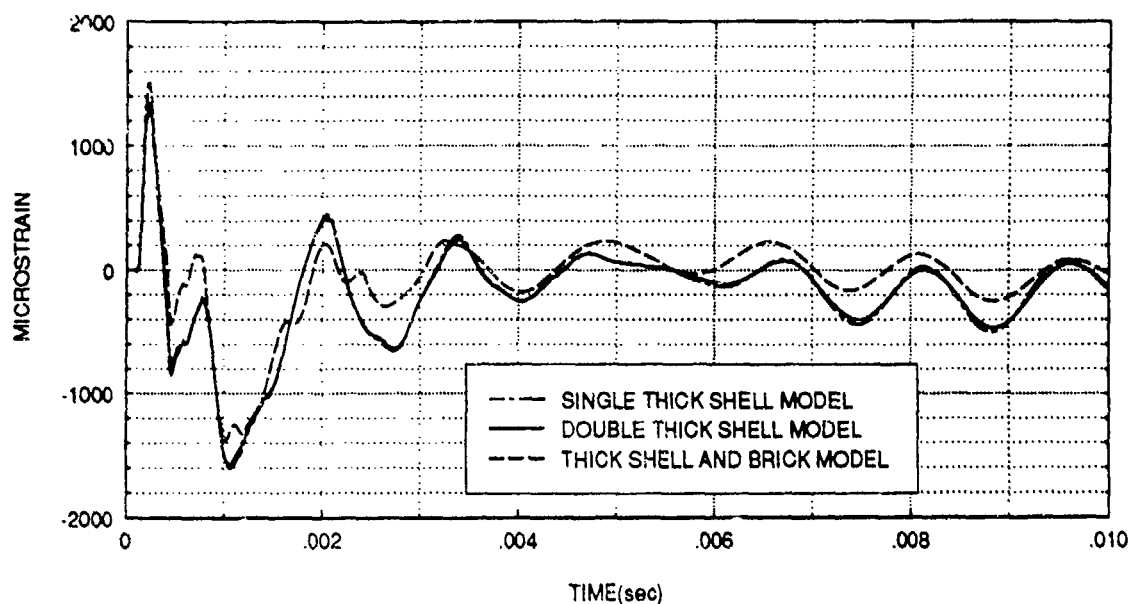


**Figure 14:** Axial strain at position B3 for different shell thickness element configurations.

# HOOP STRAIN FOR ELEMENT B3

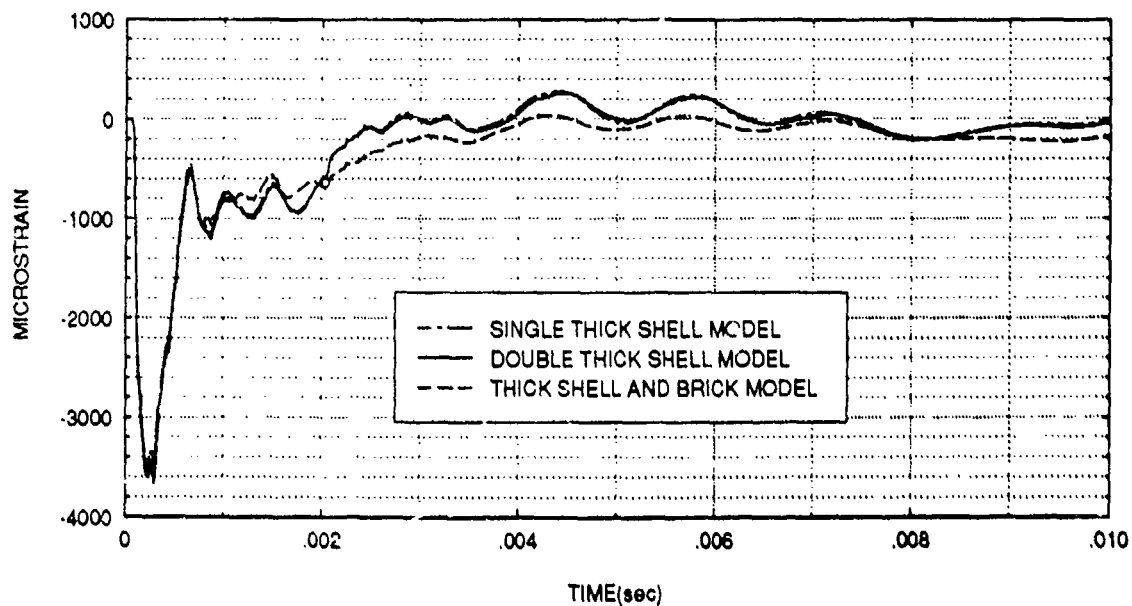


**Figure 15:** Hoop strain at position B3 for different shell thickness element configurations.

be approximately the same. At all locations, the thick shell/brick model appeared to approach the steady state more rapidly. The results indicate there was no interfacing problem or unusual behavior caused by the two different types of elements and demonstrated that the thick shell/brick model could be expected to behave consistently and provide reliable response data. The thick shell and brick (solid) elements were therefore considered to be fully compatible and were used in the subsequent study.

#### **B. EFFECT OF SURFACE COATINGS ON CYLINDERS**

The purpose of this study was to determine the effects of surface coatings on the dynamic response of cylinders subjected to underwater shock. A total of six cases were analyzed. In the first case, an uncoated aluminum cylinder was compared to two composite (coated) cylinders, one coated with tread stock rubber (referred to as Composite Model 1) and the other coated with gum stock rubber (referred to as Composite Model 2). The aluminum shell material and the rubber coating were both 0.250 inches thick. Both composite cylinders exhibited higher values of stress and strain than the uncoated cylinder. In early time, (less than 1 msec.) response was approximately the same. (Passage of the shock wave occurred at about 0.2 msec.). At most locations, the deviations became significant after 1 msec.. Axial and hoop strain were plotted for all elements of interest and are shown in Figures 16-33.

### AXIAL STRAIN FOR ELEMENT A1

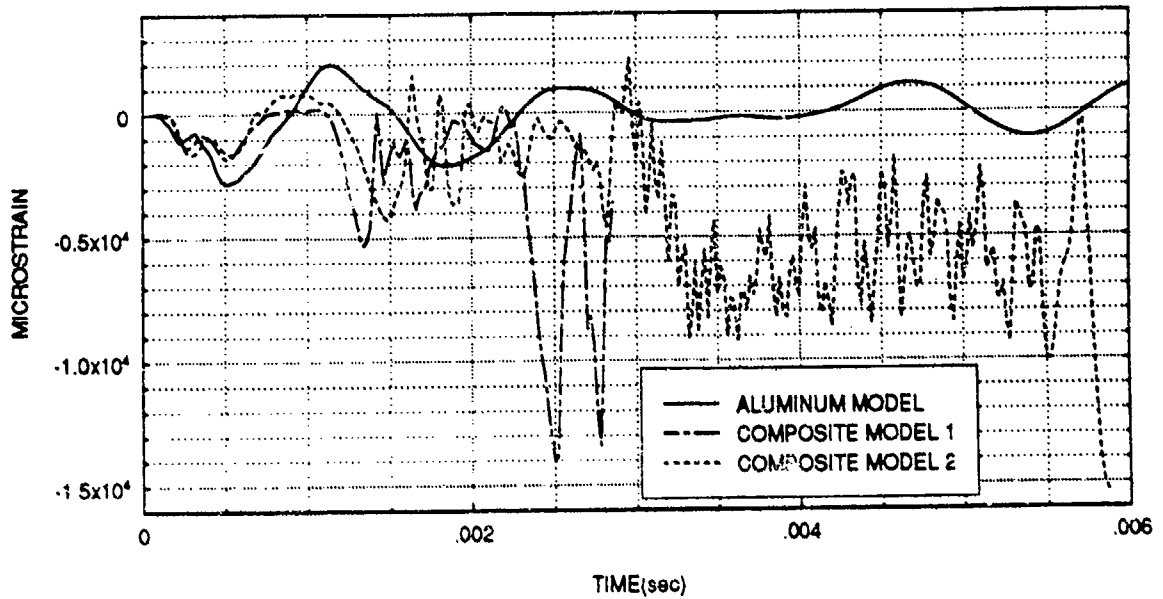


Figure 16: Axial strain at position A1 for uncoated and coated aluminum cylinders.

### HOOP STRAIN FOR ELEMENT A1

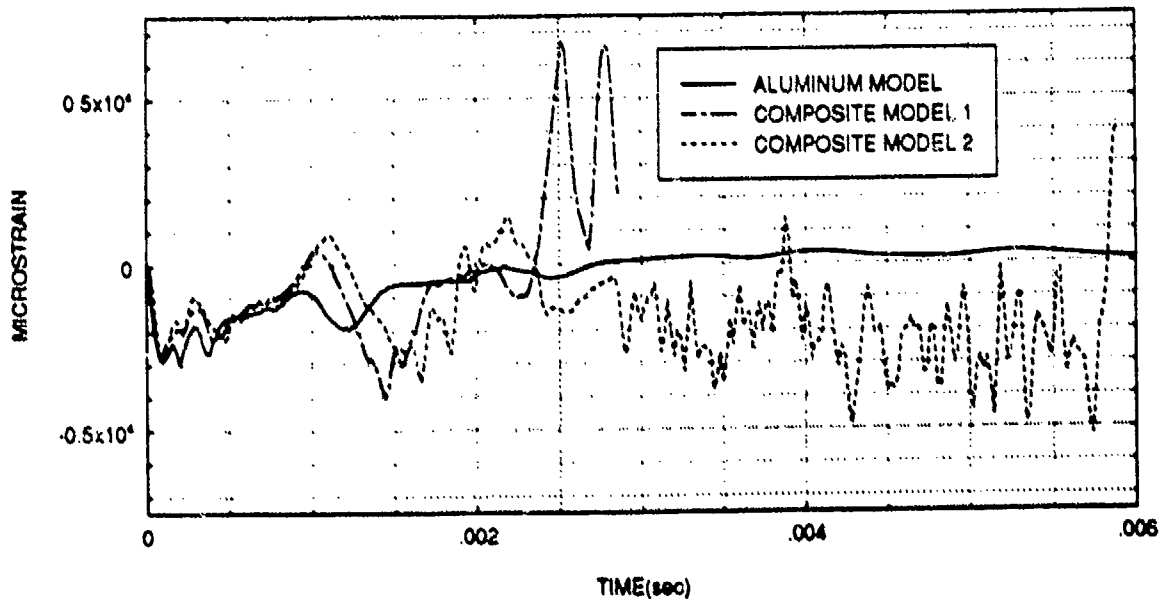
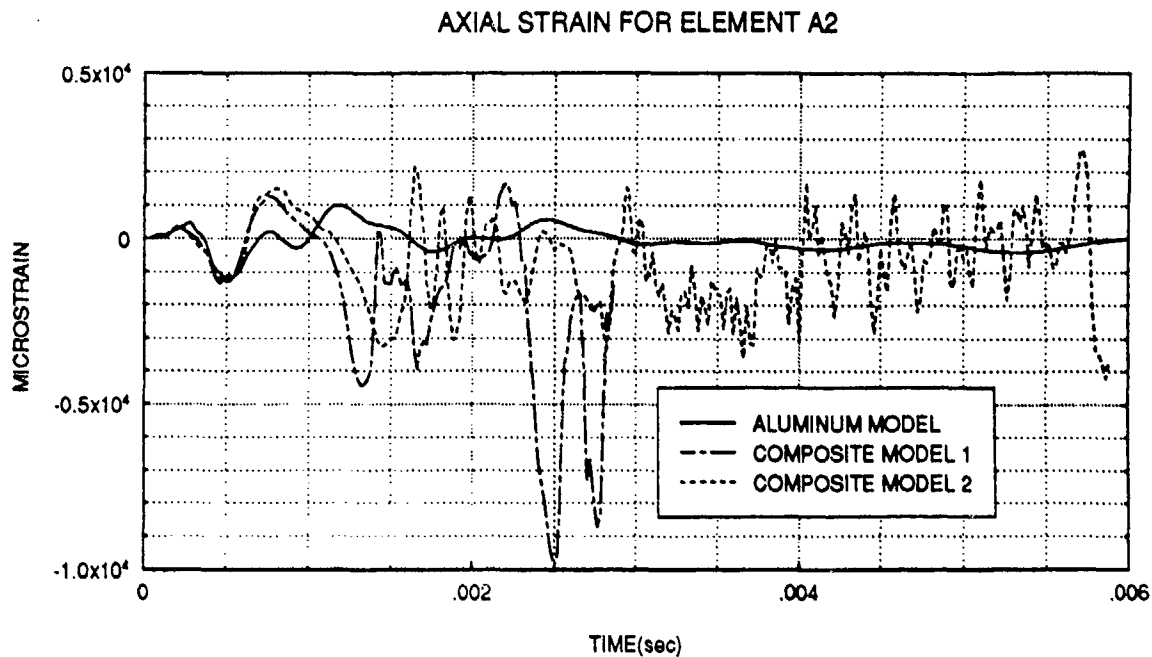
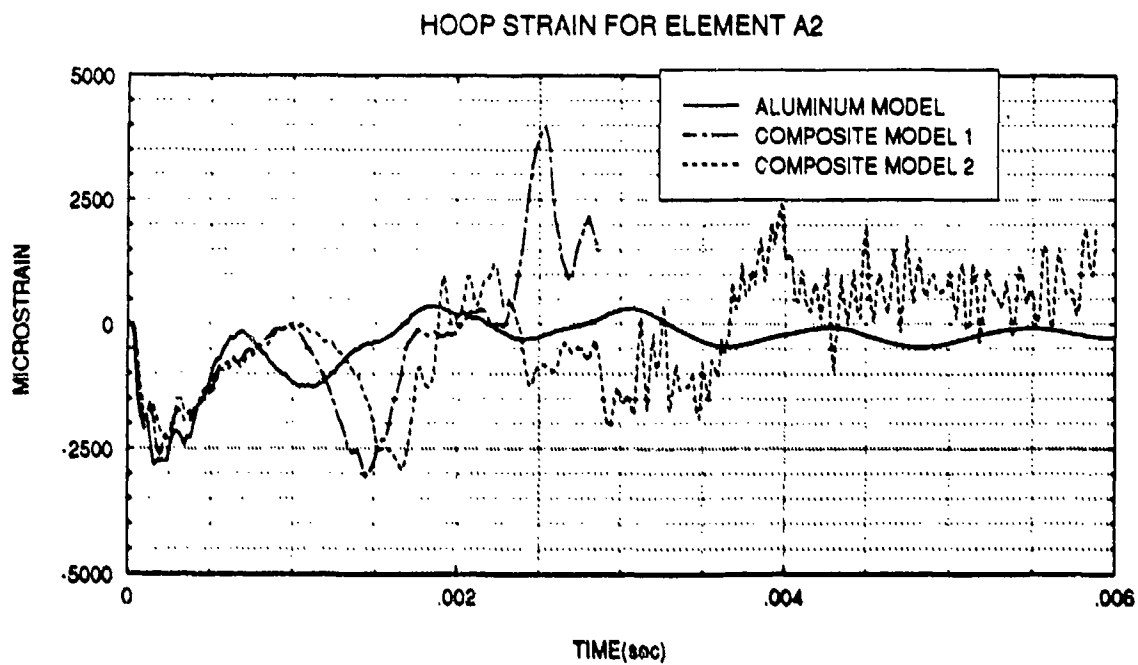


Figure 17: Hoop strain at position A1 for uncoated and coated aluminum cylinders.



**Figure 18:** Axial strain at position A2 for uncoated and coated aluminum cylinders.



**Figure 19:** Hoop strain at position A2 for uncoated and coated aluminum cylinders.

### AXIAL STRAIN FOR ELEMENT A3

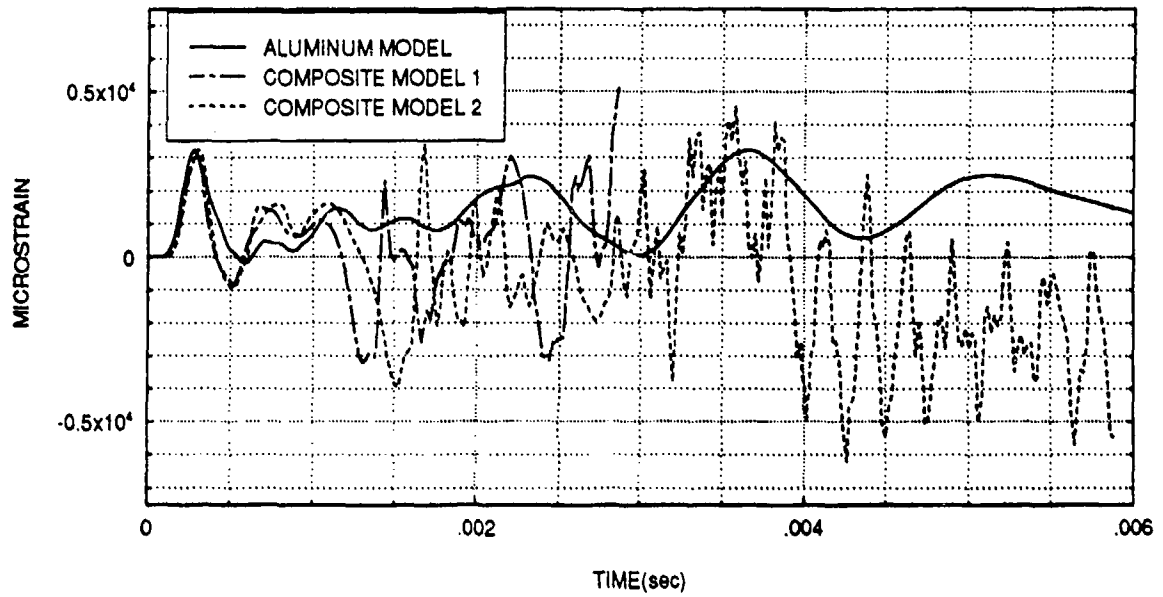


**Figure 20:** Axial strain at position A3 for uncoated and coated aluminum cylinders.

### HOOP STRAIN FOR ELEMENT A3

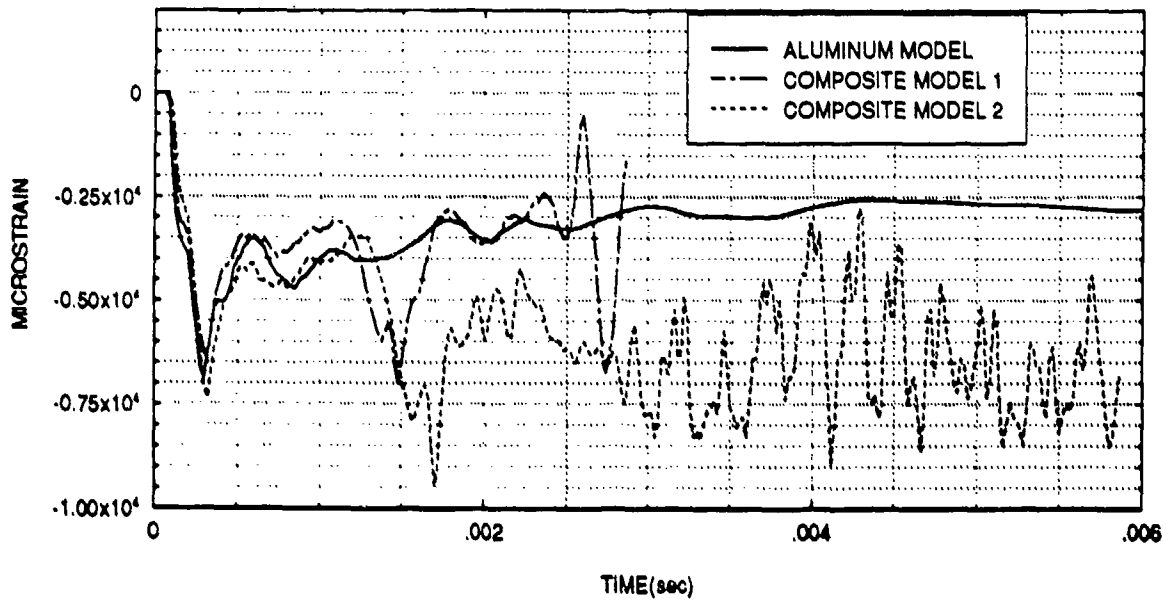


**Figure 21:** Hoop strain at position A3 for uncoated and coated aluminum cylinders.

### AXIAL STRAIN FOR ELEMENT B1

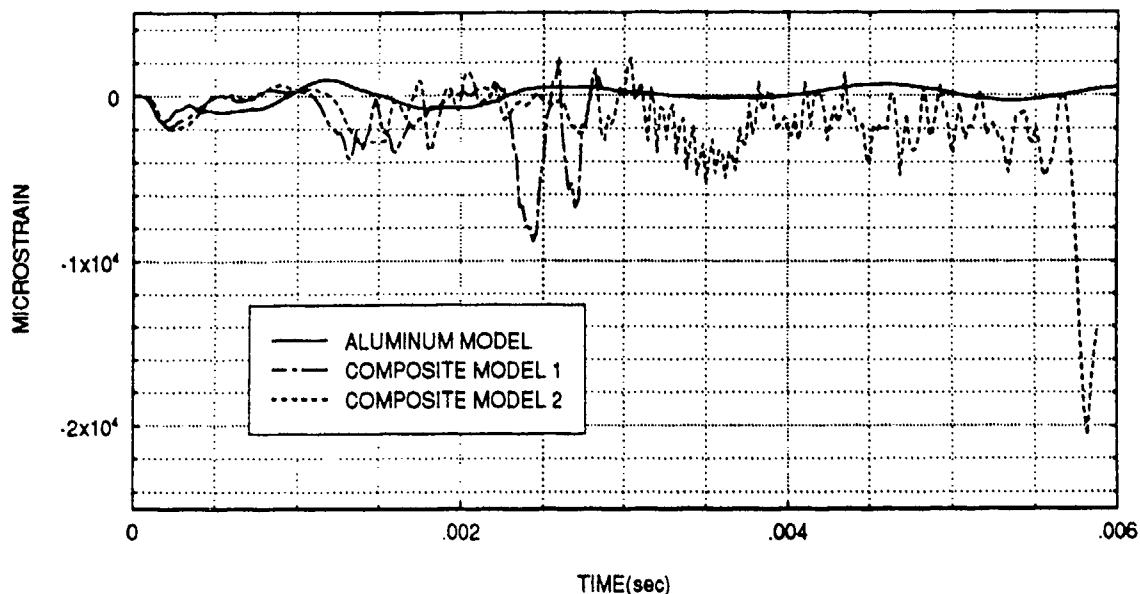


**Figure 22:** Axial strain at position B1 for uncoated and coated aluminum cylinders.

### HOOP STRAIN FOR ELEMENT B1

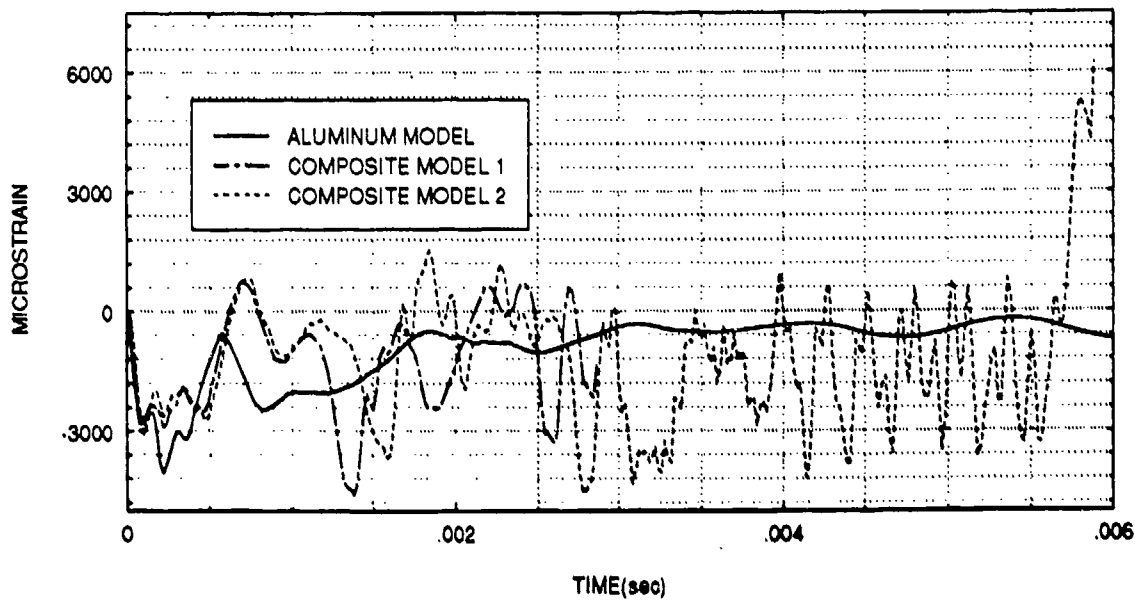


**Figure 23:** Hoop strain at position B1 for uncoated and coated aluminum cylinders.

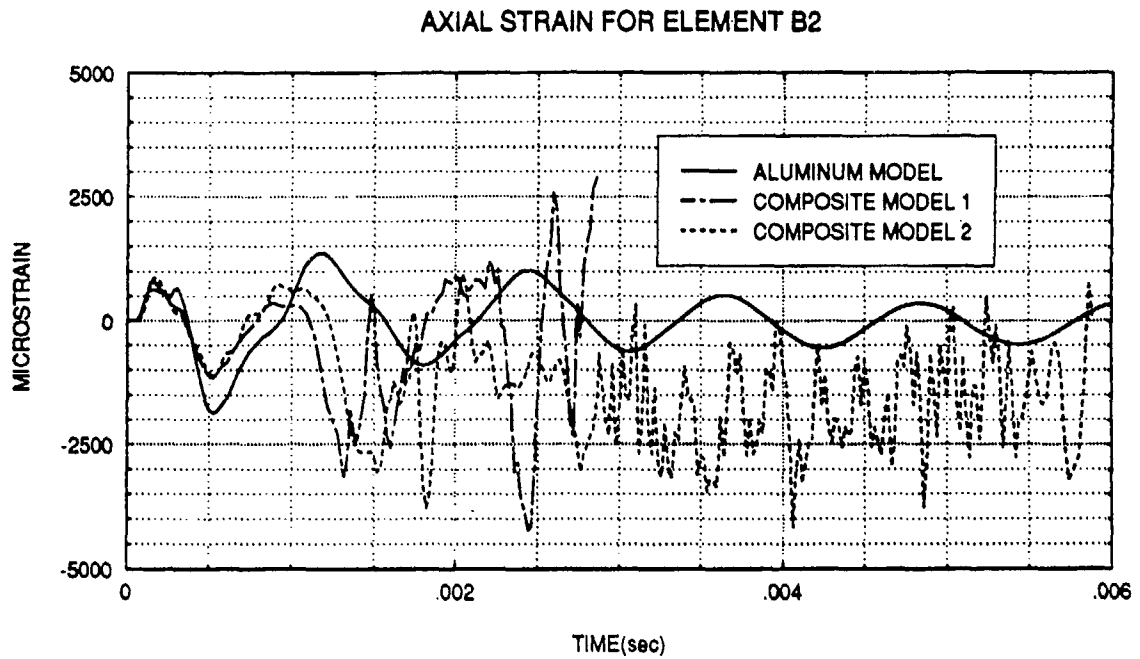


**Figure 24:** Axial strain at position B2 for uncoated and coated aluminum cylinders.

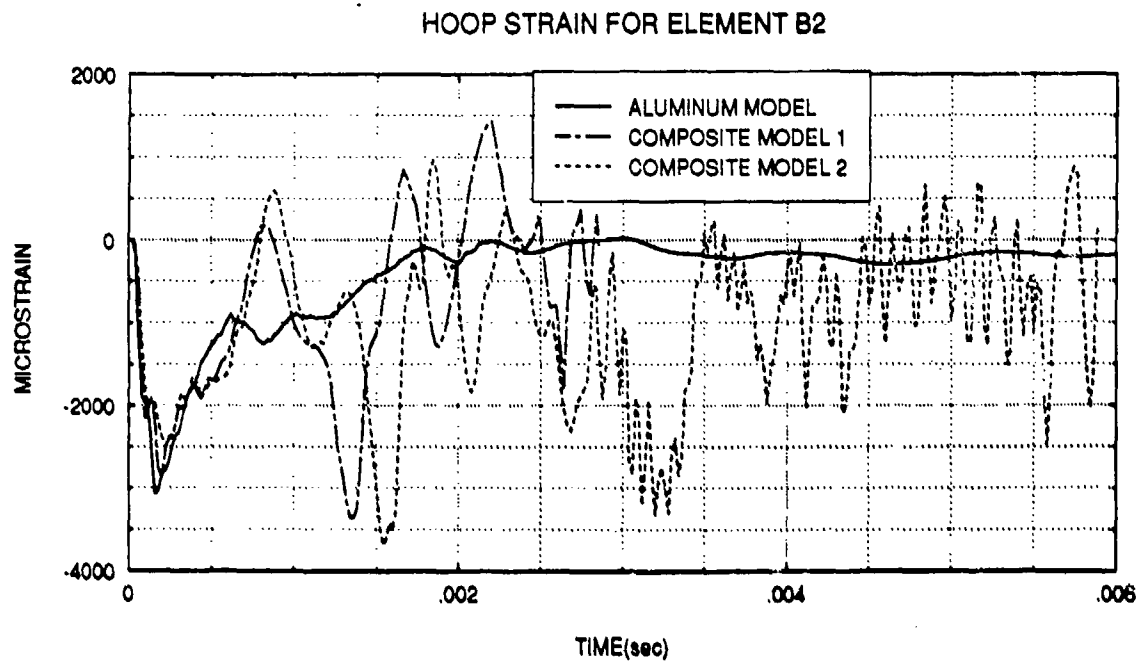


**Figure 25:** Hoop strain at position B2 for uncoated and coated aluminum cylinders.

### AXIAL STRAIN FOR ELEMENT B3

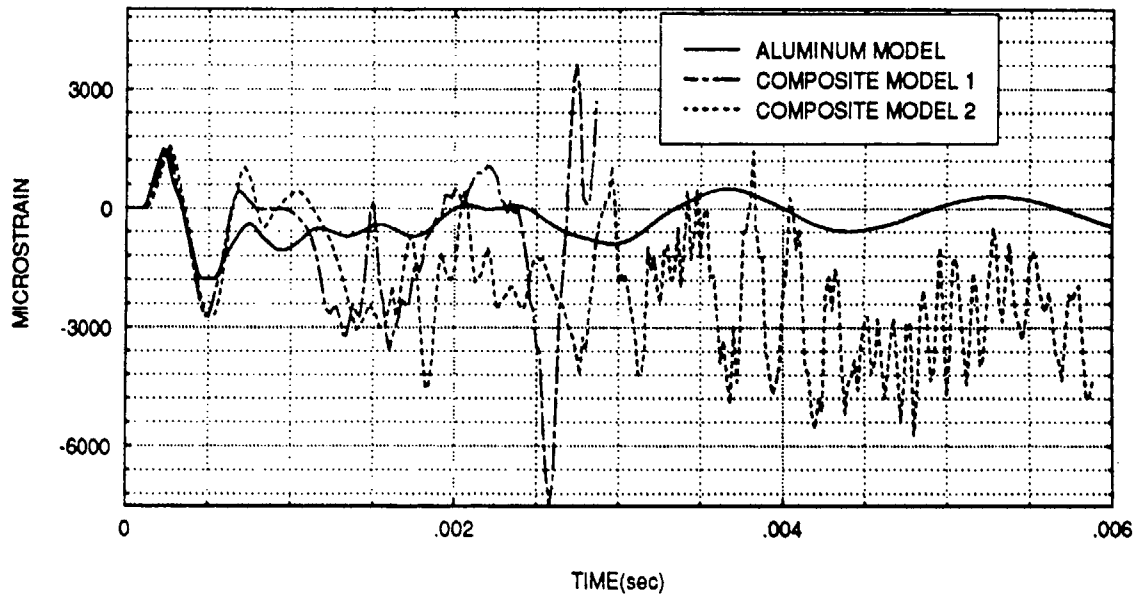


**Figure 26:** Axial strain at position B3 for uncoated and coated aluminum cylinders.

### HOOP STRAIN FOR ELEMENT B3

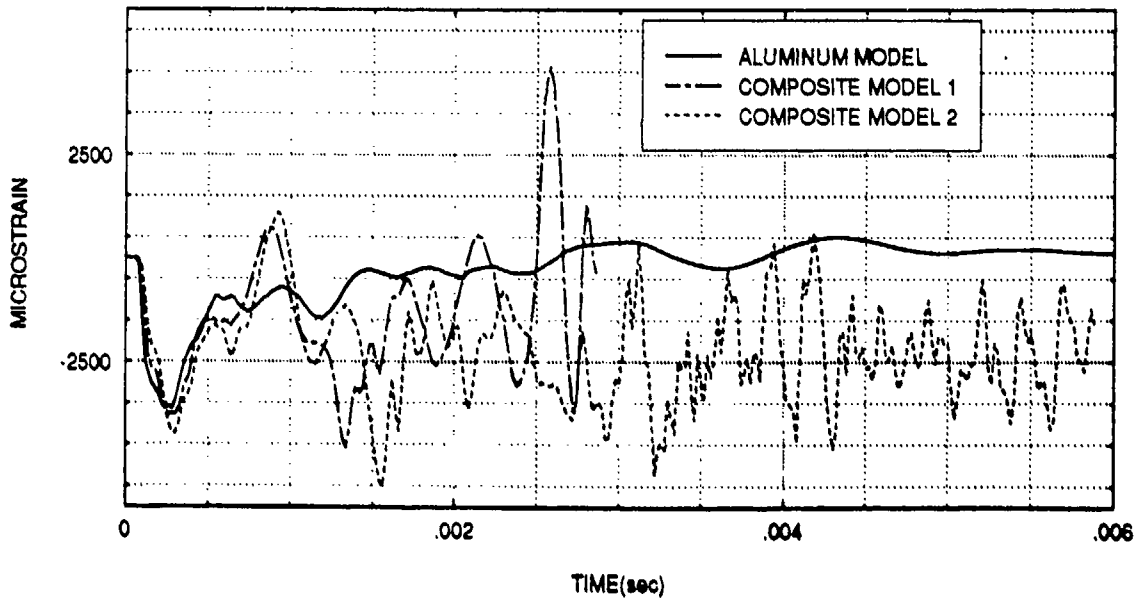


**Figure 27:** Hoop strain at position B3 for uncoated and coated aluminum cylinders.



### AXIAL STRAIN FOR ELEMENT C1

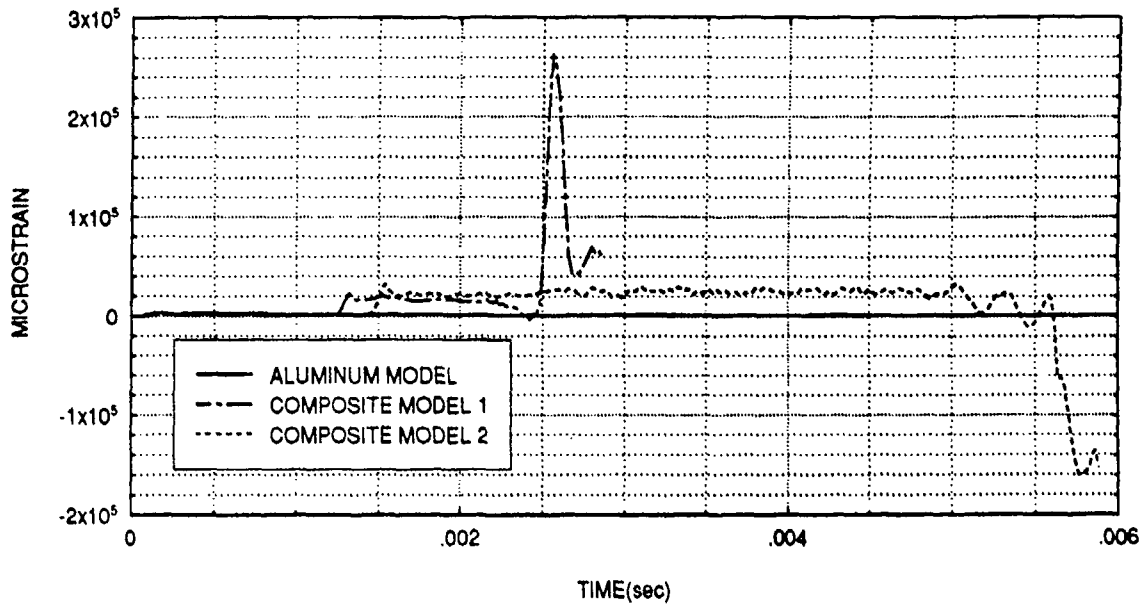


**Figure 28:** Axial strain at position C1 for uncoated and coated aluminum cylinders.

### HOOP STRAIN FOR ELEMENT C1

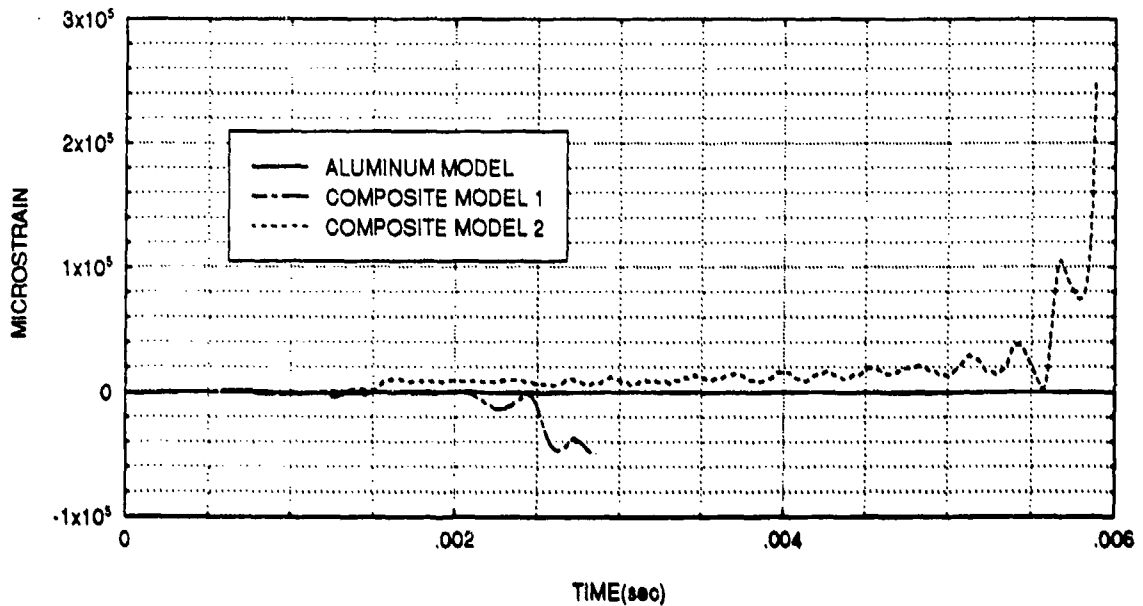


**Figure 29:** Hoop strain at position C1 for uncoated and coated aluminum cylinders.

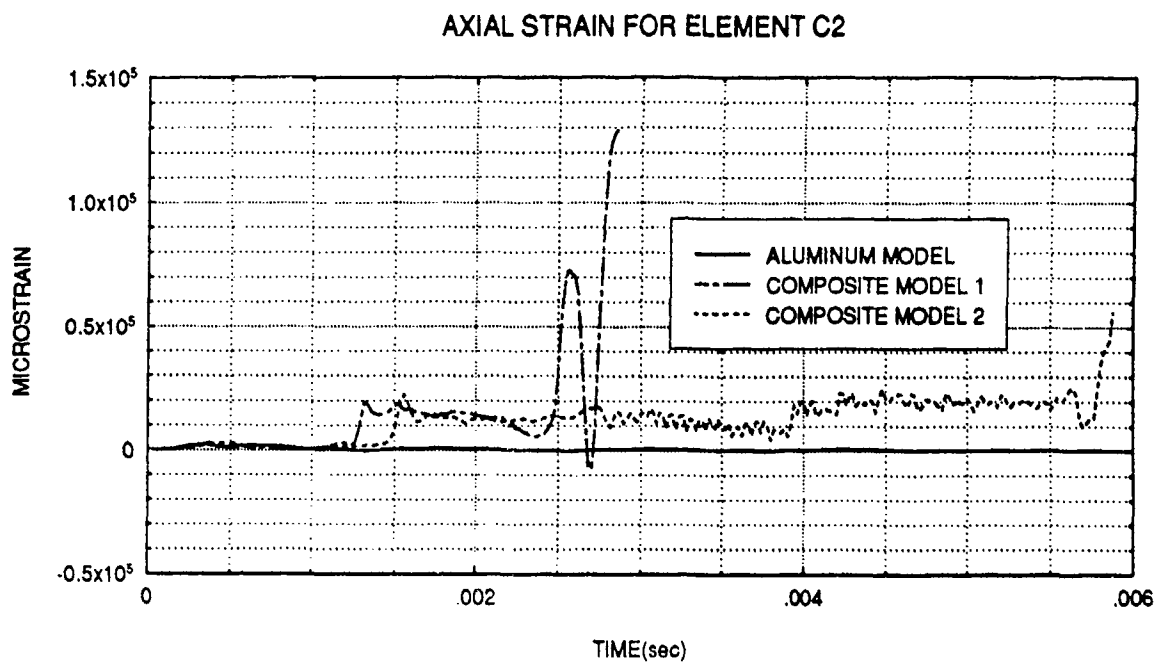


**Figure 30:** Axial strain at position C2 for uncoated and coated aluminum cylinders.

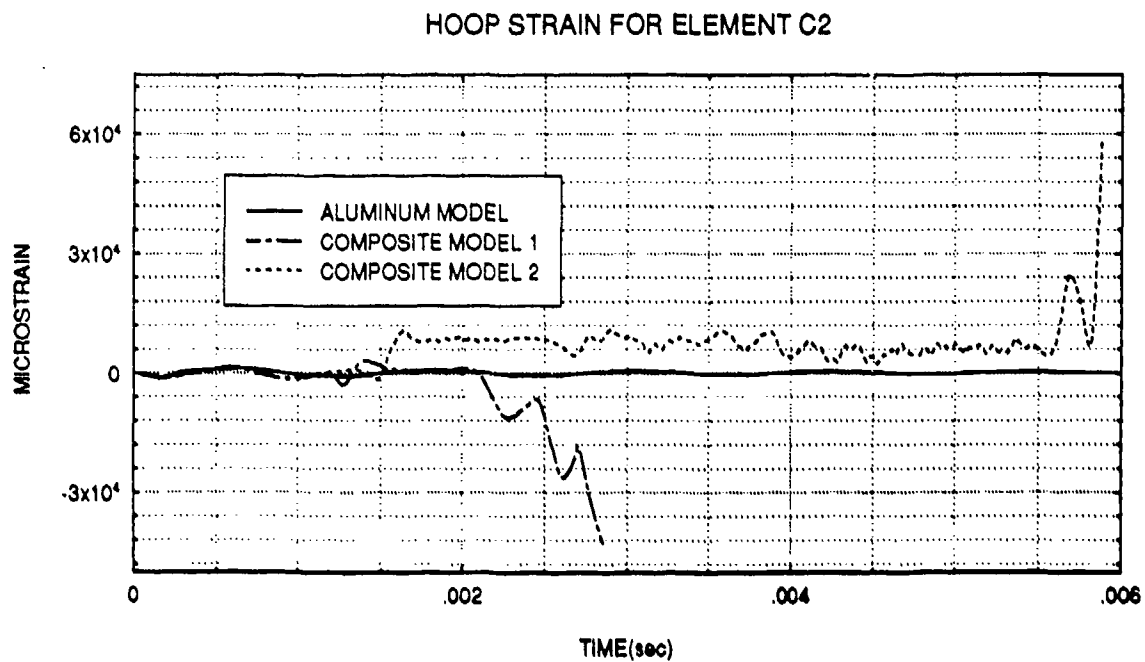


**Figure 31:** Hoop strain at position C2 for uncoated and coated aluminum cylinders.

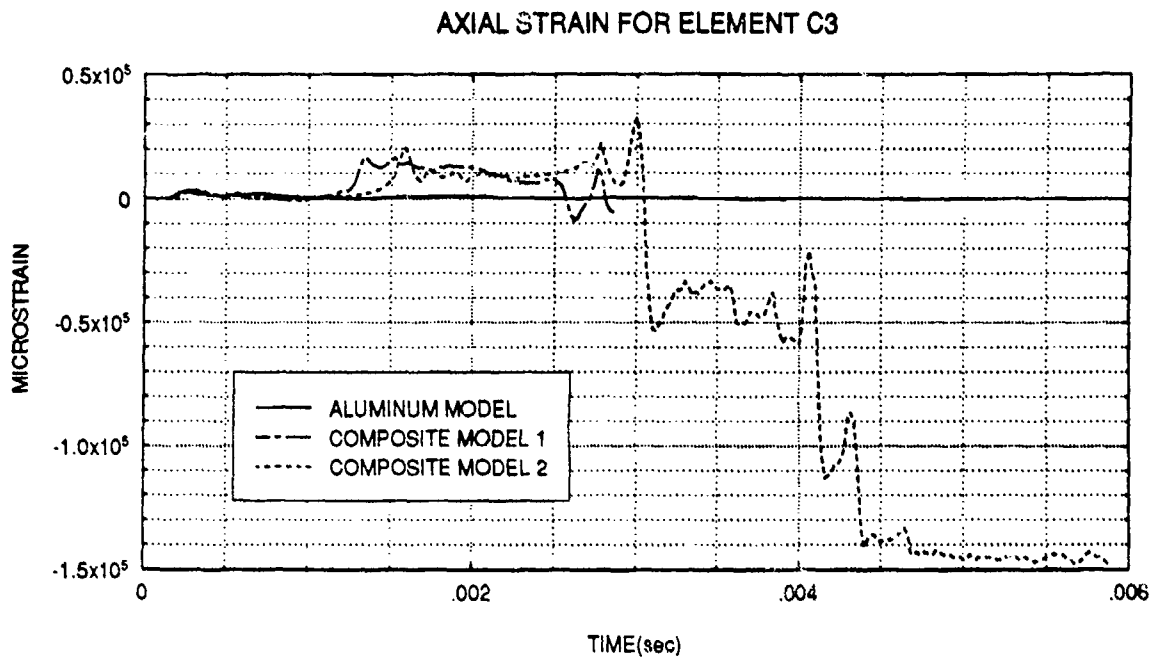


**Figure 32:** Axial strain at position C3 for uncoated and coated aluminum cylinders.

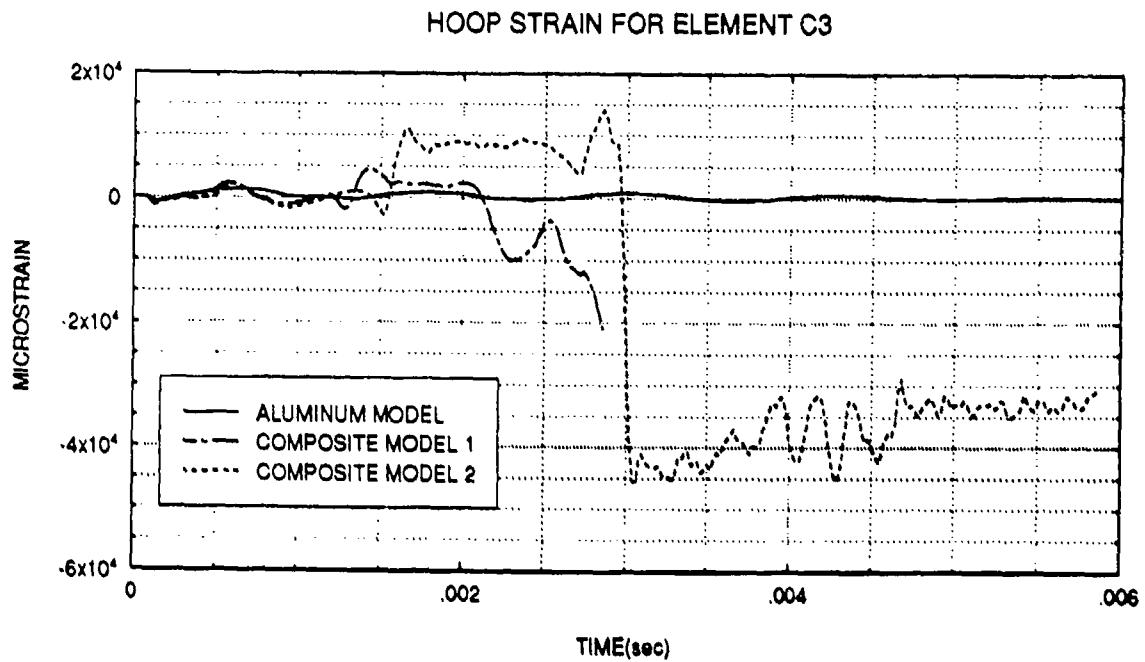
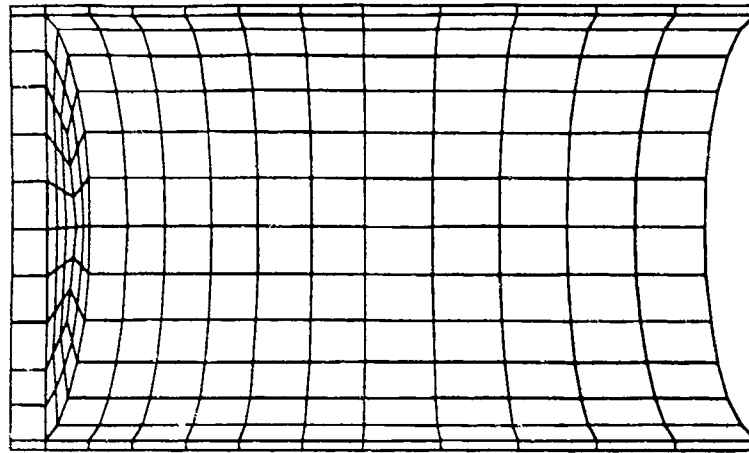


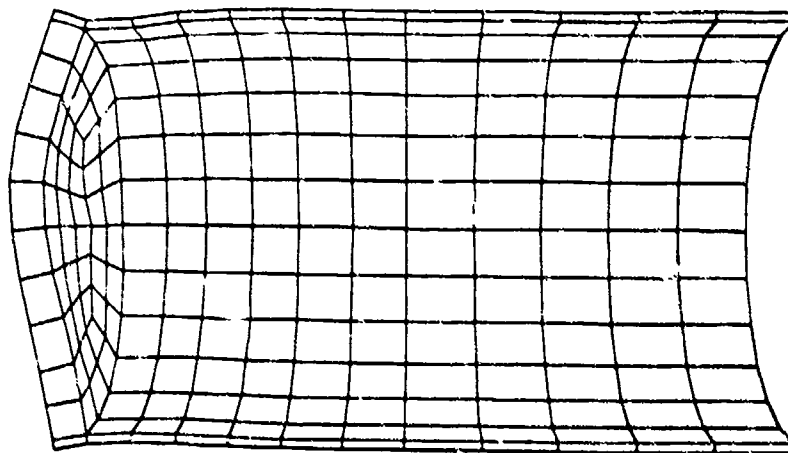
**Figure 33:** Hoop strain at position C3 for uncoated and coated aluminum cylinders.

Neither composite cylinder showed consistently higher magnitudes than the other, as this varied depending on the location analyzed. Both composite models exhibited higher oscillation than the uncoated model. The results from this study seemed to indicate that the rubber coating tended to concentrate energy into the metal cylinder rather than allow for a rapid release of energy into the water medium as in the uncoated case. The effects of the rubber coating are clearly visible in the deformation the cylinders. Figures 34 and 35 show deformation of the uncoated cylinder and composite cylinders 1 and 2 at 2.86 msec. and 5.86 msec. respectively. The unusually high values of strain attained at locations C1 and C2 may be attributed to the inertial effects of the thick endplate. Figure 36 shows a comparison of the internal energy level in the aluminum shell material for the uncoated cylinder and the two composite cylinders, the latter exhibiting significantly higher values. The effects of the rubber coatings on the cylinder were significant and it is speculated that the adverse response of the coated cylinders is related to the energy build-up in the metallic material caused by the rubber coatings.

In the next phase of study, the analysis focused on altering certain parameters to determine if they had any effect on cylinder response. In the second case, Composite Model 1 was used and the shear modulus of the rubber was reduced from 95.8 psi to 72.2 psi, with the coefficient of

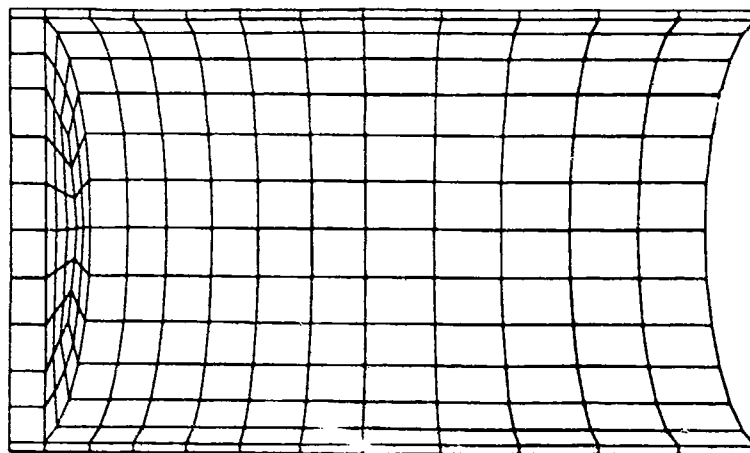


ALUMINUM MODEL

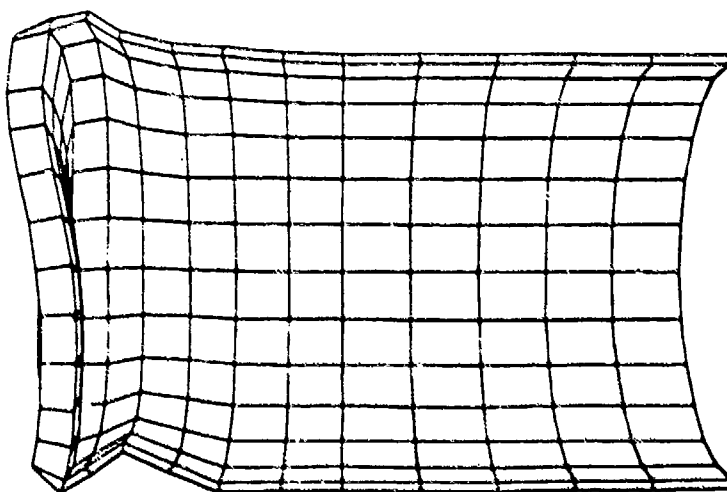


COMPOSITE MODEL 1

**Figure 34:** Deformation of (a) uncoated aluminum cylinder and  
(b) composite cylinder #1 at 2.86 msec..



ALUMINUM MODEL



COMPOSITE MODEL 2

**Figure 35:** Deformation of (a) uncoated aluminum cylinder and (b) composite cylinder #2 at 5.86 msec..

# INTERNAL ENERGY OF ALUMINUM SHELL MATERIAL

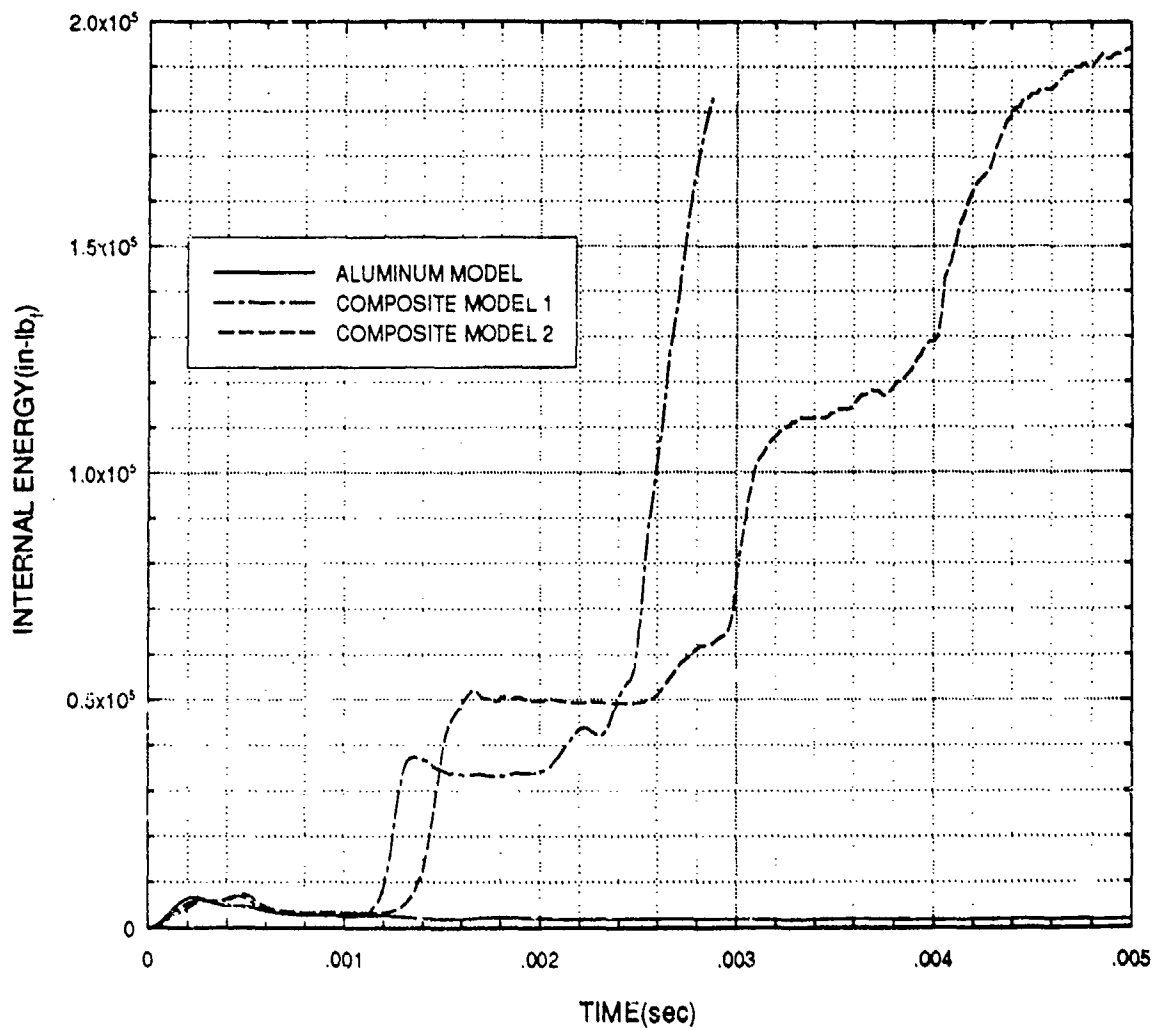


Figure 36: Internal energy of aluminum shell material for uncoated and coated aluminum cylinders.

asymmetry held constant. Values for axial and hoop strain matched closely up to about 1.4 msec.. Thereafter, the magnitudes varied and the peaks occurred at different times. Plots of axial and hoop strain are shown in Figures 37-54. Again, the location was important in determining whether the effect of lowering shear modulus resulted in a larger response. Although the variation was small, lowering the shear modulus appeared to adversely affect the response. The internal energy of the aluminum material for the two different values of shear modulus is shown in Figure 55. After 1 msec., the energy levels differed considerably. The cylinder with the lower shear modulus showed the higher internal energy. As in the previous study, the inertial effects on cylinder response are most pronounced near the endplate ("C" element locations).

The shear modulus of the rubber was then increased with the coefficient of asymmetry held constant. As the modulus was increased by orders of magnitude, the response of the cylinder dramatically improved. Effective plastic strain is plotted for element A3 and is shown in Figure 56. For shear modulus values at or above 500 psi, the aluminum exhibited significantly lower strain. To help visualize how the response was affected by a change in the material property of the rubber, radial velocity at node 49 (interior node at element A3 along the symmetric boundary) was examined. The plot is shown in Figure 57 and it indicates that at values above 500 psi, the response is not erratic as in the low shear modulus case, but rather



# AXIAL STRAIN FOR ELEMENT A1

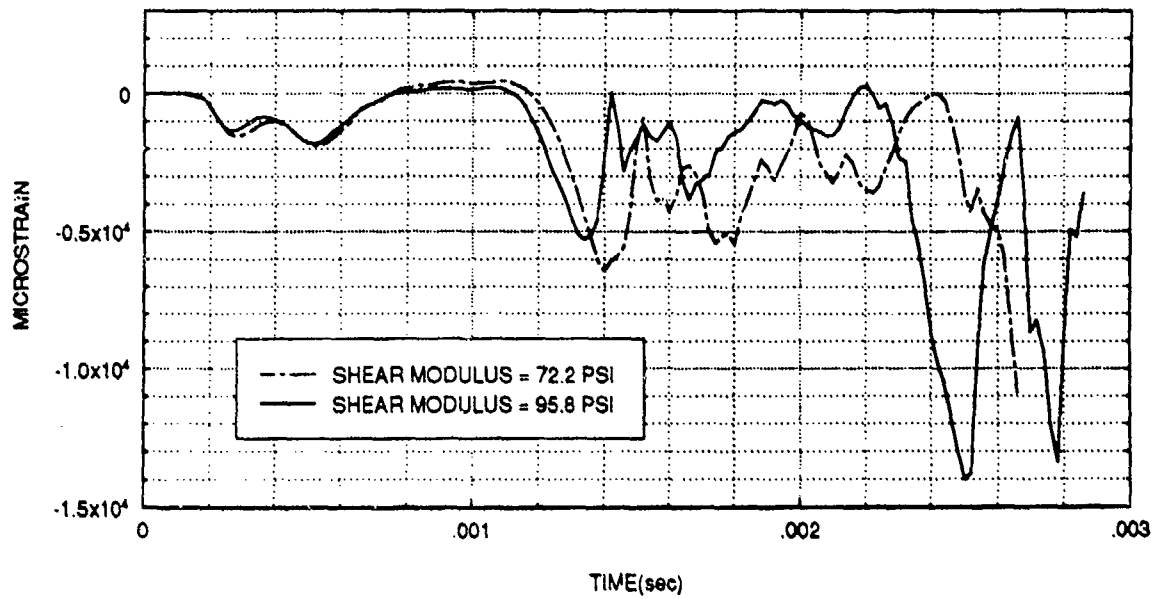


**Figure 37:** Axial strain at position A1 for coated aluminum cylinders with variation of rubber shear modulus.

# HOOP STRAIN FOR ELEMENT A1

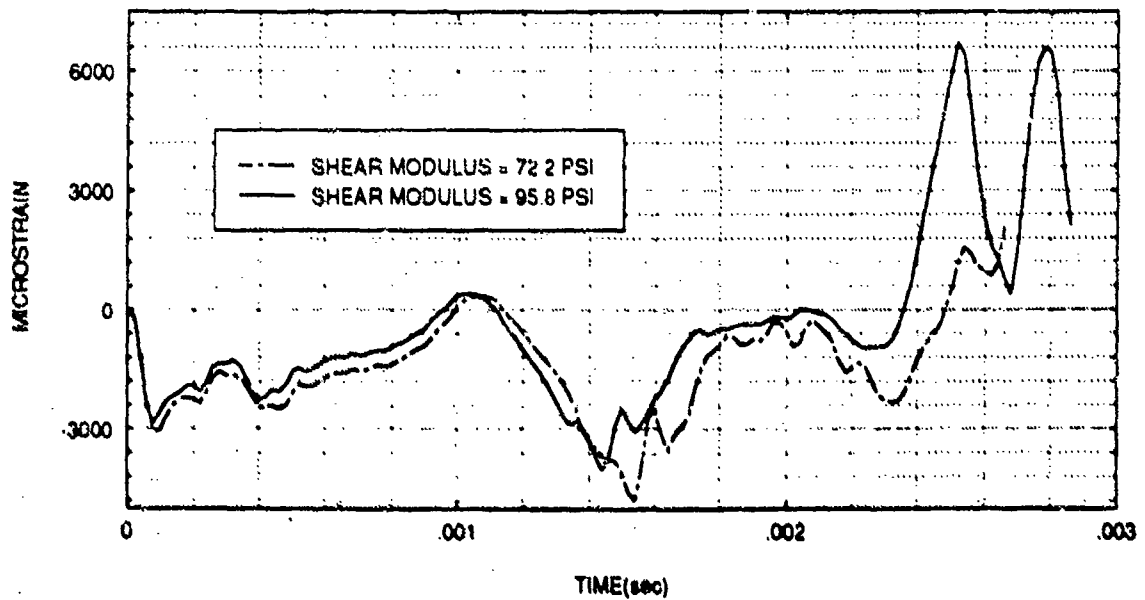


**Figure 38:** Hoop strain at position A1 for coated aluminum cylinders with variation of rubber shear modulus.

### AXIAL STRAIN FOR ELEMENT A2

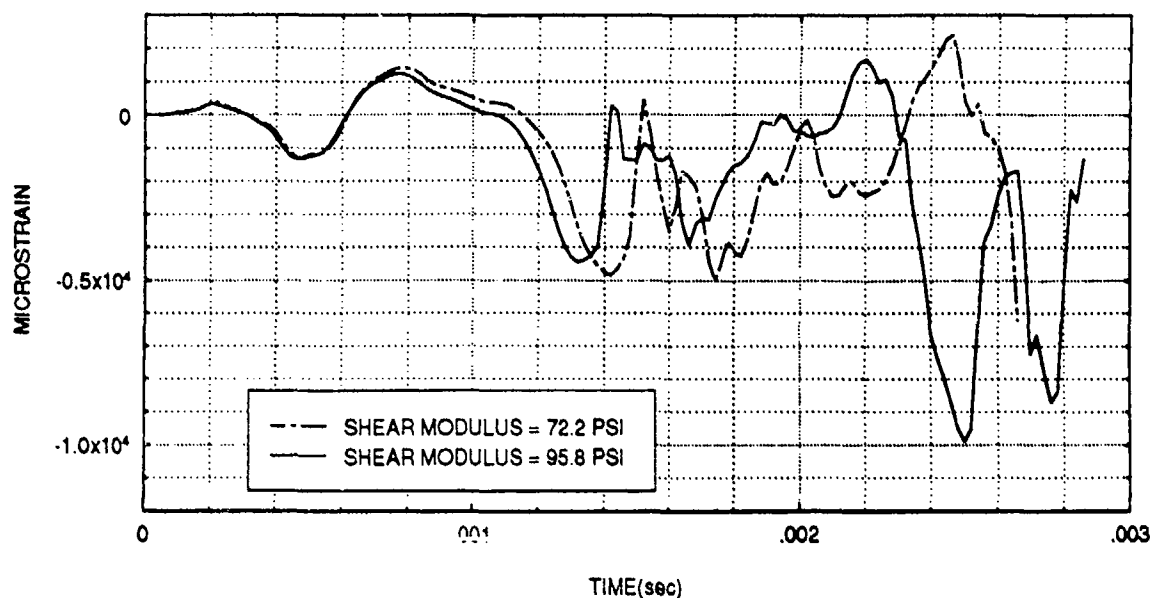


**Figure 39:** Axial strain at position A2 for coated aluminum cylinders with variation of rubber shear modulus.

### HOOP STRAIN FOR ELEMENT A2

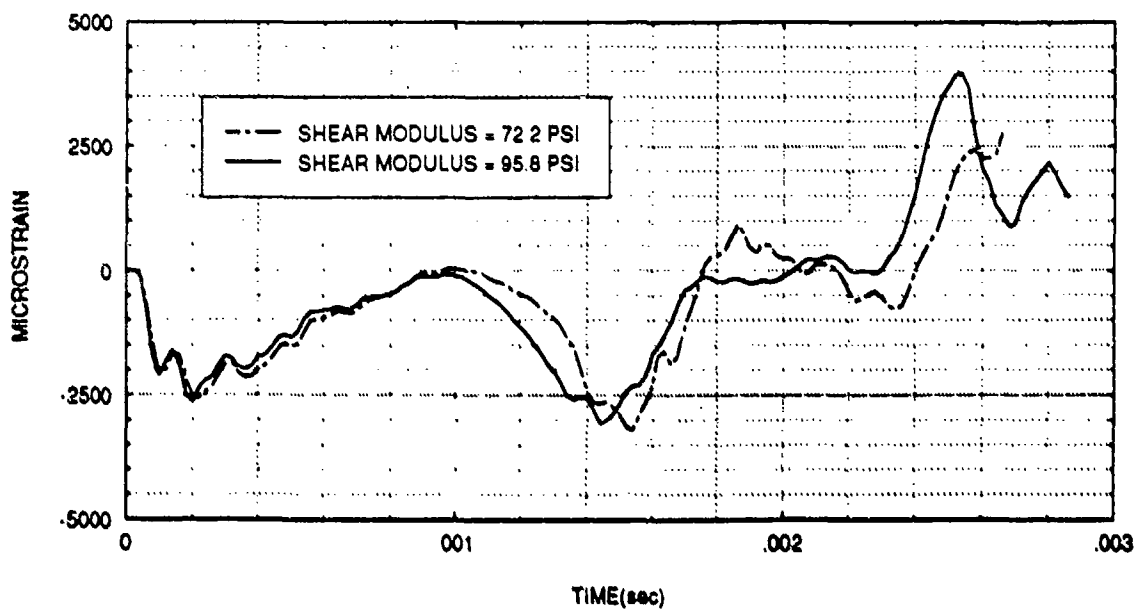


**Figure 40:** Hoop strain at position A2 for coated aluminum cylinders with variation of rubber shear modulus.

### AXIAL STRAIN FOR ELEMENT A3

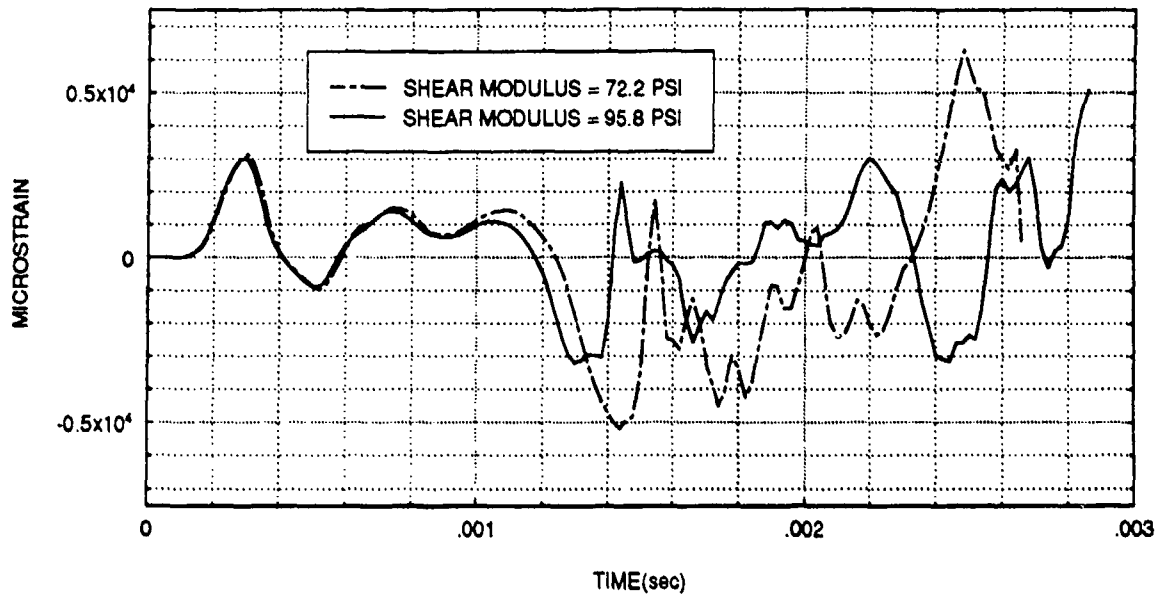


**Figure 41:** Axial strain at position A3 for coated aluminum cylinders with variation of rubber shear modulus.

### HOOP STRAIN FOR ELEMENT A3

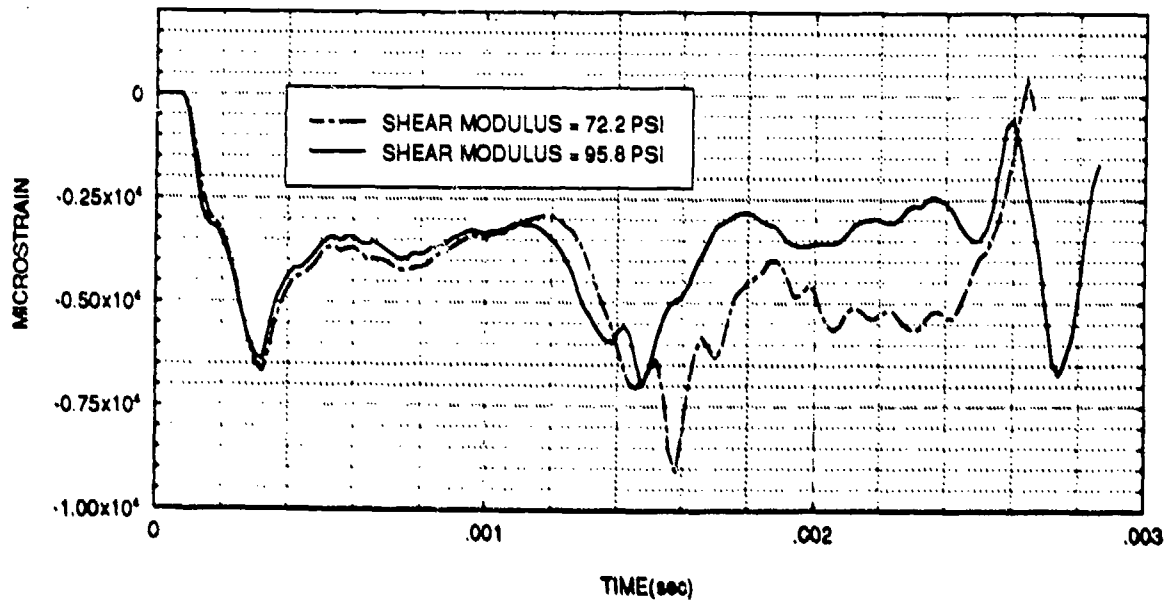


**Figure 42:** Hoop strain at position A3 for coated aluminum cylinders with variation of rubber shear modulus.

### AXIAL STRAIN FOR ELEMENT B1

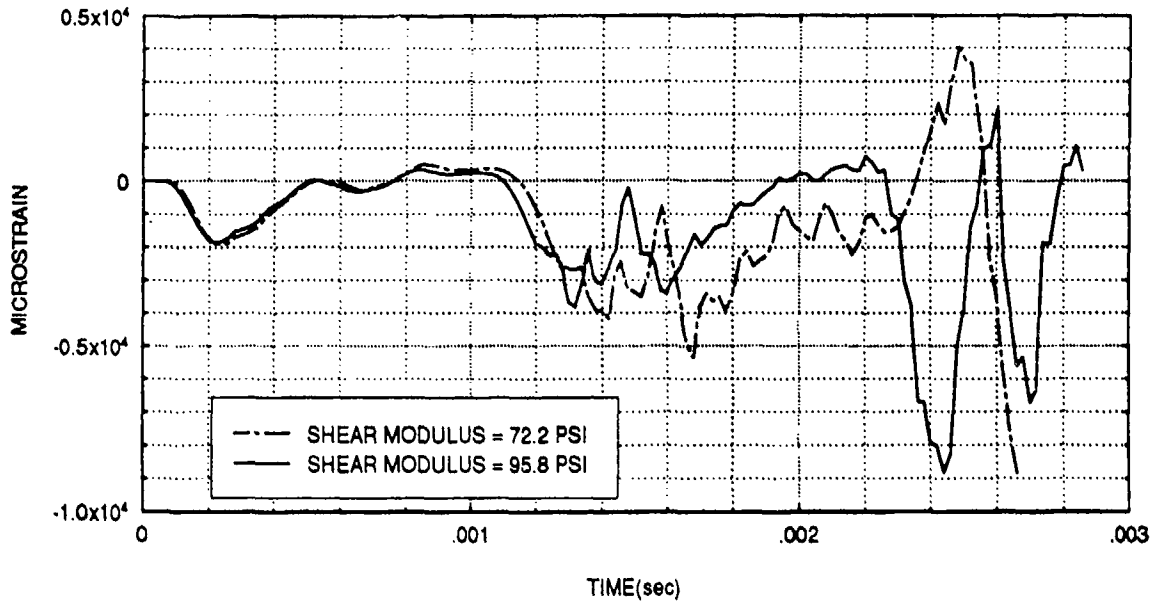


**Figure 43:** Axial strain at position B1 for coated aluminum cylinders with variation of rubber shear modulus.

### HOOP STRAIN FOR ELEMENT B1

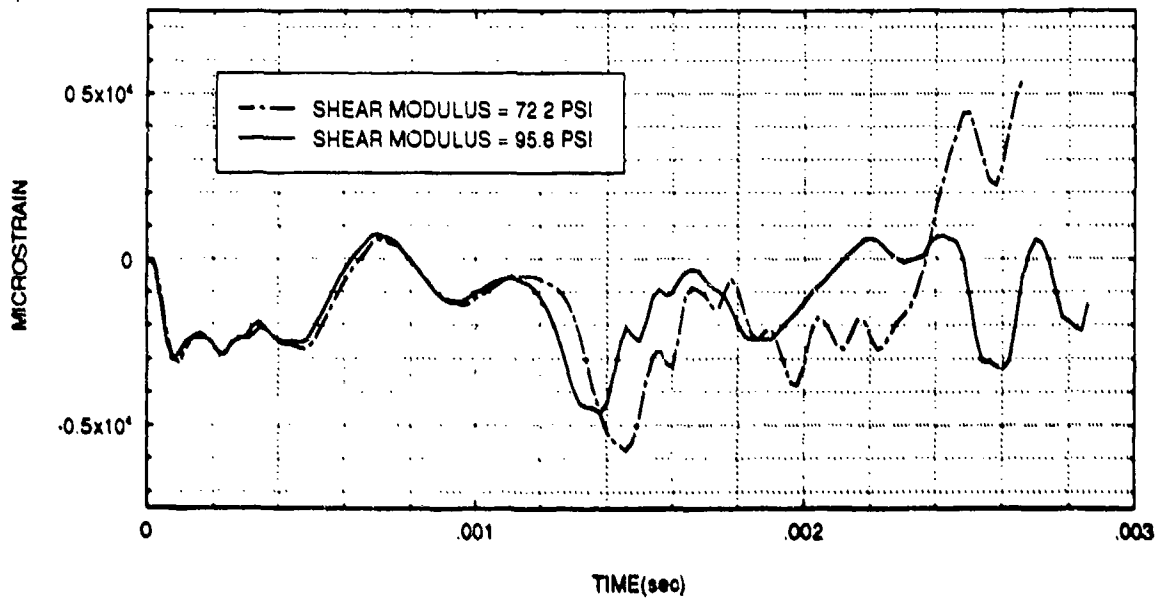


**Figure 44:** Hoop strain at position B1 for coated aluminum cylinders with variation of rubber shear modulus.

### AXIAL STRAIN FOR ELEMENT B2

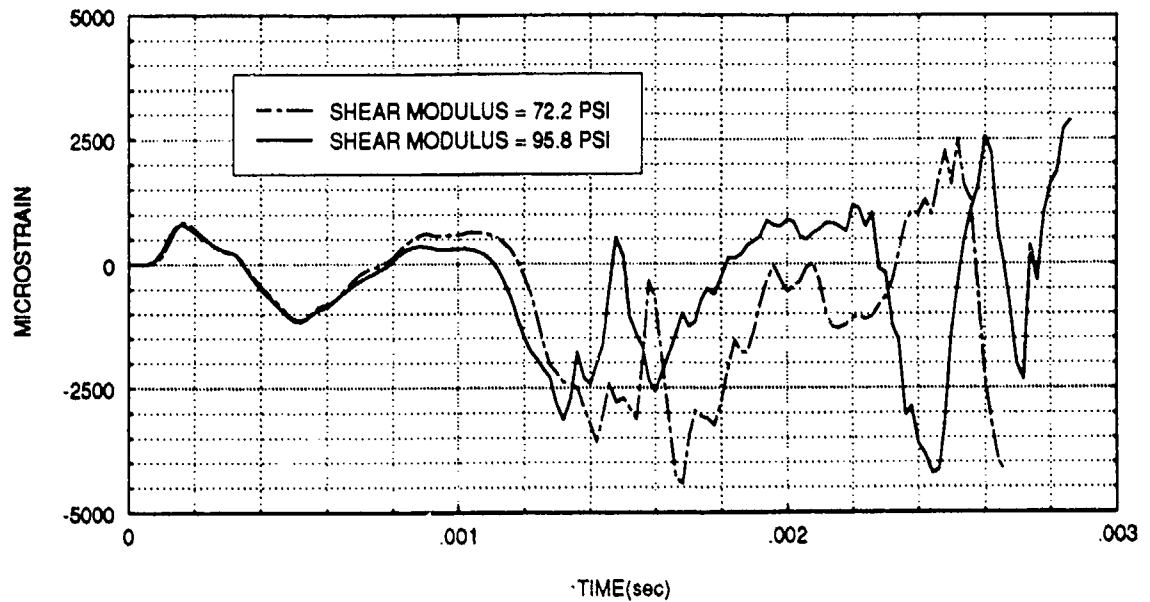


**Figure 45:** Axial strain at position B2 for coated aluminum cylinders with variation of rubber shear modulus.

### HOOP STRAIN FOR ELEMENT B2

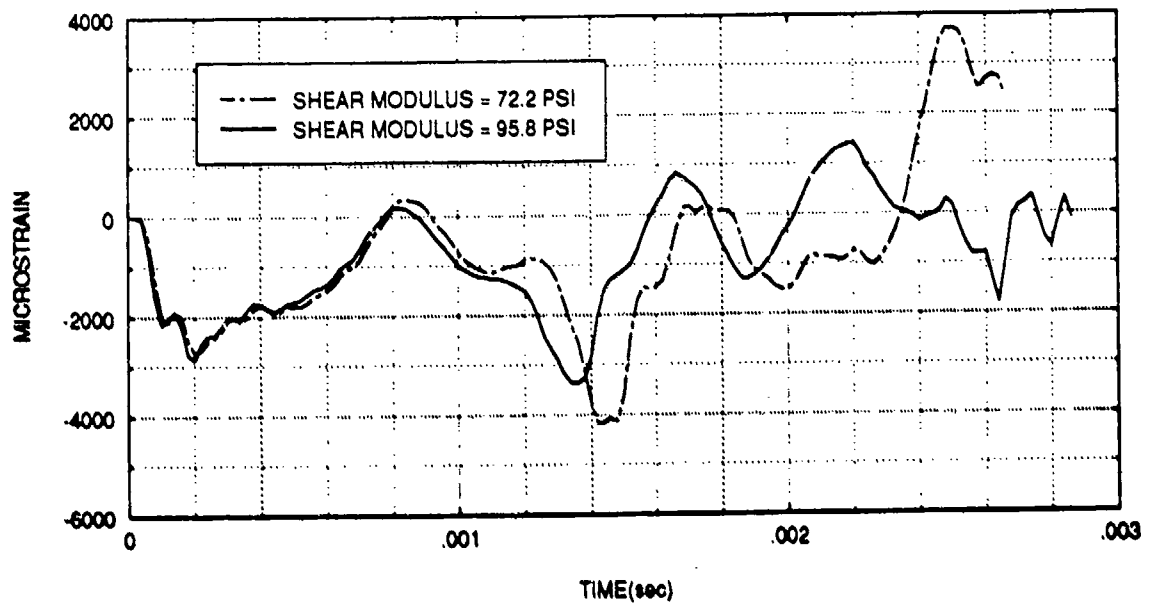


**Figure 46:** Hoop strain at position B2 for coated aluminum cylinders with variation of rubber shear modulus.

### AXIAL STRAIN FOR ELEMENT B3

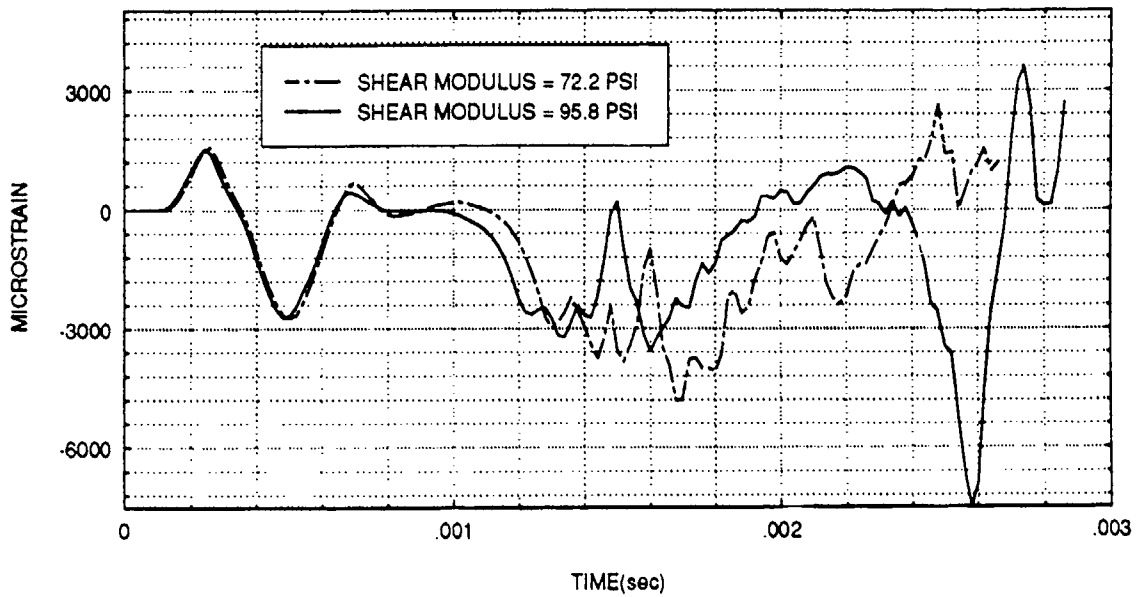


**Figure 47:** Axial strain at position B3 for coated aluminum cylinders with variation of rubber shear modulus.

### HOOP STRAIN FOR ELEMENT B3

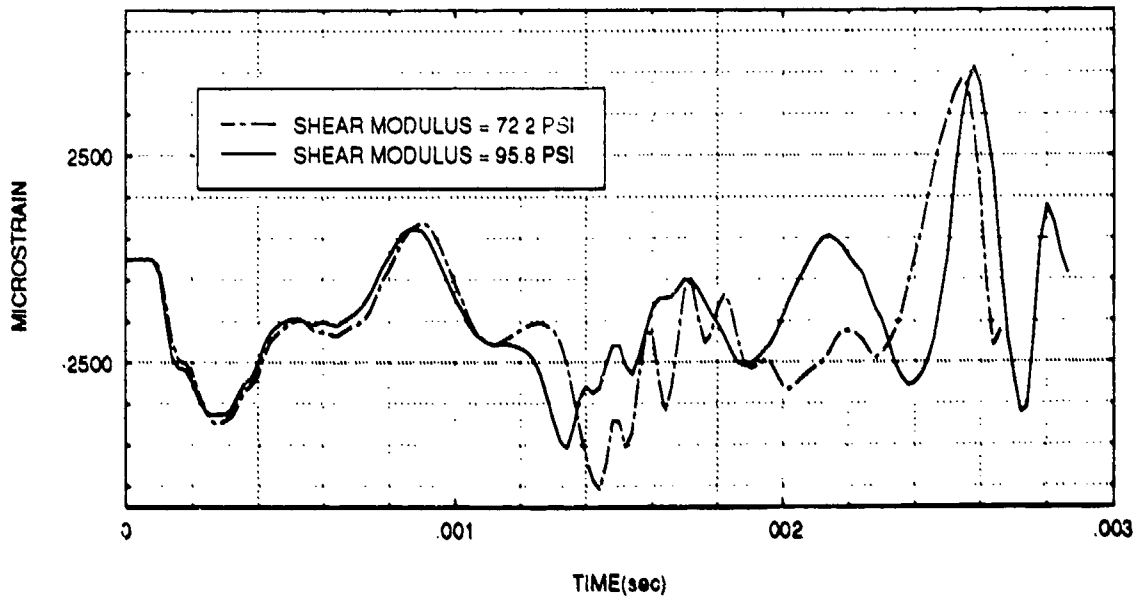


**Figure 48:** Hoop strain at position B3 for coated aluminum cylinders with variation of rubber shear modulus.

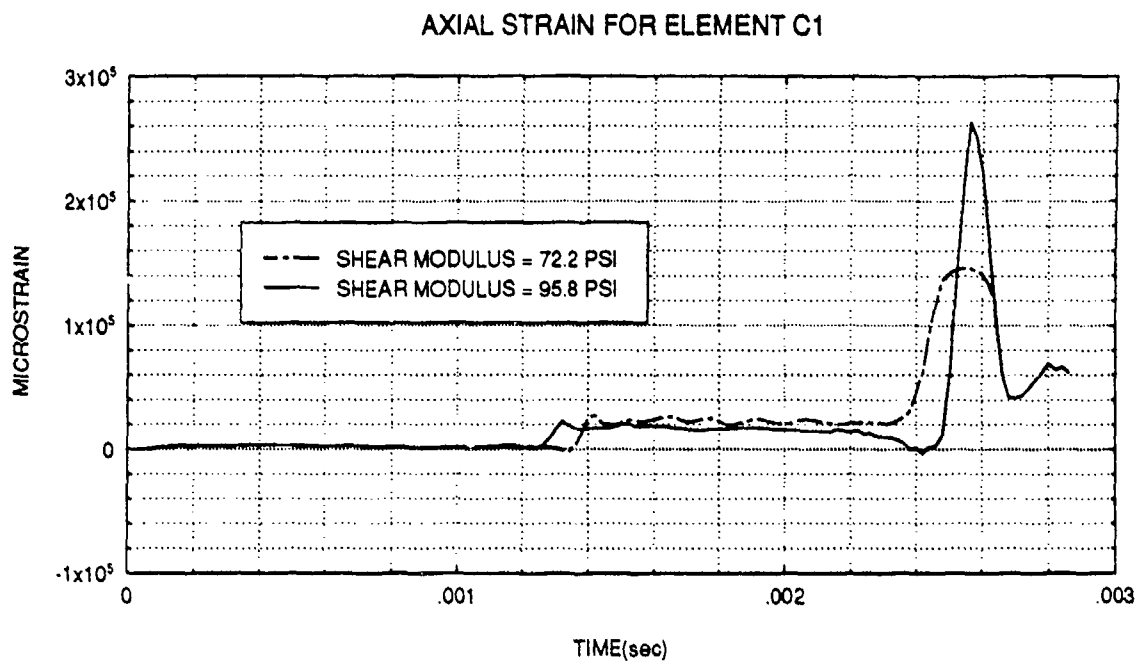


**Figure 49:** Axial strain at position C1 for coated aluminum cylinders with variation of rubber shear modulus.

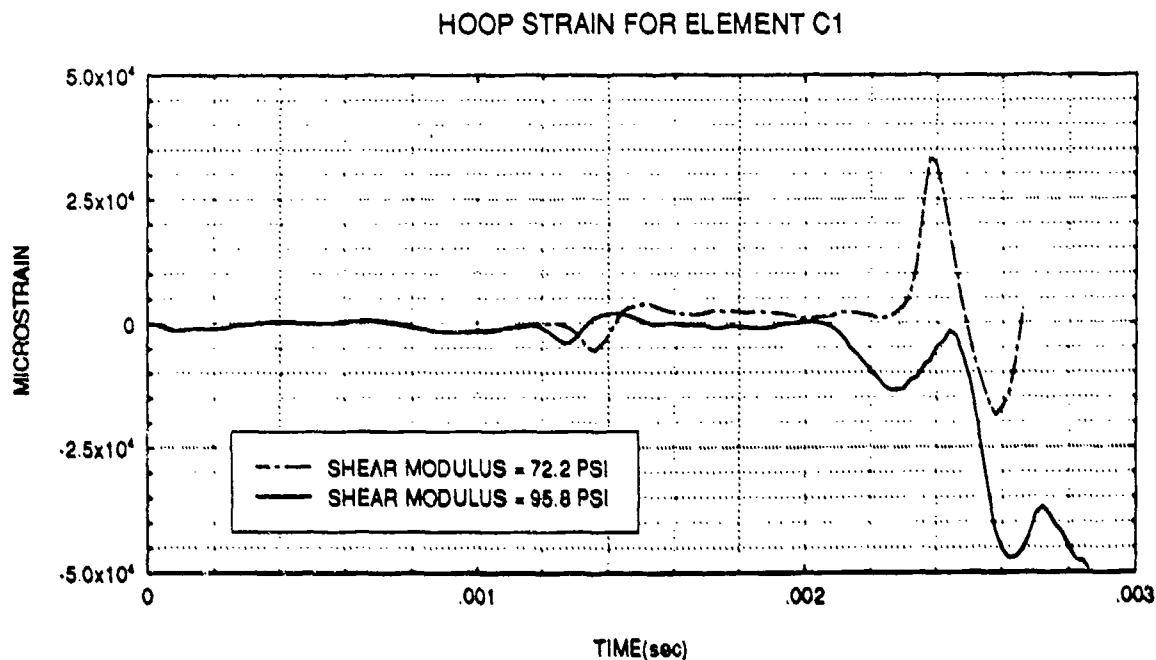


**Figure 50:** Hoop strain at position C1 for coated aluminum cylinders with variation of rubber shear modulus.

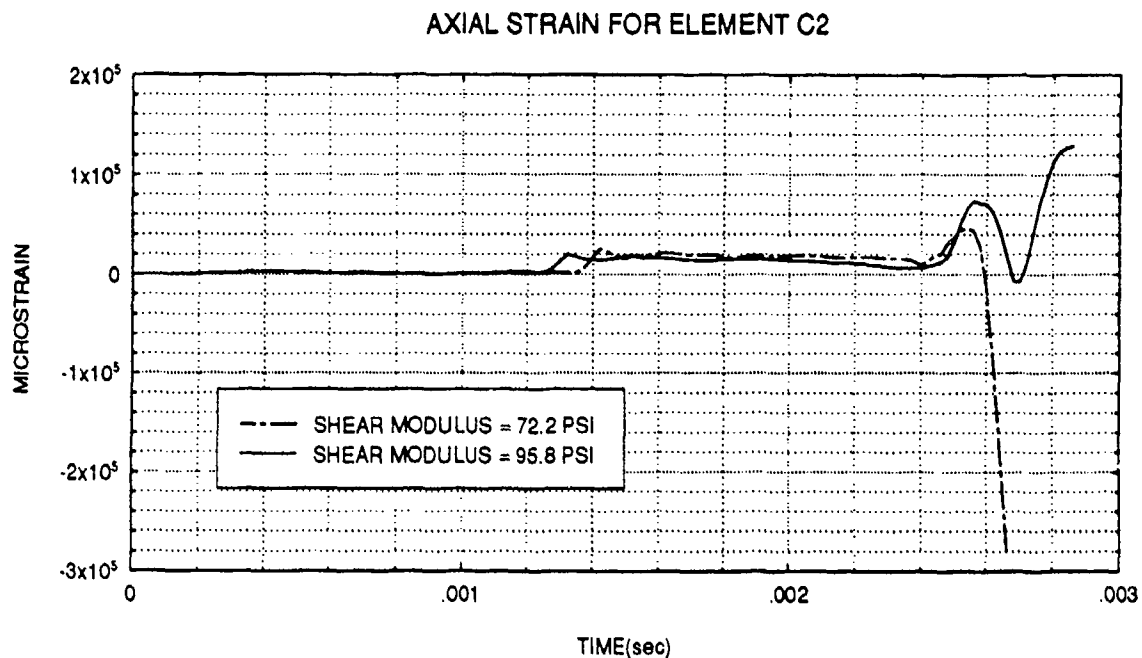


**Figure 51:** Axial strain at position C2 for coated aluminum cylinders with variation of rubber shear modulus.

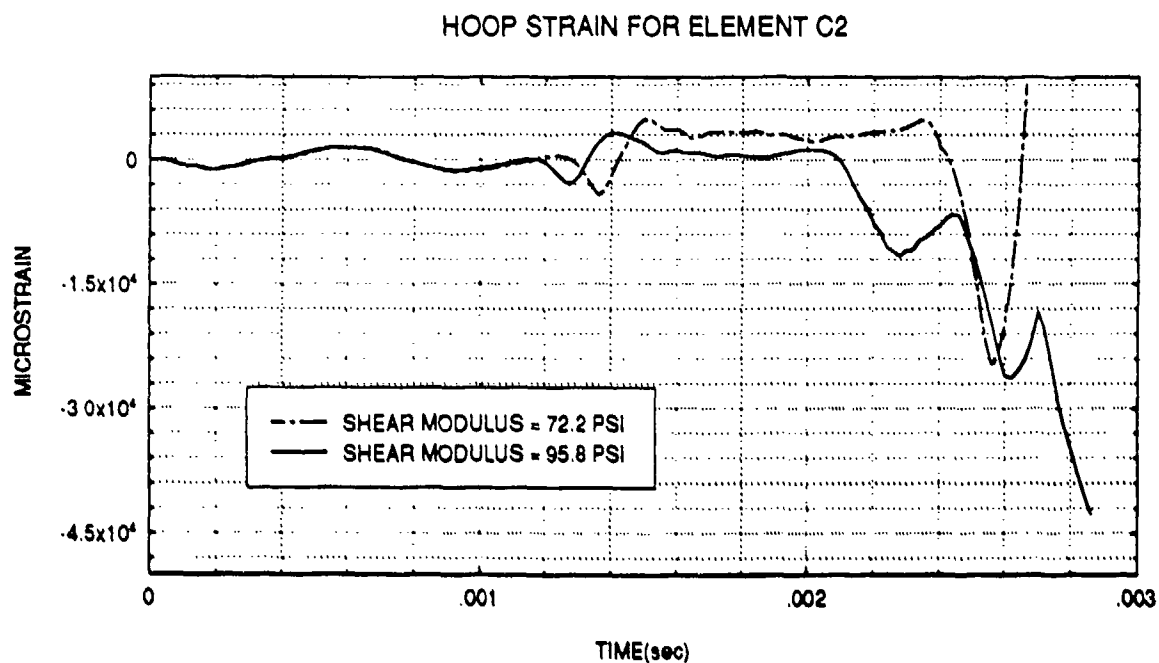


**Figure 52:** Hoop strain at position C2 for coated aluminum cylinders with variation of rubber shear modulus.



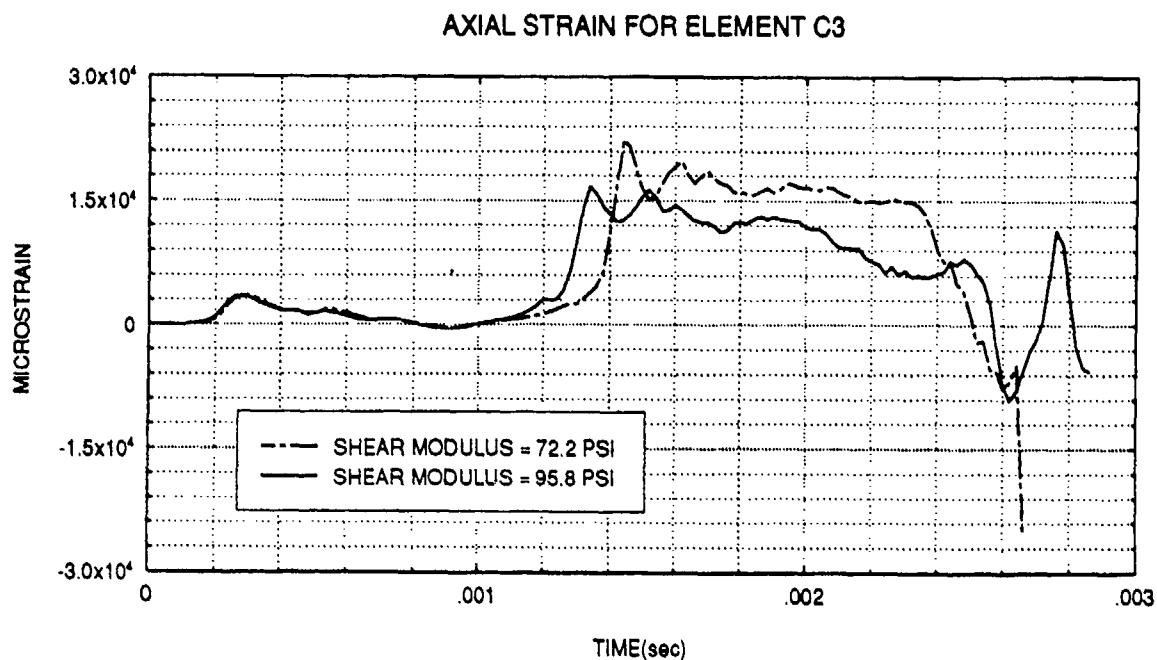


**Figure 53:** Axial strain at position C3 for coated aluminum cylinders with variation of rubber shear modulus.

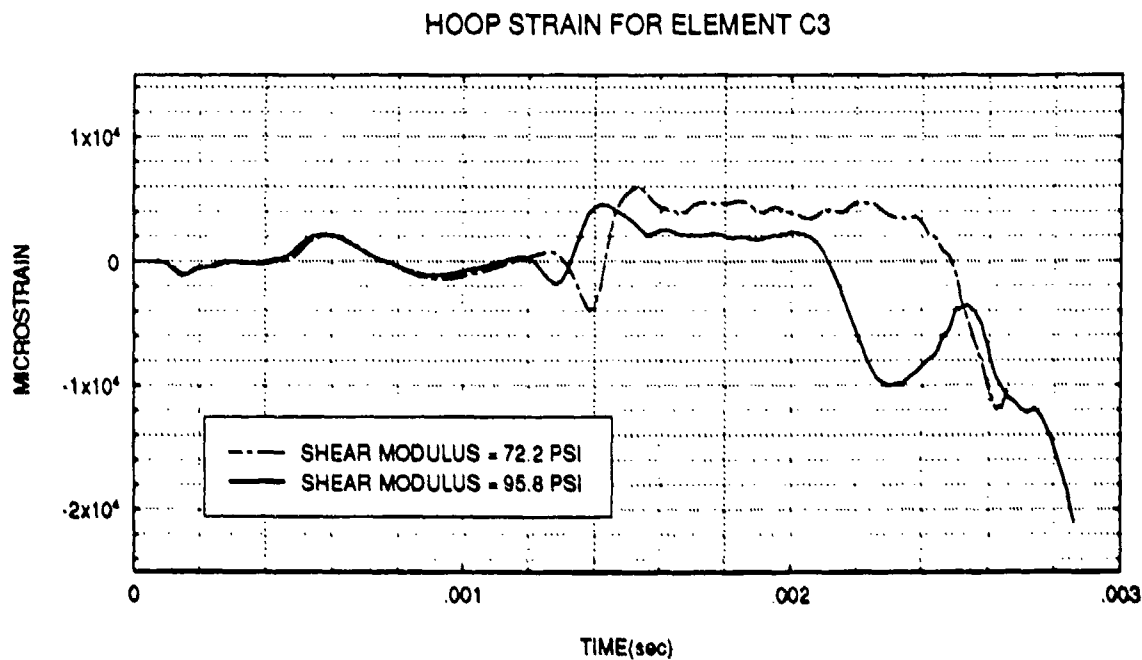


**Figure 54:** Hoop strain at position C3 for coated aluminum cylinders with variation of rubber shear modulus.

# INTERNAL ENERGY OF ALUMINUM SHELL MATERIAL

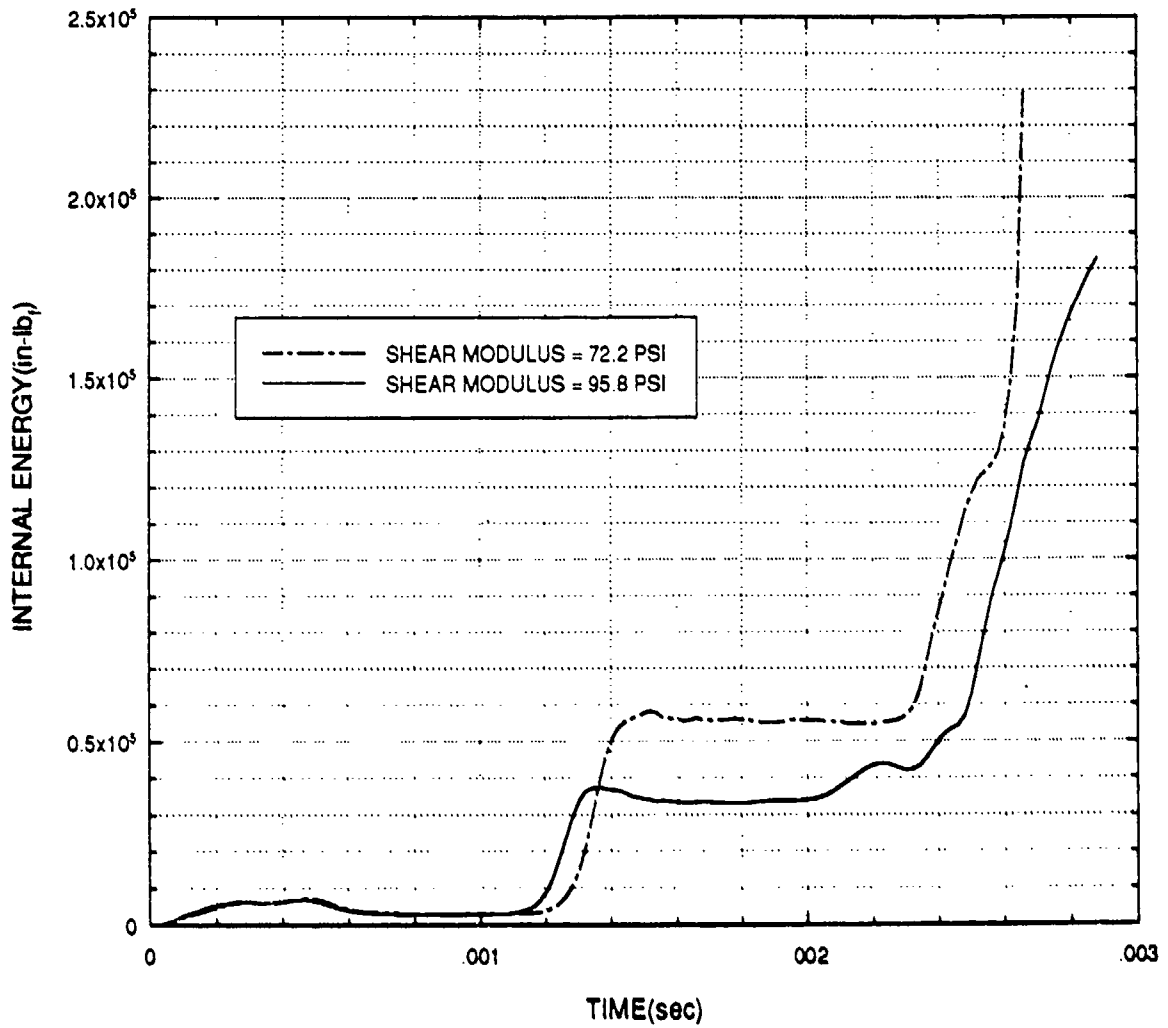


**Figure 55:** Internal energy of aluminum shell material of coated aluminum cylinders with variation of rubber shear modulus.

### EFFECTIVE PLASTIC STRAIN AT ELEMENT A3

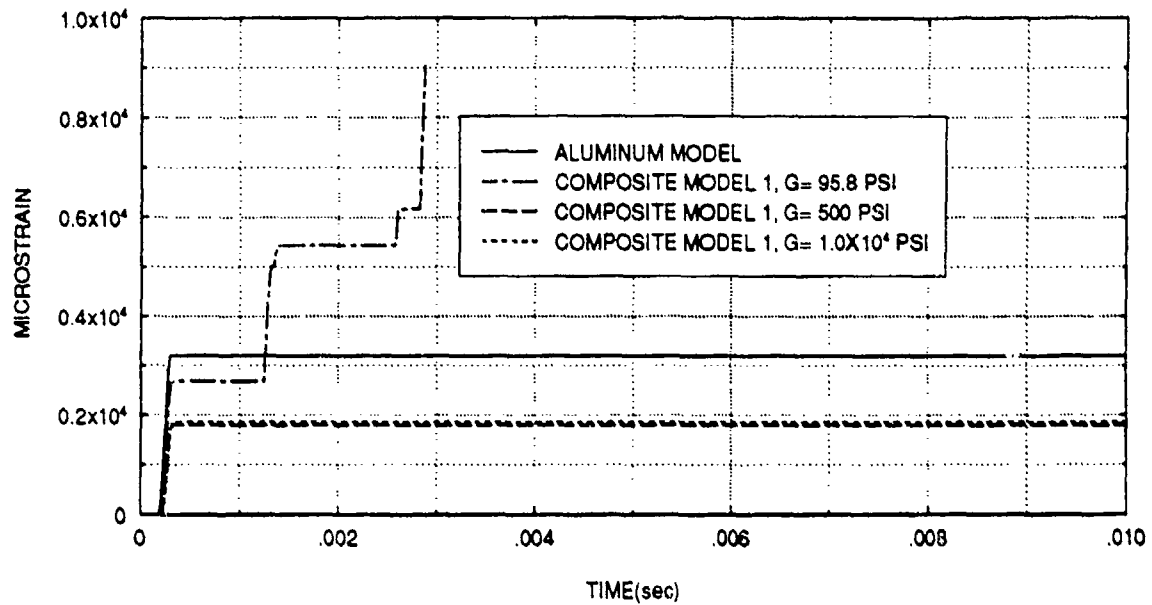


**Figure 56:** Effective plastic strain at position A3 for uncoated and coated aluminum cylinders with large variation of rubber shear modulus.

### RADIAL VELOCITY AT NODE 49

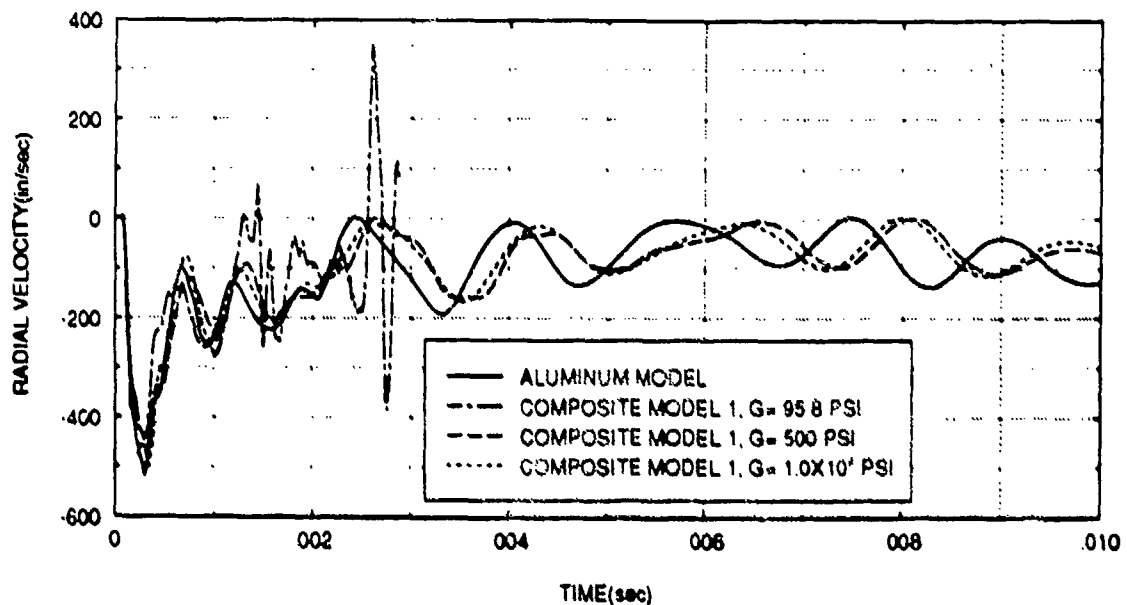
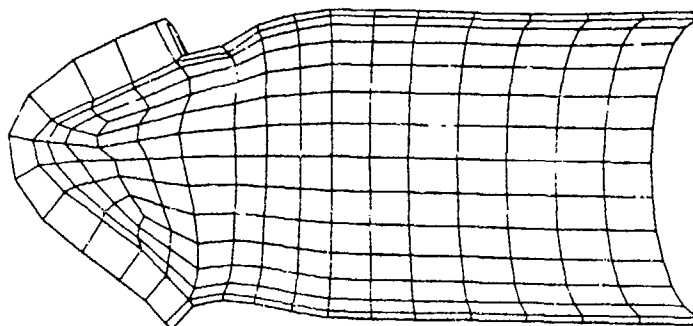


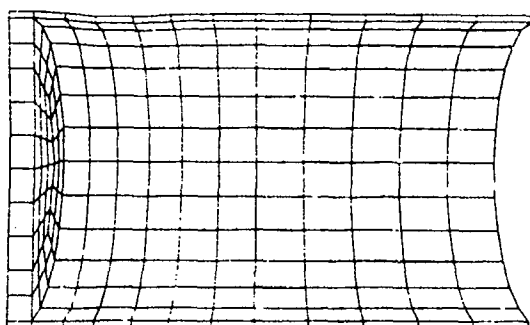
**Figure 57:** Radial velocity at node 49 for uncoated and coated aluminum cylinders with large variation of rubber shear modulus.

shows a gradual and smooth return to the steady state. The deformation of Composite Model 1 for different values of rubber shear modulus is shown in Figure 58. Larger deformation was visible in the cylinder that had a shear modulus of 95.8 psi.. However, for larger values of shear modulus, the amount of deformation is small and is commensurate with deformation observed in the uncoated aluminum cylinder model. The internal energy of the aluminum shell material is plotted for different values of rubber shear modulus and is shown in Figures 59 and 60. These plots clearly show that when the shear modulus is high, the response of the coated cylinder is almost identical to the uncoated cylinder. The results of this study seem to indicate that the dynamic response of the cylinder is related to the stiffness of the coating and is therefore affected by the value of the shear modulus. Furthermore, the dramatic change in the response of the cylinder due to a change in the shear modulus of the coating suggests the existence of a shear modulus "threshold" value, i.e. a value below which causes the coated cylinder adversely respond to an underwater shock wave.

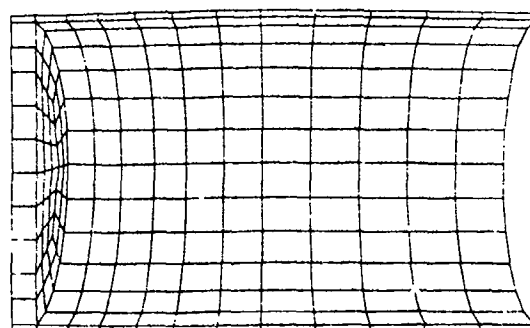
In the third case, the objective was to examine the sensitivity of the response to a change in the coefficient of asymmetry while holding the shear modulus of the rubber constant. Again, Composite Model 1 was utilized and the coefficient of asymmetry was varied from 0.223 to 0.50. At nearly all locations, axial and hoop strain values exhibited



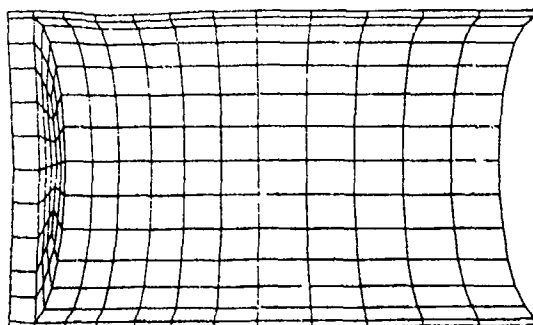
COMPOSITE MODEL 1 ( $G=95.8$  PSI)



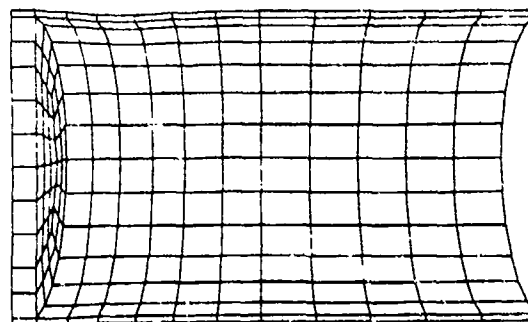
COMPOSITE MODEL 1 ( $G= 1 \times 10^4$  PSI)



COMPOSITE MODEL 1 ( $G= 1 \times 10^6$  PSI)



ALUMINUM MODEL



COMPOSITE MODEL 1 ( $G= 500$  PSI)

**Figure 58:** Deformation of uncoated and coated aluminum cylinders with large variation of rubber shear modulus at 2.86 msec. (Scale factor of 5).

# INTERNAL ENERGY OF ALUMINUM SHELL MATERIAL

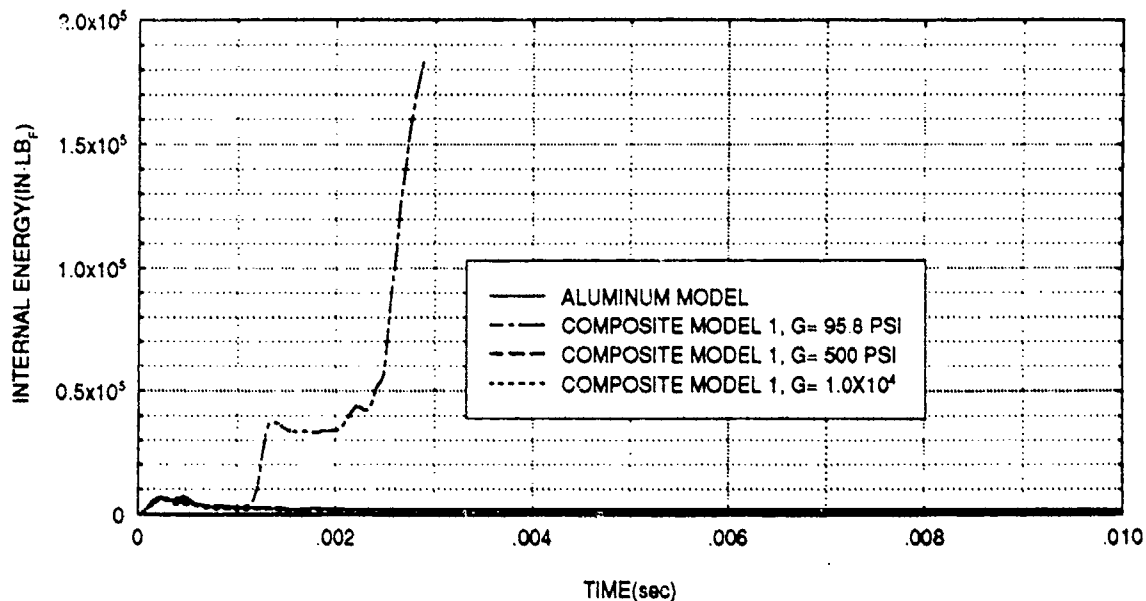


**Figure 59:** Internal energy of aluminum material for uncoated and coated cylinders with large variation of rubber shear modulus (10 msec. range).

# INTERNAL ENERGY OF ALUMINUM SHELL MATERIAL

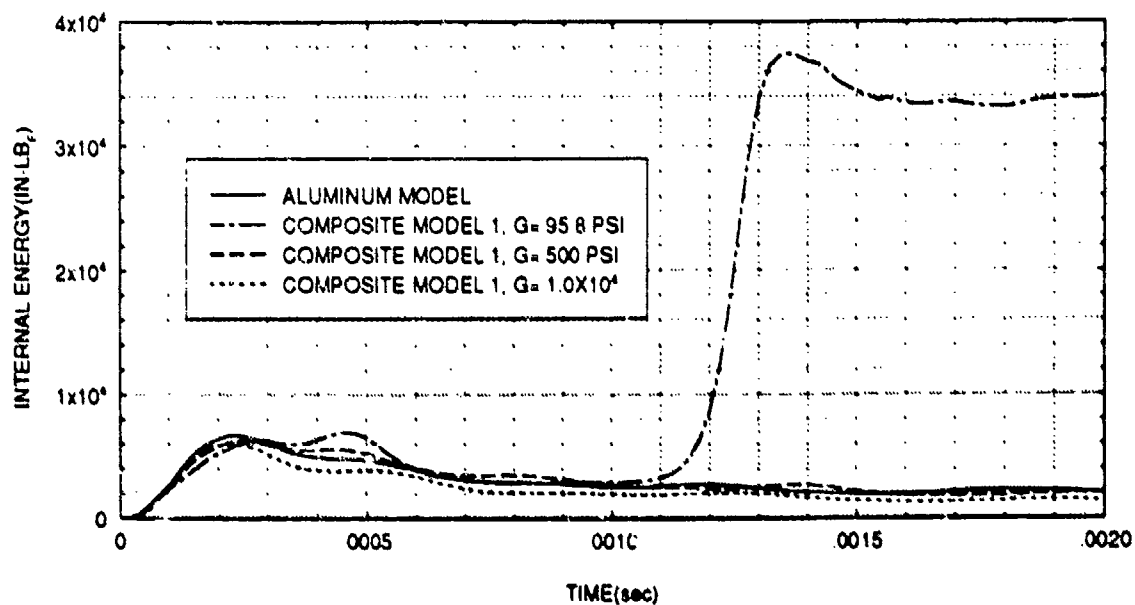


**Figure 60:** Internal energy of aluminum material for uncoated and coated cylinders with large variation of rubber shear modulus (2 msec. range)

relatively small deviations until late time (later than 2 msec.). The internal energy level of the aluminum, shown in Figure 61, was virtually identical for both cylinders up through 2.2 msec. and then showed a small deviation thereafter. Strain results are shown in Figures 62-79, and indicate that the dynamic response of the coated cylinder was weakly influenced by changes in the coefficient of asymmetry and were not evident until late time.

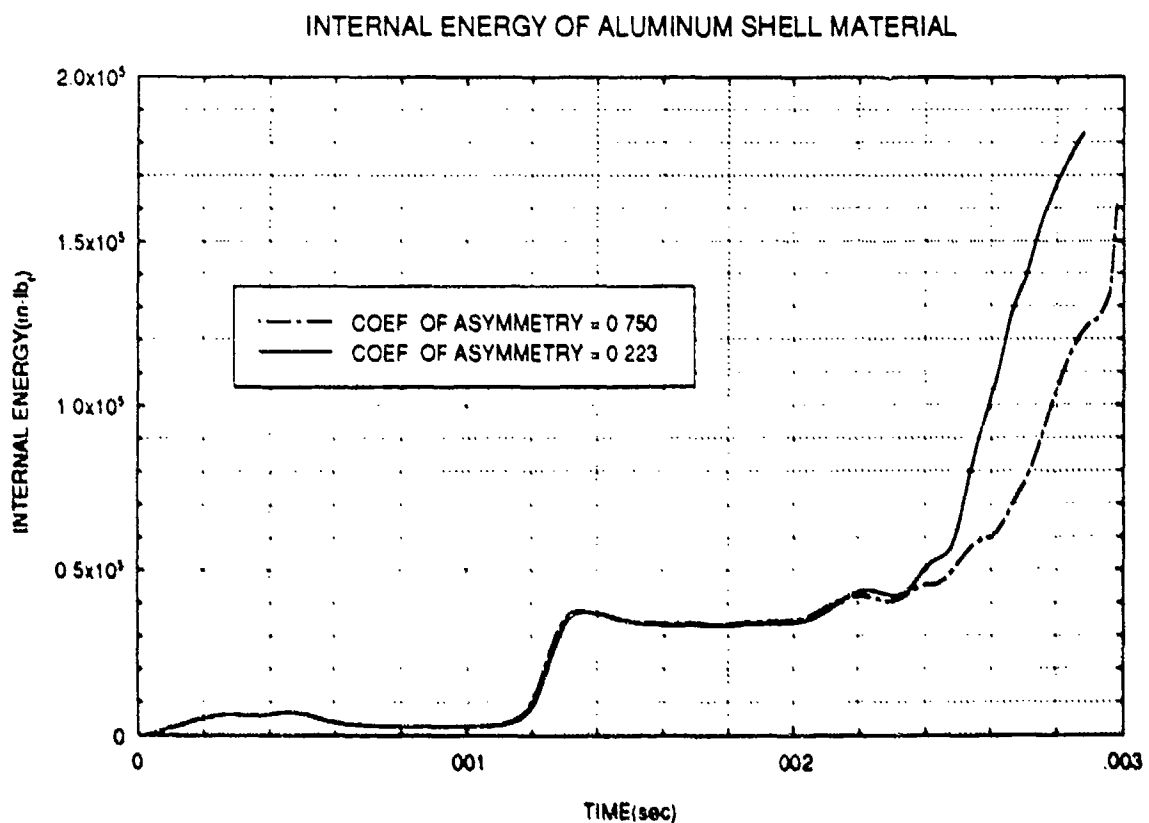


**Figure 61:** Comparison of internal energy of aluminum shell material of coated cylinder with variation in coefficient of asymmetry.

### AXIAL STRAIN FOR ELEMENT A1

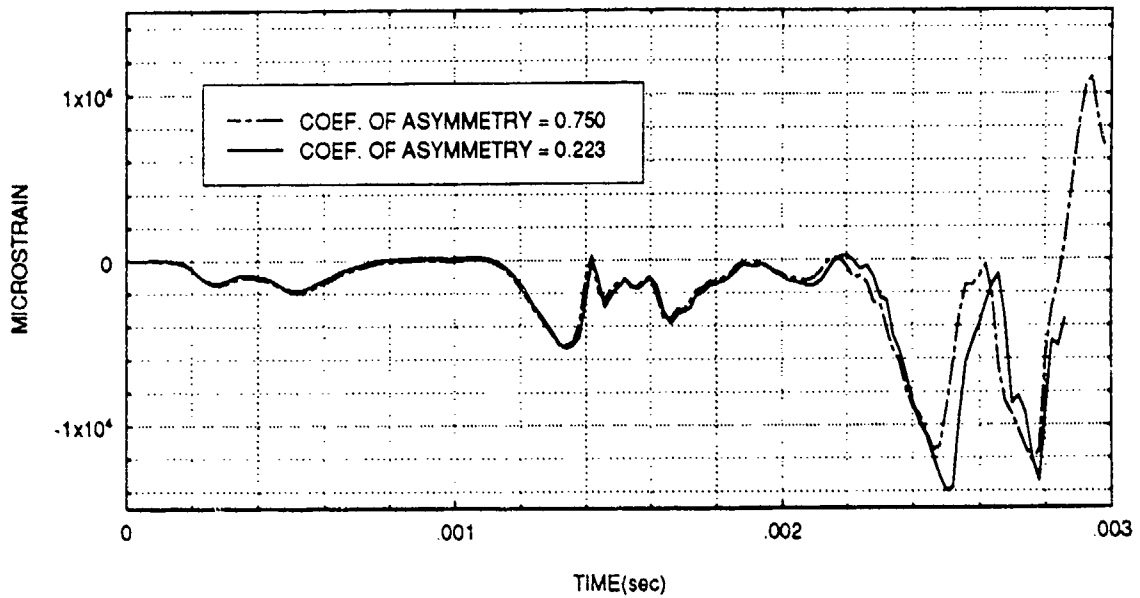


**Figure 62:** Axial strain at position A1 for coated aluminum cylinders with variation of coefficient of asymmetry.

### HOOP STRAIN FOR ELEMENT A1

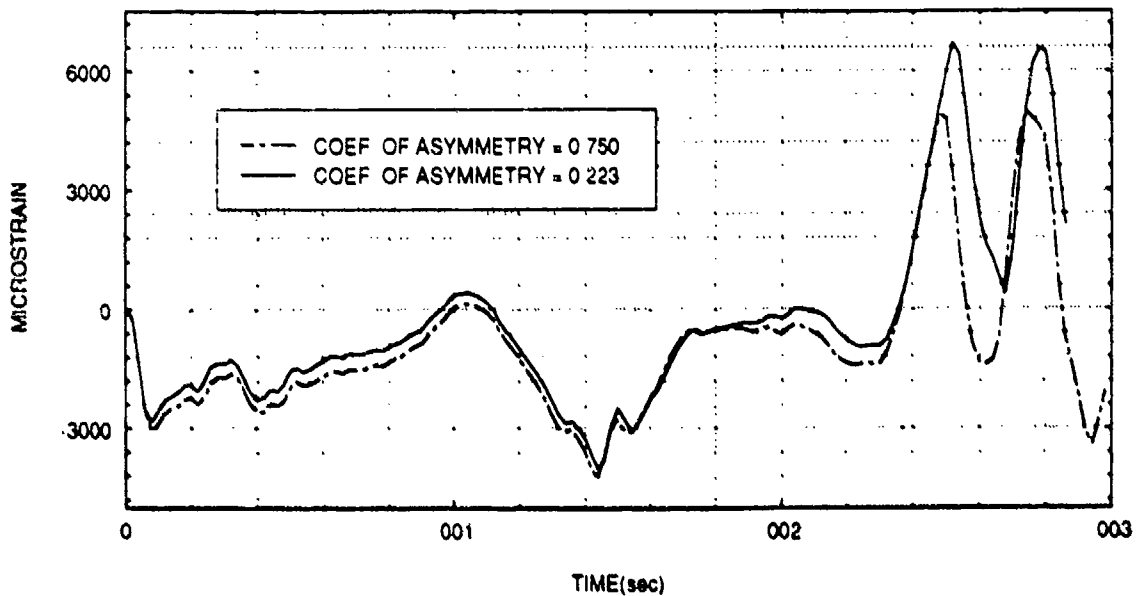


**Figure 63:** Hoop strain at position A1 for coated aluminum cylinders with variation of coefficient of asymmetry.



# AXIAL STRAIN FOR ELEMENT A2

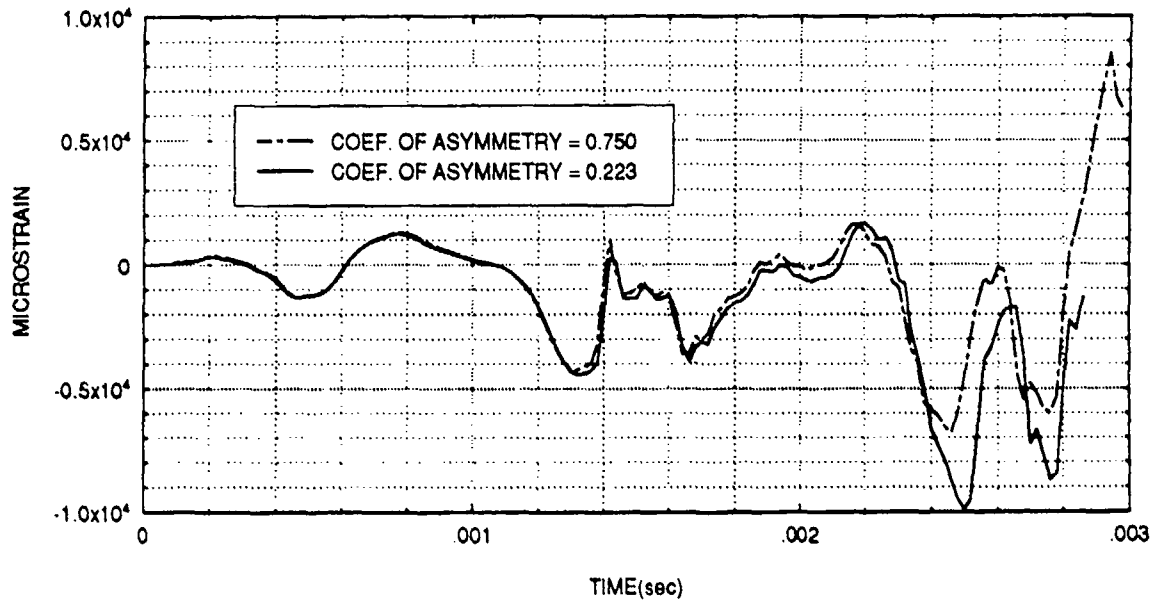


**Figure 64:** Axial strain at position A2 for coated aluminum cylinders with variation of coefficient of asymmetry.

# HOOP STRAIN FOR ELEMENT A2

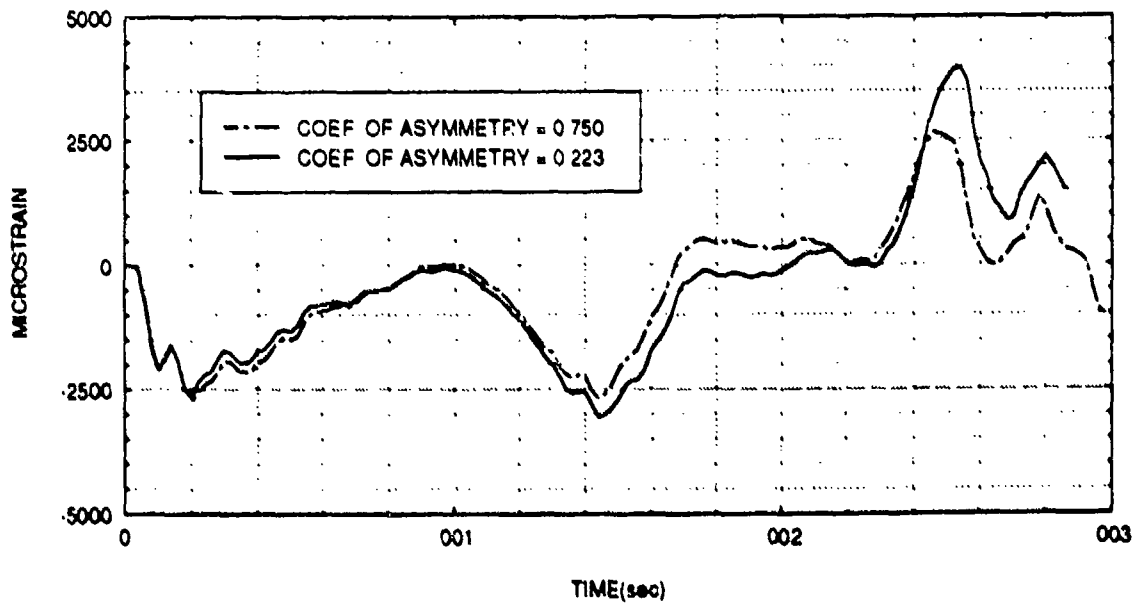


**Figure 65:** Hoop strain at position A2 for coated aluminum cylinders with variation of coefficient of asymmetry.

### AXIAL STRAIN FOR ELEMENT A3

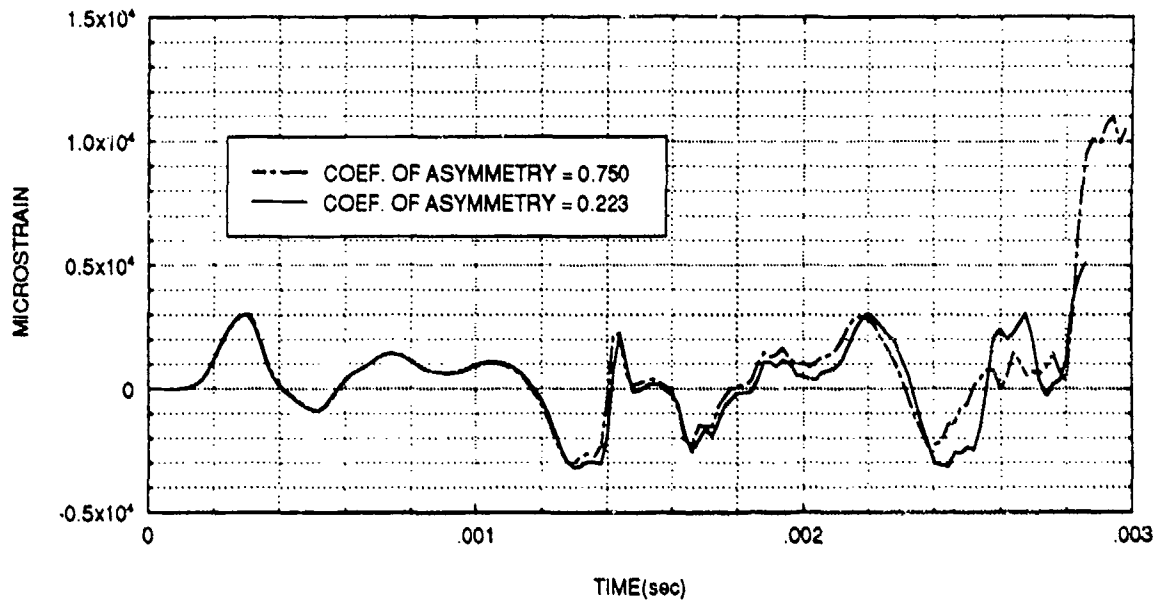


**Figure 66:** Axial strain at position A3 for coated aluminum cylinders with variation of coefficient of asymmetry.

### HOOP STRAIN FOR ELEMENT A3

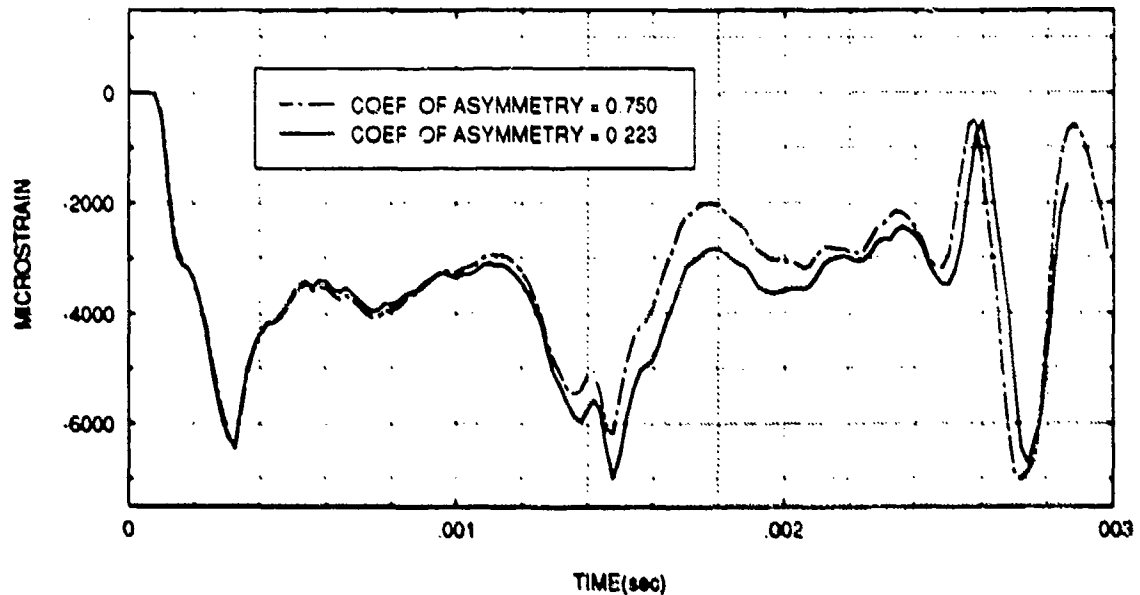


**Figure 67:** Hoop strain at position A3 for coated aluminum cylinders with variation of coefficient of asymmetry.

# AXIAL STRAIN FOR ELEMENT B1

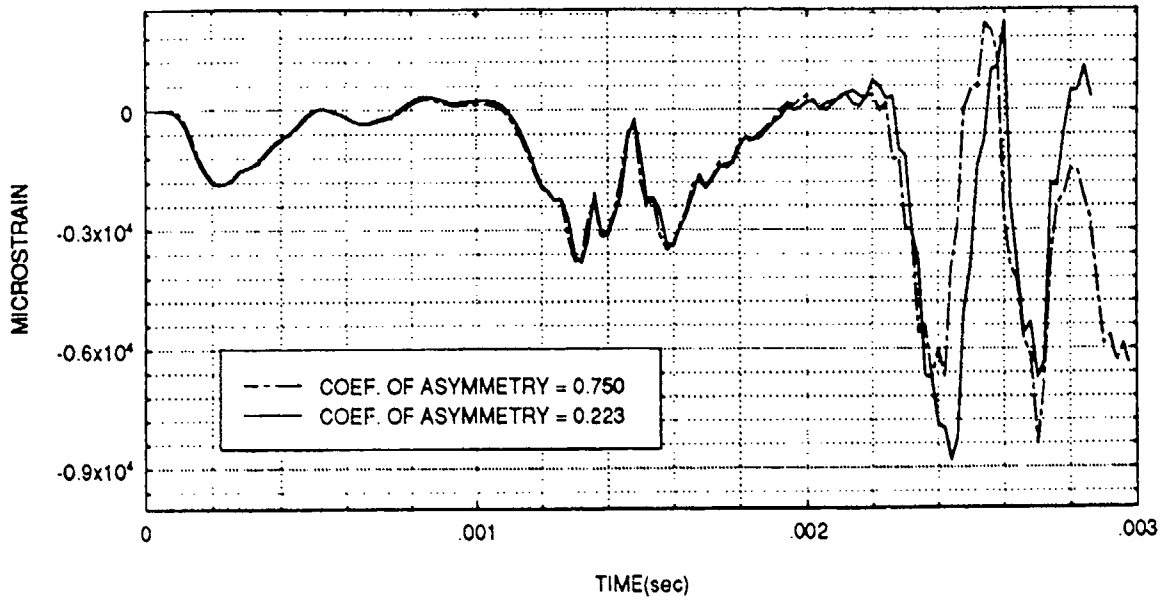


**Figure 68:** Axial strain at position B1 for coated aluminum cylinders with variation of coefficient of asymmetry.

# HOOP STRAIN FOR ELEMENT B1

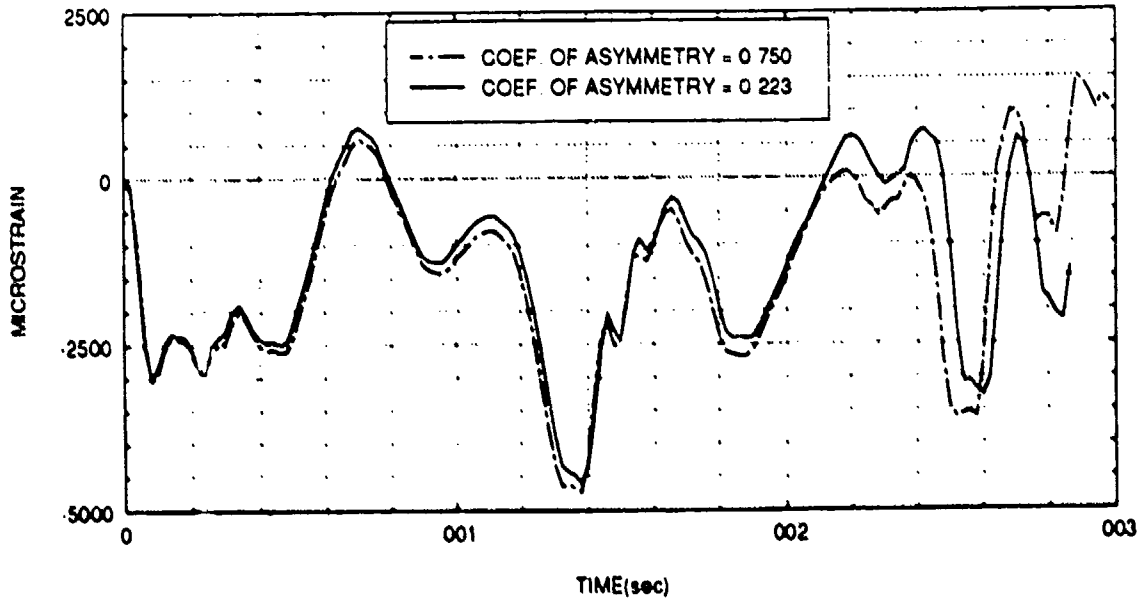


**Figure 69:** Hoop strain at position B1 for coated aluminum cylinders with variation of coefficient of asymmetry.

# AXIAL STRAIN FOR ELEMENT B2

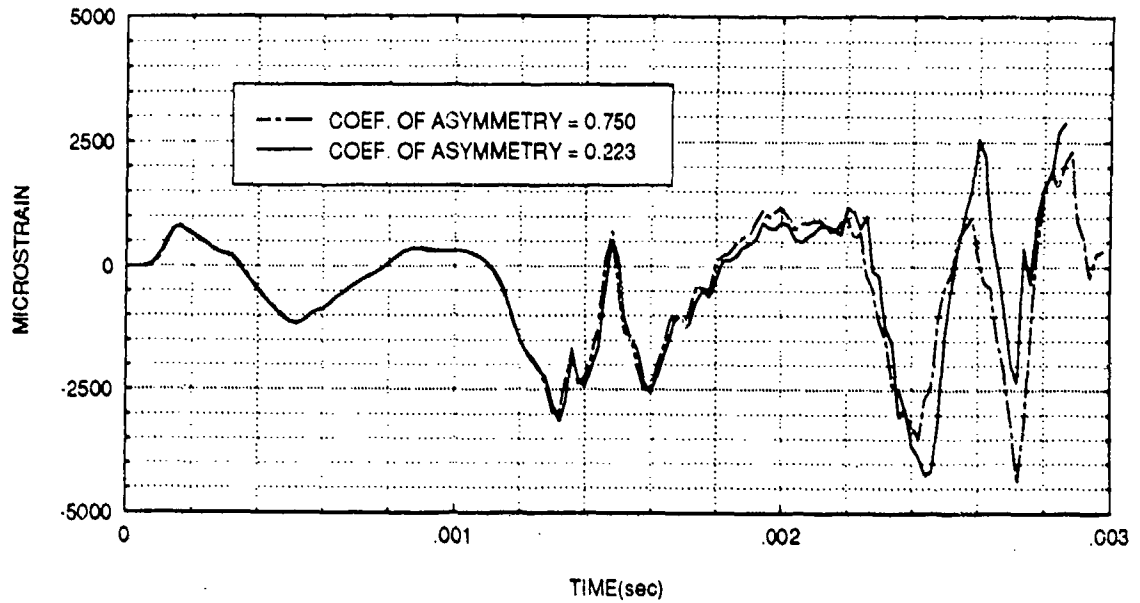


**Figure 70:** Axial strain at position B2 for coated aluminum cylinders with variation of coefficient of asymmetry.

# HOOP STRAIN FOR ELEMENT B2

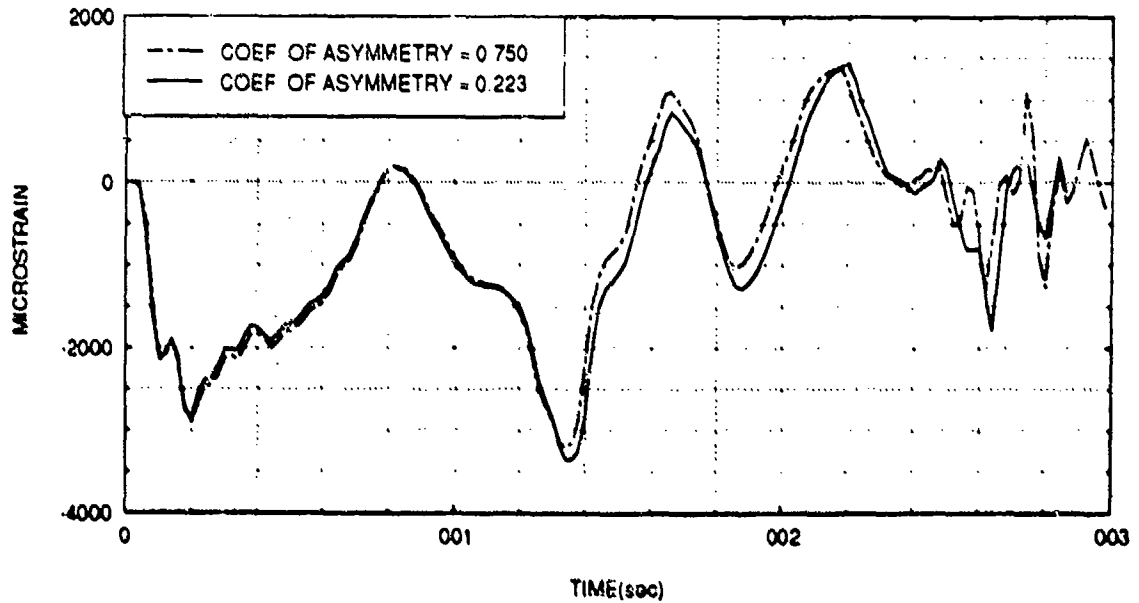


**Figure 71:** Hoop strain at position B2 for coated aluminum cylinders with variation of coefficient of asymmetry.

### AXIAL STRAIN FOR ELEMENT B3

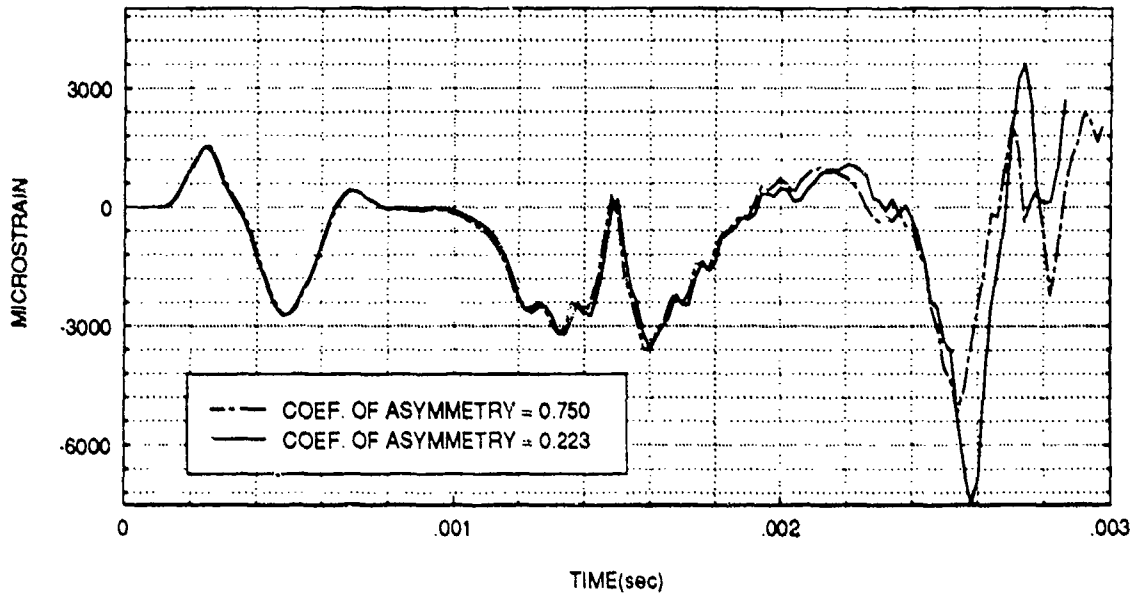


**Figure 72:** Axial strain at position B3 for coated aluminum cylinders with variation of coefficient of asymmetry.

### HOOP STRAIN FOR ELEMENT B3

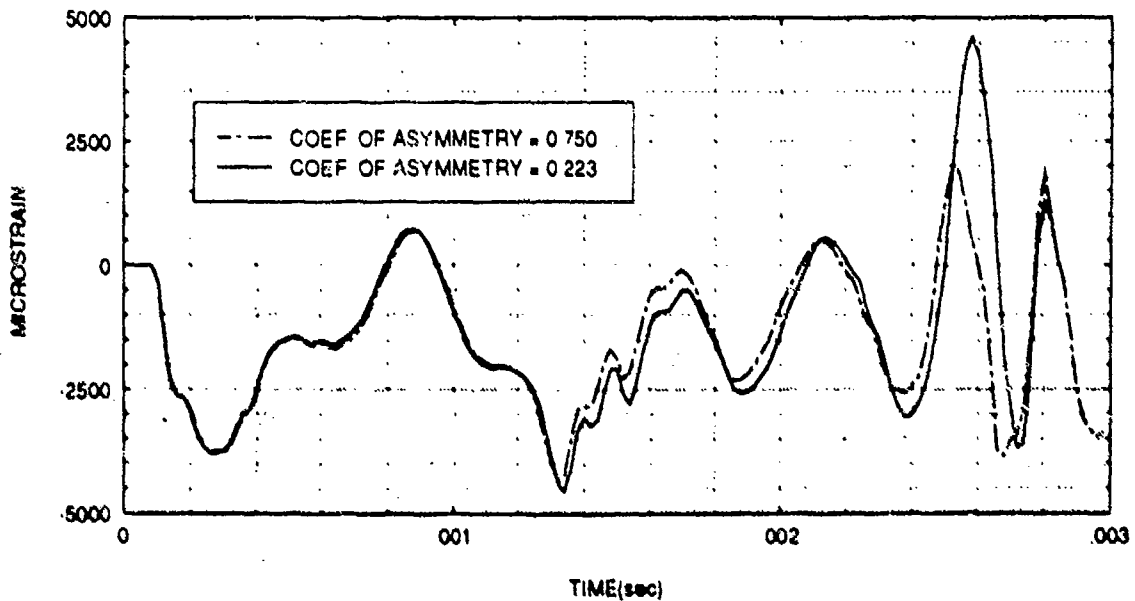


**Figure 73:** Hoop strain at position B3 for coated aluminum cylinders with variation of coefficient of asymmetry.

# AXIAL STRAIN FOR ELEMENT C1

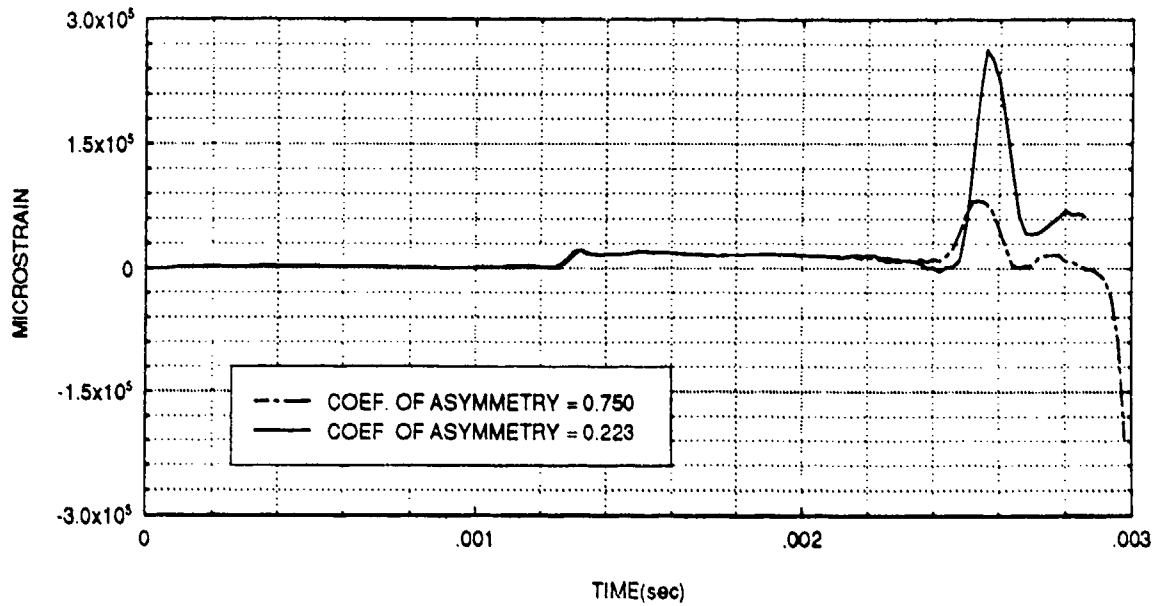


**Figure 74:** Axial strain at position C1 for coated aluminum cylinders with variation of coefficient of asymmetry.

# HOOP STRAIN FOR ELEMENT C1

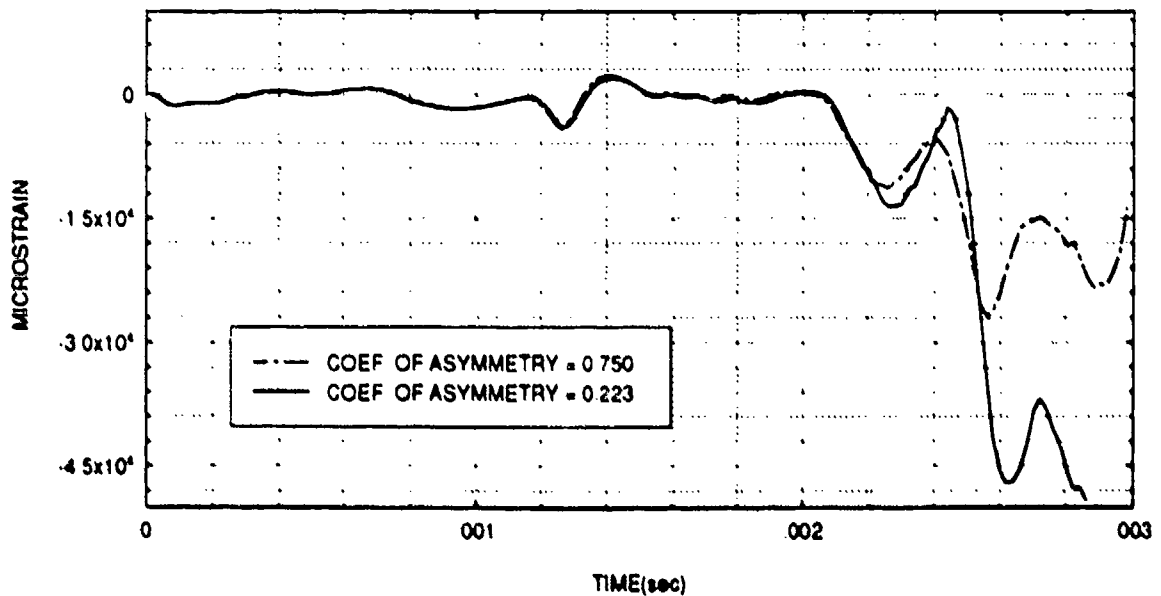


**Figure 75:** Hoop strain at position C1 for coated aluminum cylinders with variation of coefficient of asymmetry.

### AXIAL STRAIN FOR ELEMENT C2

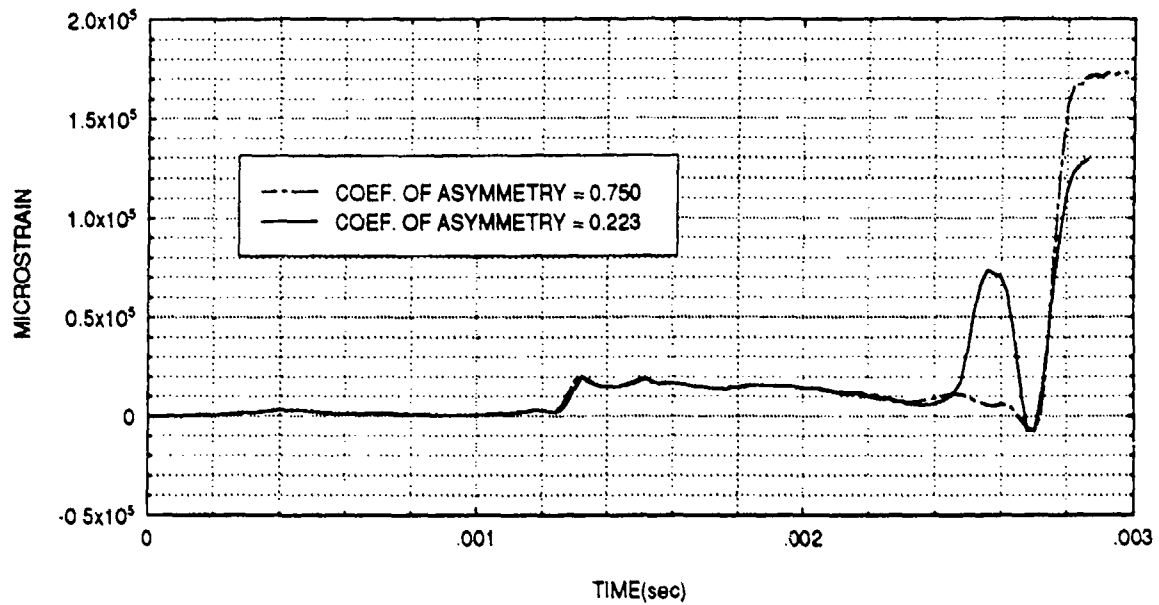


**Figure 76:** Axial strain at position C2 for coated aluminum cylinders with variation of coefficient of asymmetry.

### HOOP STRAIN FOR ELEMENT C2

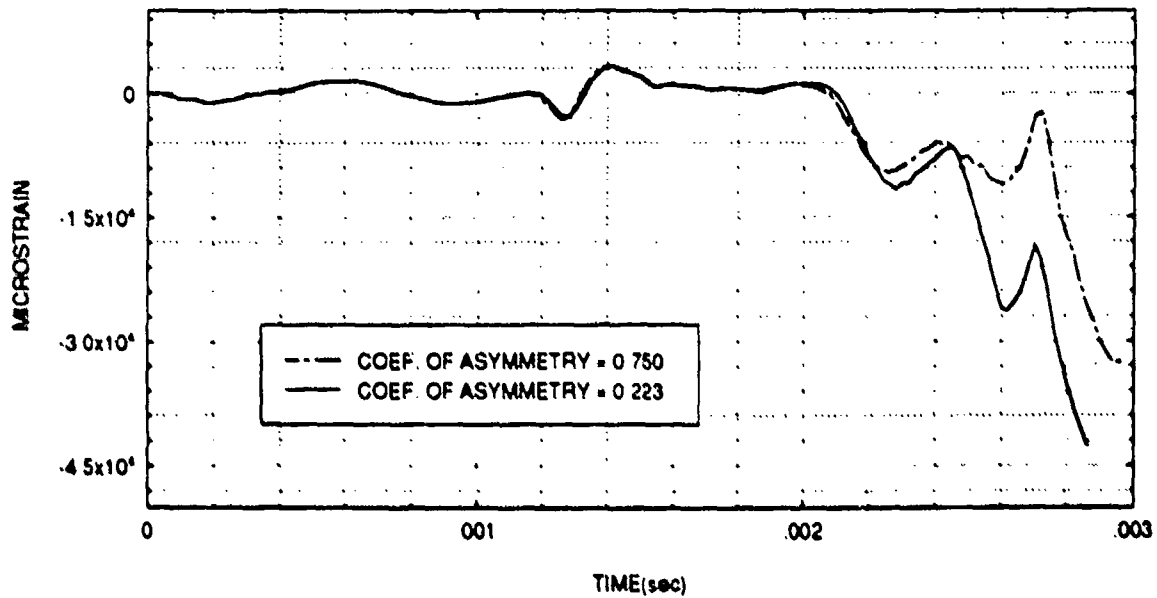


**Figure 77:** Hoop strain at position C2 for coated aluminum cylinders with variation of coefficient of asymmetry.

### AXIAL STRAIN FOR ELEMENT C3

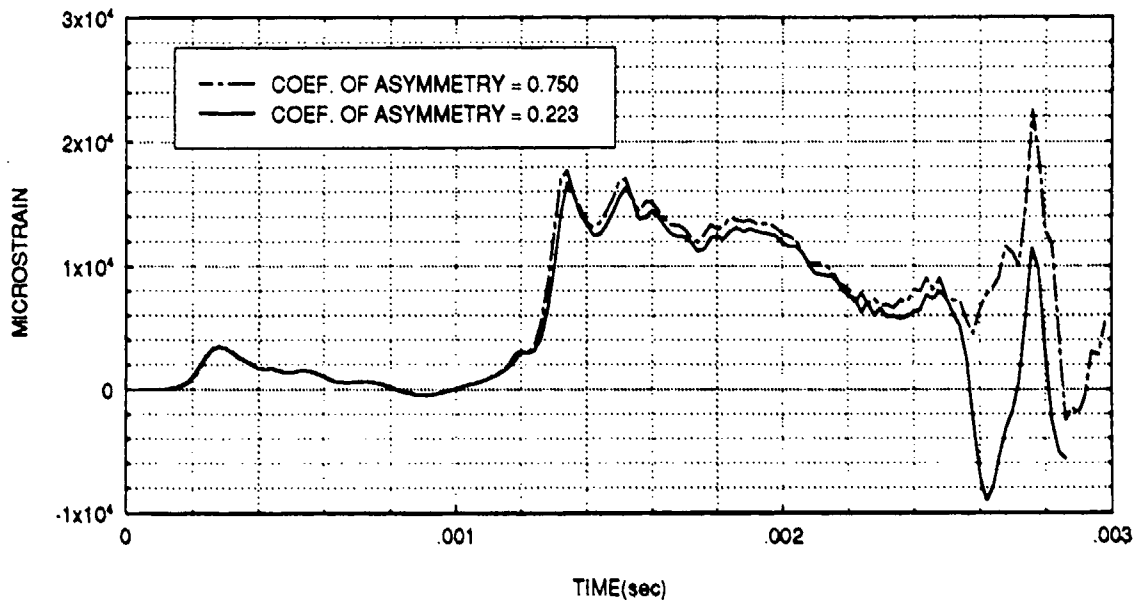


**Figure 78:** Axial strain at position C3 for coated aluminum cylinders with variation of coefficient of asymmetry.

### HOOP STRAIN FOR ELEMENT C3

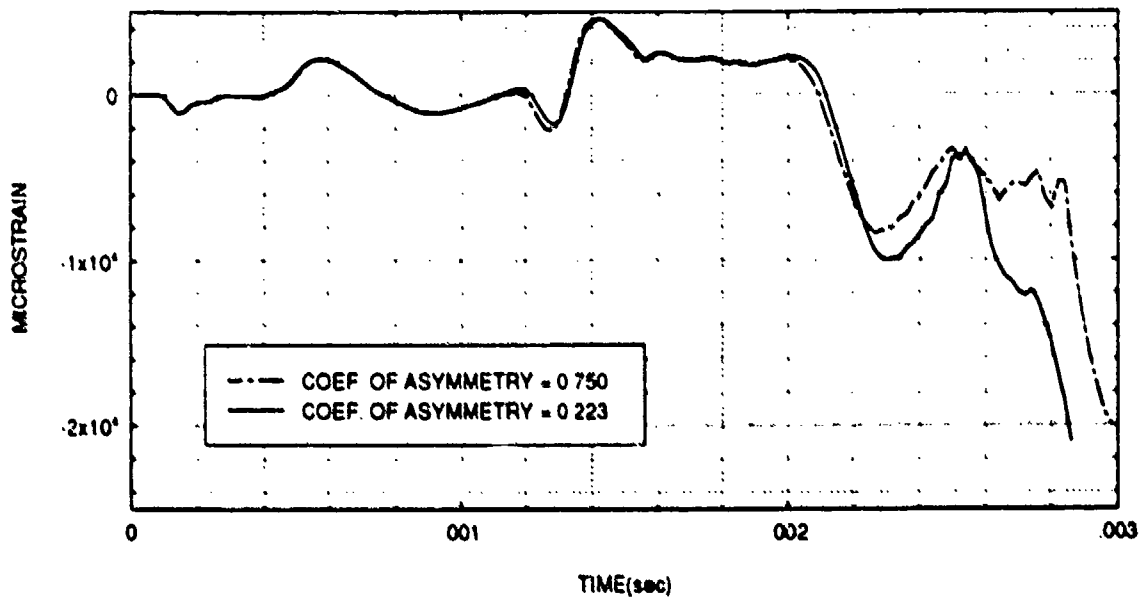


**Figure 79:** Hoop strain at position C3 for coated aluminum cylinders with variation of coefficient of asymmetry.



In the fourth case, the objective was to determine how a variation in the thickness of the aluminum would affect the dynamic response of the coated cylinder. The thickness of the aluminum shell material in Composite Model 1 was changed from 0.250 in. to 0.125 in. and 0.375 in.. The thickness of the aluminum endplate remained constant (1 in. thick). Plots of axial and hoop strain are shown in Figures 80-97. The results show that the thickness variation affected the cylinder differently depending on the location where an element was analyzed. For example, away from the endplate ("A" and "B" elements), hoop strain values were generally higher when the aluminum thickness was reduced, however the thinner aluminum resulted in lower axial strain values near the endplate. To gain a better perspective on what the overall effect was, effective plastic strain was plotted for all elements of interest and is shown in Figures 98-106. These plots showed that the thicker aluminum generally resulted in lower plastic strain at locations away from the endplate but higher plastic strain near the endplate. Aluminum deformation is shown in Figure 107 for the three different thickness cases. Deformations were scaled by a factor of five. It can not be deduced which pattern of deformation represents the most severe affect. The internal energy of the aluminum shell material was also plotted and is shown in Figure 108. The results indicate that as the metal thickness was reduced, the internal energy was also reduced. Results of this study seem

# AXIAL STRAIN FOR ELEMENT A1

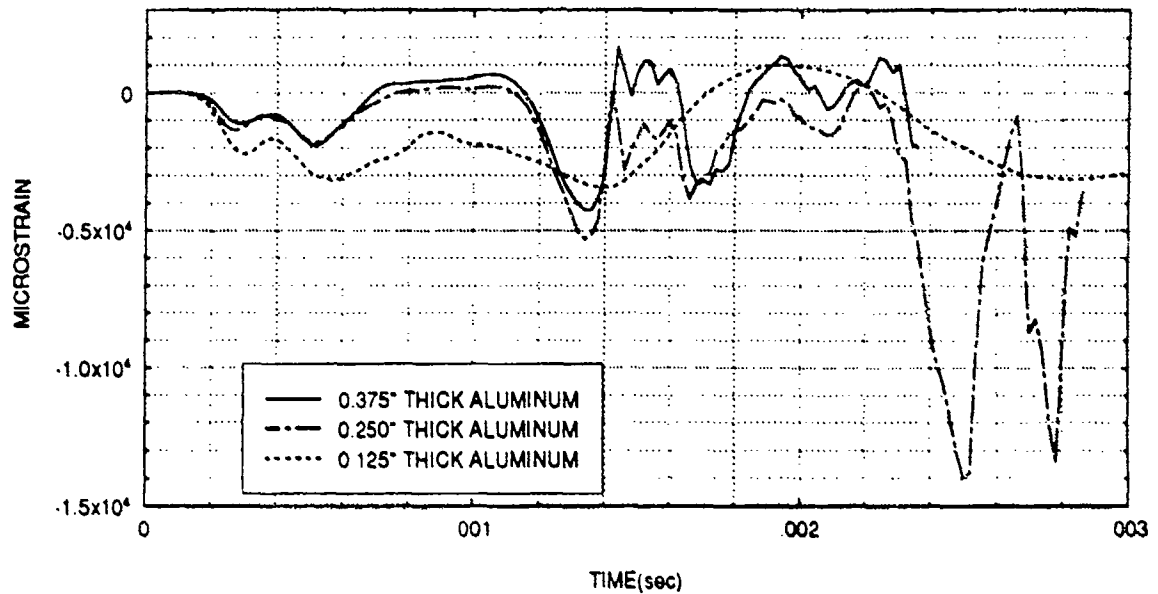


**Figure 80:** Axial strain at position A1 for coated cylinders with variation of aluminum shell thickness.

# HOOP STRAIN FOR ELEMENT A1

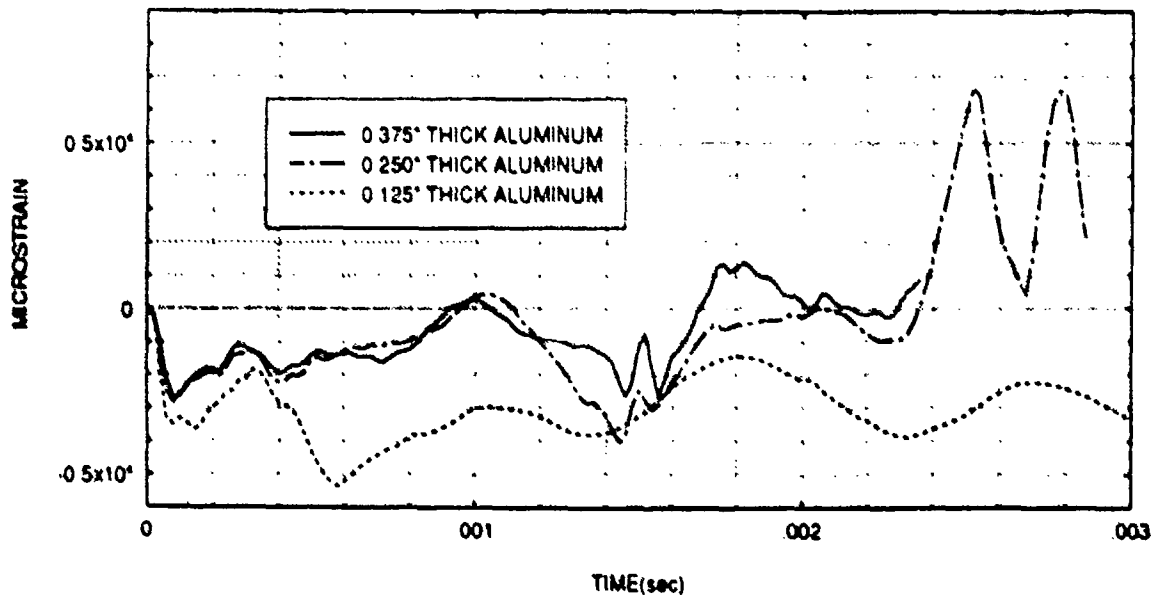


**Figure 81:** Hoop strain at position A1 for coated cylinders with variation of aluminum shell thickness.

### AXIAL STRAIN FOR ELEMENT A2

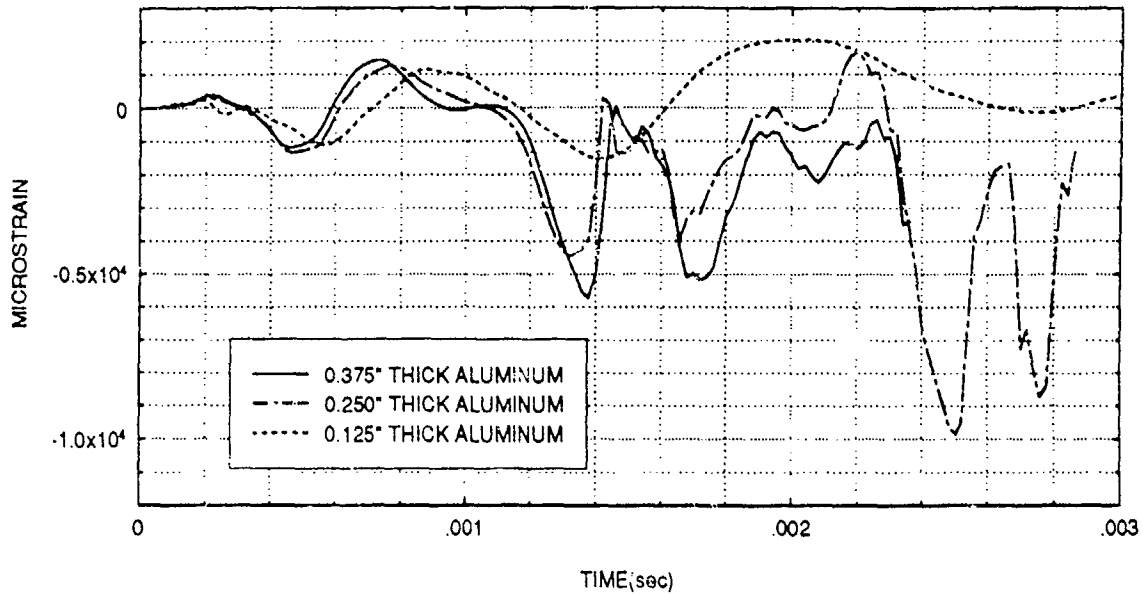


**Figure 82:** Axial strain at position A2 for coated cylinders with variation of aluminum shell thickness.

### HOOP STRAIN FOR ELEMENT A2

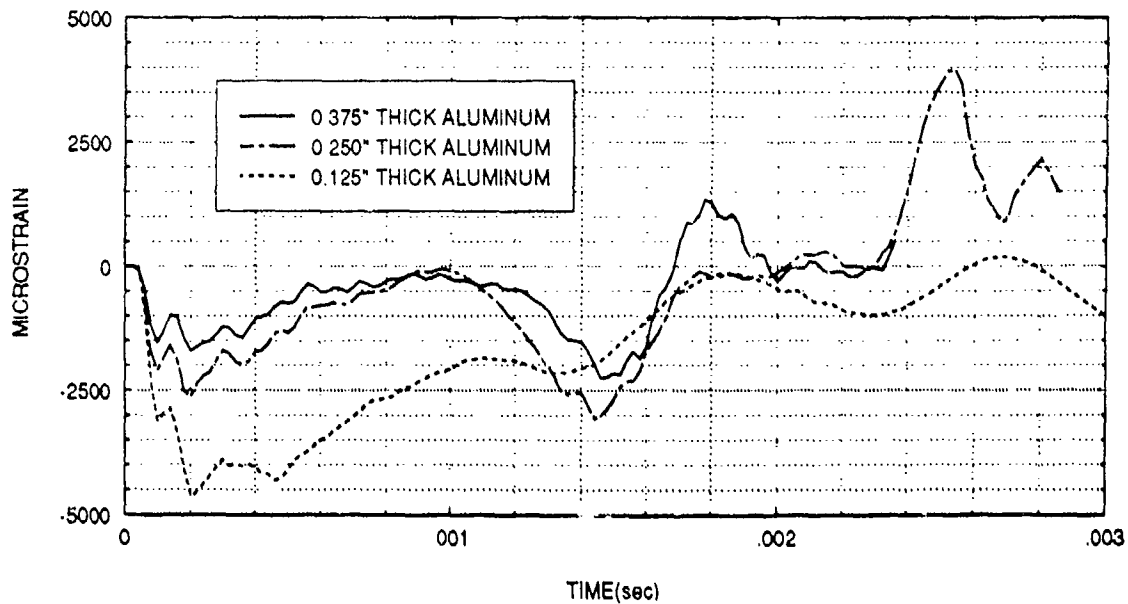


**Figure 83:** Hoop strain at position A2 for coated cylinders with variation of aluminum shell thickness.

### AXIAL STRAIN FOR ELEMENT A3

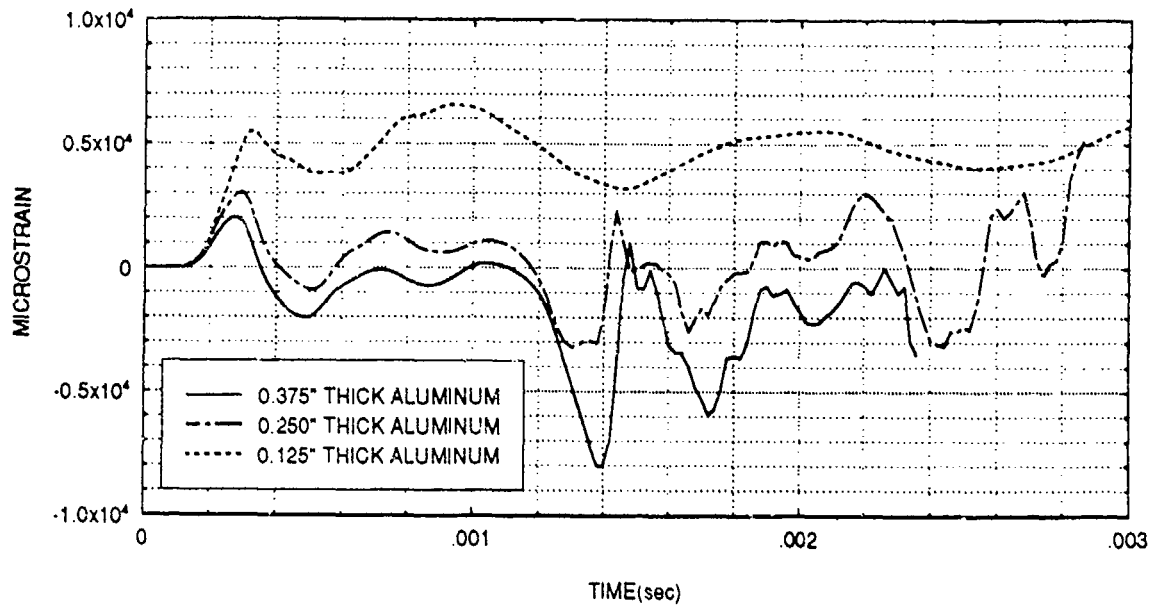


**Figure 84:** Axial strain at position A3 for coated cylinders with variation of aluminum shell thickness.

### HOOP STRAIN FOR ELEMENT A3

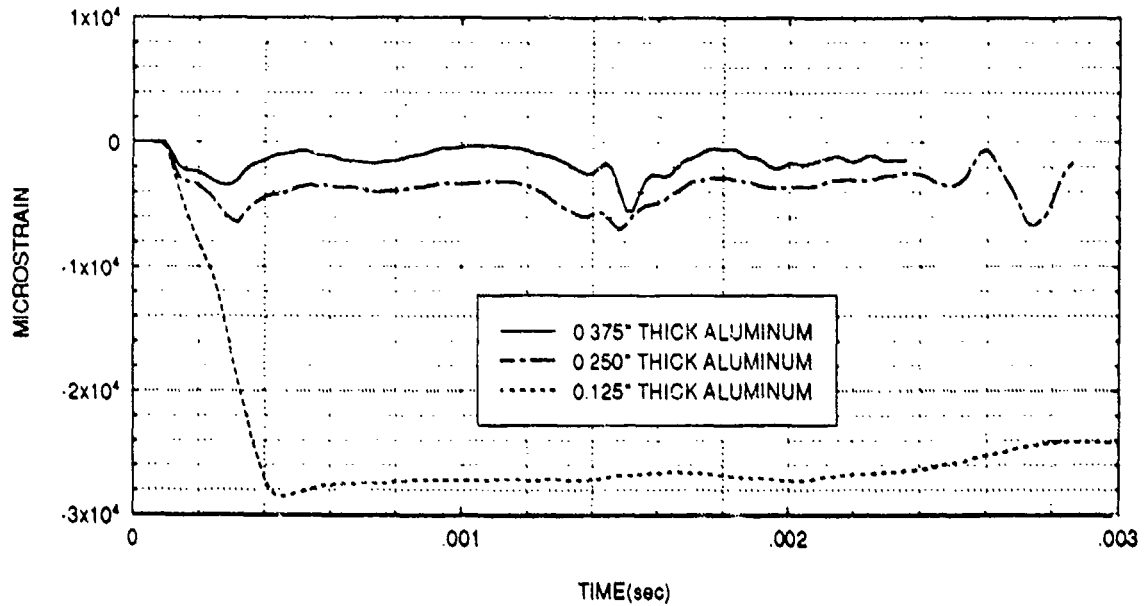


**Figure 85:** Hoop strain at position A3 for coated cylinders with variation of aluminum shell thickness.

# AXIAL STRAIN FOR ELEMENT B1

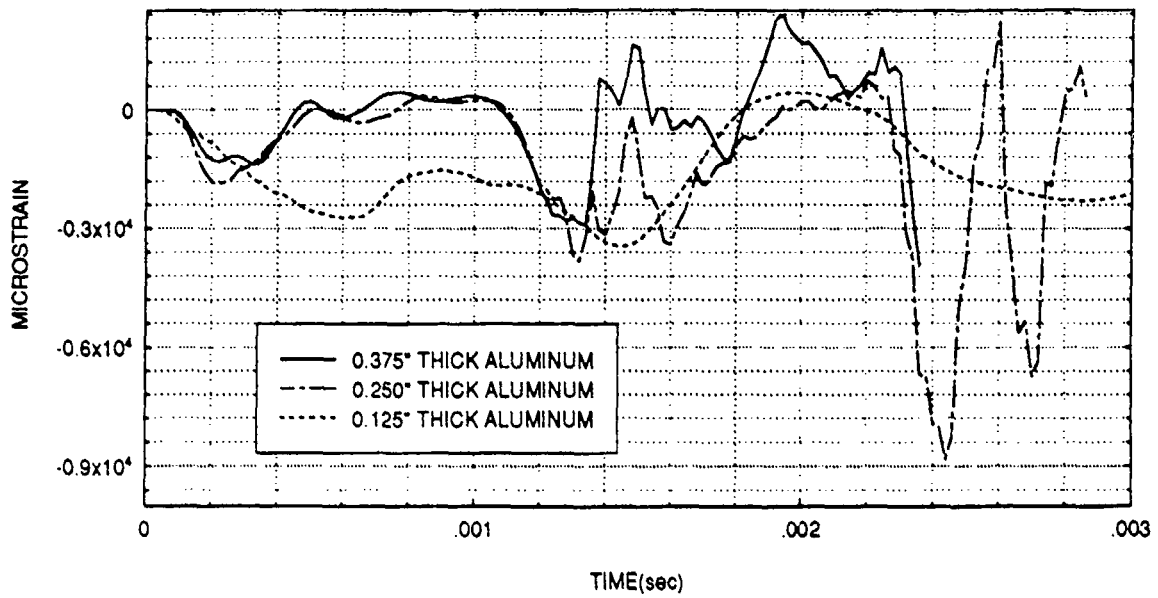


**Figure 86:** Axial strain at position B1 for coated cylinders with variation of aluminum shell thickness.

# HOOP STRAIN FOR ELEMENT B1

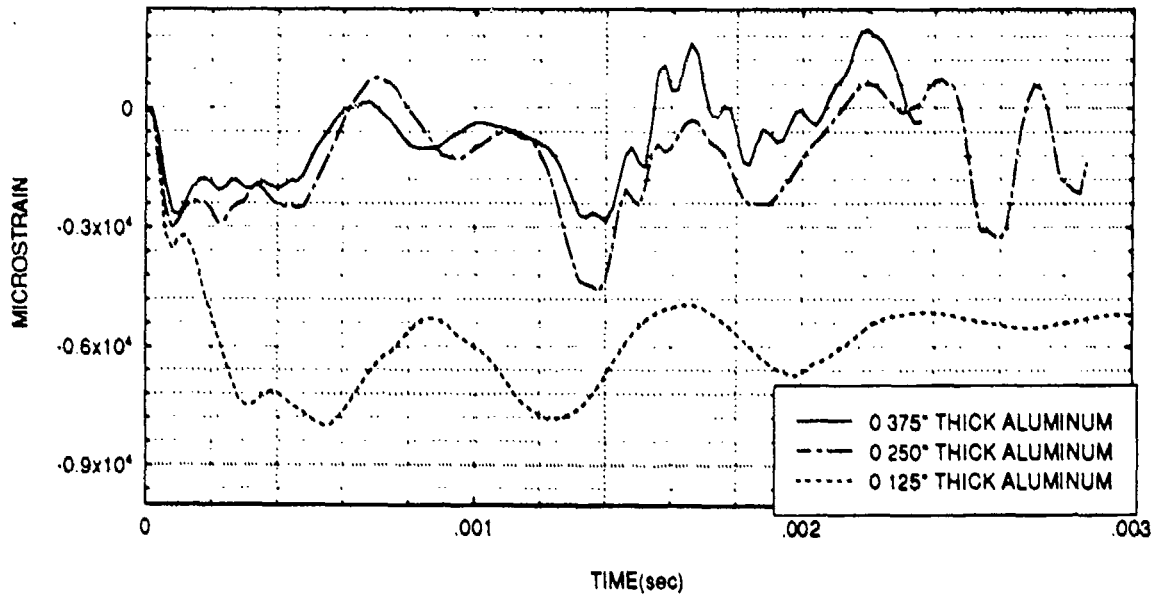


**Figure 87:** Hoop strain at position B1 for coated cylinders with variation of aluminum shell thickness.

### AXIAL STRAIN FOR ELEMENT B2

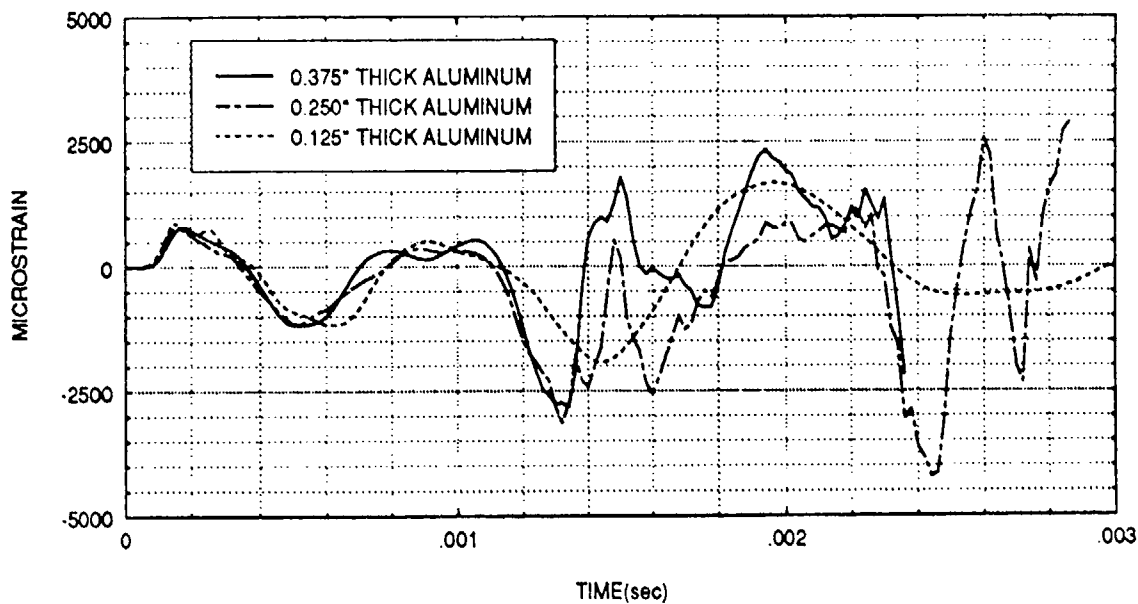


**Figure 88:** Axial strain at position B2 for coated cylinders with variation of aluminum shell thickness.

### HOOP STRAIN FOR ELEMENT B2

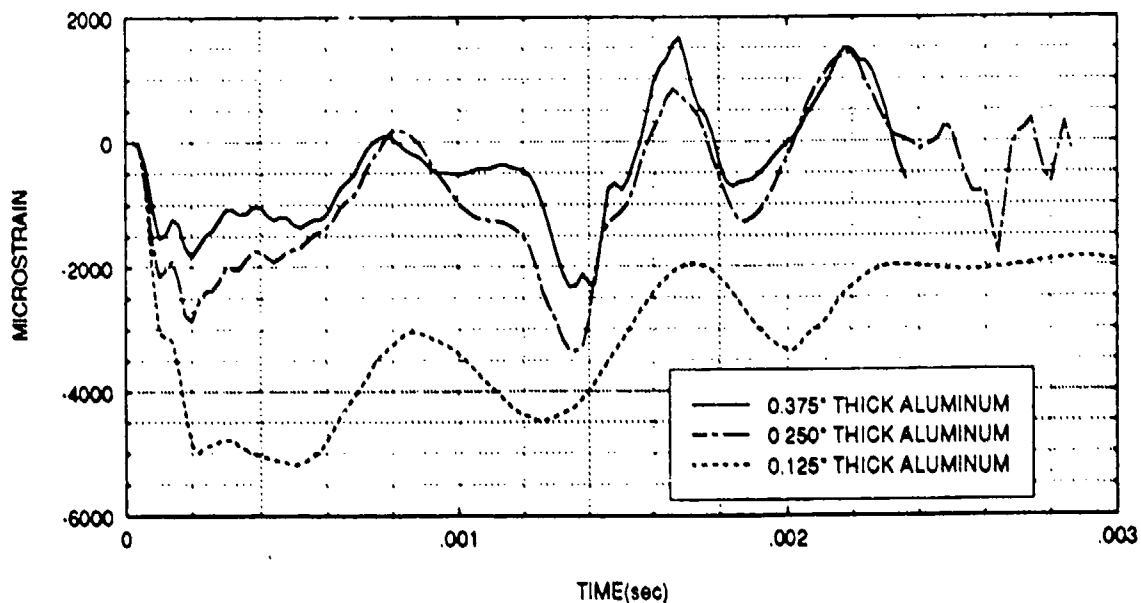


**Figure 89:** Hoop strain at position B2 for coated cylinders with variation of aluminum shell thickness.

### AXIAL STRAIN FOR ELEMENT B3

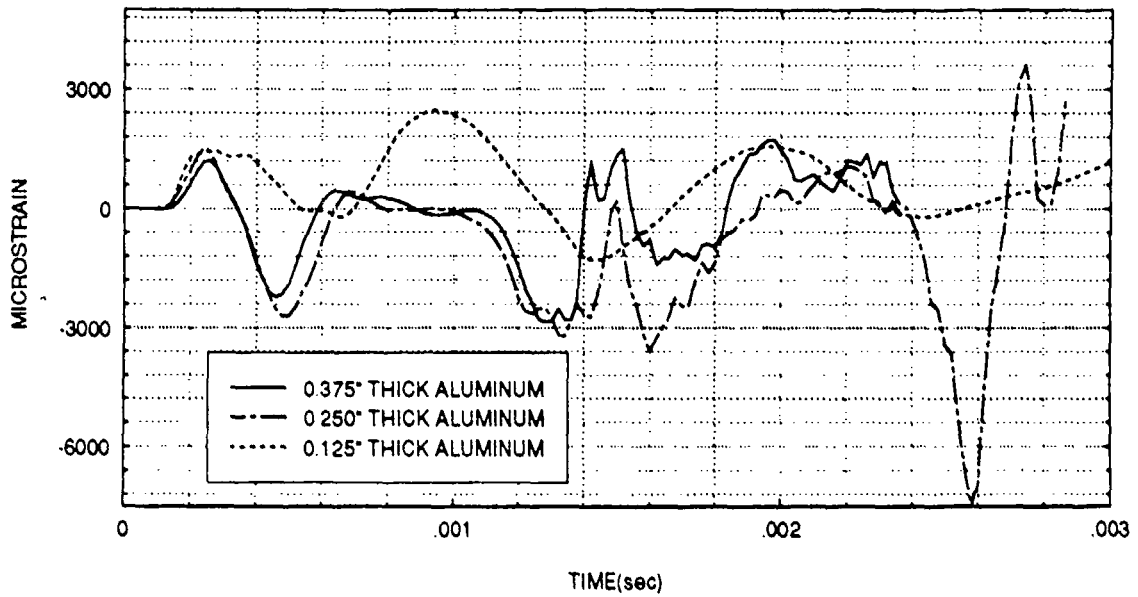


**Figure 90:** Axial strain at position B3 for coated cylinders with variation of aluminum shell thickness.

### HOOP STRAIN FOR ELEMENT B3

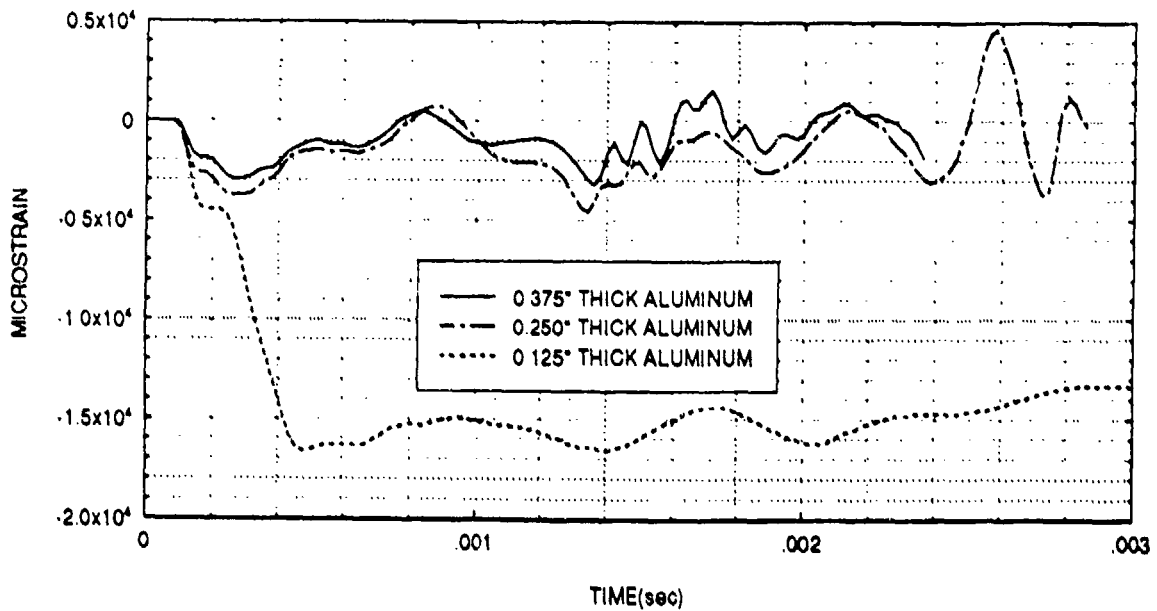


**Figure 91:** Hoop strain at position B3 for coated cylinders with variation of aluminum shell thickness.

### AXIAL STRAIN FOR ELEMENT C1

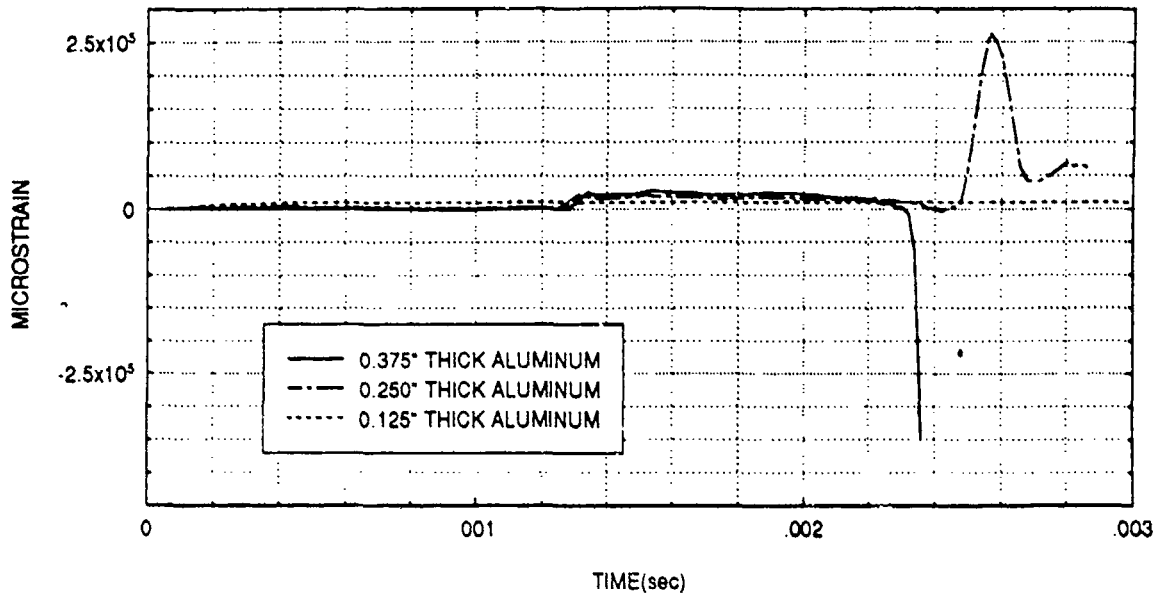


**Figure 92:** Axial strain at position C1 for coated cylinders with variation of aluminum shell thickness.

### HOOP STRAIN FOR ELEMENT C1

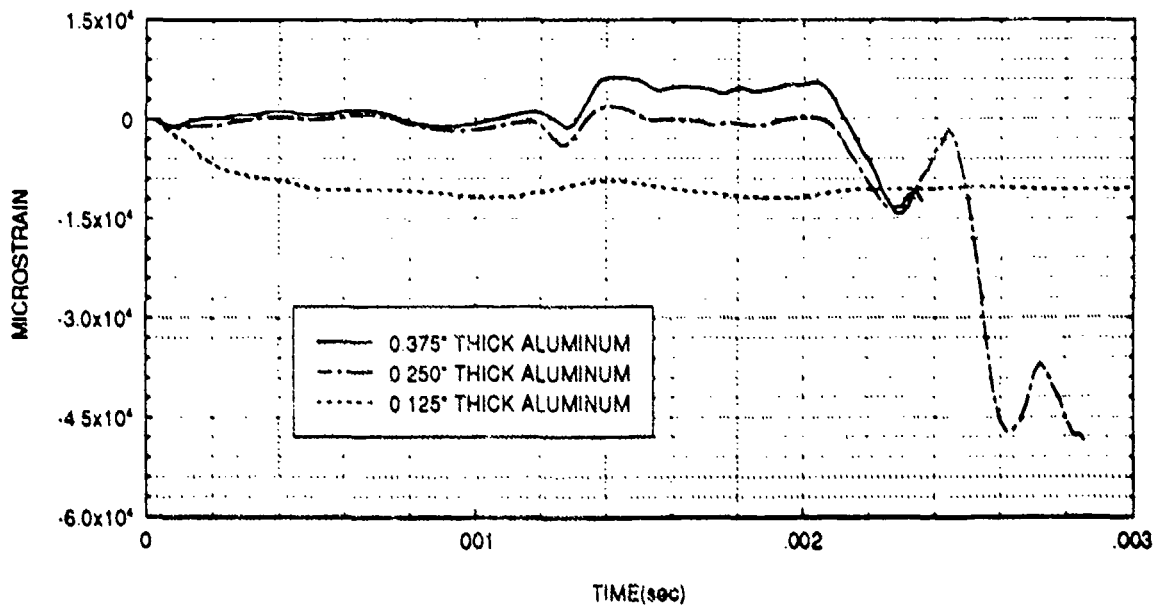


**Figure 93:** Hoop strain at position C1 for coated cylinders with variation of aluminum shell thickness.



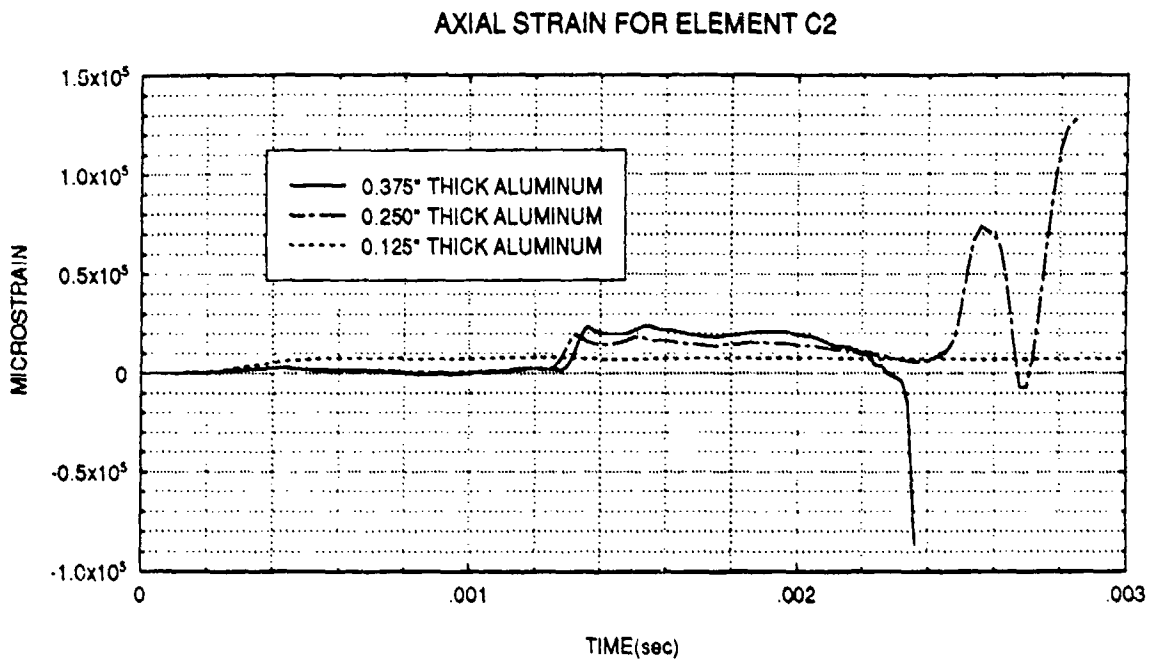


**Figure 94:** Axial strain at position C2 for coated cylinders with variation of aluminum shell thickness.

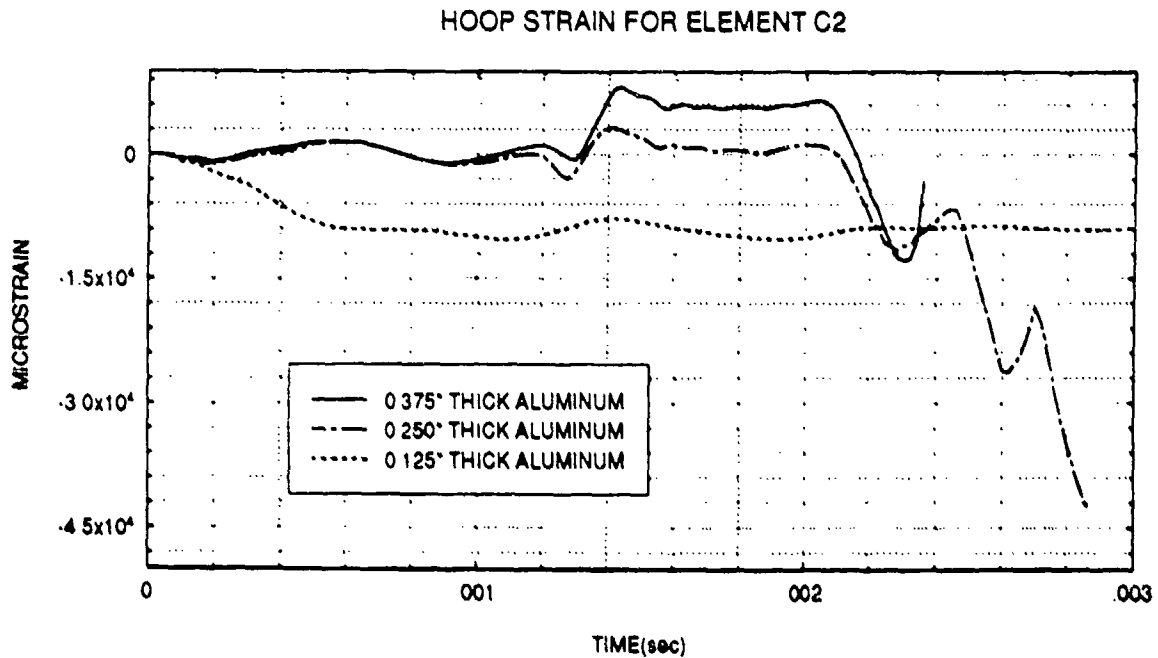


**Figure 95:** Hoop strain at position C2 for coated cylinders with variation of aluminum shell thickness.

### AXIAL STRAIN FOR ELEMENT C3

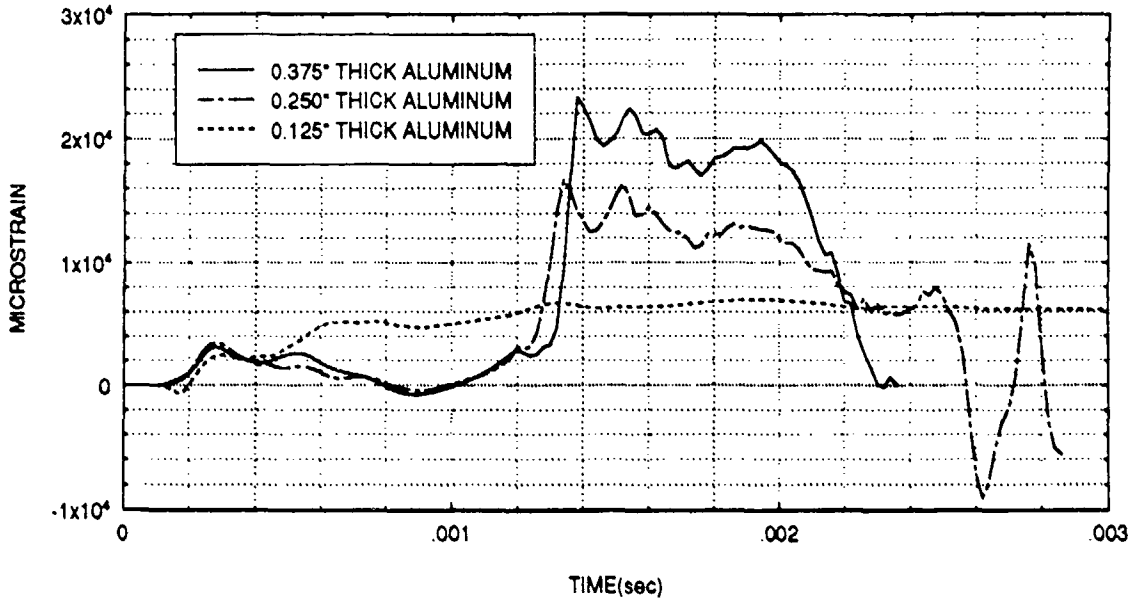


**Figure 96:** Axial strain at position C3 for coated cylinders with variation of aluminum shell thickness.

### HOOP STRAIN FOR ELEMENT C3

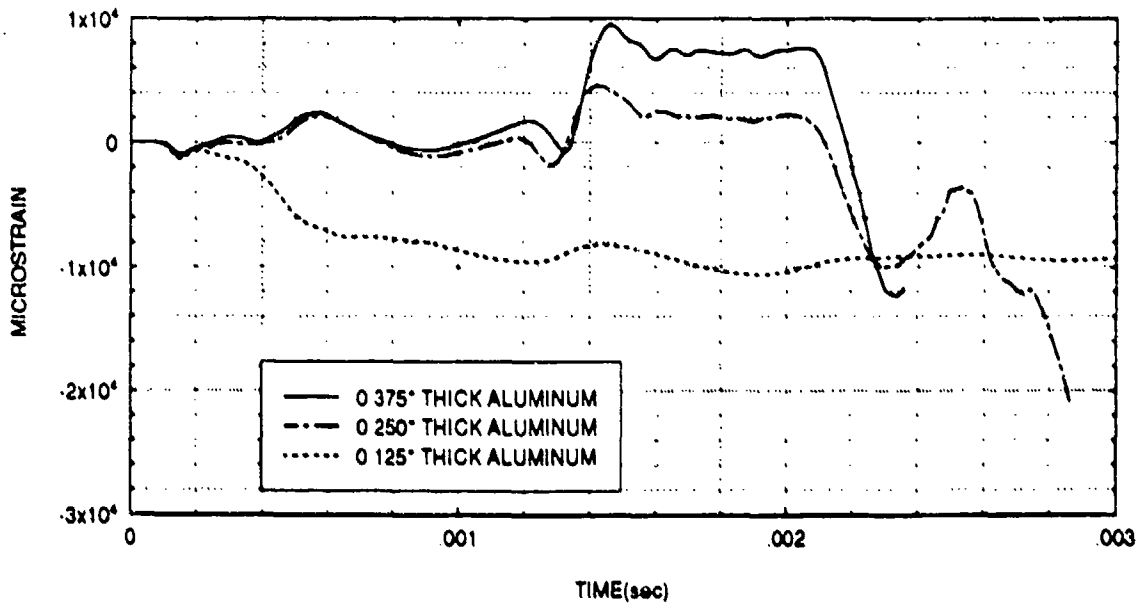


**Figure 97:** Hoop strain at position C3 for coated cylinders with variation of aluminum shell thickness.

### EFFECTIVE PLASTIC STRAIN FOR ELEMENT A1

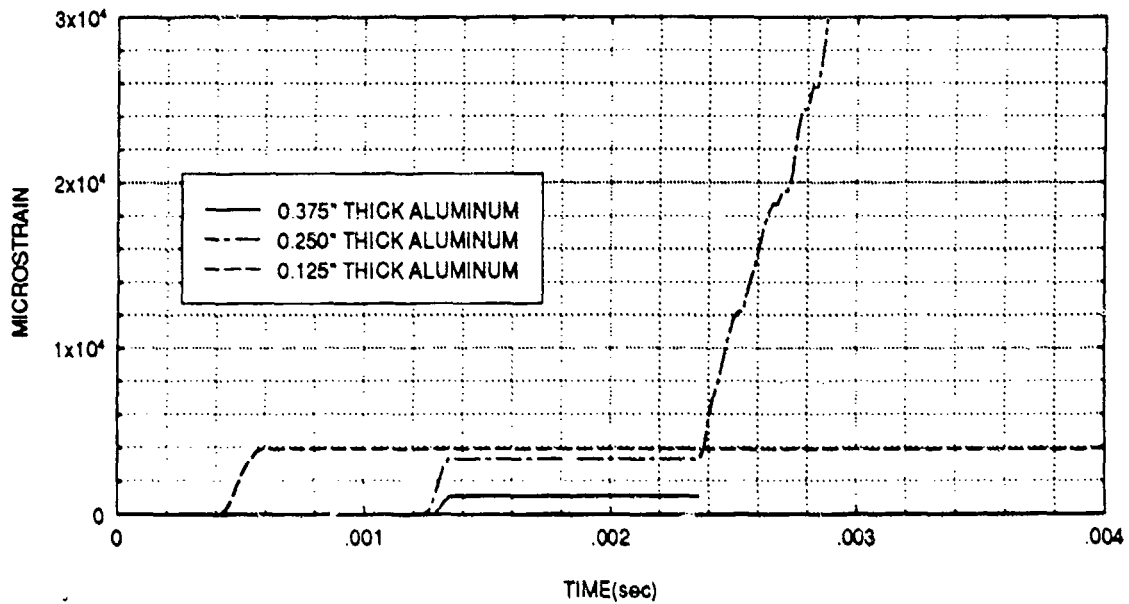


**Figure 98:** Effective plastic strain at position A1 for coated cylinders with variation of aluminum shell thickness.

### EFFECTIVE PLASTIC STRAIN FOR ELEMENT A2

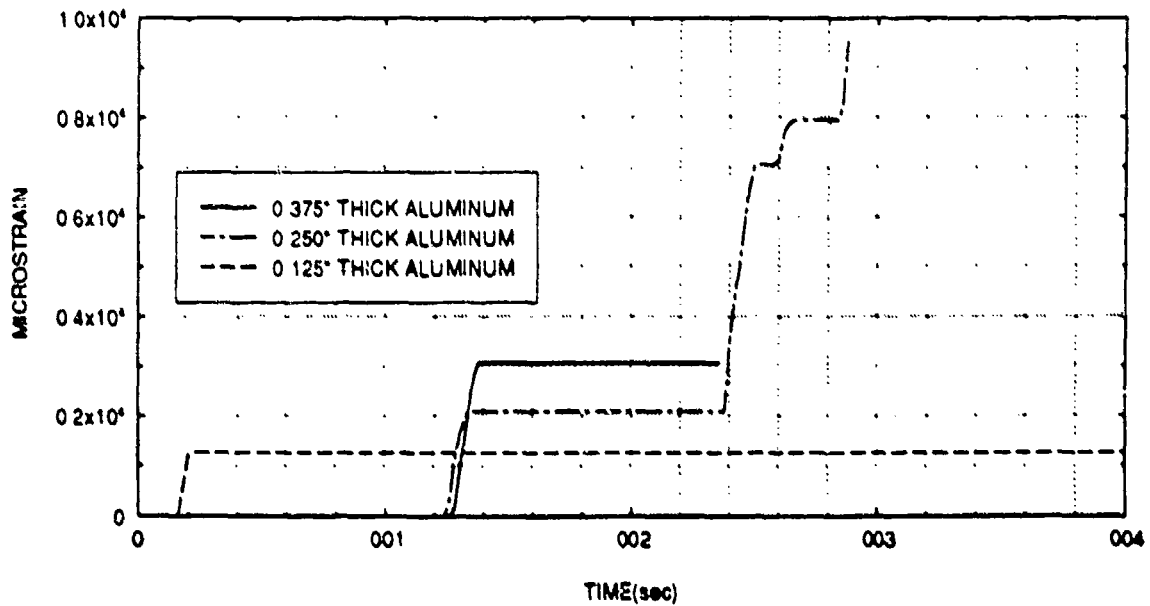


**Figure 99:** Effective plastic strain at position A2 for coated cylinders with variation of aluminum shell thickness.

### EFFECTIVE PLASTIC STRAIN FOR ELEMENT A3

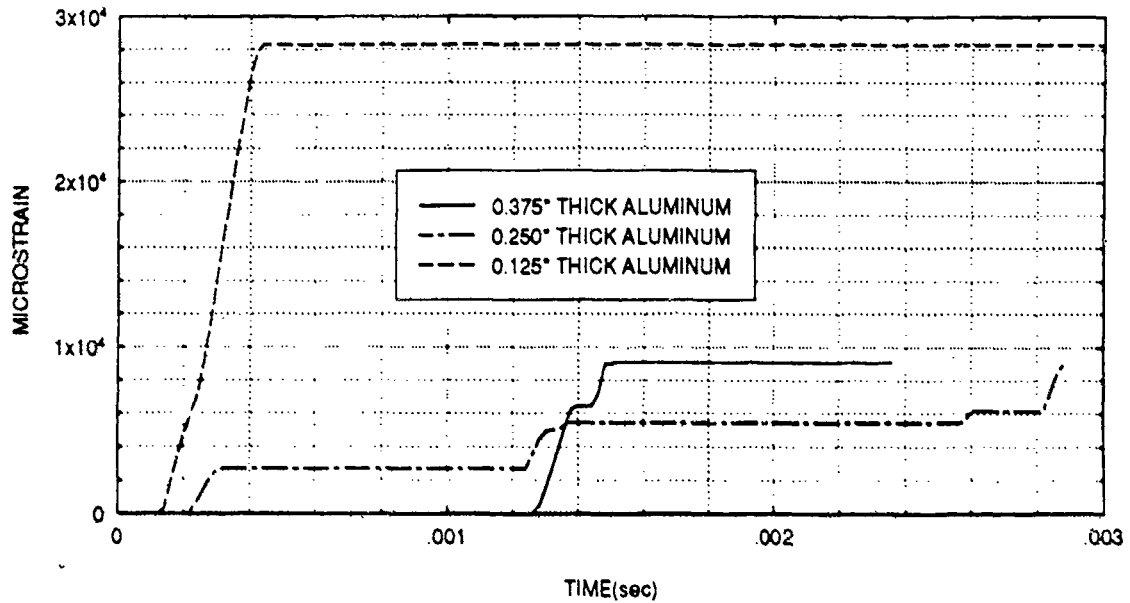


**Figure 100:** Effective plastic strain at position A3 for coated cylinders with variation of aluminum shell thickness.

### EFFECTIVE PLASTIC STRAIN FOR ELEMENT B1

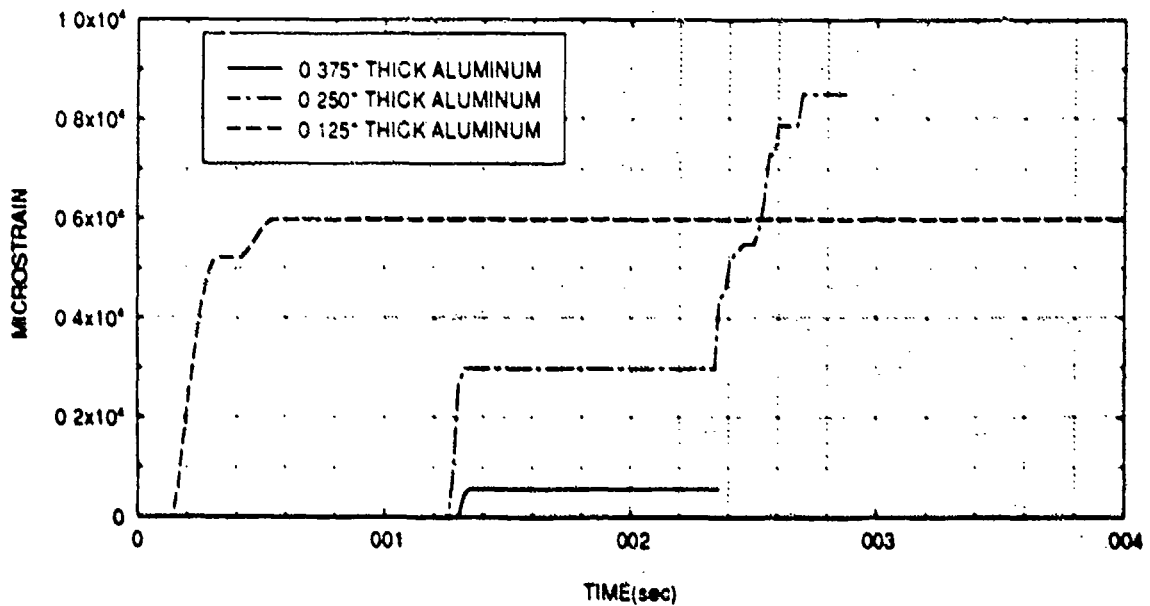


**Figure 101:** Effective plastic strain at position B1 for coated cylinders with variation of aluminum shell thickness.

### EFFECTIVE PLASTIC STRAIN FOR ELEMENT B2

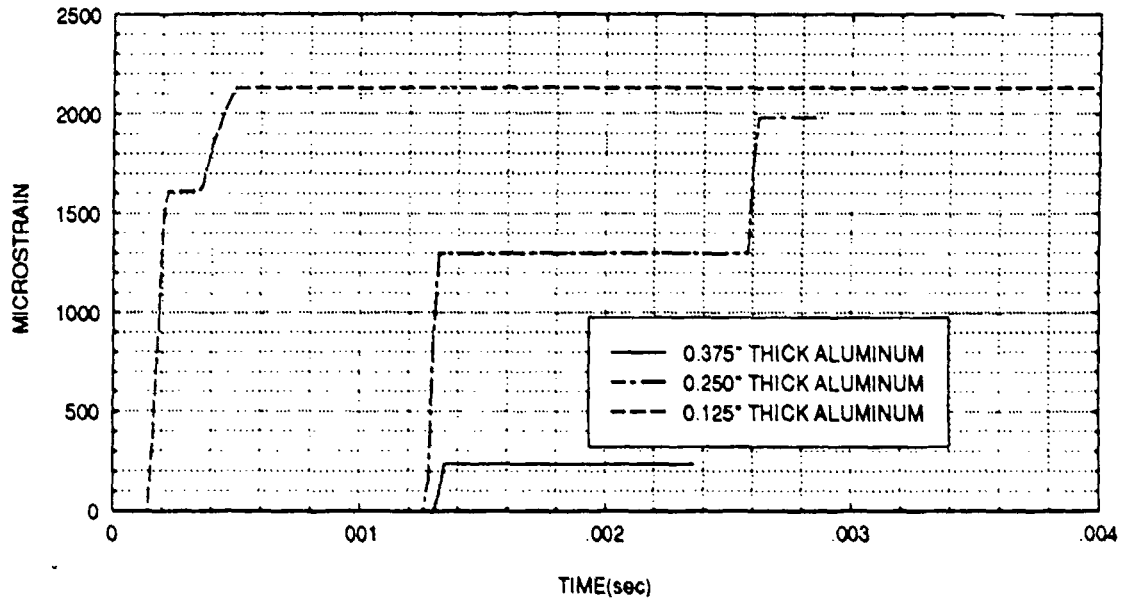


**Figure 102:** Effective plastic strain at position B2 for coated cylinders with variation of aluminum shell thickness.

### EFFECTIVE PLASTIC STRAIN FOR ELEMENT B3

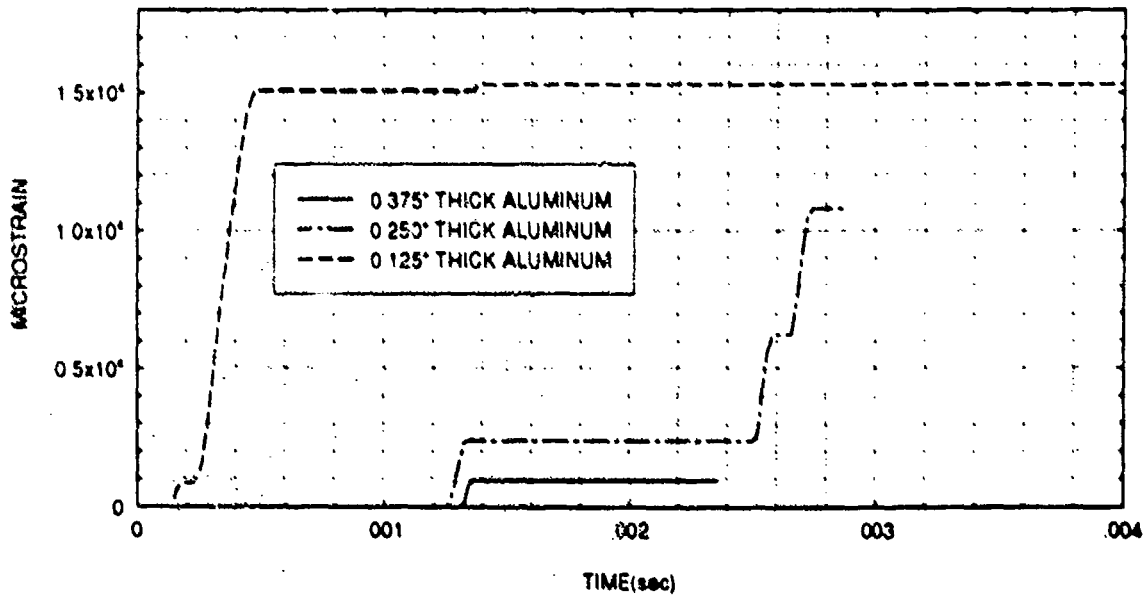


**Figure 103:** Effective plastic strain at position B3 for coated cylinders with variation of aluminum shell thickness.

# EFFECTIVE PLASTIC STRAIN FOR ELEMENT C1

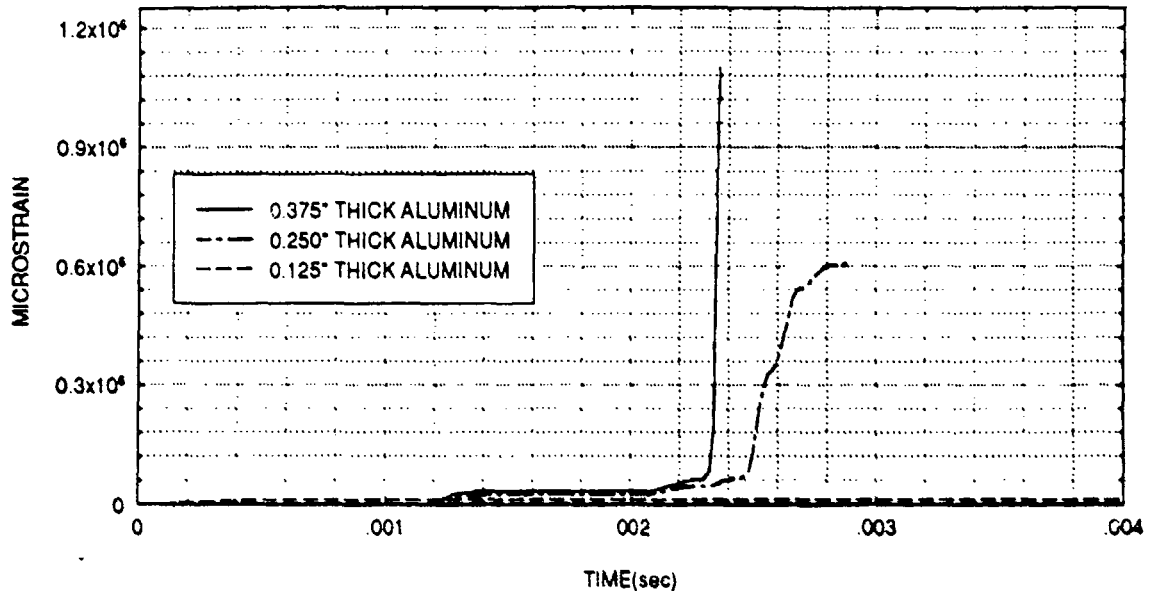


**Figure 104:** Effective plastic strain at position C1 for coated cylinders with variation of aluminum shell thickness.

# EFFECTIVE PLASTIC STRAIN FOR ELEMENT C2

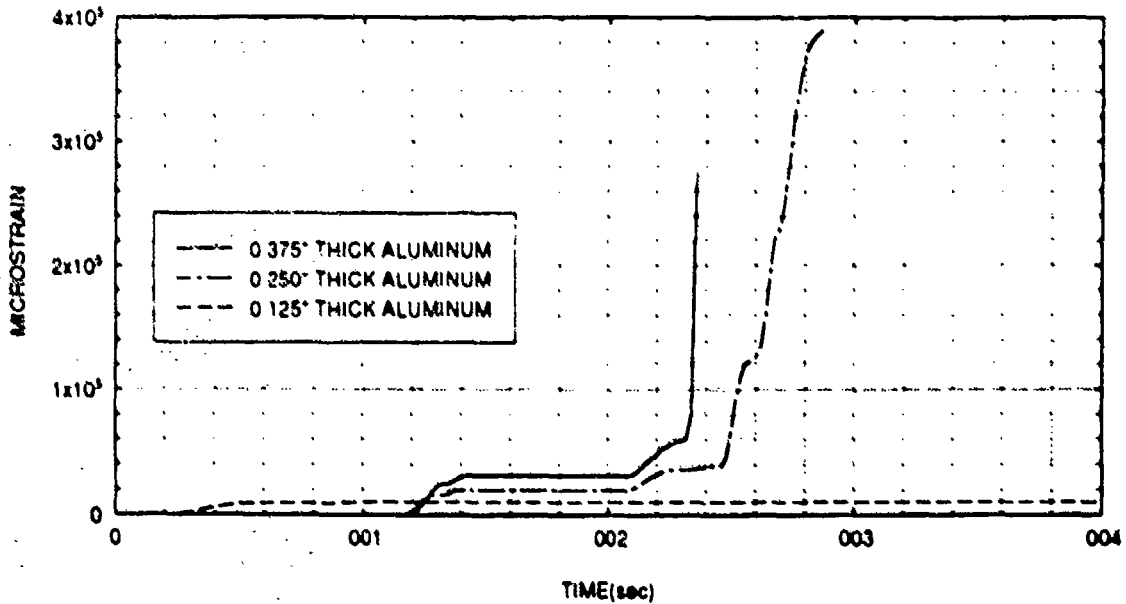


**Figure 105:** Effective plastic strain at position C2 for coated cylinders with variation of aluminum shell thickness.

### EFFECTIVE PLASTIC STRAIN FOR ELEMENT C3

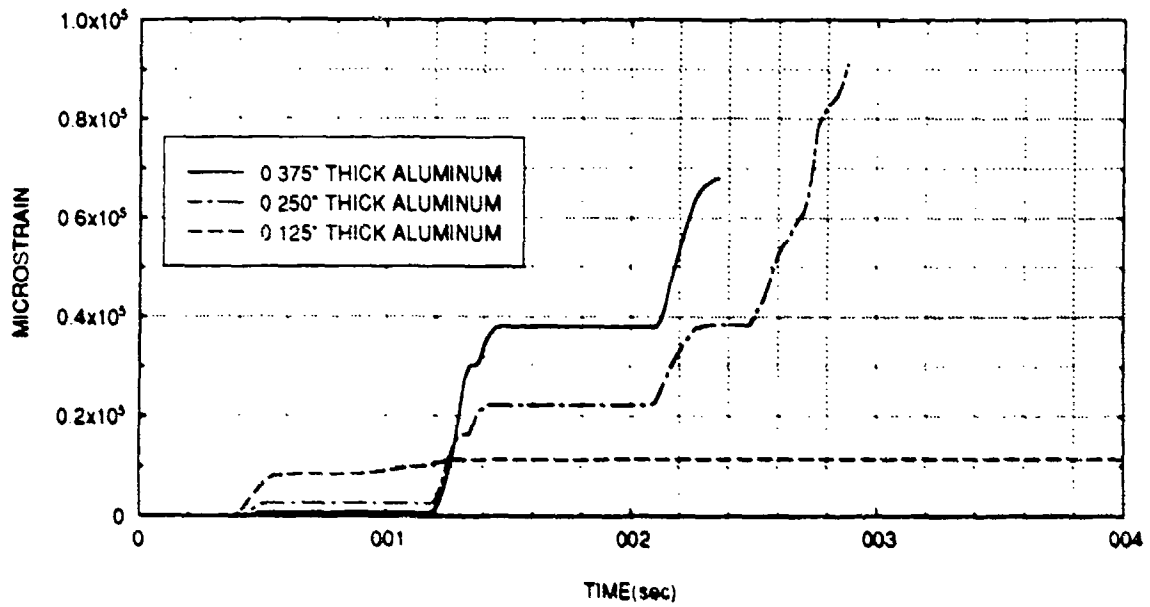
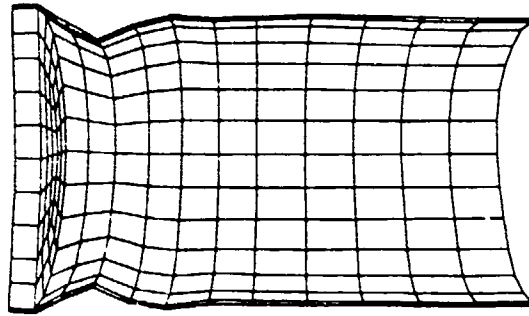
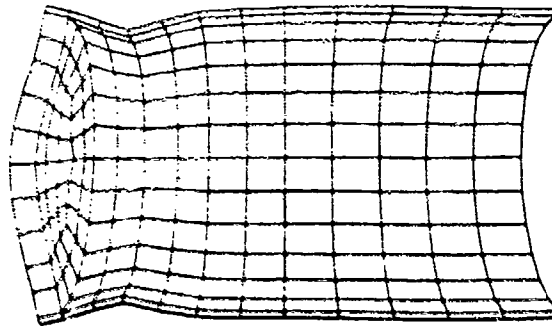


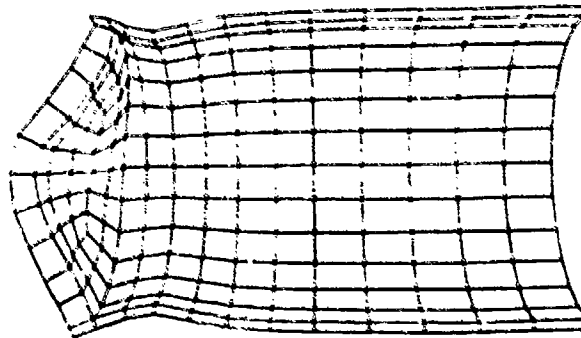
**Figure 106:** Effective plastic strain at position C3 for coated cylinders with variation of aluminum shell thickness.



0.125" THICK ALUMINUM (DISPL. SCALE FACTOR OF 5)



0.250" THICK ALUMINUM (DISPL. SCALE FACTOR OF 5)



0.375" THICK ALUMINUM (DISPL. SCALE FACTOR OF 5)

**Figure 107:** Deformation of coated cylinders with variation of aluminum shell thickness at 2.34 msec..



# INTERNAL ENERGY OF ALUMINUM SHELL MATERIAL

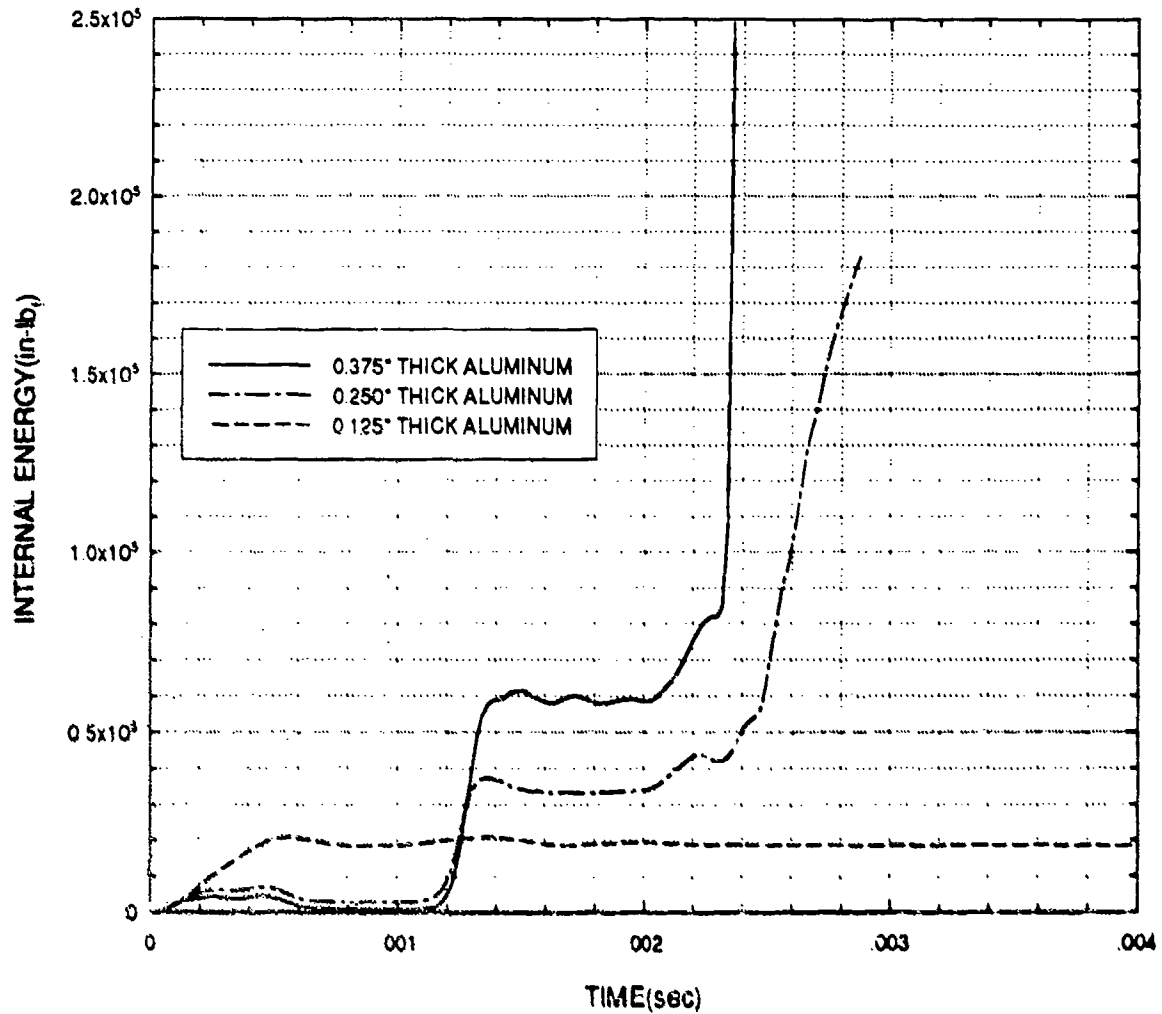


**Figure 108:** Internal energy of aluminum shell material of coated cylinders with variation of aluminum shell thickness.

to indicate that variations of metal thickness have a local effect on response and are greatly influenced by inertia effects.

In the fifth case, the objective was to determine how a variation in the coating thickness would affect the dynamic response of the cylinder. The thickness of the tread stock rubber in Composite Model 1 was changed from 0.250 in. to 0.125 in. and to 0.375 in.. Axial and hoop strain values are plotted and are shown in Figures 109-126. At nearly all locations, the response of the cylinder significantly improved when the rubber thickness was increased but was adversely affected when the rubber thickness was decreased. Early termination of the problem in the thin rubber case was due to a severe distortion of the model mesh. The effects of rubber thickness are also evident in the values of effective plastic strain that were achieved and are shown in Figures 127-135. Differences in response can be seen in the deformation of the cylinder for each case and are shown in Figures 136 and 137. The effect is more dramatic at late time and can be seen more clearly in the response at 2.86 msec. (Figure 137). Cylinder response was also examined for a rubber thickness of 0.500 in. and it was found that the response of the cylinder improved. Internal energy of the aluminum shell material is plotted for the various rubber thicknesses and is shown in Figure 138. As observed in case 2 (shear modulus variation), the results of this study also support the hypothesis that the dynamic

### AXIAL STRAIN FOR ELEMENT A1

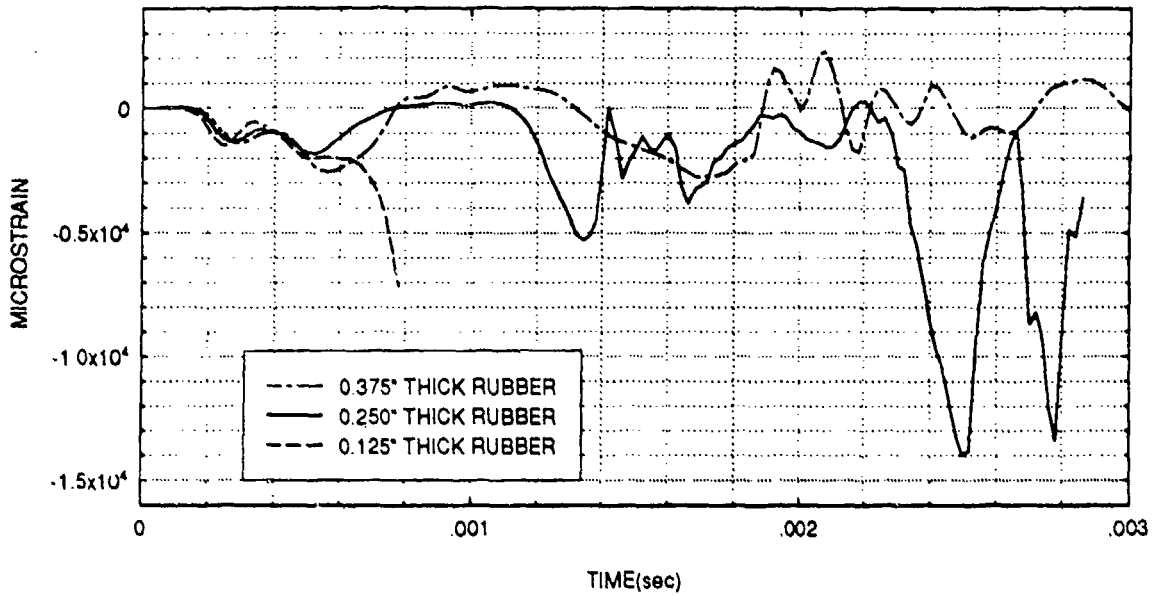


**Figure 109:** Axial strain at position A1 for coated aluminum cylinders with variation of rubber thickness.

### HOOP STRAIN FOR ELEMENT A1

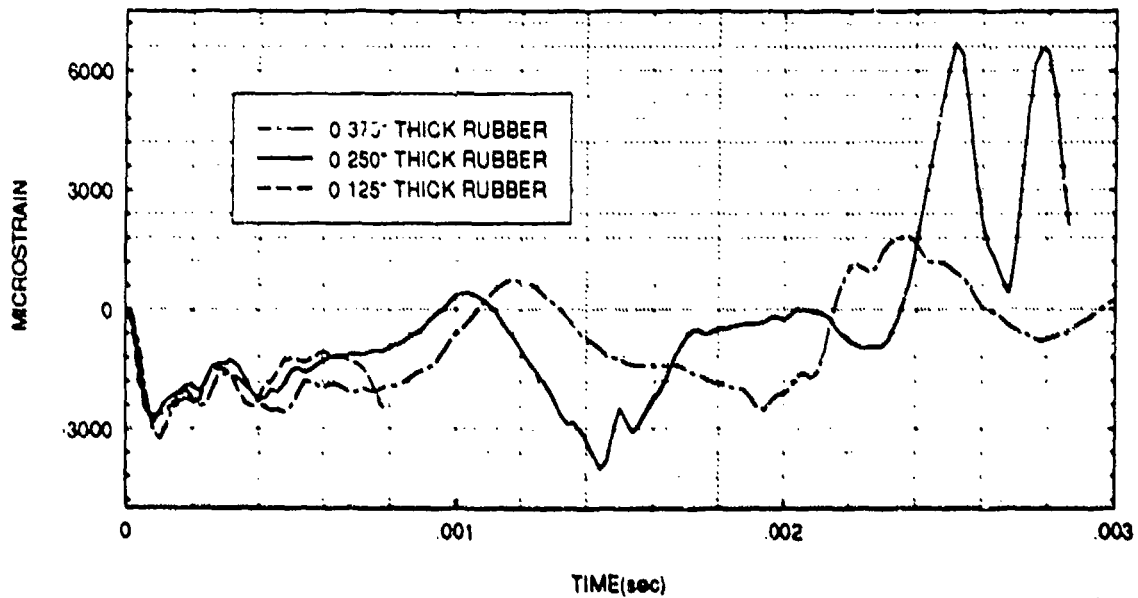


**Figure 110:** Hoop strain at position A1 for coated aluminum cylinders with variation of rubber thickness.

### AXIAL STRAIN FOR ELEMENT A2

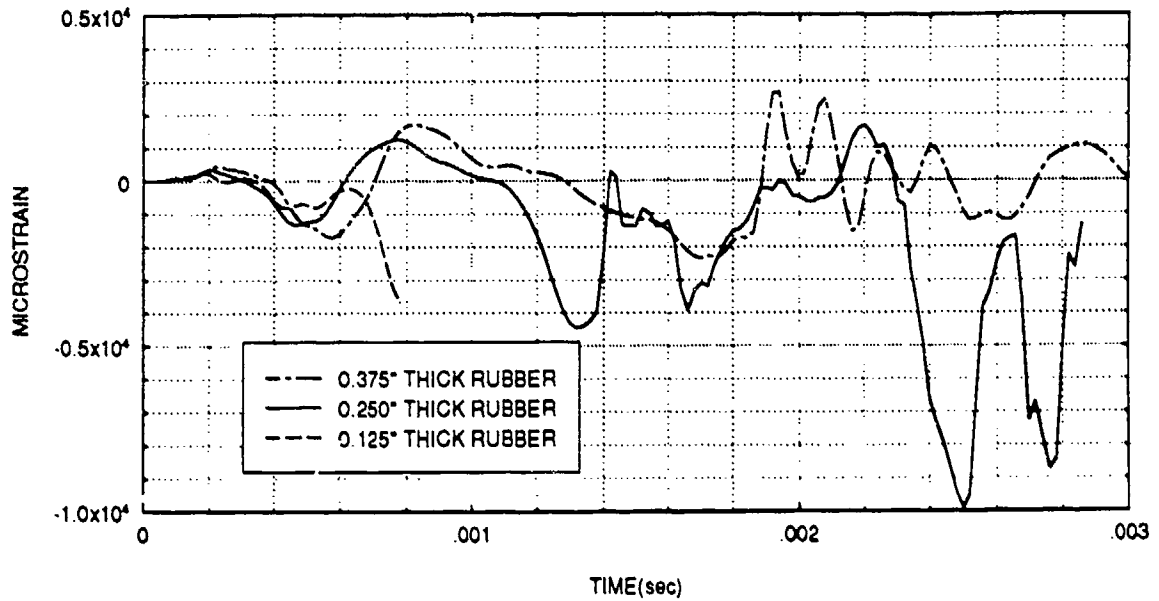


**Figure 111:** Axial strain at position A2 for coated aluminum cylinders with variation of rubber thickness.

### HOOP STRAIN FOR ELEMENT A2

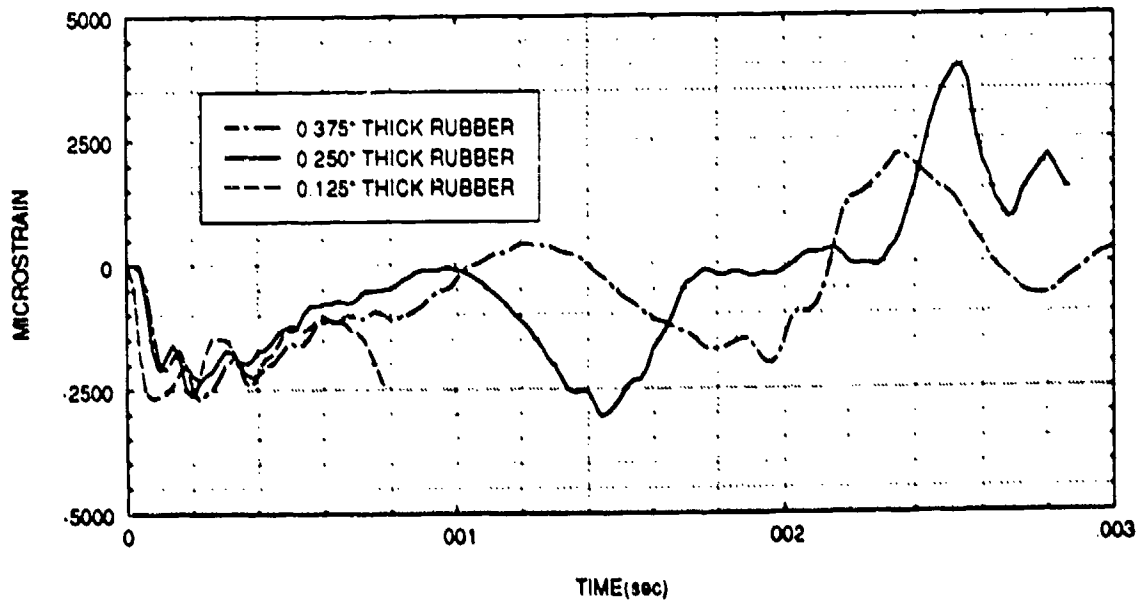


**Figure 112:** Hoop strain at position A2 for coated aluminum cylinders with variation of rubber thickness.

### AXIAL STRAIN FOR ELEMENT A3

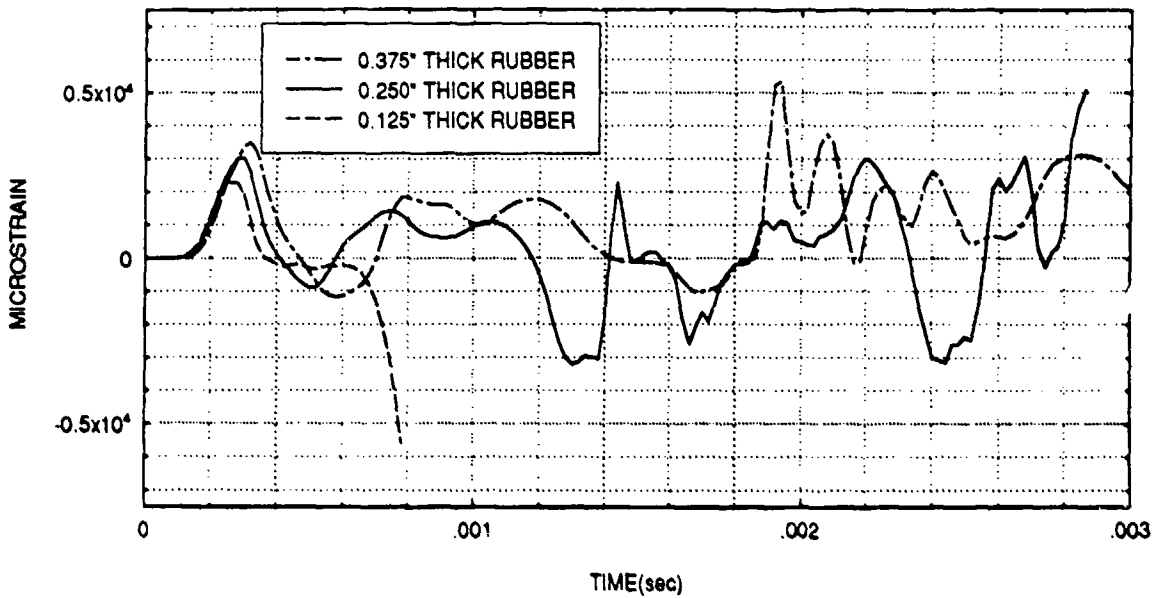


**Figure 113:** Axial strain at position A3 for coated aluminum cylinders with variation of rubber thickness.

### HOOP STRAIN FOR ELEMENT A3

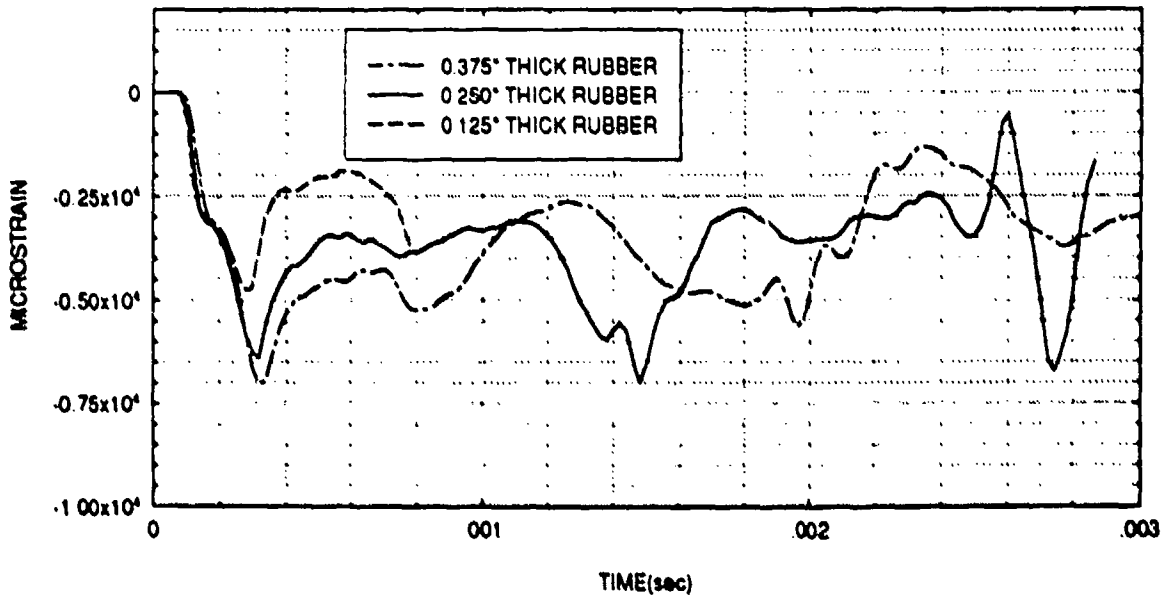


**Figure 114:** Hoop strain at position A3 for coated aluminum cylinders with variation of rubber thickness.

### AXIAL STRAIN FOR ELEMENT B1

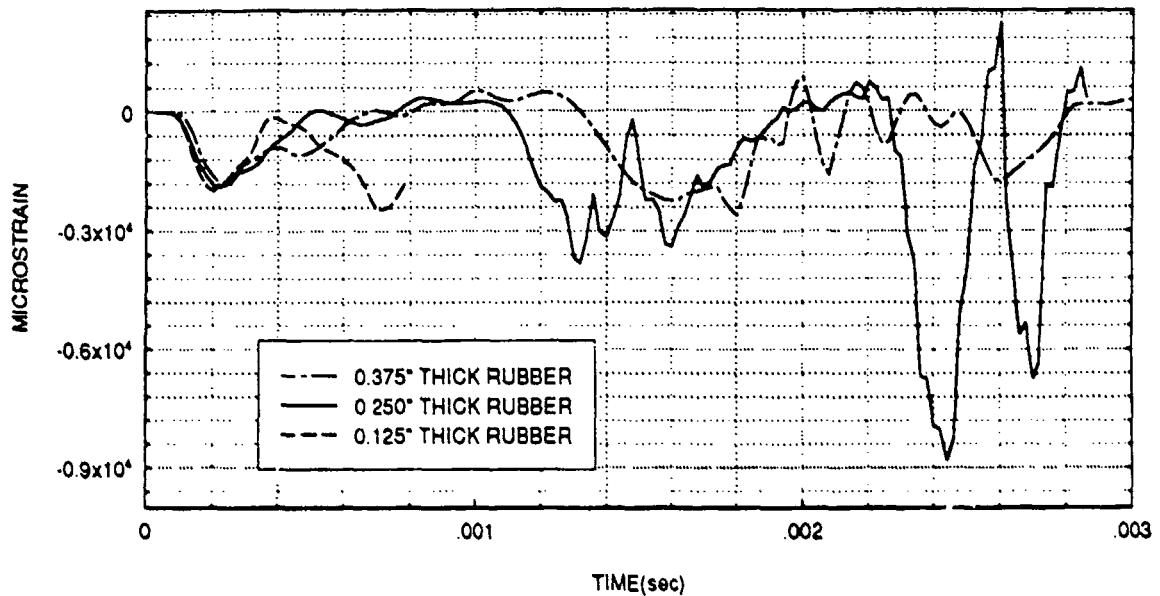


**Figure 115:** Axial strain at position B1 for coated aluminum cylinders with variation of rubber thickness.

### HOOP STRAIN FOR ELEMENT B1

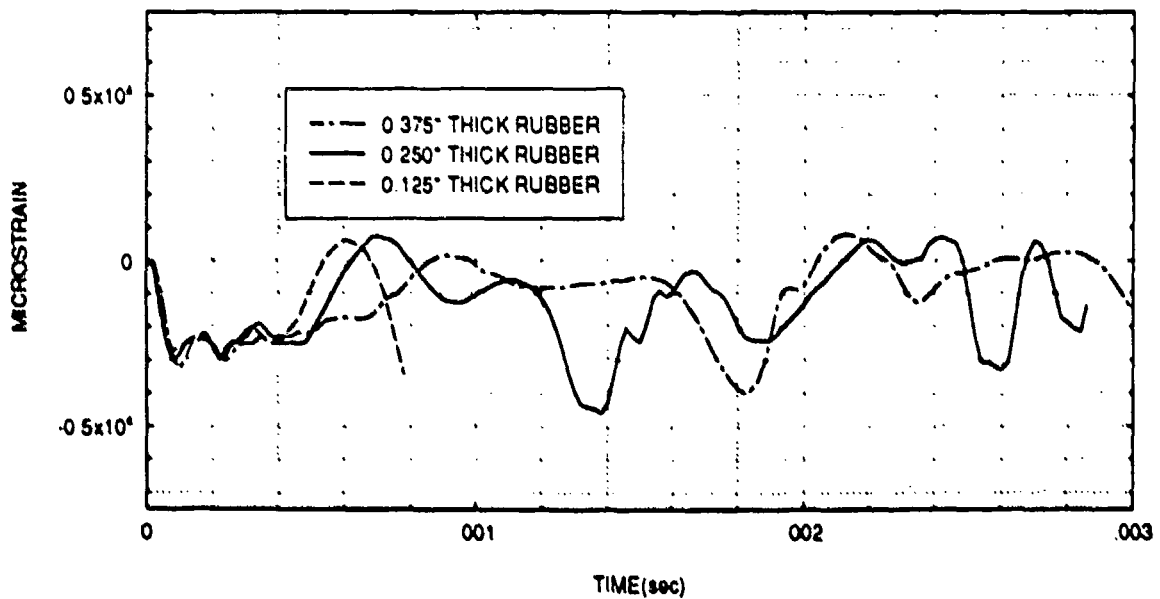


**Figure 116:** Hoop strain at position B1 for coated aluminum cylinders with variation of rubber thickness.

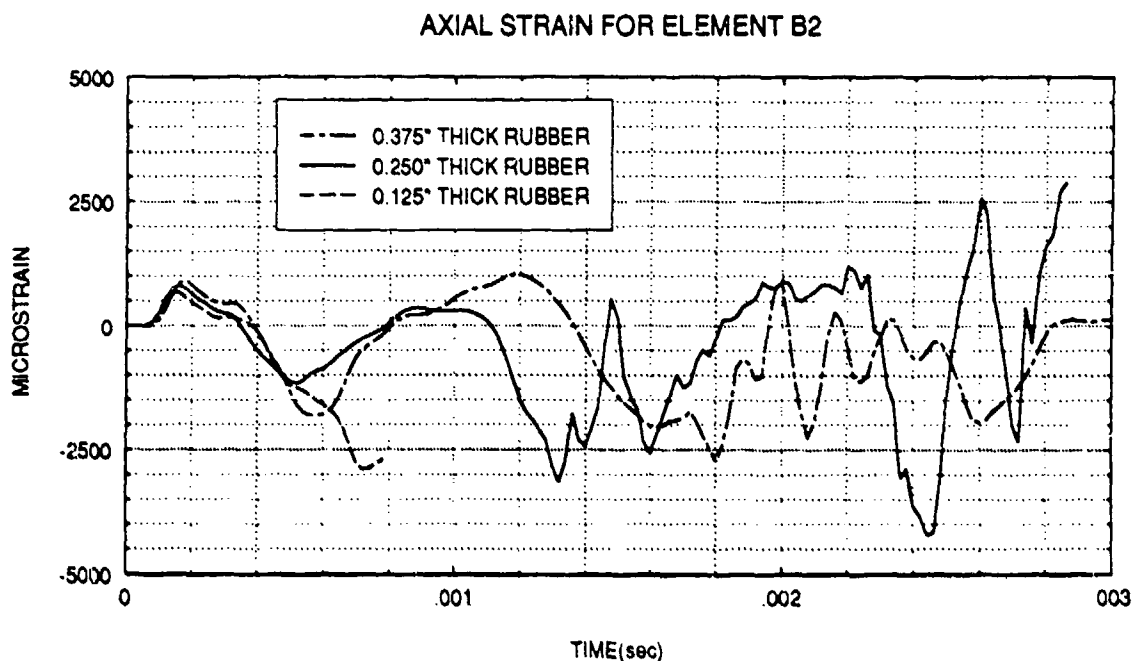


**Figure 117:** Axial strain at position B2 for coated aluminum cylinders with variation of rubber thickness.

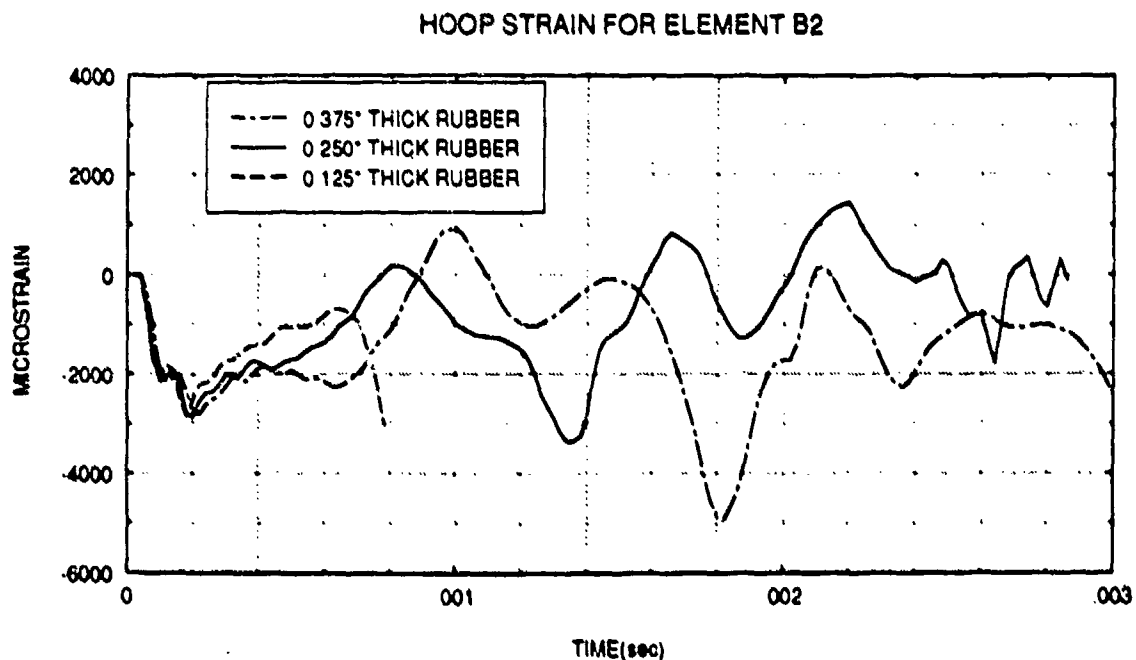


**Figure 118:** Hoop strain at position B2 for coated aluminum cylinders with variation of rubber thickness.

### AXIAL STRAIN FOR ELEMENT B3

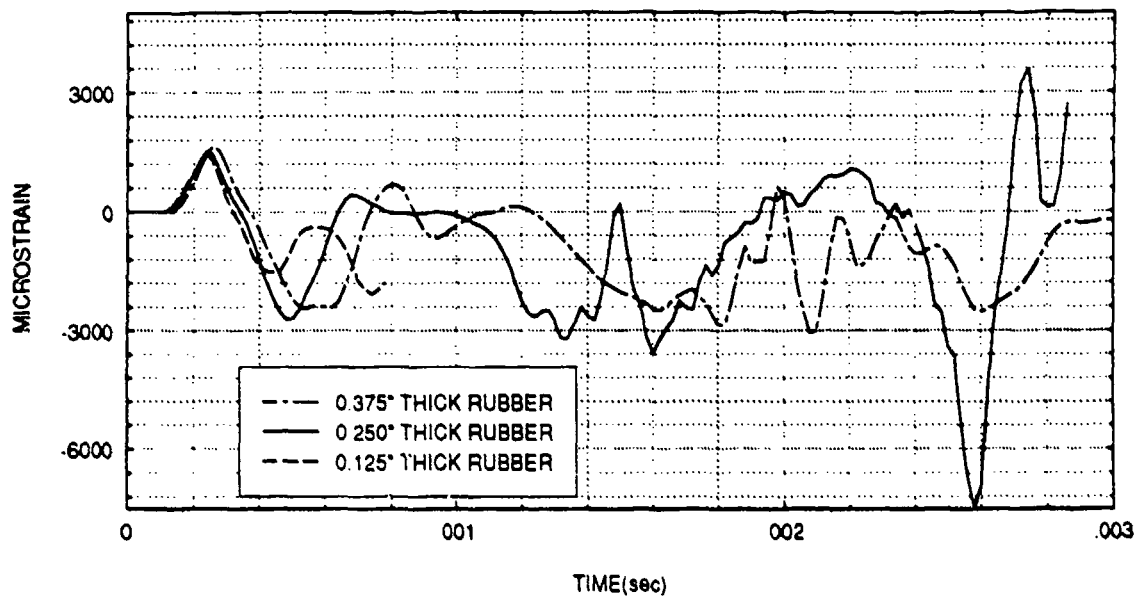


**Figure 119:** Axial strain at position B3 for coated aluminum cylinders with variation of rubber thickness.

### HOOP STRAIN FOR ELEMENT B3

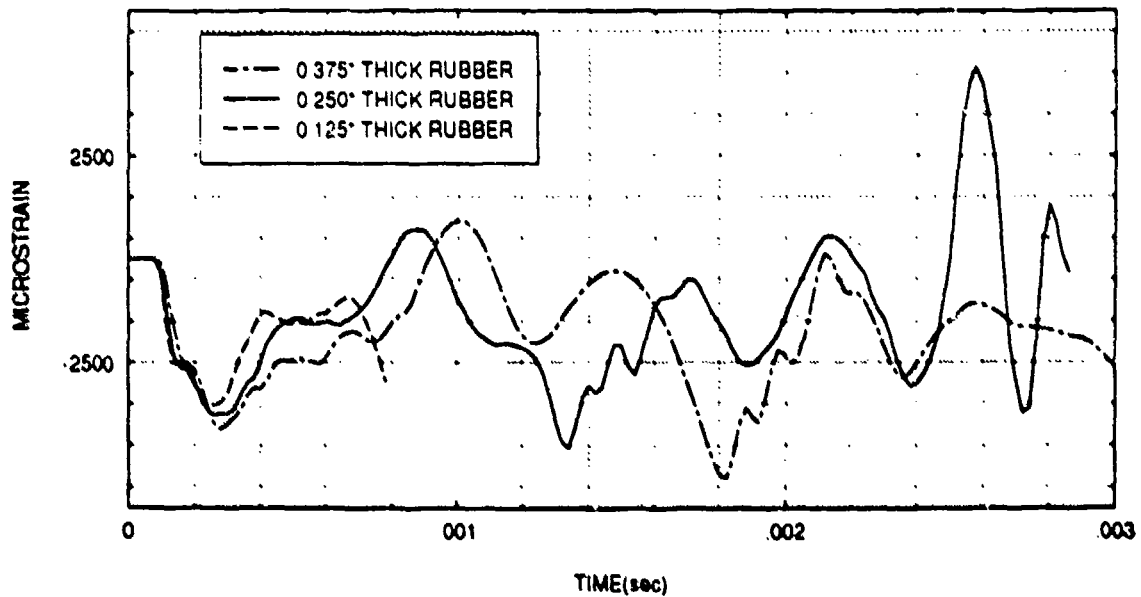


**Figure 120:** Hoop strain at position B3 for coated aluminum cylinders with variation of rubber thickness.



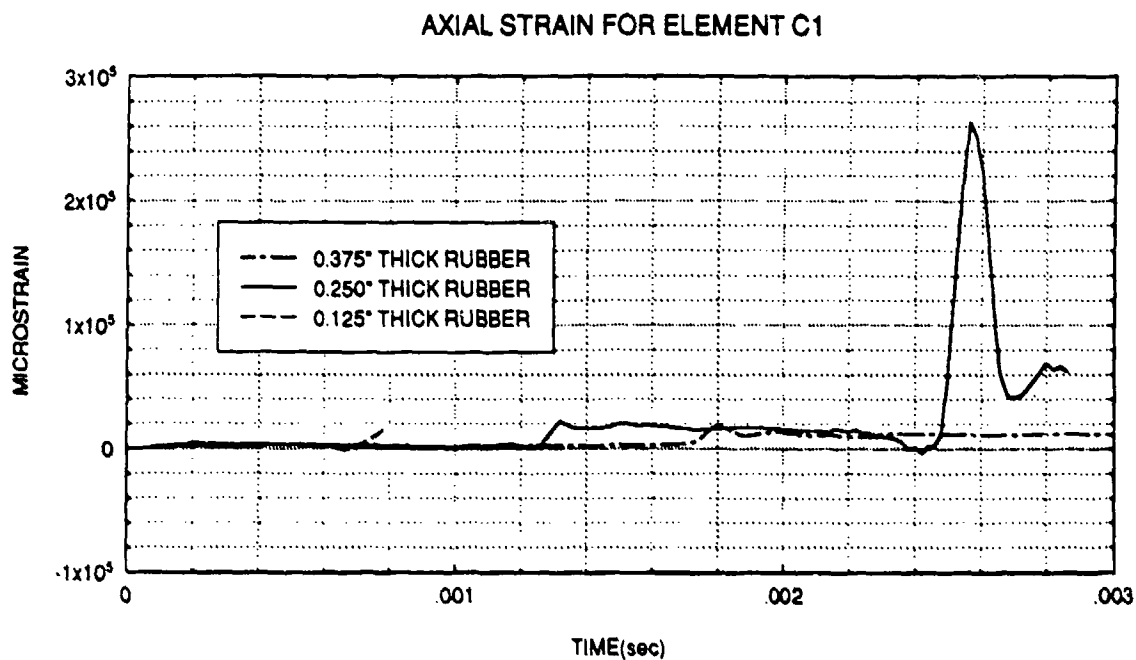


**Figure 121:** Axial strain at position C1 for coated aluminum cylinders with variation of rubber thickness.

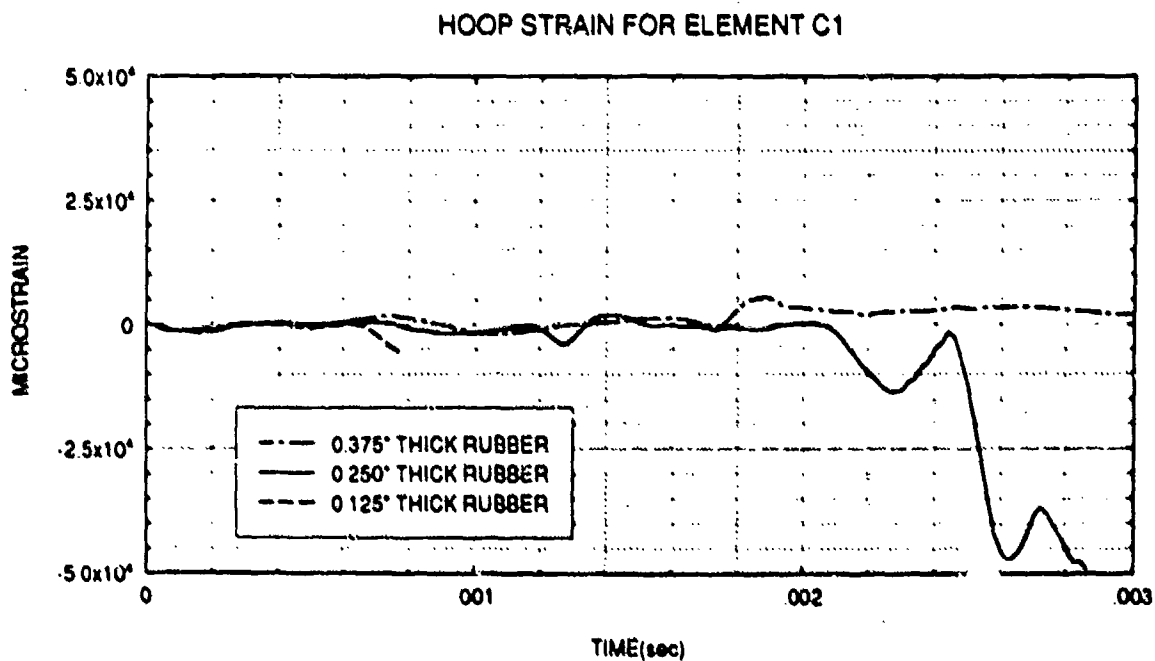


**Figure 122:** Hoop strain at position C1 for coated aluminum cylinders with variation of rubber thickness.

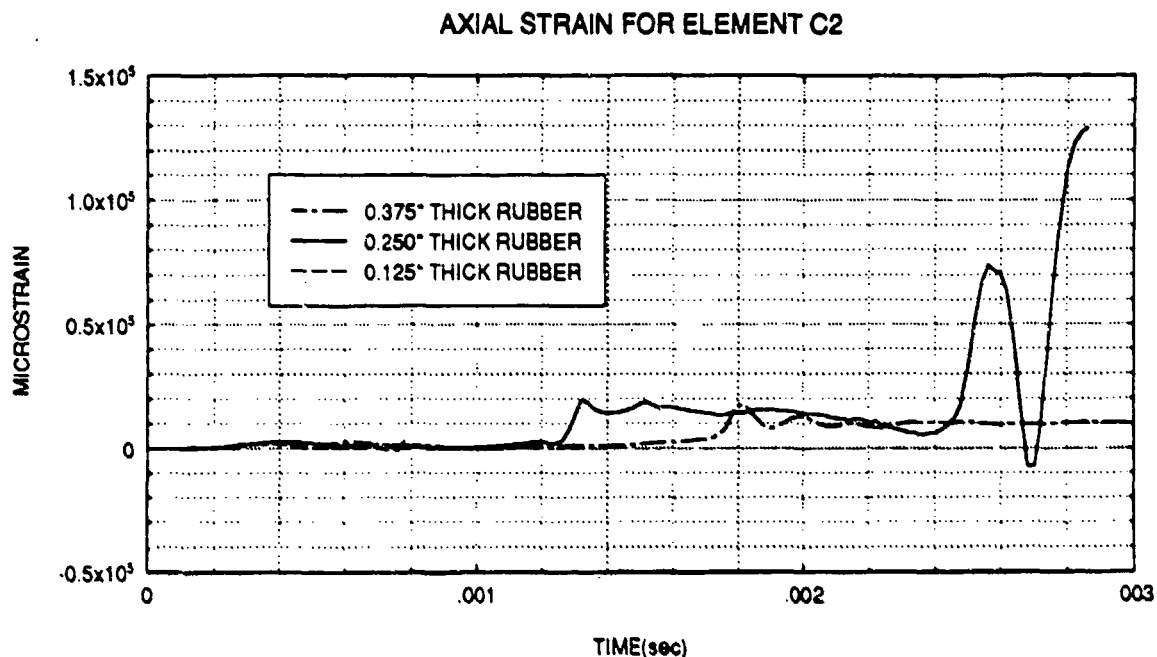


**Figure 123:** Axial strain at position C2 for coated aluminum cylinders with variation of rubber thickness.

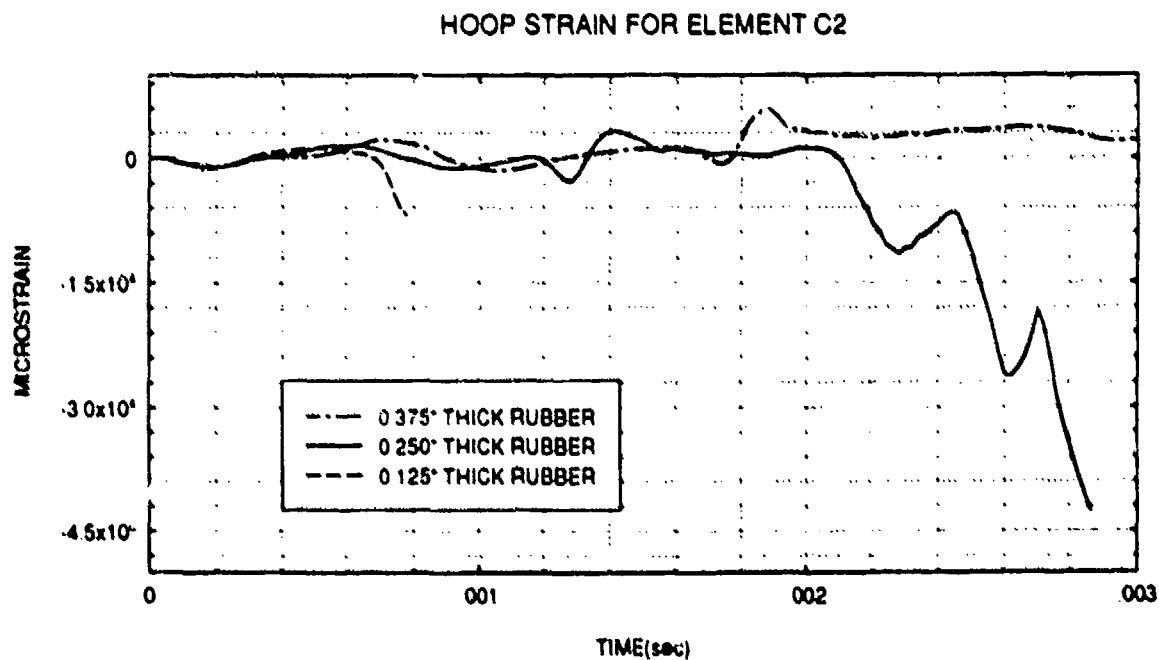


**Figure 124:** Hoop strain at position C2 for coated aluminum cylinders with variation of rubber thickness.

### AXIAL STRAIN FOR ELEMENT C3

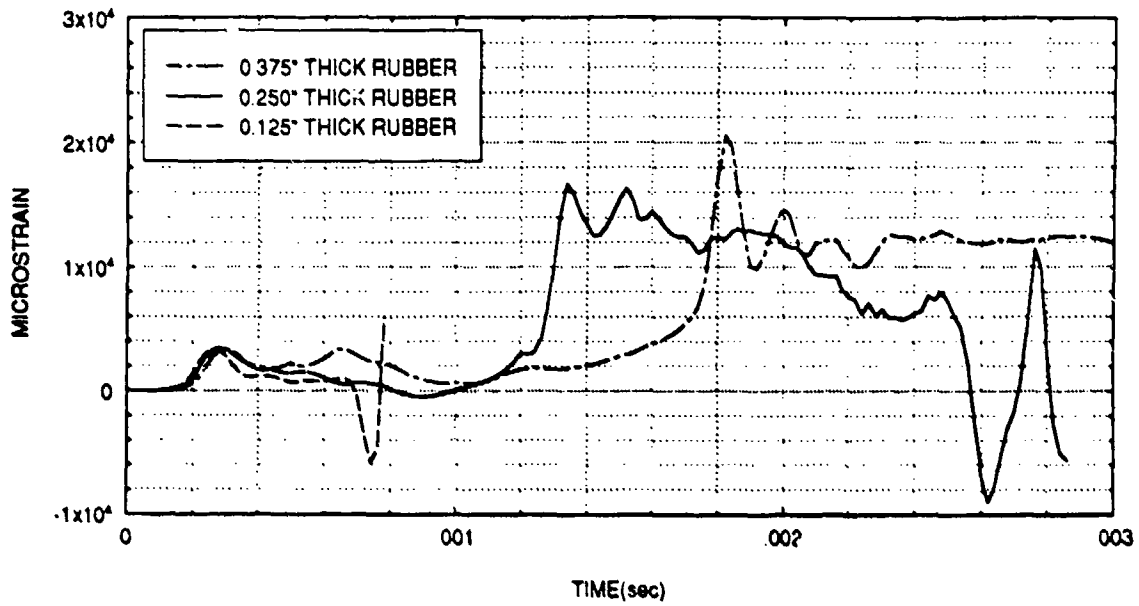


**Figure 125:** Axial strain at position C3 for coated aluminum cylinders with variation of rubber thickness.

### HOOP STRAIN FOR ELEMENT C3

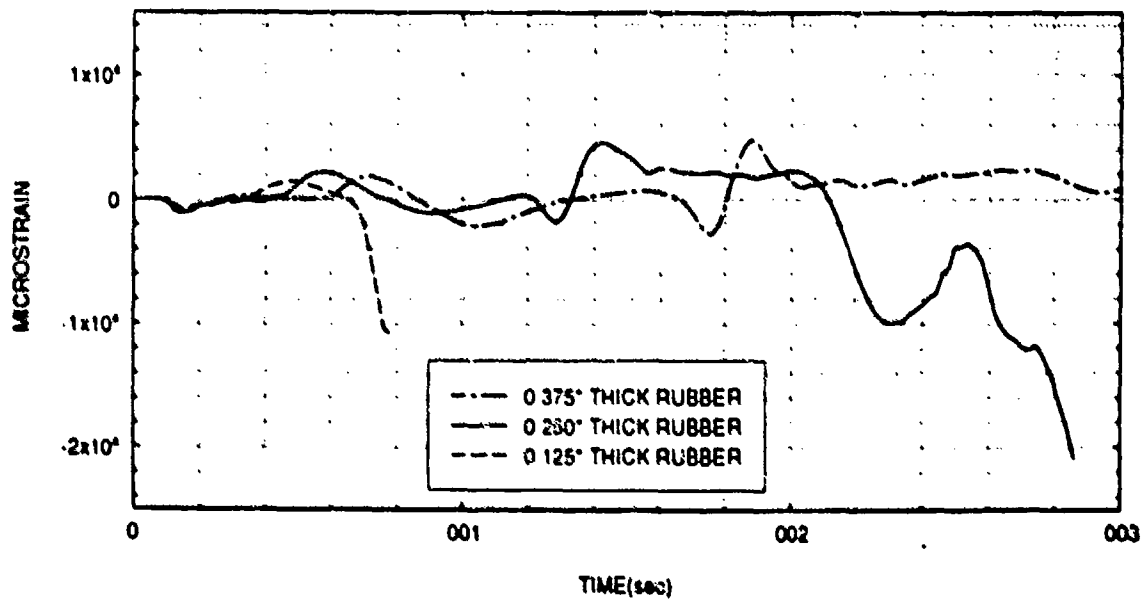


**Figure 126:** Hoop strain at position C3 for coated aluminum cylinders with variation of rubber thickness.

### EFFECTIVE PLASTIC STRAIN FOR ELEMENT A1

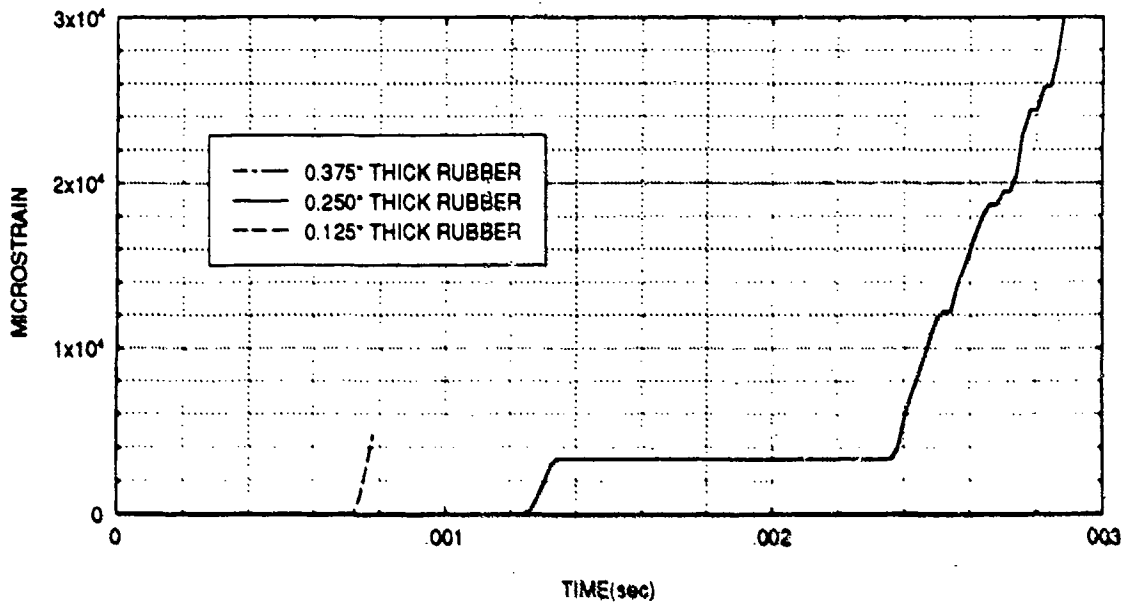


**Figure 127:** Effective plastic strain at position A1 for coated aluminum cylinders with variation of rubber thickness.

### EFFECTIVE PLASTIC STRAIN FOR ELEMENT A2

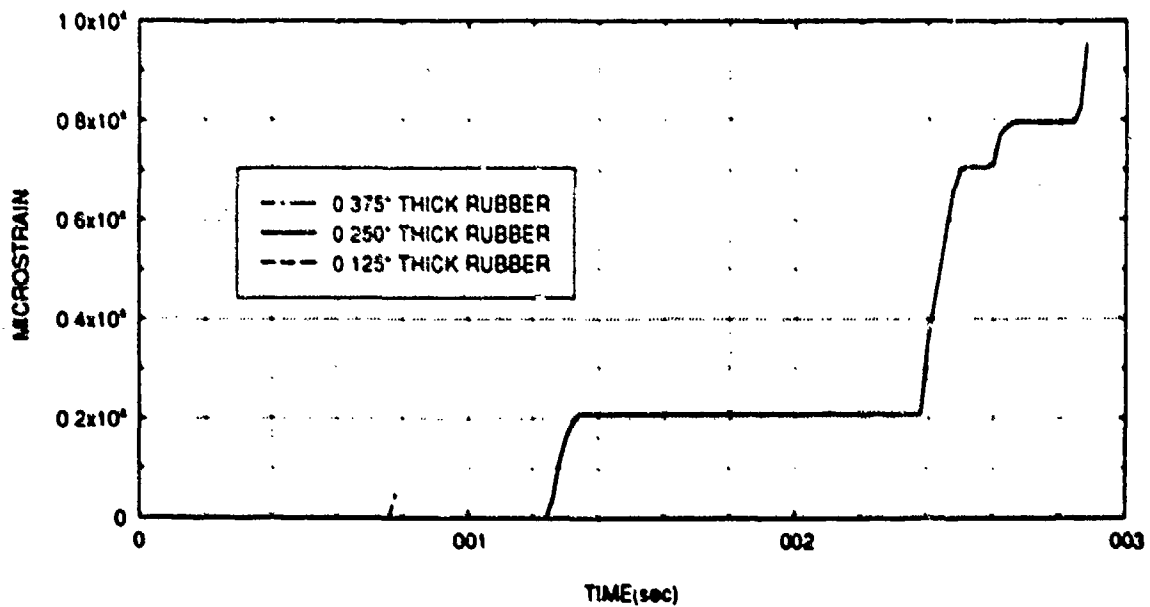


**Figure 128:** Effective plastic strain at position A2 for coated aluminum cylinders with variation of rubber thickness.

### EFFECTIVE PLASTIC STRAIN FOR ELEMENT A3

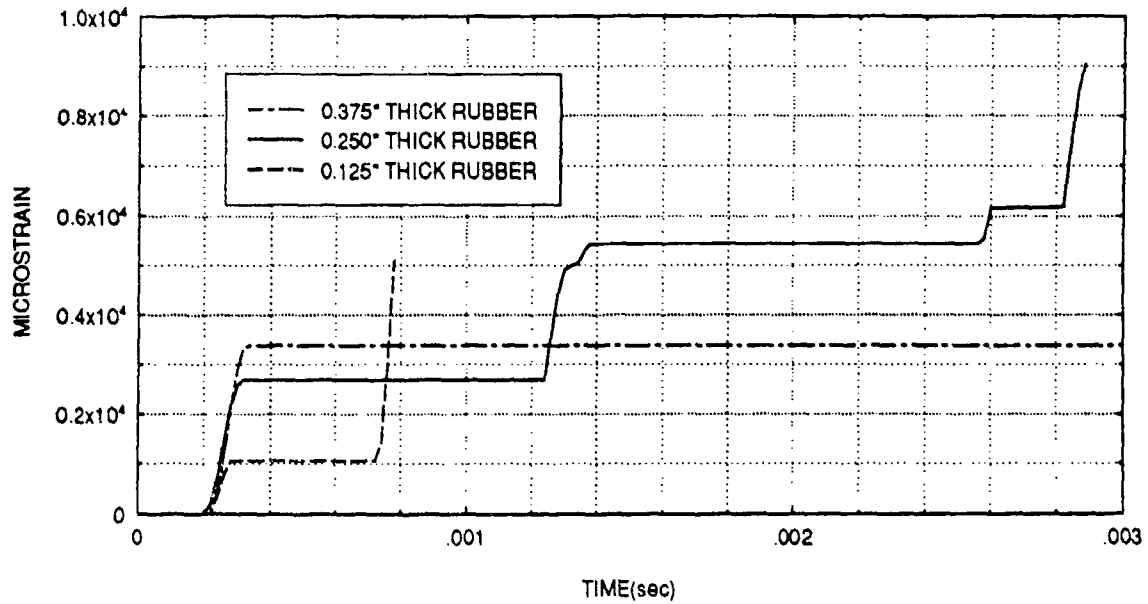


**Figure 129:** Effective plastic strain at position A3 for coated aluminum cylinders with variation of rubber thickness.

### EFFECTIVE PLASTIC STRAIN FOR ELEMENT B1

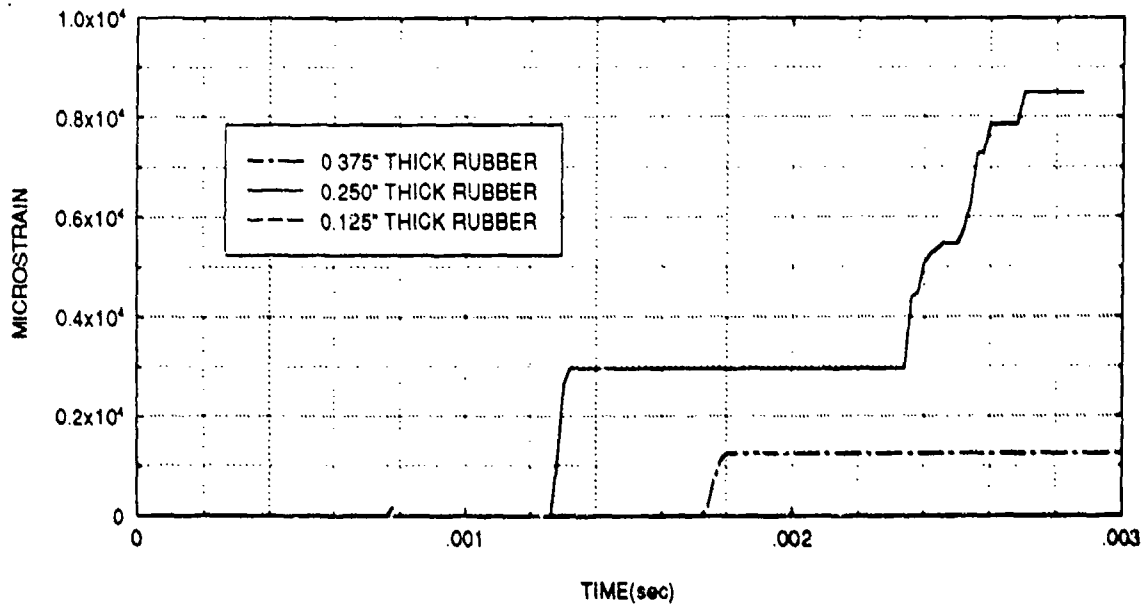


**Figure 130:** Effective plastic strain at position B1 for coated aluminum cylinders with variation of rubber thickness.

### EFFECTIVE PLASTIC STRAIN FOR ELEMENT B2

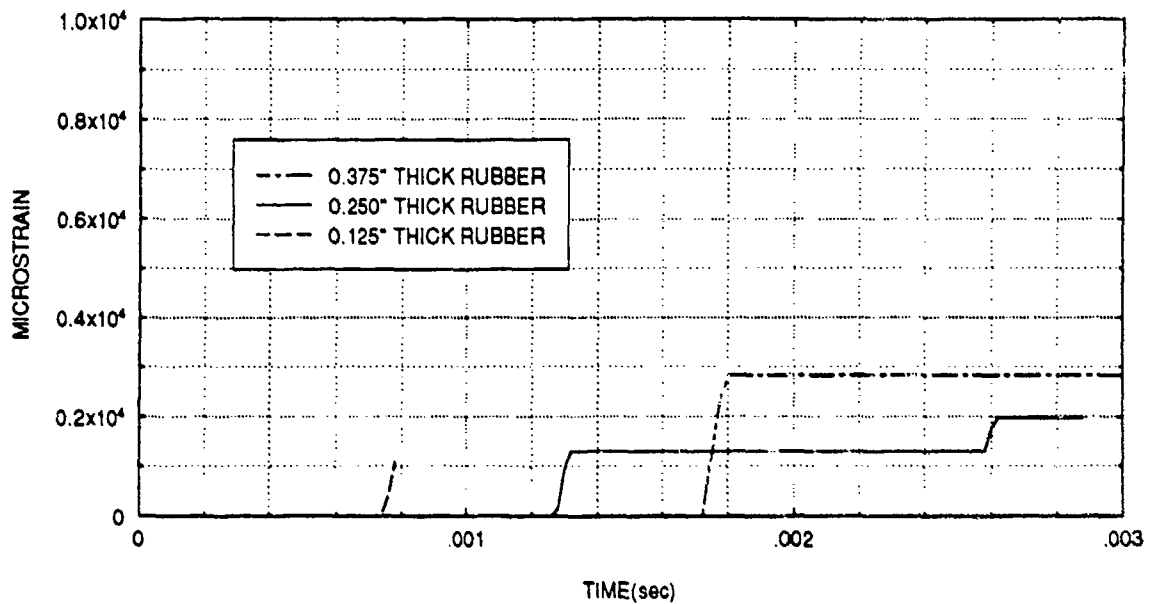


**Figure 131:** Effective plastic strain at position B2 for coated aluminum cylinders with variation of rubber thickness.

### EFFECTIVE PLASTIC STRAIN FOR ELEMENT B3

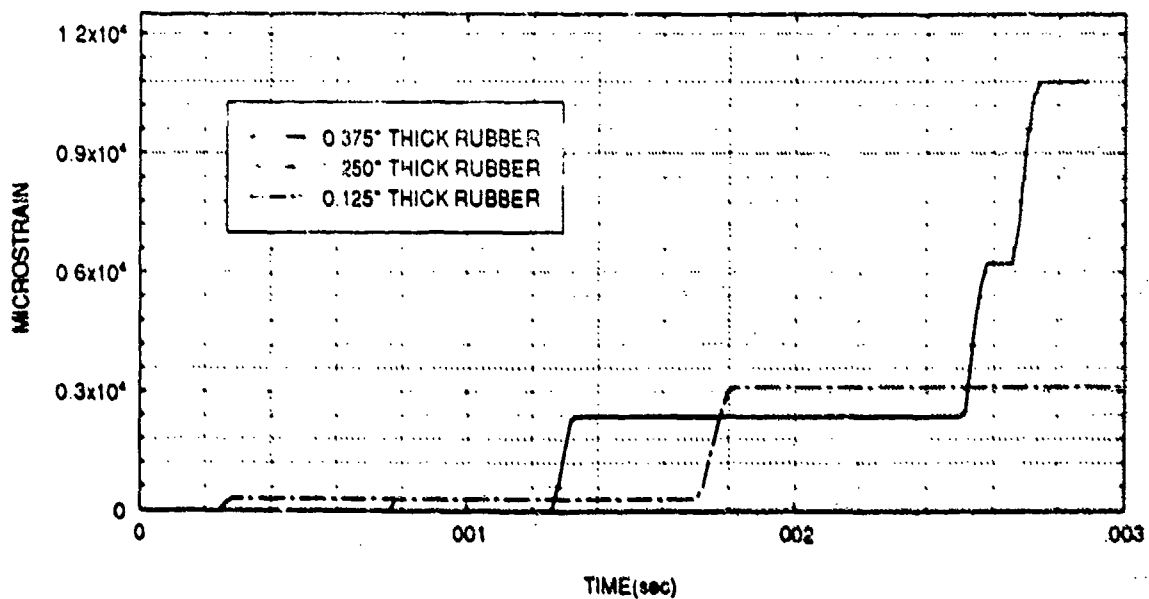


**Figure 132:** Effective plastic strain at position B3 for coated aluminum cylinders with variation of rubber thickness.

### EFFECTIVE PLASTIC STRAIN FOR ELEMENT C1

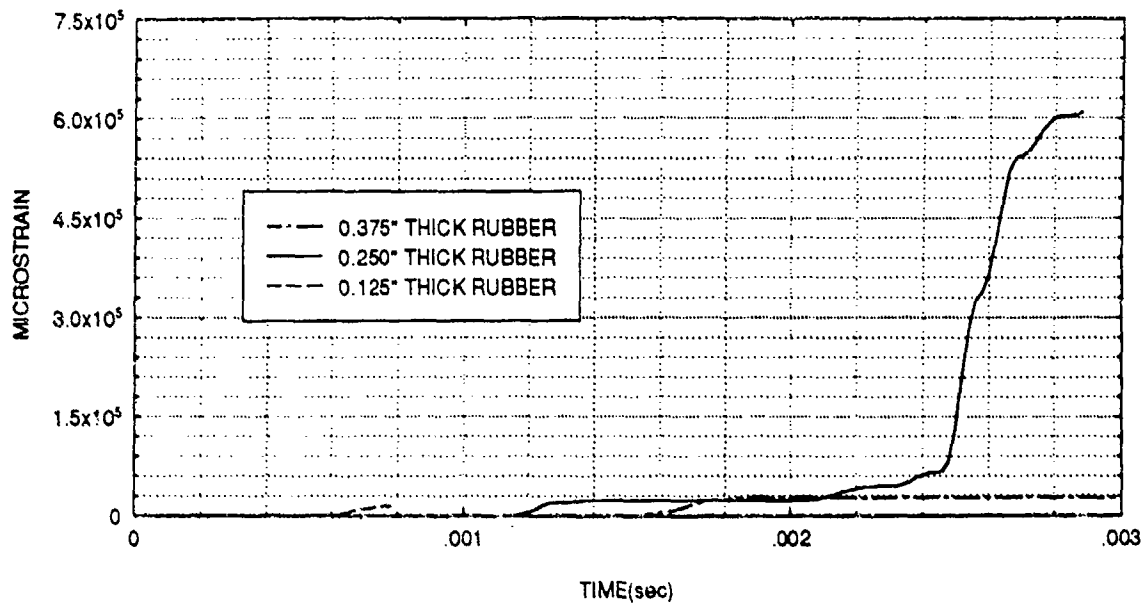


**Figure 133:** Effective plastic strain at position C1 for coated aluminum cylinders with variation of rubber thickness.

### EFFECTIVE PLASTIC STRAIN FOR ELEMENT C2

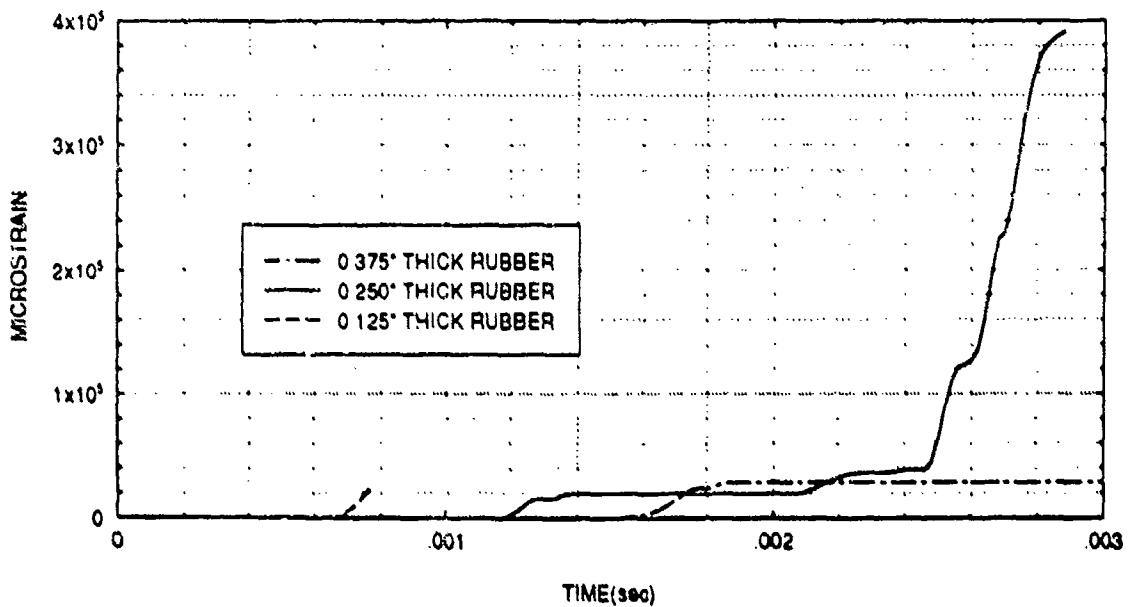


**Figure 134:** Effective plastic strain at position C2 for coated aluminum cylinders with variation of rubber thickness.

### EFFECTIVE PLASTIC STRAIN FOR ELEMENT C3

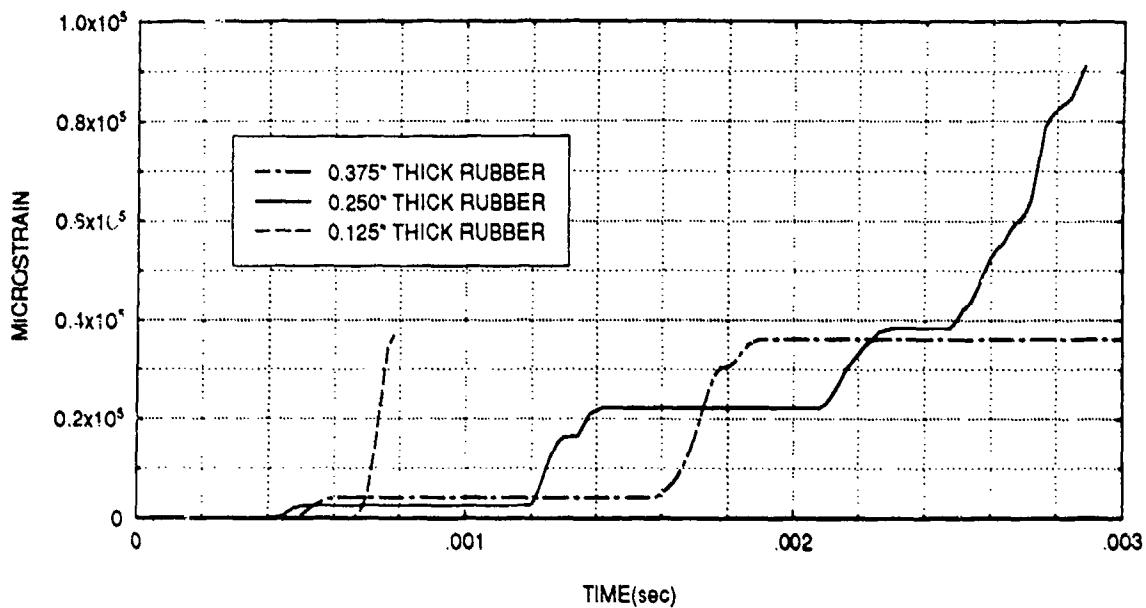
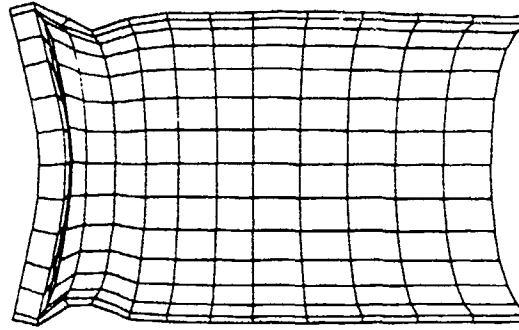
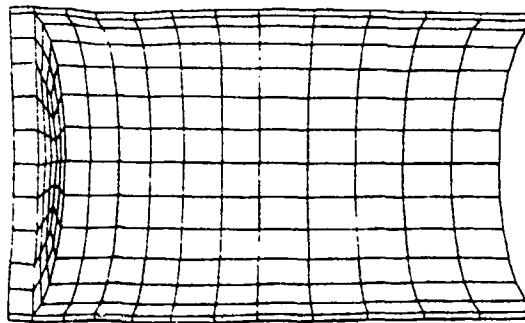


**Figure 135:** Effective plastic strain at position C3 for coated aluminum cylinders with variation of rubber thickness.

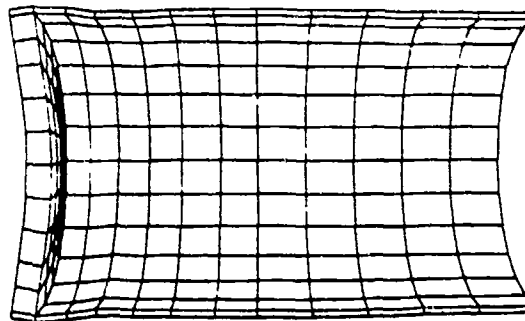




0.125" THICK RUBBER (DISPL. SCALE FACTOR OF 5)

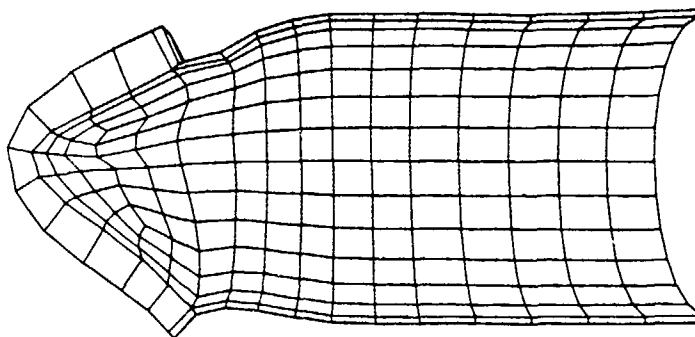


0.250" THICK RUBBER (DISPL. SCALE FACTOR OF 5)

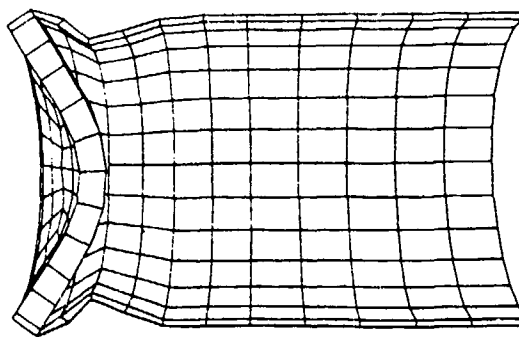


0.375" THICK RUBBER (DISPL. SCALE FACTOR OF 5)

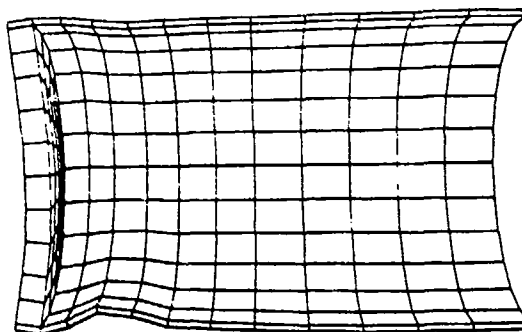
**Figure 136:** Deformation of coated aluminum cylinders with variation of rubber thickness at 0.76 msec. (Displacement scale factor of 5).



0.250" THICK RUBBER (DISPL. SCALE FACTOR OF 5)



0.375" THICK RUBBER (DISPL. SCALE FACTOR OF 5)



0.500" THICK RUBBER (DISPL. SCALE FACTOR OF 5)

**Figure 137:** Deformation of coated aluminum cylinders with variation of rubber thickness at 2.86 msec. (Displacement scale factor of 5).

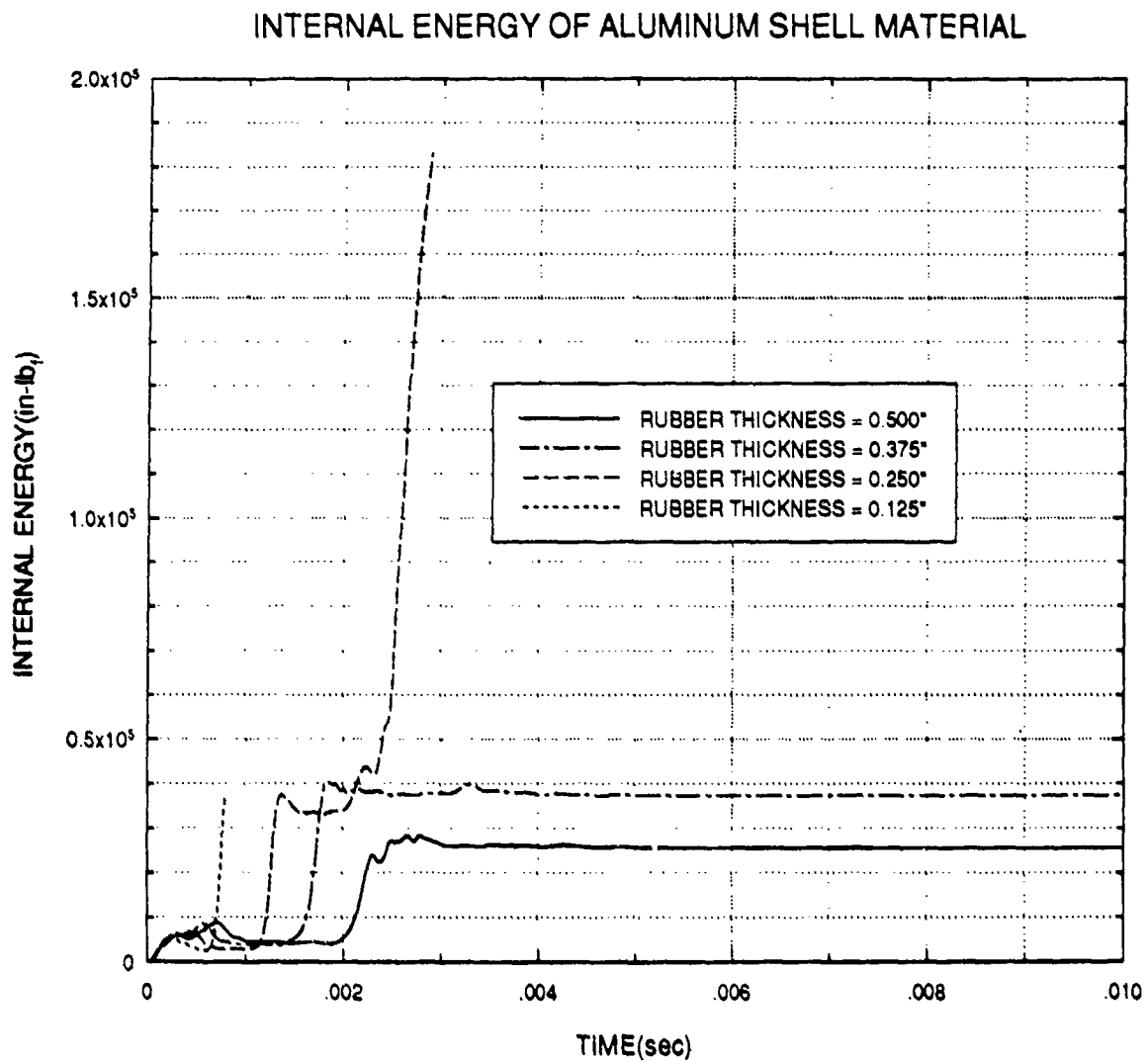


**Figure 138:** Internal energy of aluminum shell material for coated cylinders with variation of rubber thickness.

response of the cylinder is related to the stiffness of the coating and is therefore affected by the thickness of the coating. The significant difference in response due to changes in coating thickness again suggest the existence of a thickness "threshold" value, i.e. a value below which causes the coated cylinder to respond adversely to an underwater shock wave.

In the sixth case, the objective was to determine how a change in the metal material would affect the dynamic response of the cylinder. For this study, an uncoated steel cylinder was compared to a steel cylinder coated with tread stock rubber. The steel shell thickness and coating thickness were both 0.250 in.. The endplate thickness was 1 in. as in the aluminum cylinder cases. Axial and hoop strain values are plotted for all element locations and are shown in Figures 139-156. Results appeared analagous to those obtained in case 1. Again, axial and hoop strain values were larger in the coated cylinder than in the uncoated cylinder. It was noted that the ratio of the maximum response of the coated and uncoated cylinders was generally higher in the case of steel than in the case of aluminum. For example at location B3, for response up through 1.3 msec., the ratio of coated to uncoated maximum axial strain was 4.3 for steel and 1.8 for aluminum. This is likely attributable to the strain-rate sensitivity of steel. Results of this study indicate that effects of surface coatings on the response of cylinders subjected to underwater

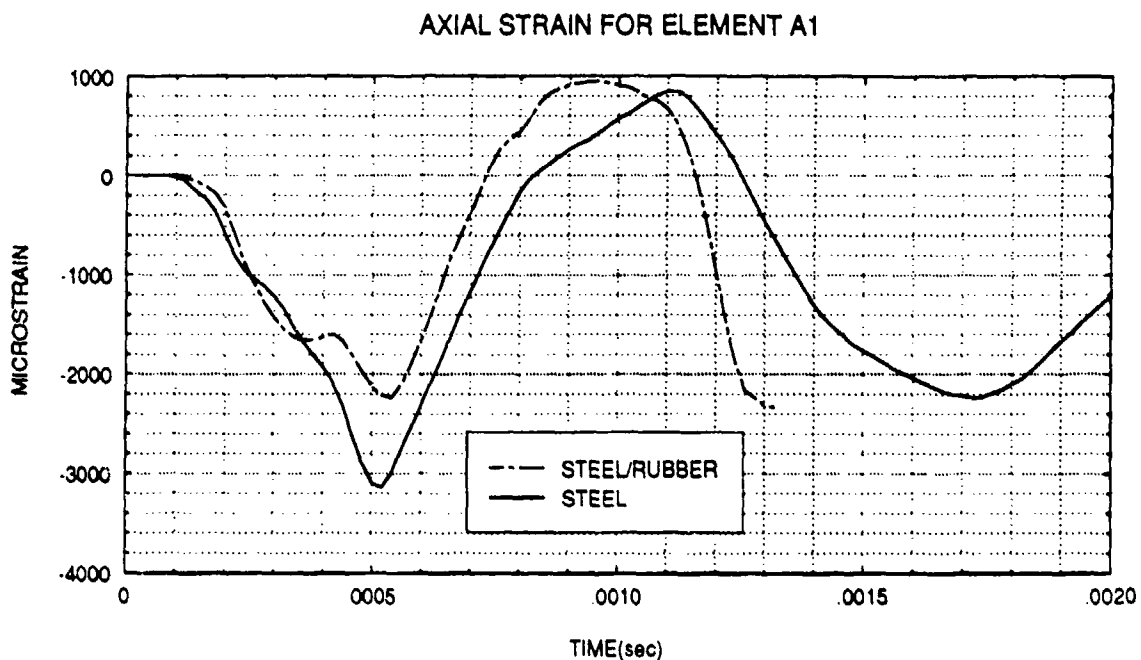


**Figure 139:** Axial strain at position A1 for uncoated and coated steel cylinders.

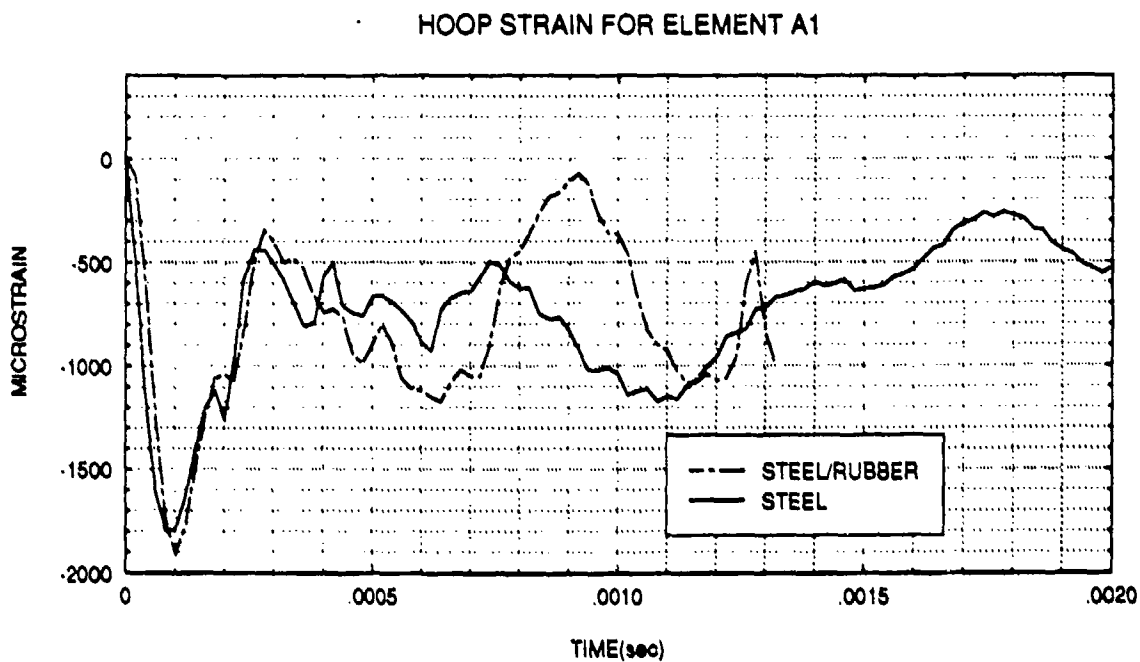


**Figure 140:** Hoop strain at position A1 for uncoated and coated steel cylinders.

### AXIAL STRAIN FOR ELEMENT A2

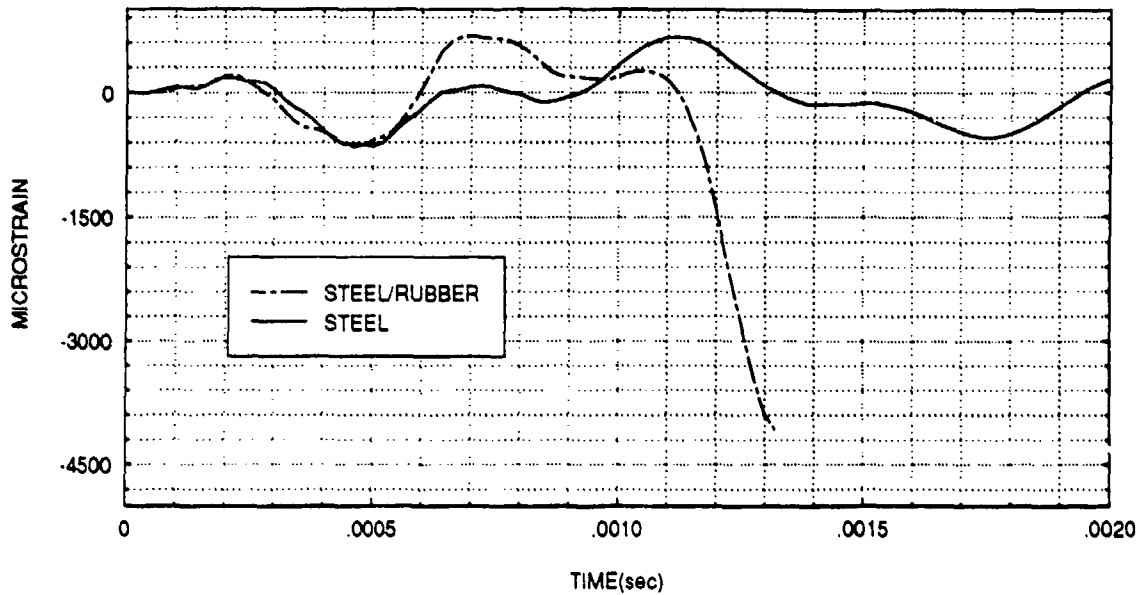


**Figure 141:** Axial strain at position A2 for uncoated and coated steel cylinders.

### HOOP STRAIN FOR ELEMENT A2

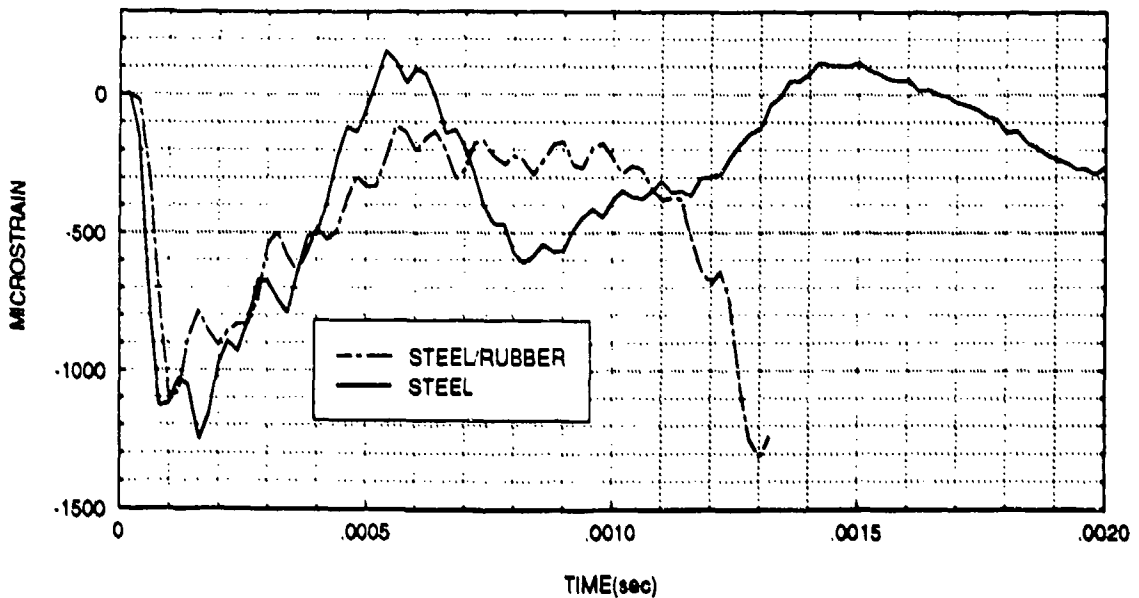


**Figure 142:** Hoop strain at position A2 for uncoated and coated steel cylinders.

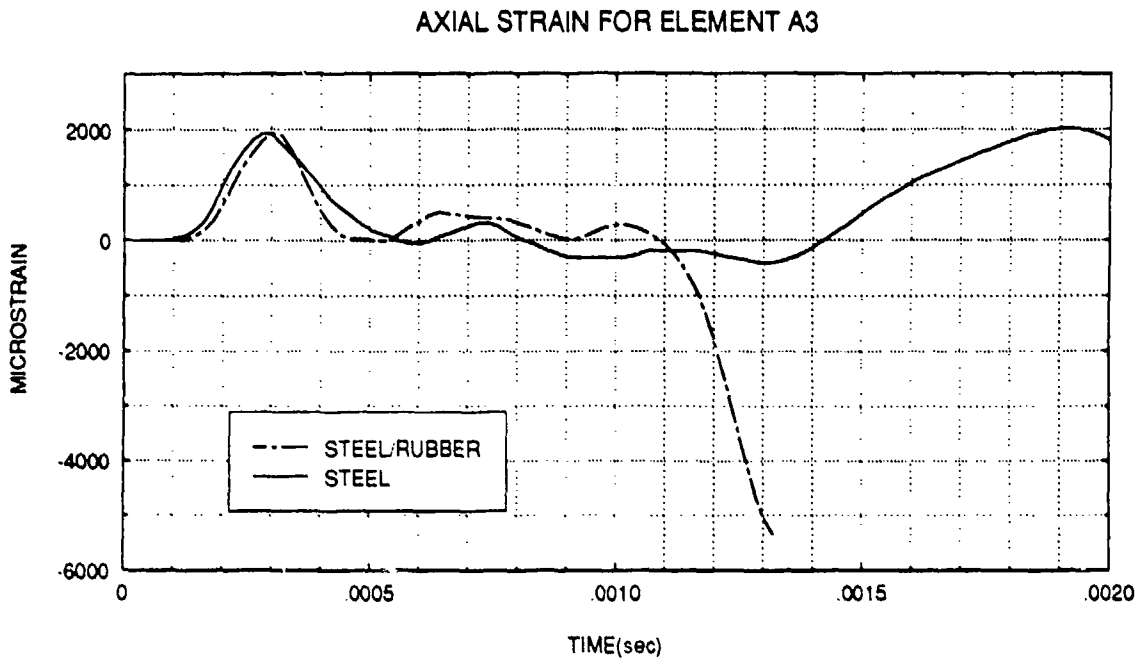


**Figure 143:** Axial strain at position A3 for uncoated and coated steel cylinders.

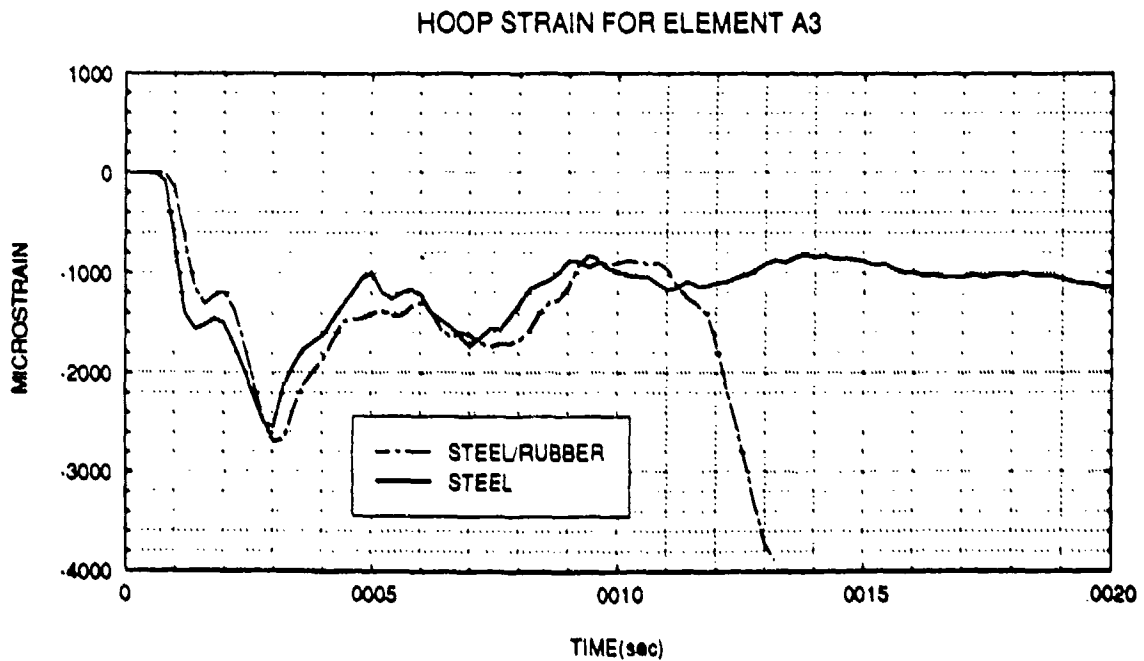


**Figure 144:** Hoop strain at position A3 for uncoated and coated steel cylinders.

### AXIAL STRAIN FOR ELEMENT B1

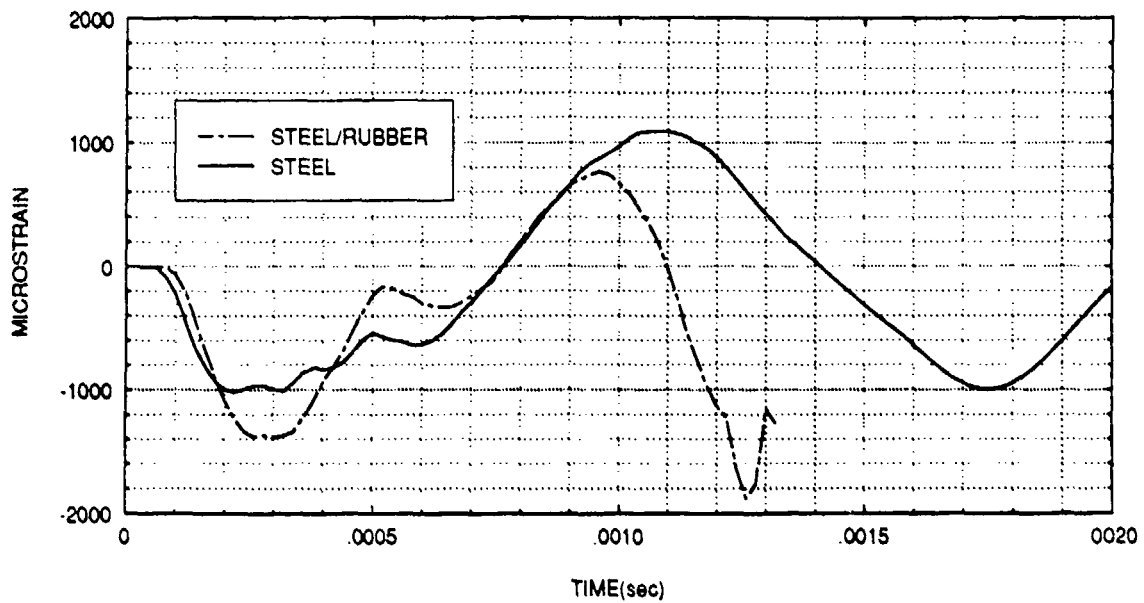


**Figure 145:** Axial strain at position B1 for uncoated and coated steel cylinders.

### HOOP STRAIN FOR ELEMENT B1

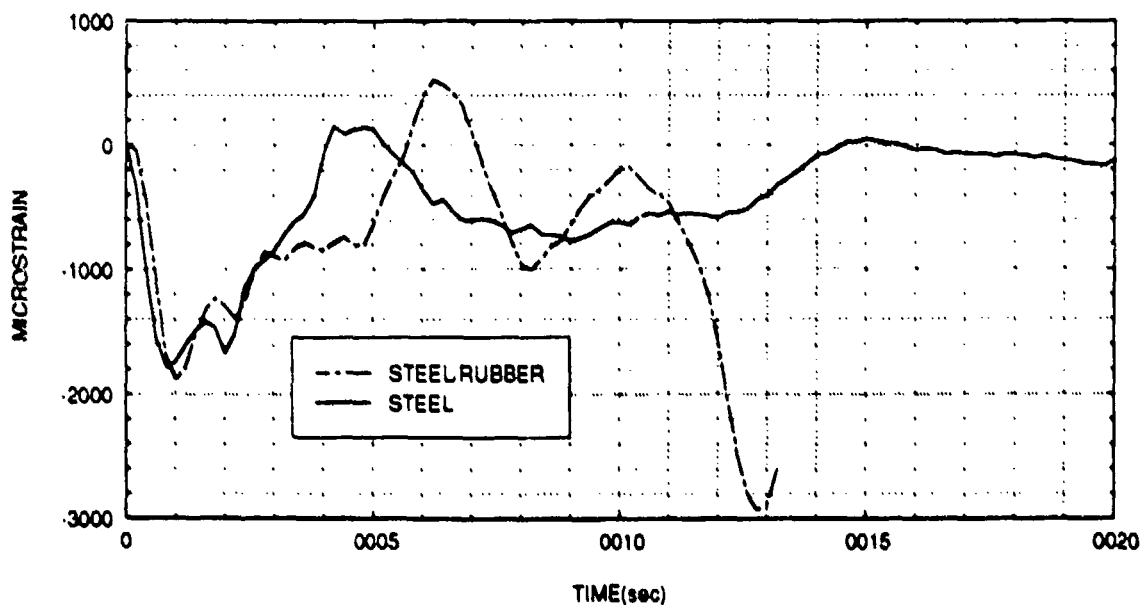


**Figure 146:** Hoop strain at position B1 for uncoated and coated steel cylinders.



### AXIAL STRAIN FOR ELEMENT B2

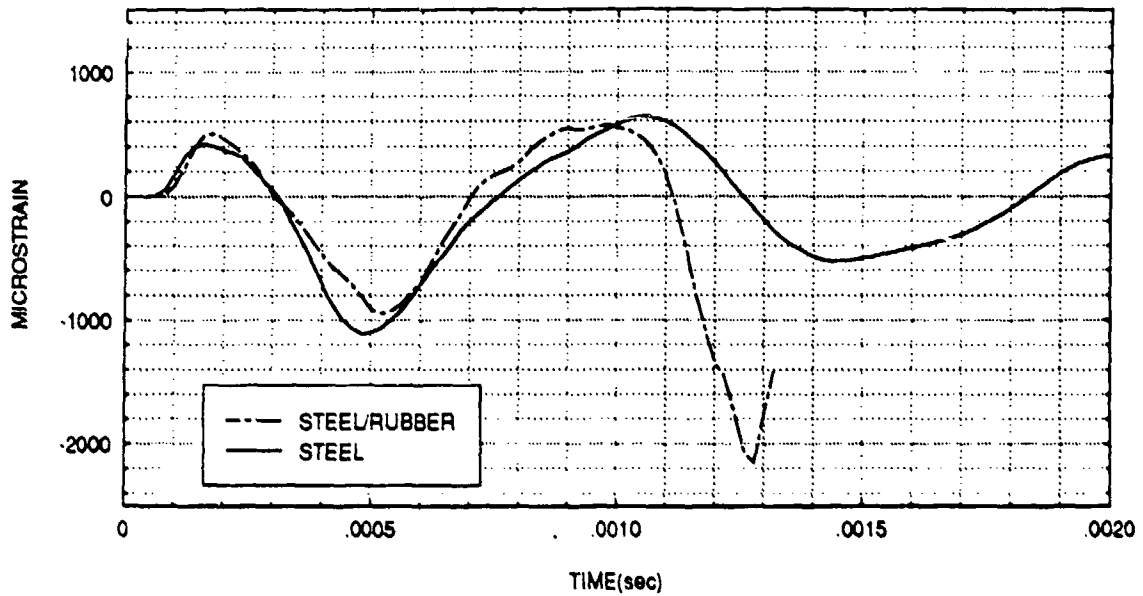


**Figure 147:** Axial strain at position B2 for uncoated and coated steel cylinders.

### HOOP STRAIN FOR ELEMENT B2

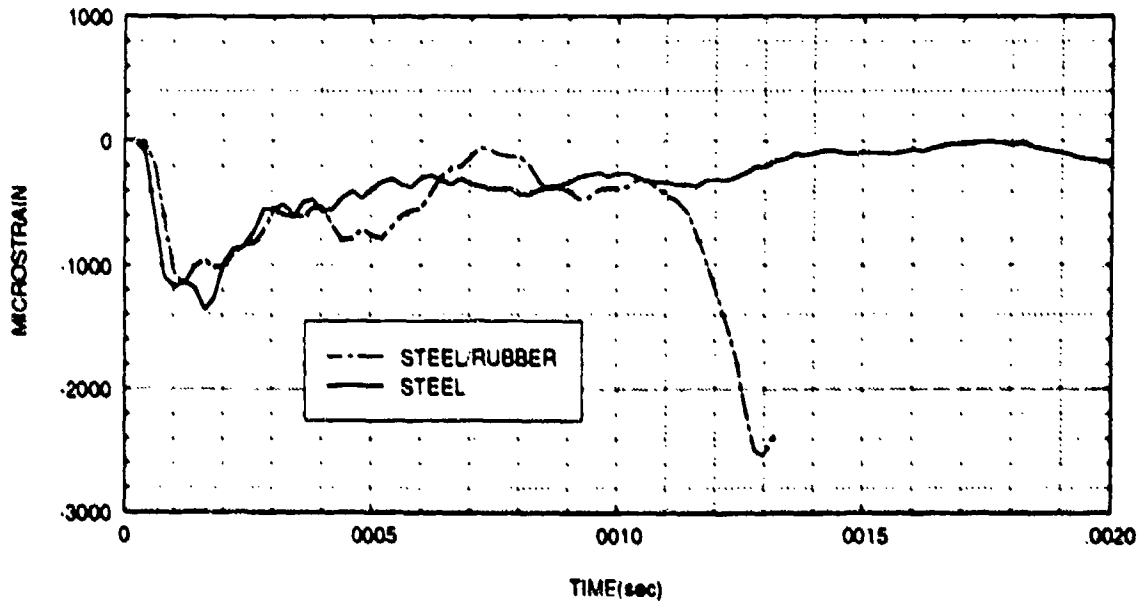


**Figure 148:** Hoop strain at position B2 for uncoated and coated steel cylinders.

### AXIAL STRAIN FOR ELEMENT B3

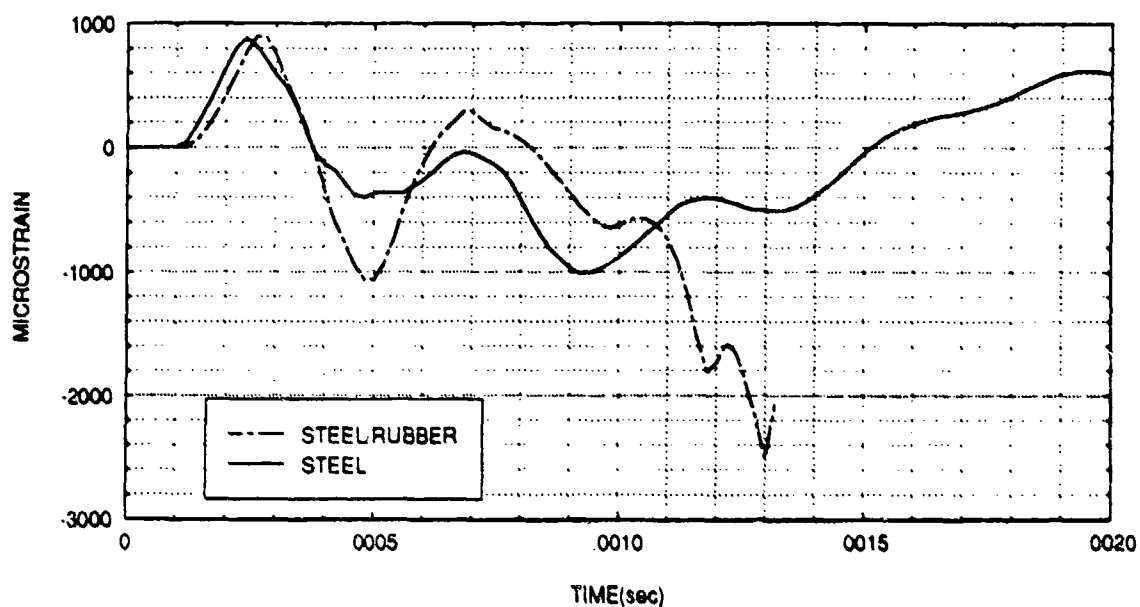


**Figure 149:** Axial strain at position B3 for uncoated and coated steel cylinders.

### HOOP STRAIN FOR ELEMENT B3

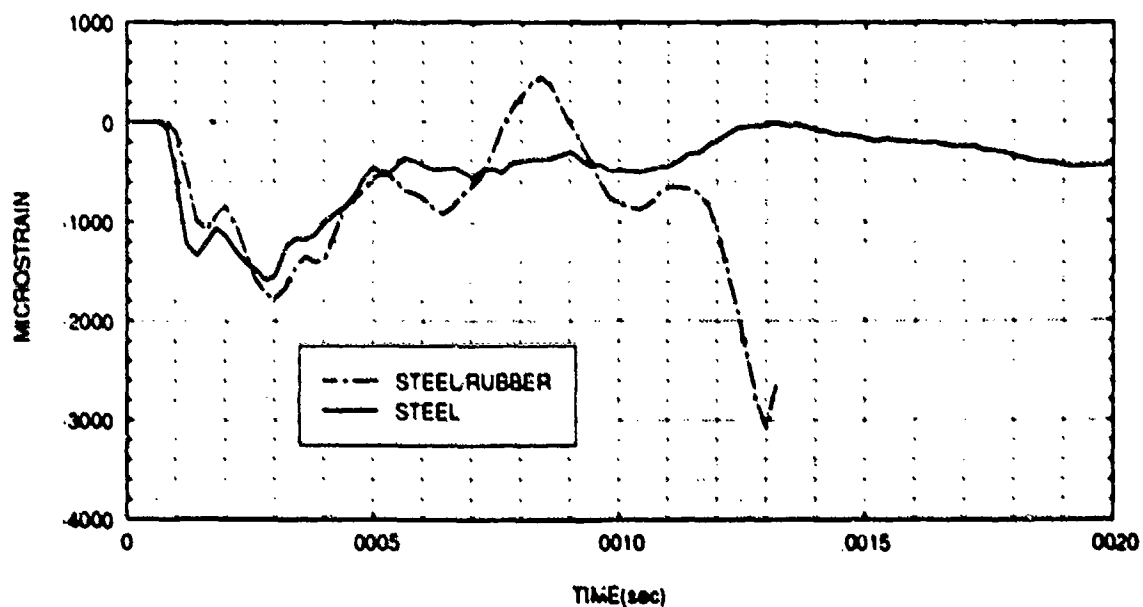


**Figure 150:** Hoop strain at position B3 for uncoated and coated steel cylinders.

# AXIAL STRAIN FOR ELEMENT C1

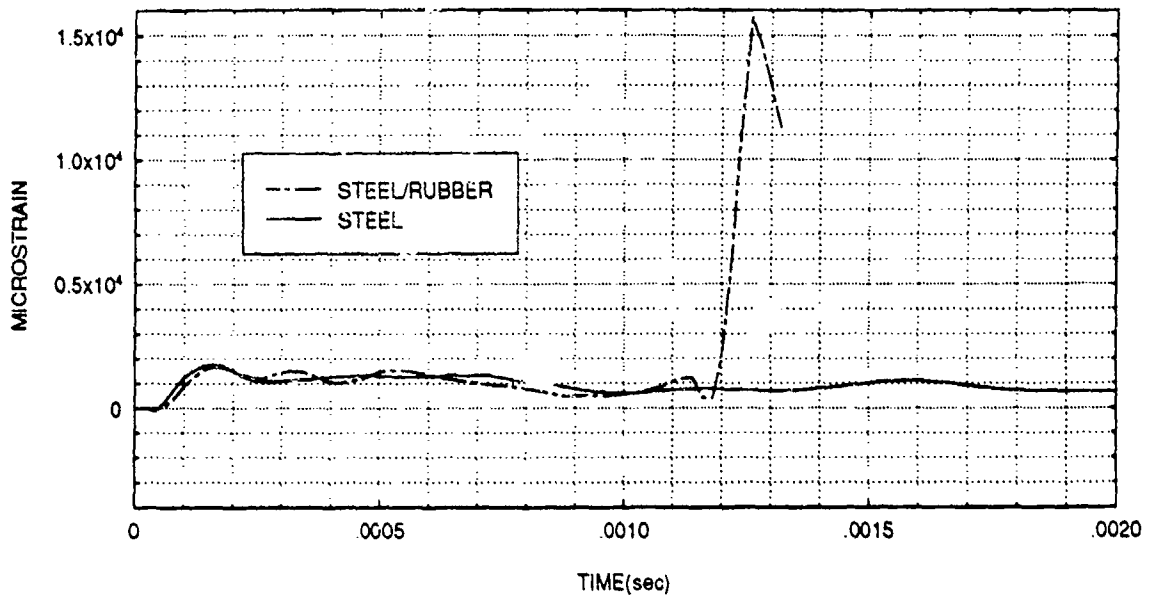


**Figure 151:** Axial strain at position C1 for uncoated and coated steel cylinders.

# HOOP STRAIN FOR ELEMENT C1

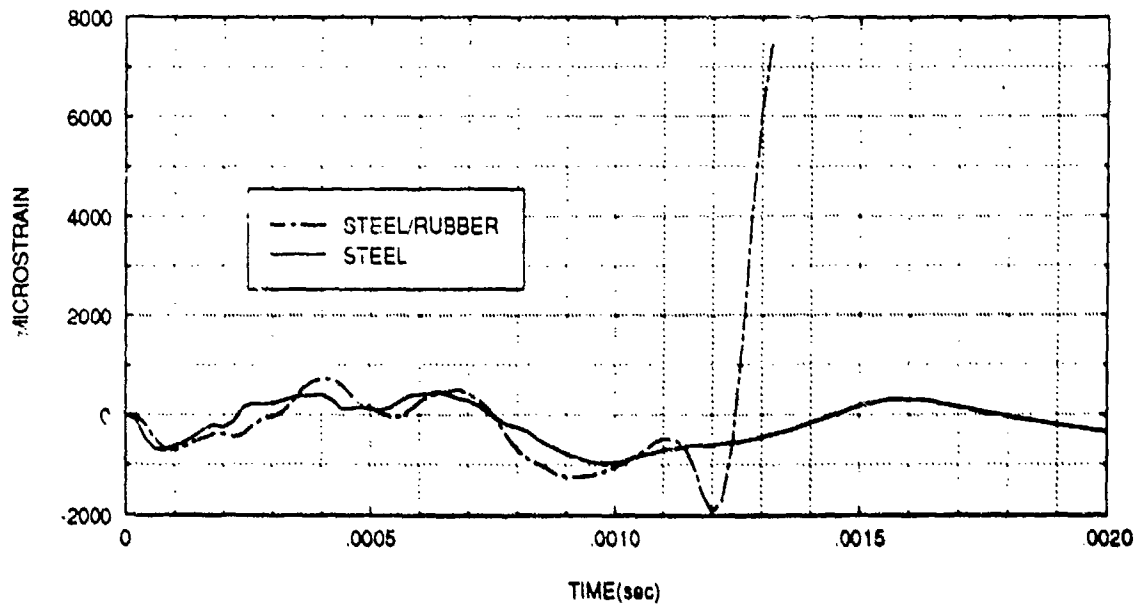


**Figure 152:** Hoop strain at position C1 for uncoated and coated steel cylinders.

### AXIAL STRAIN FOR ELEMENT C2

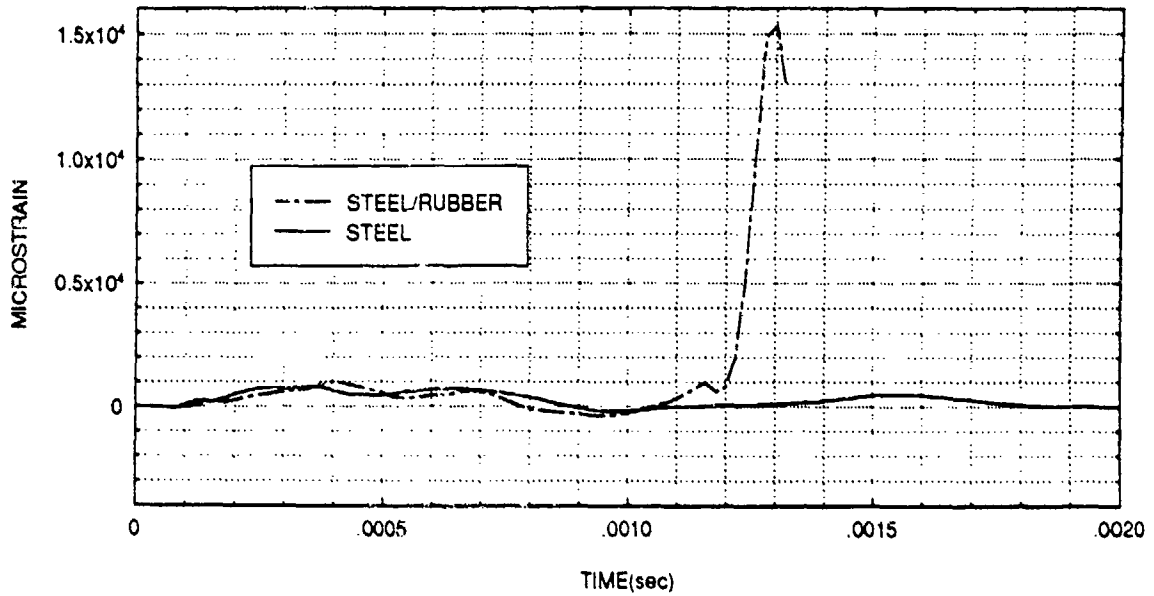


**Figure 153:** Axial strain at position C2 for uncoated and coated steel cylinders.

### HOOP STRAIN FOR ELEMENT C2

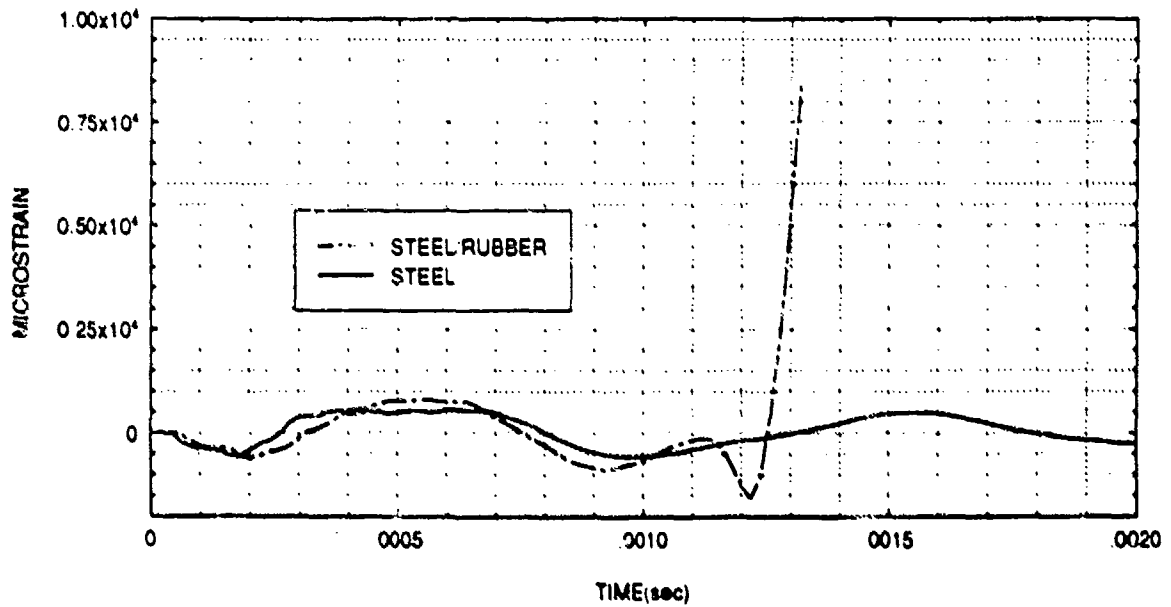


**Figure 154:** Hoop strain at position C2 for uncoated and coated steel cylinders.

### AXIAL STRAIN FOR ELEMENT C3

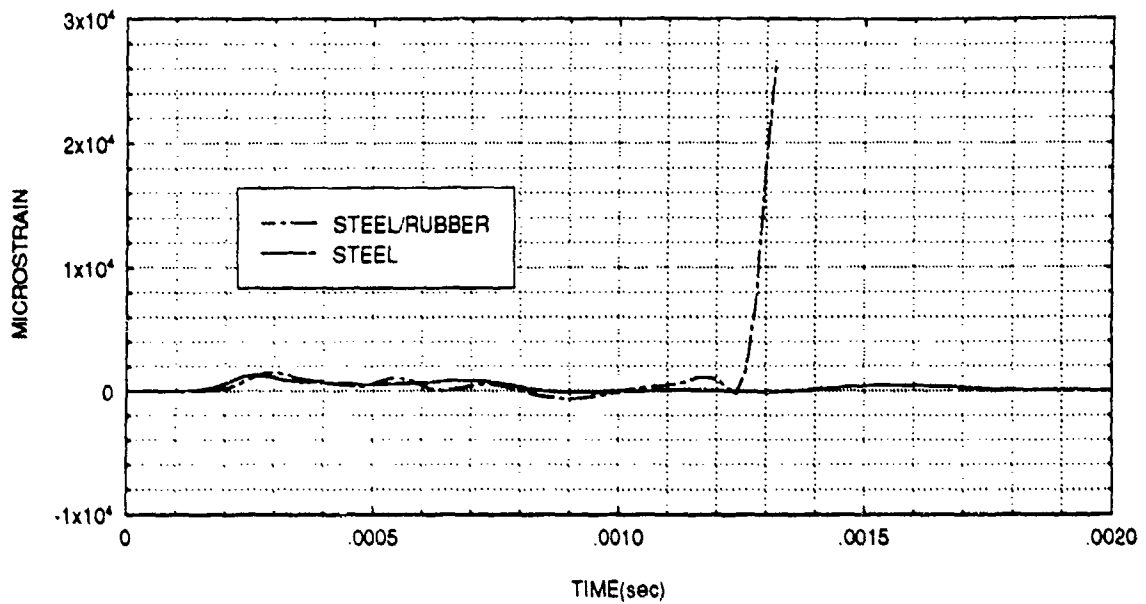


**Figure 155:** Axial strain at position C3 for uncoated and coated steel cylinders.

### HOOP STRAIN FOR ELEMENT C3

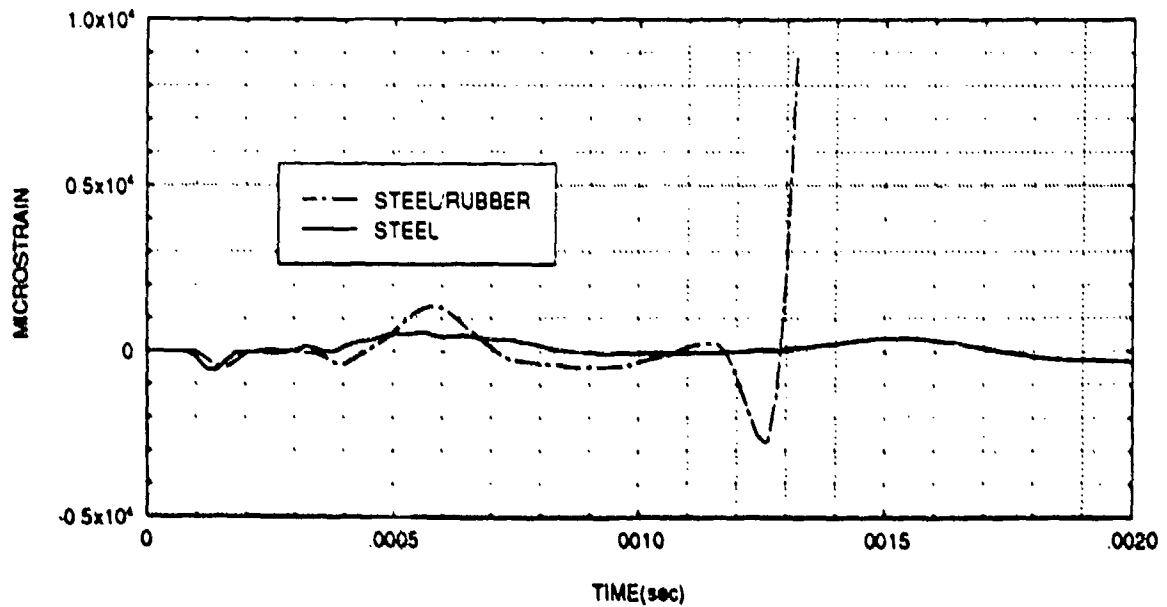


**Figure 156:** Hoop strain at position C3 for uncoated and coated steel cylinders.

shock are similar, and while the magnitudes of the response vary, the trends are the same.

#### IV. CONCLUSIONS AND RECOMMENDATIONS

Under certain conditions, when subjected to underwater shock, compliant coatings appeared to concentrate wave energy within the structure for longer duration, resulting in significantly higher magnitudes of stress and strain. Instead of a gradual release of energy into the surrounding water medium, most of the energy was retained in the metal material. Cylinder response was most influenced by changes in rubber shear modulus and rubber thickness. Increasing these values resulted in improved cylinder response. Both parameters are related to the coating stiffness and it is this property that most likely governs the extent of the energy transfer in the compliant coating and consequently the dynamic response of the cylinder. Results point to the existence of threshold values for both coating shear modulus and coating thickness, values below which lead to adverse and erratic cylinder response.

A more detailed analysis of wave transmission and reflection at the rubber-metal and rubber-water interfaces would be beneficial. An examination of the effects of stiffness changes at the microscopic level would improve our understanding of the energy transfer mechanism in the coating. A sensitivity analysis should also be conducted to investigate cylinder response for changes in endplate thickness and loading (asymmetrical vice symmetrical).

Follow on physical tests should be conducted to validate the numerical models and to enhance our understanding of the effects of compliant coatings on shock hardening.



# APPENDIX - COMPOSITE CYLINDER MODEL INGRID INPUT FILE

```
MODEL-MOONRIV.1.ING //THICKSHELL AND BRICK, ALUMINUM AND RUBBER(TREAD STOCK)//
dn3d vec term 0.010 plti 20.0e-6 prti 1000.0
```

```
mat 1 type 3 e 1.08e+7 pr 0.33 ro 2.610e-4 etan 0.0 sigy 4.0e+4
tshell quad 3 thick 0.250 endmat
```

```
mat 2 type 3 e 1.08e+7 pr 0.33 ro 2.160e-4 etan 0.0 sigy 4.0e+4
tshell quad 3 thick 1.000 endmat
```

```
mat 3 type 3 e 1.08e+7 pr 0.33 ro 2.160e-4 etan 0.0 sigy 4.0e+4
endmat
```

```
mat 4 type 3 e 1.08e+7 pr 0.33 ro 2.160e-5 etan 0.0 sigy 4.0e+4
endmat
```

```
mat 5 type 3 e 1.08e+7 pr 0.33 ro 2.160e-5 etan 0.0 sigy 4.0e+4
endmat
```

```
c Materials 3-5 are modeled as the rubber material, however the ingrid program
c will not accept this material specification. Therefore, these materials will
c be entered as if aluminum brick elements and the correct properties for the
c rubber will be edited in the ingrid file.
```

```
c The material input line for the rubber material parts should appear as
c follows:
```

```
c mat 3 type 27 a 29.291 b 18.609 pr 0.4991 ro 9.20e-05 endmat
```

```
c mat 4 type 27 a 29.291 b 18.609 pr 0.4991 ro 9.20e-05 endmat
```

```
c mat 5 type 27 a 29.291 b 18.609 pr 0.4991 ro 9.20e-05 endmat
```

```
c Materials 1 and 2 are Aluminum and are used for the inner cylindrical shell
c and inner end plate. Materials 3,4 and 5 are Tread Stock (Type of rubber)
c and are used for the outer cylindrical shell and outer end plate.
```

```
lcd 1 2 0.0 0.0 5.0e-2 0.0
lcd 2 2 0.0 2.0e-7 5.0e-2 2.0e-7
```

```
plan 2
0 0 0 0 1 0 0.001 symm
0 0 0 1 0 0 0.001 symm
```

c	name	type	point	dir	vector	size
	sd 1	cyli	0 0 0	0 1 0	6.250	
	sd 2	cyli	0 0 0	0 1 0	6.000	
	sd 3	cyli	0 0 0	0 1 0	5.750	
	sd 4	cyli	0 0 0	0 1 0	[5.750*2./3.]	

```
c ***** Generate Inner Cylindrical Shell *****
```

```
start
```

1	2	3	6	9	10	11 ;
1	2	4	6	8	13	18 20 22 24 25 ;
1	2	3	6	9	10	11 ;

-1.	-1.	-1.	0.	1.	1.	1.
-21.0	-20.0	-17.5	-14.5	-11.0	0.0	11.0 14.5 17.5 20.0 21.0
1.	1.	1.	0.	-1.	-1.	-1.

```
or 6 0 0 7 0 0 k j
or 1 0 0 2 0 0 j k
or 0 0 1 0 0 2 i j
or 0 0 6 0 0 7 j i
```

```

di 1 3 0 5 7 ; ; 1 3 0 5 7 ;
d 2 0 2 6 0 6

sfi -1 -7 ; ; -1 -7 ; sd 2
sfi -2 -6 ; ; -2 -6 ; sd 3

d 0 1 0 0 6 0
d 1 0 0 4 0 0

mate 1

end

c ***** Generate Inner End Plate *****
start

1      3      6      9      11 ;
1      2 ;
1      3      6      9      11 ;

-1.    -1.    0.    1.    1.
20.0   21.0
-1.    -1.    0.    1.    1.

or 0 0 0 0 0 0 k i

di 1 2 0 4 5 ; ; 1 2 0 4 5 ;

sfi -1 -5 ; ; -1 -5 ; sd 3
sfvi -2 -4 ; ; -2 -4 ; sd 4

d 1 0 0 3 0 0

mate 2

end

c ***** Generate Outer Cylindrical Shell Coating *****
start

1      2      3      6      9      10      11 ;
1      2      3      5      7      9      14      19      21      23      25      26      27 ;
1      2      3      6      9      10      11 ;

-1.    -1.    -1.    0.    1.    1.    1.
-21.25 -21.0 -20.0 -17.5 -14.5 -11.0 0.0 11.0 14.5 17.5 20.0 21.0 21.25
1.      1.      1.      0.    -1.    -1.    -1.

or 6 0 0 7 0 0 k j
or 1 0 0 2 0 0 j k
or 0 0 1 0 0 2 i j
or 0 0 6 0 0 7 j i

pri -1 -7 ; ; -1 -7 ; 1 -1.0 0.0 0.0 0.0

di 1 3 0 5 7 ; ; 1 3 0 5 7 ;
d 2 0 2 6 0 6

sfi -1 -7 ; ; -1 -7 ; sd 1
sfi -2 -6 ; ; -2 -6 ; sd 2

d 0 1 0 0 7 0

```

```

d 1 0 0 4 0 0
mate 3
end
c ***** Generate Outer End Plate Coating (Small Ring Area) *****
start
      1      2      3      6      9      10      11 ;
      1      2 ;
      1      2      3      6      9      10      11 ;
      -1.     -1.     -1.      0.      1.      1.      1.
      21.0    21.250
      -1.     -1.     -1.      0.      1.      1.      1.
or 6 0 0 7 0 0 k j
or 1 0 0 2 0 0 j k
or 0 0 1 0 0 2 i j
or 0 0 6 0 0 7 j i
di 1 3 0 5 7 ; ; 1 3 0 5 7 ;
d 2 0 2 6 0 6
sfi -1 -7 ; ; -1 -7 ; sd 2
sfi -2 -6 ; ; -2 -6 ; sd 3
d 1 0 0 4 0 0
mate 4
end
c ***** Generate Outer End Plate Coating (Large Plate Area) *****
start
      1      3      6      9      11 ;
      1      2 ;
      1      3      6      9      11 ;
      -1.     -1.      0.      1.      1.
      21.0    21.250
      -1.     -1.      0.      1.      1.
or 0 0 0 0 0 0 k i
pr 1 2 1 5 2 5 1 -1.0 0.0 0.0 0.0
di 1 2 0 4 5 ; ; 1 2 0 4 5
sfi -1 -5 ; ; -1 -5 ; sd 3
sfvi -2 -4 ; ; -2 -4 ; sd 4
d 1 0 0 3 0 0
mate 5
end
end

```

## LIST OF REFERENCES

1. Fox, P. K., *Nonlinear Dynamic Response of Cylindrical Shells Subjected To Underwater Side-On Explosions*, Master's Thesis, Naval Postgraduate School, Monterey, California, 1992.
2. Fox, P. K., Kwon, Y. W., Shin, Y. S., *Nonlinear Response of Cylindrical Shells to Underwater Explosion: Testings and Numerical Prediction Using USA/DYNA3D*, Report NPS-ME-92-002, Naval Postgraduate School, Monterey, California, March 1992.
3. Chisum, J. E., *Response Predictions for Double Hull Cylinders Subjected to Underwater Shock Loading*, Master's Thesis, Naval Postgraduate School, Monterey, California, 1992.
4. Los Alamos Technical Associates, *Test Plan for Microsphere Effects on Shock Waves*, LATA031-00, Report DNA-001-86-C-0024, Defense Nuclear Agency, Washington, D.C., 1992.
5. Livermore Software Technology Corporation Report 1018, *VEC/DYNA3D User's Manual (Nonlinear Dynamic Analysis of Structures in Three Dimensions)*, by D. W. Stillman and J. O. Hallquist, June 1990.
6. Livermore Software Technology Corporation Report 1019, *LS-INGRID: A Pre-Processor and Three-Dimensional Mesh Generator for the Programs LS-DYNA3D, LS-NIKE3D and TOPAZ-3D*, version 3.0, by D. W. Stillman and J. O. Hallquist, June 1991.
7. Livermore Software Technology Corporation Report 1009, *LS-TAURUS, An Interactive Post-Processor for the Programs LS-DYNA3D, LS-NIKE3D and TOPAZ-3D*, by J. O. Hallquist, April 1990.
8. Deruntz, J. A. Jr., *The Underwater Shock Analysis Code and its Applications*, Paper presented at the 60th Shock and Vibration Symposium, Virginia Beach, Virginia, 1989.
9. Geers, T. L., "Residual Potential and Approximate Methods for Three Dimensional Fluid-Structure Interaction Problem," *Journal of the Acoustic Society of America*, v. 49, pp 1505-1510, 1971.
10. Geers, T. L., "Computational Methods for Transient Analysis," *Boundary-Element Methods for Transient Response*, Elsevier Science Publishing Co., Inc., New York, New York, p. 231, 1983.

11. Mooney, M., "A Theory of Large Elastic Deformation,"  
*Journal of Applied Physics*, v. 11, pp 582-592, 1940.

# INITIAL DISTRIBUTION LIST

	No. of Copies
1. Defense Technical Information Center Cameron Station Alexandria, Virginia 22304-6145	2
2. Library, Code 52 Naval Postgraduate School Monterey, California 93943-5002	2
3. Professor Y. W. Kwon, Code ME/Kw Department of Mechanical Engineering Naval Postgraduate School Monterey, California 93940	1
4. Professor Y. S. Shin, Code ME/Sg Department of Mechanical Engineering Naval Postgraduate School Monterey, California 93940	1
5. Department Chairman, Code ME Department of Mechanical Engineering Naval Postgraduate School Monterey, California 93940	1
6. Naval Engineering Curricular Office (Code 34) Naval Postgraduate School Monterey, California 93943-5002	1
7. Dr. Kent Goering Defense Nuclear Agency 6801 Telegraph Road Alexandria, Virginia 22310	1
8. Mr. Douglas Bruder Defense Nuclear Agency 6801 Telegraph Road Alexandria, Virginia 22310	1
9. Dr. Phillip B. Abraham Office of Naval Research Solid Mechanics Division, Code 1132 800 North Quincy Street Arlington, Virginia 22217-5000	1

- |   |   |
|---|---|
| 10. Mr. Gene Remmers, ONT-23<br>Director, Office of Naval Technology<br>800 North Quincy Street<br>Arlington, Virginia 22217-5000                           | 1 |
| 11. Mr. Roshty S. Barsoum<br>Office of Naval Research<br>Solid Mechanics Division, Code 1132SM<br>800 North Quincy Street<br>Arlington, Virginia 22217-5000 | 1 |
| 12. Dr. Bill Sykes<br>David Taylor Research Center<br>Bethesda, Maryland 20084-5000   | 1 |
| 13. LCDR John K. Bergersen<br>1501 Dickinson Rd.<br>Havertown, Pennsylvania 19083   | 1 |